AUSTENITIC NITRIDING OF IRON AND IRON-CARBON ALLOYS

BRYAN GEORGE FRANCIS ROE B.Eng. M.I.M.

Thesis submitted in accordance with the requirements of the University of Liverpool for the degree of Doctor in Philosophy.

July 1976

To Liz

'to dream the impossible dream'

ACKNOWLEDGEMENTS

I would like to thank Dr. T. Bell for his advice and criticism in the supervision of the project.

Thanks are also due to Professors J. Stringer and D.Hull for the provision of laboratory facilities, Mr. F. Woodland for assistance in workshop facilities, Mr. J. Gillies for assistance in photography and members of the Heat Treatment Research Group for their help and criticism at various stages of the work.

In addition, special thanks are due to Messrs. D. Harding, J. Hughes, J.Gould and their staff at Vauxhall.Motors, Ellesmere Port for the provision of their Quantovac analysis facility without which much of the work described in this thesis could not have been carried out.

Financial support in the form of a Science Research Council 'Instant' Award is also gratefully acknowledged.

Finally, help and encouragement from my parents over many years of study and the assistance of Mrs. B. Sloan in the typing of the thesis are also gratefully acknowledged.

SUMMARY

Some of the scientific and technological limitations in the field of austenitic thermochemical treatments involving the diffusion of nitrogen have been investigated.

New methods of accurately analysing the nitrogen concentration gradient in surface hardened components have been evolved, using standards based on a controlled nitriding process. As a result of this work, (a) emission spectrometry is now being used as a quality control tool in industrial austenitic carbonitriding and (b) quantitative electronprobe microanalysis for nitrogen is now a powerful tool for physical metallurgical research into nitrogen-rich iron-based systems. In addition, methods of accurately determining the residual ammonia level in heat treatment atmospheres have been evolved using both infra-red gas analysis and gas chromatography.

Using the analytical methods just described, an investigation of the iron-carbon-nitrogen system was undertaken. This has resulted in the following information about the system:

(a) the diffusion coefficient of nitrogen in austenite is compositionally dependent, in a similar manner to that for carbon in austenite,

(b) using existing D_{γ}^{N} data for very low nitrogen levels, it is possible to estimate nitrogen concentration gradients in surface hardened components, by means of equations based on compositionally dependent diffusion coefficients,

(c) D_{γ}^{N}, at a fixed nitrogen level, increases with increase in base carbon level of iron-carbon alloys,

(d) the iron-carbon-nitrogen ternary system at temperatures in the range 748°C to 845°C has been investigated and the austenite phase field partly delineated,

(e) the mechanism of gas void formation in the austenitic nitriding of pure iron, which has in the past restricted its application, has been investigated and shown to be due to overlapping of advancing austenite interfaces in thin sheet material. This has important industrial implications in that relatively thick components can be surface hardened with high nitrogen levels without fear of blistering due to gas void formation.

CONTENTS

CHAPTER 1

INTRODUCTION

Over the years heat treatment processes have begun as small laboratory investigations, and when their commercial importance has been recognised, a scaling up operation has taken place and the particular process established on a mass production scale. Thermochemical processes for the surface hardening of iron and its alloys are no exception to this trend. Indeed, the vast majority of industry would function in a very inefficient manner without such treatments to combat wear and fatigue.

Occasionally treatments are used where their practical value and importance has been establisned on largely empirical data, but their scientific principles are not fully understood. Such a process is austenitic carbonitriding, involving the diffusional addition of both carbon and nitrogen to the steel surface. Similarly, a treatment which has been investigated scientifically, but as yet has only remained a laboratory treatment, is austenitic nitriding. The common link between the two treatments is the addition of nitrogen to the steel surface.

The present project has been undertaken to examine the scientific deficiencies in austenitic carbonitriding, and further investigate austenitic nitriding with a view to its commercial establishment. Many of the barriers to both objectives are concerned with the performance and detection of nitrogen, both in the surface of the treated component and in the atmosphere in which the components are treated. The role of nitrogen in iron has been firmly established, but its commercial importance

has only really been emphasised in ferritic thermochemical processes such as nitriding and various nitrocarburising treatments. In these latter processes, the degree of control required is not as critical as that required for the austenitic processes and is one reason for their widespread use.

Therefore to firmly establish the austenitic nitriding process commercially, process control parameters would need to be examined from both scientific and technological viewpoints.

Fortunately, these main objectives complement each other as neither one can proceed without the other, and the project has been established to investigate them simultaneously.

After reviewing the present state of austenitic thermochemical treatments in chapter 2, the full scope and objectives of the project are outlined in chapter 3. Each subsequent chapter deals with particular topics, and further reviews and full discussion of results are contained within these chapters as appropriate. The final chapter 8 contains a summary of all the progress and results of objectives of the project.

In this thesis, the tables and figures relevant to each chapter have been positioned at the end of each chapter, and a full list of tables and figures is included at the end of the thesis, together with page numbers.

CHAPTER 2.

REVIEW OF AUSTENITIC THERMOCHEMICAL TREATMENTS AND CURRENT INDUSTRIAL PRACTICE.

2.1. Introduction

Thermochemical treatments are used by industry as a means of improving the wear resistance and fatigue life of critical components. The austenitic thermochemical treatments currently used for steels are carburising, involving the diffusional addition of carbon to the steel surface, and carbonitriding, involving the diffusional addition of both carbon and nitrogen to the steel surface. Austenitic nitriding, involving only the diffusional addition of nitrogen, has had some investigation on a laboratory scale[1-3], but is not yet practiced industrially.

The aim of this present review is to describe both the scientific principles and the current industrial practice of austenitic thermochemical processes. In particular, emphasis will be placed on identifying the constraints on

(a) a complete understanding of the carbonitriding process and

(b) the industrial acceptance of austenitic nitriding, in order to provide the background to the objectives of the present project, which are described in chapter 3.

2.2 Classification of Thermochemical Treatments

Thermochemical treatments of steels can be divided into two classes

(a) Austenitic treatment - diffusional addition of carbon and/or nitrogen at temperatures in the austenite phase field.

(b) Ferritic treatment - diffusional addition of carbon and/or nitrogen at temperatures in the ferrite phase field.

A more detailed breakdown of the various thermochemical processes can be seen in table 1, and it can also be seen that similarities exist between some of the treatments

This present work is essentially concerned with austenitic treatments which will now be reviewed in detail, but where particular control or analysis techniques are pertinent to both types of treatment the appropriate distinctions will be made.

2.3 Carburising.

As indicated in table 1, carbon is transferred from a carburising medium into the surface of steel by a diffusion process and its distribution within the steel depends mainly on three factors:

(a) the carbon potential of the carburising medium

(b) the diffusion time

(c) the temperature of treatment.

The main variation is effected through factor (a) because by varying the carbon potential the surface carbon concentration can be controlled such that the process can be used to

(1) control the carbon level to the same level as the base carbon level

(2) restore the carbon level in a decarburised layer to the original carbon level

(3) increase the carbon level at the surface and thus create a concentration gradient between the surface and the inner part of the component.

It is function (3) which is most commonly known as carburising, although functions (1) and (2) are both part of the carburising process.

By producing a concentration gradient in the component a composite material is made, because by quenching in a suitable medium such as oil, the high carbon outer portion - the case - is transformed to a hard martensitic structure, whilst the low carbon inner portion - the core - is transformed to a relatively soft structure (ferrite + pearlite or bainite depending on the hardenability of the steel). In addition to this, because of the different transformation rates of the case and core, after completion of the quench the case remains in compression, and so its resistance to any cyclic stressing is greatly enhanced.

One of the most common uses for carburised components is in power transmission parts of automobiles such as gearbox parts subjected to high alternating stresses and frequent contact with other components. In order to sustain the frequent contact good wear resistance is required and this can be achieved by producing a high surface hardness. It is known [4] that the hardness of quenched martensite varies with its carbon content up to a maximum hardness of 64 HRC (850 HV) at 0.85 w/o carbon. It follows therefore that the maximumwear resistance should be obtained by treating a component such that its surface carbon content is close to this value. Further increase in carbon content results in no further increase in hardness, and invariably results in a decrease in hardness at the surface due to retained austenite. Consequently most industrial carburising processes aim at a surface carbon content of 0.85 w/o.

2.3.1. Methods of carburising.

The carburising media can be solid, liquid or gaseous and a brief outline of each technique will now be given.

2.3.1.1. Solid or pack carburising.

This is the original form of carburising in which a component was surrounded with charcoal and heated to red heat, carbon was thus transferred from the charcoal to the component. However this technique was not always successful, and further development work produced catalysers which improved the efficiency and reproducibility of the process. Pack carburising is still used, but is mainly confined to treatment of small parts or 'one-off' jobs.

The modern pack carburising compounds are normally a mixture of coke, charcoal and a catalyst such as $BaCO_3$ or Na_2CO_3. Components are packed with these compounds in sealed steel boxes which are then heated in a conventional furnace. At temperature the coke and charcoal, under the action of the catalysers, produce carbon monoxide which reacts with the steel surface as follows:

$$2CO + Fe = Fe + C_{in\ Fe} + CO_2 \qquad (1)$$

The equilibrium constant for this reaction is

$$K = \frac{(CO)^2}{CO_2} \qquad (2)$$

and so control of the reaction is through control of the quantity of carbon monoxide released from the compound. Some control can be achieved by control of the catalysts, but is not very successful in practice, and is one of the reasons for the limited use of the process. In addition, a further austenitising

treatment after the components have cooled from the pack treatment is necessary to produce the required case profile and a quench to produce the hardened case.

2.3.1.2. Liquid carburising.

Taking the pack carburising method one step further by producing a carbonaceous solid which is molten at the carburising temperature is the basis of liquid carburising. Suitable compounds are mixtures of sodium cyanide and alkaline earth salts, although occasionally chlorides of barium, calcium or strontium are used. . The compounds are available commercially as fused salts under a variety of trade names for specific temperature applications. Full details of these and their operating practice is documented in the 'Cassel' Manual of Heat Treatment[5].

The mechanism of the reaction is very complex, but the underlying principle is that at temperature the cyanide and salt compounds react to form an alkaline earth cyanide, which readily decomposes in contact with the iron surface to produce carbon:

$$Ba(CN)_2 + Fe = Fe + C_{in\ Fe} + BaCN_2 \qquad (3)$$

In addition, a small amount of nascent nitrogen is formed which also diffuses into the surface, so that strictly speaking this is a carbonitriding reaction.

Temperatures normally used for this process are between 840 and 900°C, with possible extension up to 1050°C, but at high temperatures the life of the salt pots is very short.

Control of the carbon potential is achieved by additives or buffers and to maintain efficiency regular chemical analysis of the bath must be made, and the specified working composition maintained by appropriate additions of salts.

Liquid carburising is in widespread use throughout the world and has considerable advantages over pack carburising. Its main advantages are

(a) rapid heat transfer

(b) the ability to quench directly into water, oil or neutral salt.

However it has disadvantages in the poisonous nature of the salts used, and the safe disposal of both expended salt mixtures and the effluent used to clean parts and equipment. This is particularly relevant at the present time with so much emphasis being placedon the protection of the environment from pollution.

2.3.1.3 Gas carburising.

By far the most widely used carburising process is gas carburising with its main advantage being in the controllability of the process. The control aspects will be dealt with in a later section.

In gas carburising, the work is heated in a neutral atmosphere in a gas-tight furnace until the required temperature is reached. The furnace atmosphere is then enriched with a suitable gas to act as a carburising agent, and the work held at this temperature for sufficient time to allow carbon to diffuse into the work. Quenching is then performed on completion of

the diffusion time and is normally performed under a protective atmosphere. Suitable carburising agents are hydrocarbon gases such as methane, propane and butane and sometimes town gas is used. It is also possible to use organic liquid mixtures which volatilise in the heat of the furnace chamber. The hydrocarbons are rarely used in undiluted form because they tend to deposit soot, once the saturation carbon content of the steel is reached. It is more usual to generate a neutral carrier gas, to which small quantities of the hydrocarbons can be added to achieve the desired carbon potential. This neutral carrier gas is normally produced from an endothermic generator which catalytically breaks down town gas or, more commonly in this country, liquid propane. Endothermic atmospheres also provide a background carbon potential during the heating-up period in the carburising process. A typical composition of 'endo' gas is:

N_2	35-40 v/o	H_2	35-45 v/o
CO	25-15 v/o	CH_4	0.5-1.5 v/o
CO_2	0-1.0 v/o		

The background carbon potential is provided by the reaction:

$$2CO + Fe = Fe + C_{in\ Fe} + CO_2 \qquad (4)$$

The presence of hydrogen in the 'endo' gas also produces the reaction:

$$CO + H_2 + Fe = Fe + C_{in\ Fe} + H_2O \qquad (5)$$

which is more efficient than reaction (4), and also allows the carbon potential to be related to the water vapour content or dew point. This as will be shown later is one method of control.

By adding hydrocarbons to the 'endo' gas the dew point and CO_2 levels can be reduced, and thus provide more carbon potential by the following reactions:

$$CH_4 + H_2O = CO + 3H_2 \quad (6)$$

$$CH_4 + CO_2 = 2CO + 2H_2 \quad (7)$$

$$CH_4 + Fe = Fe + C_{in\ Fe} + 2H_2 \quad (8)$$

Similar atmospheres are generated when organic liquid mixtures are used - the drip feed method. Suitable mixtures are based on methyl, ethyl or propyl alcohol, with additions of benzene and other liquid hydrocarbons. Carbon potential in this method is normally controlled by controlling the rate of flow of the liquid into the furnace and forced circulation of the used gases. The latter act in a similar manner to 'endo' gas and dilute the freshly vapourised gases to prevent sooting.

2.3.2. Control of gas carburising atmospheres.

From equations (4) to (7) possibilities for control exist through monitoring of the CO_2 and H_2O levels. In fact in the carburising atmosphere these levels are interrelated, because by combining equations (6) and (7) the following reaction results:

$$CO_2 + H_2 = CO + H_2O \quad (9)$$

whose equilibrium constant is :

$$K = \frac{(CO)\ (H_2O)}{(CO_2)(H_2)} \quad (10)$$

$$\text{or} \quad \frac{(H_2O)}{(H_2)} = \frac{K(CO_2)}{(CO)} \quad (11)$$

Control is also possible through equation (4) whose equilibrium constant is:

$$K = (CO_2) / (CO)^2 \quad (12)$$

Here K is independant of water vapour content, but the equation is not a simple ratio.

The equilibrium constant for reaction (11) has been calculated by Harris [6] from the data of Wagman et al [7]. Data[8] are also available for the equilibrium of CO_2 and CO with various carbon concentrations in plain carbon steel at various temperatures so that complete solution of reaction (9) is possible. Hence monitoring of any of the gases should provide adequate control, although to be strictly accurate the ratios on either side of the equation should be monitored, to account for any variation in the composition of the 'endo' gas supplied from the generator. However, in practice it is usually sufficient to monitor one gas in the ratio.

The methods available for monitoring the above reaction and some other types of reaction are shown in table 2 and will now be described in more detail.

2.3.2.1. Dew point meter.

This is one of the earliest methods of control and is based on the principle that at a certain temperature, for a given pressure, a mixture of gases will precipitate its moisture content. The exact relationship between moisture content and dew point is known and the method is therefore fairly straightforward. The principle is still widely used in carburising and instruments are now available which will perform the measurement automatically. it should be remembered however that the moisture content determined will only accurately reflect the carbon potential when the gas atmosphere is in equilibrium, a state rarely obtained in short time treatments.

2.3.2.2. Infra-red gas analysis.

This is perhaps the most common type of control used and, as can be seen from table 2, can be used to monitor a variety of gases, but normally in carburising an instrument is set up to measure and monitor CO_2. The commercial infra-red analyser is the absorption type based on the principle that certain gases will absorb infra-red radiation of different wavelengths, depending on the particular gas in question. These gases - elemental gases excluded as they do not absorb infra-red radiation - will absorb the infra-red radiation in proportion to their concentrations in a gas mixture, and so this variation can readily be monitored electronically and displayed on a meter or chart. By linking the instrument to suitable control valves, the composition of the carburising gas can be maintained within certain limits. In practice one infra-red analyser set up for CO_2 is often linked to a bank of up to six furnaces and switched into the gas stream automatically. The accuracy of the infra-red meter is extremely good; a typical carburising atmosphere might contain 0.1v/o CO_2 and the meter will read this to an accuracy in the order of 0.005v/o CO_2.

2.3.2.3. Orsat gas analysis

This method is an early attempt at complete gas analysis and uses a chemical absorption principle to determine CO_2, CO, O_2, H_2, CH_4 and C_2H_6. It has two main disadvantages;

(a) the complete analysis takes about 30 mins and is therefore not suitable for automatic control

(b) its accuracy in determining CO_2 is very poor and consequently carbon potential cannot be accurately controlled.

2.3.2.4. Gas chromatography

Small gas samples taken from the carburising atmosphere are separated into their component gases on a special column and analysed normally by passing over a thermal conductivity detector. This method has the advantage that virtually all gases can be separated and analysed very accurately, but up to quite recently the method has been rejected because it is not continuous, it has been slow and there has been difficulty in interpreting readings. However recent advances in chromatographic science have eliminated some of these difficulties and consequently there has been renewed interest in the chromatograph as a control tool.

2.3.2.5. Shim stock.

The control methods so far described have all been based on monitoring of certain furnace gases. In this method the actual carbon content of the work being treated is measured, by introducing a piece of pure iron or low alloy steel approximately 0.1mm thick into the furnace and calculating its weight gain. Depending on the temperature the shim stock is maintained in the furnace for approximately 1.5 hours, and therefore in long time treatments can be extracted, carbon content measured and any necessary adjustment to the atmosphere made. The sheet reaches temperature very quickly and also becomes through carburised quickly, so that the actual equilibrium carbon content is measured. It must be borne in mind that the components may never reach equilibrium and therefore the method should only be used as a guide. Actual chemical analysis of work pieces should be made to determine their exact carbon content. The method is slow and

therefore cannot be used for accurate atmosphere control. It is usually used as a check on actual conditions inside the furnace, whilst atmosphere control is maintained by another method.

2.3.2.6. Hot wire resistivity.

It is known that the resistivity of austenite varies approximately linearly with its carbon content, so that by making a wire thin enough to respond rapidly to changes in the carbon content of the atmosphere, a continuous recording technique is possible. In practice a probe, consisting of a 0.05mm diameter Fe-5w/o Ni wire, is maintained inside the furnace with the atmosphere continuously sucked over the wire which forms part of a Wheatstone bridge. Hence any change in carbon level of the wire is reflected in an imbalance in the bridge and can be displayed on a chart. The furnace atmosphere can also be controlled by this method, and it is claimed to be accurate to 0.005w/oC. The method known as 'Microcarb' control is patented by Leeds and Northrup[9] who make the appropriate furnace which operates on the drip feed principle.

2.3.2.7. Oxygen probe

It is known that oxygen is present in carburising atmospheres and is related to the CO/CO_2 ratio. However the quantity present is very small and has never been measureable to any accuracy until quite recently. The development of a new type of electrochemical oxygen meter by BISRA[10] enables oxygen levels from 100v/o down to 10^{-20} atmospheres to be measured at high temperatures.

A solid electrolyte, zirconia is used at high temperatures, has two chemically inert platinum electrode contacts. An e.m.f. E is developed in this cell related to the partial pressures of oxygen at the two electrodes:

$$E = KT\log (P_1/P_2) \quad (13)$$

K is a constant and T is temperature in ^{o}K.

By maintaining a constant oxygen potential at one electrode, the oxygen partial pressure at the other electrode can easily be calculated from equation (13). The application of this technique to the control of carburising atmospheres is discussed by Fairbank[11] and the detailed performance of a commercial probe is discussed by Record [12,13].

With the probe air is used as the reference gas, therefore the oxygen partial pressure is 0.21 atmospheres and the output of the probe is then given by

$$E = 45.355\mu_1 + 40 \text{ mV} \quad (14)$$

μ_1 being the oxygen potential at the measuring electrode in $kJmol^{-1}$

or

$$E = 10.84\mu_1 + 40 \text{ mV} \quad (15)$$

μ_1 being expressed in $kcalmol^{-1}$

μ_1 can be expressed in terms of the oxygen partial pressure through the following equation:

$$\mu_1 = 0.00457T\log_{10}(pO_2 \times 10^{-5}) \text{ kcalmol}^{-1} \quad (16)$$

T is in ^{o}K and pO_2 is in Nm^{-2}

In the carburising atmosphere the relationship:

$$2CO + O_2 = 2CO_2 \quad (17)$$

exists between CO, CO_2 and oxygen and the oxygen potential can be given by [12]

$$\mu O_2 = 0.0415T - 135 - 0.00915T\log_{10}(pCO/pCO_2)\ kcalmol^{-1} \quad (18)$$

Using existing thermodynamic data for 'endo' gas atmospheres[14] it is possible to calculate the oxygen potential corresponding to carbon potentials at various temperatures. This data is given in fig. 1, and has been shown in practice to work extremely well. Data has also been calculated[13] for the relationship between oxygen potential and CO_2 and dew point at various temperatures.

2.4 Carbonitriding.

Having outlined the principles behind carburising and methods of process control, it will now be shown how carbonitriding is related to the process. As can be seen from table 1 carbonitriding involves the diffusional addition of both carbon and nitrogen to the steel surface and this is readily achieved in both liquid and gaseous media.

2.4.1. Methods of carbonitriding.

2.4.1.1. Liquid carbonitriding.

As was seen with liquid carburising, a small amount of nitrogen is produced from the carburising cyanide salt. In order to increase the amount of nitrogen produced by the salt an ample supply of oxygen in the bath is necessary, as greater quantities of nitrogen can be produced from the cyanate salt - the oxidised cyanide. The following reactions are believed to take place: [15]

$$2NaCN + O_2 = 2NaNCO \quad (19)$$

$$4NaNCO = Na_2CO_3 + 2NaCN + CO + 2N_{in\ Fe} \quad (20)$$

$$2CO = C_{in\ Fe} + CO_2 \quad (21)$$

$$NaCN + CO_2 = NaNCO + CO \quad (22)$$

As can be seen from these equations, the carbon and nitrogen potentials will depend on the rate of formation and subsequent decomposition of the cyanate salt. The rates can be increased by increasing the temperature of operation, therefore increasing the carbon and nitrogen potentials.

However because of the complexity of the bath composition, and possibilities of other side reactions becoming rate controlling, the degree of control is not very good. The bath efficiency can only be maintained by regular analysis and readjustment. Despite these disadvantages the process is in common use and is cheaper than liquid carburising mainly due to its lower operating temperature.

2.4.1.2. Gas carbonitriding.

The modification to a gas carburising atmosphere to enable carbonitriding to take place is the simple addition of ammonia which breaks down on the steel surface as follows:

$$NH_3 = N_{in\ Fe} + \frac{3}{2} \times H_2 \quad (23)$$

It is not sufficient to introduce nitrogen gas into the furnace because the solubility of nitrogen in iron is pressure dependent. At one atmosphere pressure a maximum solubility of 0.03w/oN can be achieved in equilibrium with pure iron[16] at temperatures near 900°C, see fig. 2. In carburised low alloy steels maximum solubilities of nitrogen in the case[17] of the order of 0.025w/oN are achieved due to the presence of nitrogen gas in the carburising atmosphere. In order to obtain

solubilities of nitrogen of the order of 0.5w/o,pressures of nitrogen gas of the order of several thousand atmospheres would be required, and consequently this is not a practical proposition especially from the safety aspects.

Fortunately, ammonia gas in contact with an iron surface produces a high chemical activity of nitrogen which is equivalent to the high pressures of nitrogen gas required for high solubilities. Although reaction (23) is the one normally associated with nitriding and carbonitriding, two other reactions are possible[16]:

$$NH_3 = \tfrac{1}{2}N_{2\,(gas)} + \frac{3}{2} \times H_{2(gas)} \qquad (24)$$

$$NH_3 = \tfrac{1}{2}N_{2(gas)} + 3H_{\text{in Fe}} \qquad (25)$$

neither of which produce nitrogen in steel. Reaction(24) is commonly associated with the thermal decomposition of ammonia, and reaction (25) occurs only to a limited extent.

From reaction (23) the solubility of nitrogen in steel will be proportional to the equilibrium constant:

$$K = \frac{(pH_2)^{3/2}}{(pNH_3)} \qquad (26)$$

It should be appreciated when ammonia is added to a gas carburising atmosphere that the equilibrium conditions determined for gas carburising will not be valid for carbonitriding, because of the interaction of ammonia and its decomposition products with the constituent gases in the carburising atmosphere. However new equilibrium data for various levels of ammonia additions have recently been determined[18-20], and this will be discussed more fully in the review of current industrial practice - section 2.8.

Gas carbonitriding atmospheres can also be generated by the drip feed method, similarly to gas carburising, in this case an organic liquid containing nitrogen is used. Typical liquids are aniline, piridine, ethanolamine, triethanolamine, tetraethylenopentamine, urea and formamide. Triethanolamine[21] is perhaps the most commonly used liquid, it easily breaks down at high temperatures and is easy to feed into the furnace. Gases formed on its decomposition are CH_4, CO, H_2 and HCN. HCN readily breaks down on the steel surface to produce nitrogen and carbon, in addition to the carbon produced by the other gases. Consequently the atmosphere produced has high carburising and nitriding potentials, and very slow flow rates must be used to avoid sooting.

2.4.2. Control of gas carbonitriding atmospheres

It would be partially true to say that there is little control over carbonitriding atmospheres, however this is unfair on the operators because the process itself has developed largely on an empirical basis until recent scientific interest had been aroused. Because the carbonitriding atmosphere is more complex than the carburising atmosphere control is normally in two parts; one concerned with the carburising potential and one concerned with the nitriding potential.

2.4.2.1. Control of carburising potential

All the methods of control described in section 2.3.2. could be used for controlling the carburising potential, but certain reservations must be made for each method of control.

Those methods concerned with gas atmosphere analysis must take

account of the shift of equilibrium for carburising by the addition of ammonia[18-20] to the atmosphere already referred to in section 2.4.1.2. - this applies to all methods except shim stock (2.3.2.5.) and hot wire resistivity (2.3.2.6.)

The shim stock method is not normally used because

(a) carbonitriding cycles are normally short - 1-3 hours

(b) simple weight gain measurement will not produce the carbon weight gain, as nitrogen is also absorbed in the specimen. A rapid chemical analysis technique is required to determine carbon and nitrogen levels, if the method is considered for control.

In the case of hot wire resistivity, nitrogen behaves in a similar manner to carbon by increasing the resistivity of austenite and hence its effect on the wire cannot be separated.

In the case of atmospheres produced by drip feed methods, independent control of carburising potential can only be maintained by splitting the atmosphere generation into two liquids; one for carburising and one for nitriding.

2.4.2.2. Control of nitrogen potential.

Until very recently no methods of controlling the nitrogen potential within a carbonitriding atmosphere have been available. It is for this reason that the process has developed on an empirical basis, with the only exterior methods of control being the flow rate of ammonia gas into the furnace. In the case of atmospheres generated by drip feed methods control of the flow rate of compounds such as urea[22] and formamide[22] which break down to give only active nitrogen offer some means

of control.

2.5. Vacuum Carburising.

One of the newer austenitic thermochemical treatments is vacuum carburising which has stemmed from a need to quicken process times and improve on quality of the finished product. The process on an industrial scale[23,24] employs a 'cold wall' vacuum furnace containing an oil quench tank. Work is preheated to the required carburising temperature in the range 1000-1150°C under a reduced pressure of 10^{-3} torr, then held at temperature for a short time for cleaning and outgassing. The carburising gas in the form of methane or purified natural gas then back fills the chamber to the required sub-atmospheric pressure and treatment then takes place for several hours. The carburising action occurs by reaction (8) - section 2.3.1.3.

$$CH_4 + Fe = Fe + C_{(in\ Fe)} + 2H_2 \qquad (8)$$

Because of the relatively high temperature of reaction, grain growth can occur and this is minimised by rapid cooling in nitrogen gas and reheating to about 850°C to refine the grain size, after which the work is finally quenched in oil. A typical production cycle is shown in fig.3[25]. Overall cycle times are approximately 2/3rds of conventional gas carburising times, due to the use of elevated temperatures. Advantages from environmental viewpoints - no fumes or excess heat - and technical viewpoints - cleaner parts, more controllable process and possible elimination of surface oxidation products - are claimed.

2.5.1. Control of Vacuum Carburising.

Because of the relative simplicity of the process compared to conventional gas carburising, control of the process is exercised through either

(a) partial pressure of CH_4 in work chamber

and/or

(b) temperature of carburising.

These controls have been exercised somewhat empirically from the initial development of the process [23-26], but recent work[27] has confirmed the relationship between methane partial pressure and carbon uptake in the work piece.

2.6. Ion or Plasma Thermochemical Treatments

Following the successful development of the ion or plasma nitriding processes [28-31] for ferritic thermochemical treatments, analogues of the austenitic thermochemical treatments are now being developed[32].

The ion or plasma processes operate in the following manner. The workpiece is contained within a vacuum chamber evacuated to a pressure of between 1 and 10 torr. An electrical potential of 600-800 volts is then connected between the chamber wall and the work piece, and in the presence of a suitable gas a glow discharge is created around the surface of the workpiece. The glow discharge or plasma is confined to a layer a few millimetres thick around the workpiece surface, the temperature of the surface being controlled automatically through control of the glow discharge power by temperature sensors attached to the workpiece.

The process initially developed for nitriding uses cracked

ammonia or nitrogen and hydrogen mixtures as the discharge gas. In the plasma, kinetic energy induced into nitrogen ions causes detachment of iron ions from the workpiece which then combine and form an Iron Nitride on the surface of the workpiece.

In translating the process to carburising and carbonitriding a methane or methane/nitrogen gas respectively is normally used, the plasma producing carbon or carbon and nitrogen atoms which then diffuse into the surface.

2.6.1. Control of Ion Thermochemical treatments.

In a similar manner to vacuum carburising, control is exercised through

a) type of discharge gas and partial pressure

b) temperature of workpiece - through power supplied to discharge.

In addition for a carbonitriding process, control is also exercised through the relative partial pressures of the gases in the discharge gas mixture.

Jones etal[28] have shown that in ion nitriding optimum surface hardness and case depth occur at a discharge current of 6mA and discharge voltage drop of 220 volts, further increase in discharge current to 28mA has little or no effect. Seybolt[33] has found that nitrogen partial pressure in ion nitriding is also critical, a partial pressure corresponding to equilibrium with Fe_4N is necessary ($\sim$ 1.3 torr), below which nitriding is not practicable.

Whilst ion nitriding is now an industrially accepted process[31], the ion carburising and carbonitriding processes[30,32,34] are still being investigated on a laboratory scale and the full control parameters have not been evaluated.

2.7 Austenitic Nitriding.

As was noted in the introduction (section 2.1.), austenitic nitriding has only been investigated on a laboratory scale to date [2,3,], Bell has outlined the background to this work and some of its theoretical concepts[1]

The same ammonia decomposition reaction used in ferritic nitriding is employed - reaction (23)

$$NH_3 \rightleftharpoons N_{(\text{in Fe})} + 3/2H_2 \quad - \quad (23)$$

but the ammonia gas is diluted with hydrogen to reduce the nitriding potential so that nitrogen absorbed into the steel surface does not exceed that required to form nitrides. Work[2] on thin foil material has shown that austenitic Fe-N alloys behave in a similar manner to austenitic Fe-C alloys; on rapid quenching from the austenite phase an Fe-N martensite is formed whose hardness varies in a similar manner to Fe-C martensites, see fig. 4, and the martensite transformation temperature is similarly depressed with increase in nitrogen level, see fig. 5.

Isothermal transformation can be used to produce a range of transformation products in Fe-N alloys analagous to those in Fe-C alloys[3], however only one type of bainite is formed analagous to upper bainite in Fe-C alloys. Perhaps the most interesting property from the industrial viewpoint is the

capability of age hardening by tempering the quenched Fe-N austenite, this is illustrated in fig.6. The distinct hardening peaks are due to

(1) at about 60°C - formation of coherent $Fe_{16}N_2$ precipitates in the matrix

(2) at about 200°C - decomposition of retained austenite to a form of nitrogen bainite.

The Fe-2.7^{W}/oN alloy only undergoes the second reaction and a large hardening increase is observed with complete transformation of the austenite.

2.7.1. Control of Austenitic Nitriding.

Because of appreciable thermal dissociation of ammonia above 600°C, the equivalent nitriding potential derived from equation (23) is small, due to the low partial pressure of ammonia in equilibrium with nitrogen and hydrogen. A high nitriding potential can be obtained by maintaining a high gas flow rate, approximately 15cm/min, over the specimen. For the austenitic nitriding of pure iron specimens under these conditions, Atkinson[35] has derived the nitriding potential corrected for thermal decomposition of ammonia.

$$r = \frac{PNH_3(OUTLET)}{\left[1 - \frac{(PNH_3(INLET) + PNH_3(OUTLET)}{2}\right]^{3/2}} \qquad (27)$$

and correlated this to equilibrium nitrogen contents in Fe-N alloys. The relationship at 660° and 810°C is shown in fig.7. The theory of austenitic nitriding is fully discussed in Chapter 6

2.8 Current Industrial Practice in Austenitic Thermochemical Treatments.

The development of the austenitic thermochemical treatments has progressed from solid and liquid media to the more controllable gaseous media. Whilst solid and liquid media are still used, the practices are dying out particularly for volume production. In the case of liquid media there is also pressure from environmentalists to restrict their use due to the highly poisonous cyanide compounds which are used. The vast majority of current austenitic thermochemical treatments are therefore using gaseous media to which the control methods already described can be applied. It is not unlikely that in the forseeable future the conventional gaseous processes will be superceded by the plasma techniques which would appear to offer even more advantages in control, quality of processed product and lack of pollution.

Of the current austenitic thermochemical treatments carbonitriding is the one in most need of further investigation, because of the lack of a full understanding of the scientific principles behind the process; technological problems in the control of nitrogen potential also exist. These deficiencies have been made clear in a recent survey[36] of heat treatment practice in the U.K., Europe and the U.S.A. Because of the close similarity of species involved, the mechanism of nitriding and possible technological constraints in control of nitriding potential in austenitic nitriding, it is also appropriate to consider this process for further investigation.

Therefore it is proposed to review recent and current research

work in the field of austenitic carbonitriding and austenitic nitriding with a view to defining the constraints on further development and increased acceptance of both processes.

2.8.1. The Influence of Nitrogen In Surface Hardened Layers. With the widespread use of carburising processes and their satisfactory control, the question must be asked why carbonitriding and its somewhat unsatisfactory control and poorly understood principles should be used. Many of the reasons are concerned with the influence of nitrogen on the structural properties of iron and its alloys.

(a) When the two binary systems Fe-N[16] and Fe-C[37] are examined closely (figs.8 and 9 respectively), it can be seen that very similar phase relationships occur in the temperature range 500 - 1000°C at contents less than in 3^{W}/o. However it is also seen that nitrogen is a far more effective austenite stabiliser than carbon, depressing the eutectoid temperature down to 590°C with 2.34^{W}/oN in solid solution, compared with 727°C with 0.765^{W}/oC. Nitrogen austenite also sustains more nitrogen in solid solution than carbon austenite; 2.7^{W}/oN at 650°C compared with 2.04^{W}/oC at 1149°C. This means that carbonitriding can be performed at a lower temperature than carburising, because ternary Fe-C-N austenite will be stable to a lower temperature than Fe-C austenite. Normally temperatures up to 100°C lower can be used with subsequent savings in energy and extended furnace life.

(b) In discussing austenitic nitriding in section 2.7, it was shown that the hardnesses of the respective Fe-N and Fe-C martensites are very similar, both peaking at about 900HV for similar interstitial levels, see fig.4. Consequently no loss of hardness would result in partial or complete replacement of

carbon by nitrogen in the case.

(c) Addition of nitrogen to Fe-C martensite cases has been shown to increase the wear resistance of the case and improve fatigue resistance, the later is probably due to different residual stress patterns[38]

(d) Nitrogen improves the hardenability of the case[39,40], so that carbonitrided plain carbon steels can be fully hardened in oil. Full oil hardening after carburising requires the use of low alloy steels, with their associated cost penalty. Distortion should therefore be minimised because of the slower critical cooling rate required to produce the martensitic case.

(e) Nitrogen containing cases are more temper resistant than carbon containing cases[1]

From these considerations, there would be good reason to increase the nitrogen levels at present used in carbonitrided layers or to completely substitute nitrogen for carbon by using an austenitic nitriding process.

Current industrial practice determined in a recent survey[41] showed the use of 0.16 to 0.27^{w}/oN, and 0.8 to 1.0^{w}/oC at the surface of carbonitrided components, with case depths in the range 0.25 to 0.5 mm. Retained austenite occurred with combined interstitial levels greater than 0.85^{w}/o, but none of the users seemed unduly worried.

Work in Germany has shown that retained austenite in the surface of carburised components such as gears and shafts improves resistance to wear pitting[42] and improves fatigue strength[43] The reason for the improvement was thought to be

transformation of austenite to martensite due to deformation, further work[44] presented recently has confirmed this effect. These further considerations suggest that the properties of higher nitrogen cases with retained austenite should be investigated.

The present knowledge of the effect of nitrogen in surface hardened layers has been largely due to physical metallurgical investigations of the Fe-N binary system[1,3,45-47]. There is a limited amount of knowledge on the Fe-C-N system, but this is restricted to phase relationships at temperatures below 700°C[48,49] and physical metallurgical data of alloys produced at 500°C[50].

2.8.2. The Effect of Ammonia on Carburising Atmospheres.

In discussing the control of carburising potential in carbonitriding atmospheres (section 2.4.2.1.), it was pointed out that the addition of ammonia to the atmosphere causes a shift in equilibrium. The shift is due to dilution of the atmosphere by ammonia, its interaction with other gases and its decomposition products. It is this aspect of atmosphere equilibrium which has attracted considerable attention in recent years.

Bello et al[19,51], Salonen and Sulonen[18], Chatterjee-Fischer and Schaaber[52] and Slycke[20] have all investigated this phenomena. Experimentally it has been shown[18,19,51,52] that for a fixed CO_2 carburising level the addition of 5 v/o ammonia to the atmosphere causes a reduction in carbon potential of the atmosphere (see fig.10) by increasing the

CO_2 level; consequently the equilibrium CO_2 level must be lowered to maintain the same carburising potential. Slycke has developed a mathematical model for calculating this change for various levels of ammonia added to the atmosphere, based on assumptions that the ammonia completely dissociates,[20] graphical representations of this data are shown in figs.11 and 12. From the calculated results it was shown that the water vapour content is insignificantly affected by ammonia additions up to 10^{v}/o, confirmed experimentally by the other investigators[18,19,51,52]. The conclusion thereby being drawn that the carburising potential can be controlled on water vapour equilibrium data developed for carburising, irrespective of the ammonia level added to the atmosphere.

The same experimental investigations showed that the CO level of the atmosphere was also affected by the ammonia addition, but to a lesser extent with the consequence that the $\frac{(CO)^2}{CO_2}$ ratio remained essentially constant. Slycke's calculations[20] also confirmed this, together with actual atmosphere analysis. Therefore a second control possibility exists through the monitoring of the $\frac{(CO)^2}{CO_2}$ ratio, however this is likely to be significantly more expensive, due to the need to purchase a second infra-red analyser to monitor COlevel or use a top-gas analyser, normally employed to measure this ratio in blast furnaces.[36].

2.8.3. The Nitrogen Potential of Carbonitriding Atmospheres. Chatterjee-Fischer[53] has shown that the nitrogen content of thin foils is directly related to the inlet ammonia content of the atmosphere, see fig.13. This is not unexpected from Darken's results[16]. The nitrogen content of the foils was only significantly affected by the carburising potential when ammonia levels of 10% were used; this is related to the problem discussed in section 2.8.2. Bell$_o$ et al[19, 54]

working on the same problem have related the nitrogen potential to the residual ammonia in the exhaust gas stream, a proposal also made by Ogawa and Otomo[55]. This is the same concept proposed by Atkinson for austenitic nitriding[35,56].

Bello et al[19] also claim to have detected hydrogen cyanide levels of up to 0.08^{v}/o with 12^{v}/o ammonia additions at 850^{o}C. They proposed directly relating the HCN level to carbon and nitrogen potentials because of the decomposition reaction

$$HCN \rightleftharpoons \tfrac{1}{2}H_2 + C_{(\text{in Fe})} + N_{(\text{in Fe})} \qquad (28)$$

but have not pursued the concept because of the lack of a suitably rapid analysis method for HCN. They have employed a standard wet chemistry titration with silver nitrate on gas samples absorbed in KOH[22].

Slycke[20] has investigated this possibility and claims to have detected HCN by chromatography. The height of the HCN chromatogram peak has been directly related to the ammonia addition to the furnace. The actual HCN levels in the gas atmosphere have been determined on dissolved gas samples using a specific ion electrode[57], and then nitrogen content in carbonitrided foils directly related to HCN content, see fig.14. Using existing thermodynamic data, the nitrogen activity of HCN in the gas atmosphere has been calculated, and experimental points show some deviation from the theory at high nitrogen activities, see fig.15.

2.8.4. The Decomposition of Ammonia in Carbonitriding Atmospheres.

Ammonia is known to thermally decompose rapidly at the

temperatures involved in carbonitriding furnaces and the material of the furnace chamber is also known to have some effect[35]. Recent Japanese work[58] has studied this latter effect in detail in a range of materials likely to be used in carbonitriding furnaces, these results are shown in fig.16; 18/8 stainless steel having the greatest catalytic effect and alumina the least.

This behaviour was then examined from the viewpoint of activation energy of decomposition of ammonia, as calculated from the measured decomposition rates in contact with the various materials. A direct relationship to the standard heat of formation of the relevant oxides of the materials was found, shown in fig. 17.

The most significant contribution from this work was the experimental detection of different rates of ammonia decomposition at different points between the furnace wall and the specimen. This could then be correlated to their previous data on effect of furnace materials; the furnace wall was a Ni-Cr heat resisting steel tube with an iron specimen in the centre. It therefore follows that significant variations in surface nitrogen and case depth can occur depending on the specimens position in the furnace. Further data then showed that the critical gas flow required to give uniform dissociation increased in proportion to the ammonia content of the atmosphere and the minimum flow rate required to cover conventional carbonitriding was 110cc/cm^2min. The inference therefore is that very high flow rates or rates of forced circulation should be used in commercial furnaces to give uniformity of treatment.

2.8.5. The Measurement and Control of Ammonia in Carbo-nitriding Atmospheres.

Until very recently determination of ammonia content in gas atmospheres has only been possible by the dissociation pipette. This method relies on the great affinity of ammonia for water; the amount of ammonia present being determined by reduction in volume of a known gas sample which is subsequently exposed to contact with water. The method is reasonably reliable but not particularly convenient.

Chatterjee-Fischer[59] has attempted to control the nitrogen potential by using the hot-wire resistivity technique (see section 2.3.2.6). As both carbon and nitrogen in solid solution in austenite increase its resistivity, then their individual effects cannot be separated and only a combined interstitial content can be measured. This difficulty was eliminated by monitoring the carbon potential separately on an infra-red analyser, and the nitriding potential derived by difference. The method in itself is practical, once properly calibrated, but a major problem occurs in the decarbonitriding of the measuring wire prior to each treatment cycle. A nitrogen/hydrogen gas mixture can be used, but the decarbonitriding cycle proceeds much more slowly than the decarburising cycle, this would also imply an insensitivity in response to sudden changes in the gas atmosphere. In investigating this technique on a drip feed carbonitiriding furnace with Microcarb control[17], it was discovered that element life was much shorter in carbo-nitriding than plain carburising; possibly due to the method of decarbonitriding the wire which employed an air stream rather than a nitrogen/hydrogen mixture.

Direct monitoring and controlling of ammonia in thermo-chemical treatment atmospheres has been made by Kolozsvary [60]. An alphameter (α being the symbol normally designating degree of dissociation) was constructed on a conductivity principle, which would allow determination of degree of dissociation of ammonia in pure ammonia or the partial pressure of ammonia in a gas mixture. The hydrolysis of ammonia in a constant gas volume is monitored by the conductivity cell, and the result displayed on a suitable chart recorder or meter. The instrument can also be used to maintain a constant ammonia level in the exhaust by control of the input gases. Reproducibility of better than 2% is claimed and the instrument has been used on both laboratory and industrial furnaces with what appears to be good success. The results obtained are not directly relevant to normal gas carbonitriding processes, as Kolozsvary et al have been investigating a nitrocarburising treatment in the temperature region of 600-650°C. However the principle of the instrument is independent of the temperature of furnace operation.

A data curve is presented in the paper showing the effect of temperature of the dissociation of ammonia indicating that dissociation is virtually complete at temperatures 700°C. What is not indicated however is the limit of detectability of ammonia, which would be an important consideration in the application of such an instrument to gas carbonitriding, where residual ammonia levels are likely to be very low. However conductivity measurments are normally very sensitive, and no doubt suitable modifications

if necessary can be made to adapt the instrument to gas carbonitriding

Simultaneously with development of the alphameter the Heat Treatment Research Group (HTRG) at Liverpool University were investigating possibilities of using infra-red meters to detect ammonia. Enquiries to companies making infra-red equipment revealed that no such equipment was available for ammonia, consequently HTRG co-operated with The Analytical Development Company in constructing a direct reading infra-red ammonia meter. At the time of the development, HTRG was involved in research in ferritic nitiriding and the instrument was shown to be capable of accurately monitoring ammonia levels normally used in nitriding, culminating in the development of a new nitriding process for eliminating 'white layer'[61]. The meter - fig.18 - has a 0-100^{v}/o Ammonia range, with a facility added since its original development of a 0-10^{v}/o range. Continuous recording or monitoring of ammonia is possible and, as in common with most infra-red meters, it is possible to switch inputs from different sources into the meter. Reproducibility is better than 2% of full scale on 0-100^{v}/o range, with limit of detection of 1^{v}/o ammonia. However, water vapour must be eliminated from the gas sample by a suitable trap as interference with the ammonia infra-red spectrum can be observed.

2.8.6. Physical Metallurgical Aspects of Carbonitriding.

Much of the physical metallurgy aspects of carbonitriding has been concerned with the improved hardenability of the case due to the presence of nitrogen[62]. Holm[40] has studied the surface hardenability of a carbonitrided low alloy steel

over a wide range of carbon and nitrogen contents - 0.12 to $1.10^{W}/oC$ and 0 to $0.75^{W}/oN$. It was concluded that carbon increased hardenability more than nitrogen, and hardenability drops off at total interstitial levels of $> 1.5^{W}/o$. However hardenability for carburised only specimens dropped off at carbon levels above $1.0^{W}/oC$, so there is obviously some effect due to nitrogen. Several anomalies did occur however, and also the highest hardenabilities occurred in specimens containing $0.89^{W}/oC + 0.65^{W}/oN$ and $0.88^{W}/oC + 0.69^{W}/oN$.

Lallemant[63] has studied hardenability of carbonitrided steels and shown a beneficial effect due to nitrogen. Also in this work it was shown that the structural anomalies of surface soft spots was due to a lack of surface hardenability due to removal of nitrogen from solid solution in austenite by chromium to form a carbonitride compound. This may explain some of Holm's anomalies[40] as his steel contained 0.18w/oCr.

Guimier[64] also points out that structural anomalies and lack of hardenability occasionally occur in carbonitrided cases, as well as confirming the improved hardenability due to presence of nitrogen in the case.

Several authors[40,64] have made reference to implied improvement of diffusivity of carbon due to presence of nitrogen but no data has been presented.

Guimier[64] also refers to the improved temper resistance of carbonitrided cases over carburised cases, see fig.19.

A problem which has often been raised with regard to high nitrogen levels in iron is that of void formation. Prenosil[65] points out that nitrogen levels greater than 0.6^{w}/o could lead to void formation due to the thermodynamic instability of high levels of nitrogen in solid solution in equilibrium with nitrogen at atmosphere pressure[16]. This type of situation arises in the very high levels of nitrogen associated with $Fe_{2-3}(CN)$ type compound layers in ferritic intro-carburising[66]. Holm[40] has also reported voids in carbonitrided steels with nitrogen levels $>$ 0.5^{w}/o. This problem of void formation has had little attention from the physical metallurgical viewpoint, and needs further consideration especially in view of the apparent benefits of raising the nitrogen levels of the case.

2.9 Conclusions.

In examing the field of austenitic thermochemical treatments, austenitic carbonitriding is one treatment which appears to be in need of further investigation, both from the physical metallurgy viewpoint and from the process control viewpoint. Whilst austenitic nitriding has shown very promising results on a laboratory scale[1], it needs to be further explored in order to translate it to an industrial process.

Similarities in the two processes (a) in their diffusion of nitrogen into steel surfaces and (b) in potential benefits of increasing the nitrogen contents of surface hardened cases, warrant further investigation into the problems of controlling the nitrogen potential of atmospheres and more precise knowledge of the physical metallurgical behaviour of Fe-N and Fe-C-N alloys.

TABLE 1. - CLASSIFICATION OF THERMOCHEMICAL TREATMENTS

DIFFUSIONAL ADDITIONS OF NON METALS TO STEEL SURFACES.

FERRITIC

NITRIDING - addition of nitrogen from gaseous or liquid medium in temperature range 490-530°C.

NITROCARBURISING - addition of nitrogen and carbon from gaseous or liquid medium in temperature range 565-575°C

ION NITRIDING - addition of nitrogen from a glow discharge under sub-atmospheric pressure. Temperatures are variable through the specimen thickness.

AUSTENITIC

CARBURISING - addition of carbon from solid, liquid or gaseous medium in temperature range 800-950°C

CARBONITRIDING - addition of carbon and nitrogen from liquid or gaseous medium in temperature range 720-900°C

VACUUM CARBURISING - addition of carbon from gaseous medium at sub atmospheric pressure in temperature range 1000 - 1150°C.

ION CARBURISING AND CARBONITRIDING - addition of carbon and carbon and nitrogen from glow discharge at sub-atmospheric pressure. Temperatures are variable through the specimen thickness.

NITRIDING - addition of nitrogen from gaseous medium in the temperature range 590 - 900°C

TABLE 2.

METHODS OF MONITORING GAS CARBURISING ATMOSPHERES.

	METHOD	MEASURES.
(1)	Dew Point Meter	Atmosphere moisture content.
(2)	Infra-Red Gas Analysis	Principally CO_2, but also CO, H_2O, CH_4.
(3)	Orsat Gas Analysis	CO_2, CO, O_2, CH_4, C_2H_6
(4)	Gas Chromatography.	Virtually all gases present.
(5)	Shim Stock.	Actual carbon content of a suitable test piece.
(6)	Hot Wire (Resistivity)	Actual carbon content of a fine wire.
(7)	Oxygen Probe	Oxygen partial pressure.

FIG. 1

RELATIONSHIP BETWEEN OXYGEN POTENTIAL AND CARBON POTENTIAL AT VARIOUS TEMPERATURES FOR 'ENDO' GAS PREPARED FROM PROPANE AND CONTAINING 31% (H_2 + H_2O) AND 23% (CO + CO_2)[12]

FIG. 2

SOLUBILITY OF NITROGEN IN IRON IN EQUILIBRIUM WITH NITROGEN GAS AT 1 ATMOSPHERE.[16]

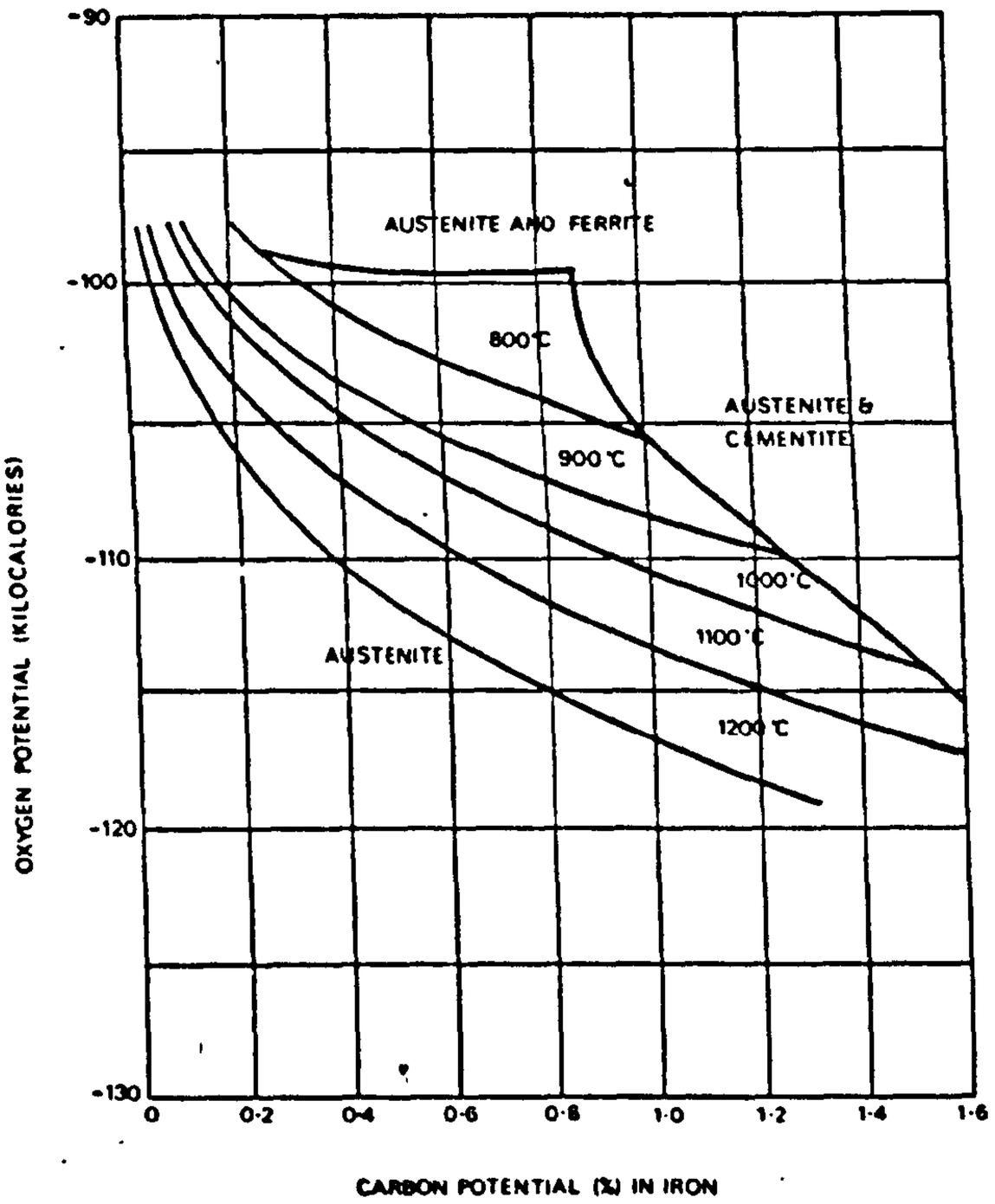
-90
-100
-110
-120
-130
AUSTENITE AND FERRITE
800°C
900°C
AUSTENITE &
CEMENTITE
1000°C
1100°C
AUSTENITE
1200°C
0
0·2
0·4
0·6
0·8
1·0
1·2
1·4
1·6
OXYGEN POTENTIAL (KILOCALORIES)
CARBON POTENTIAL (%) IN IRON

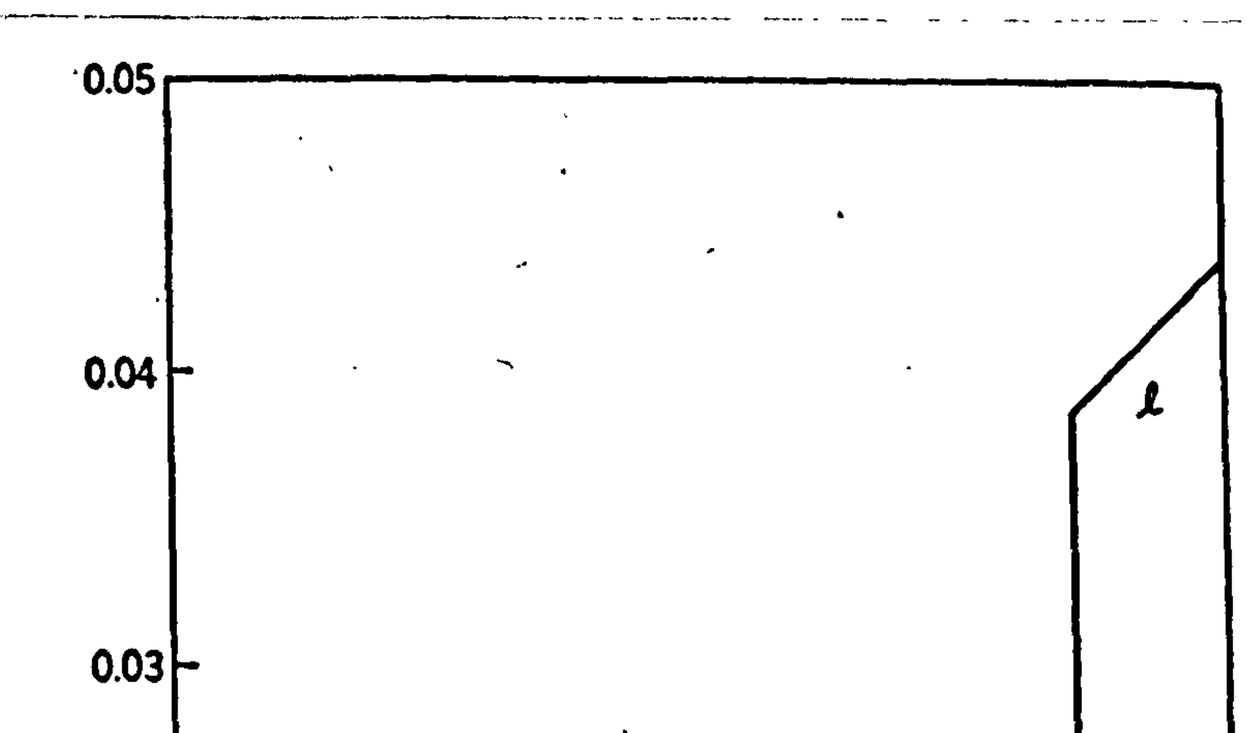
0.05
0.04
0.03
0.02
0.01
0
Wt % N
γ
l
δ
α
0
500
1000
1500
Degrees C

FIG. 3

TYPICAL PRODUCTION CYCLE FOR CARBURISING AT SUB-ATMOSPHERIC PRESSURES IN COLD-WALL VACUUM FURNACE(25)

FIG. 4

THE VARIATION OF THE HARDNESS OF Fe-N AND Fe-C MARTENSITES WITH INTERSTITIAL CONTENT(1)

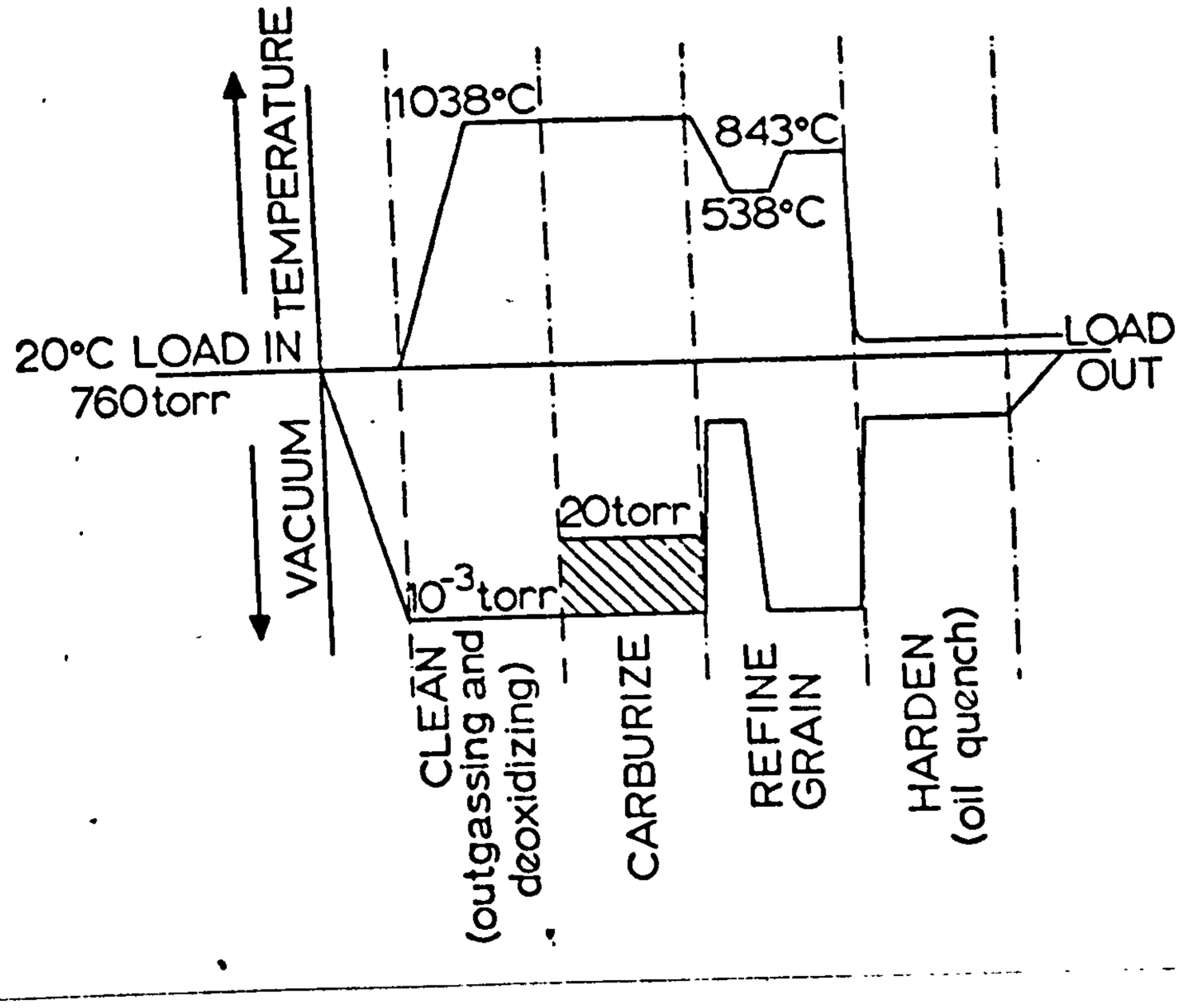
TEMPERATURE
VACUUM
20°C LOAD IN
760torr
1038°C
843°C
538°C
LOAD OUT
10^{-3} torr
20torr
CLEAN (outgassing and deoxidizing)
CARBURIZE
REFINE GRAIN
HARDEN (oil quench)

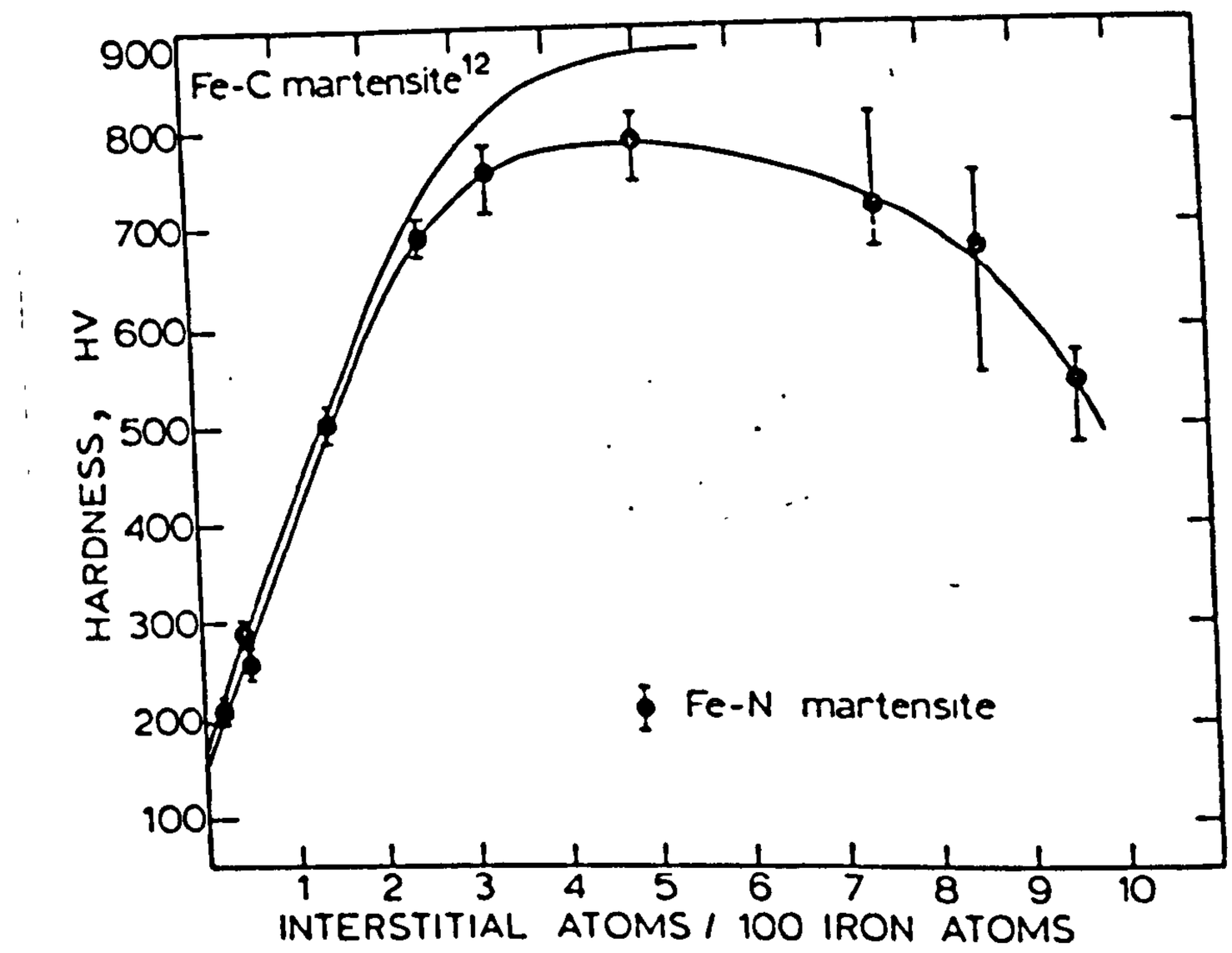
Fe-C martensite[12]
HARDNESS, HV
900
800
700
600
500
400
300
200
100
Fe-N martensite
1 2 3 4 5 6 7 8 9 10
INTERSTITIAL ATOMS / 100 IRON ATOMS

FIG. 5

VARIATION OF THE M_S TEMPERATURE WITH INTERSTITIAL CONTENT FOR Fe-N AND Fe-C ALLOYS.(1)

FIG. 6

THE HARDNESS OF THREE QUENCHED Fe-N ALLOYS AFTER TEMPERING FOR 30 MIN. AT THE TEMPERATURES INDICATED.(1)

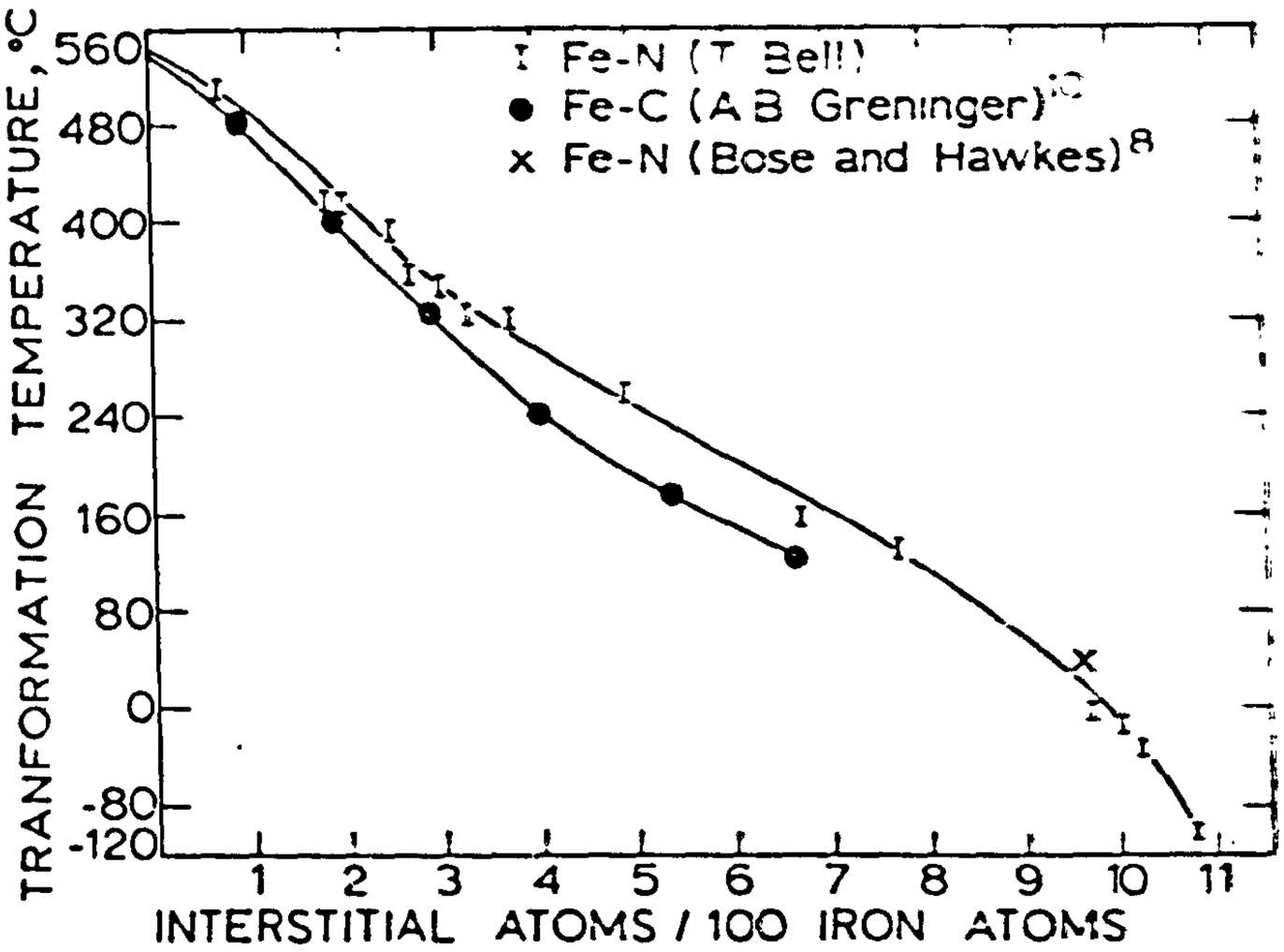
I Fe-N (T Bell)
● Fe-C (A B Greninger)[10]
x Fe-N (Bose and Hawkes)[8]
TRANFORMATION TEMPERATURE, °C
560
480
400
320
240
160
80
0
-80
-120
1 2 3 4 5 6 7 8 9 10 11
INTERSTITIAL ATOMS / 100 IRON ATOMS

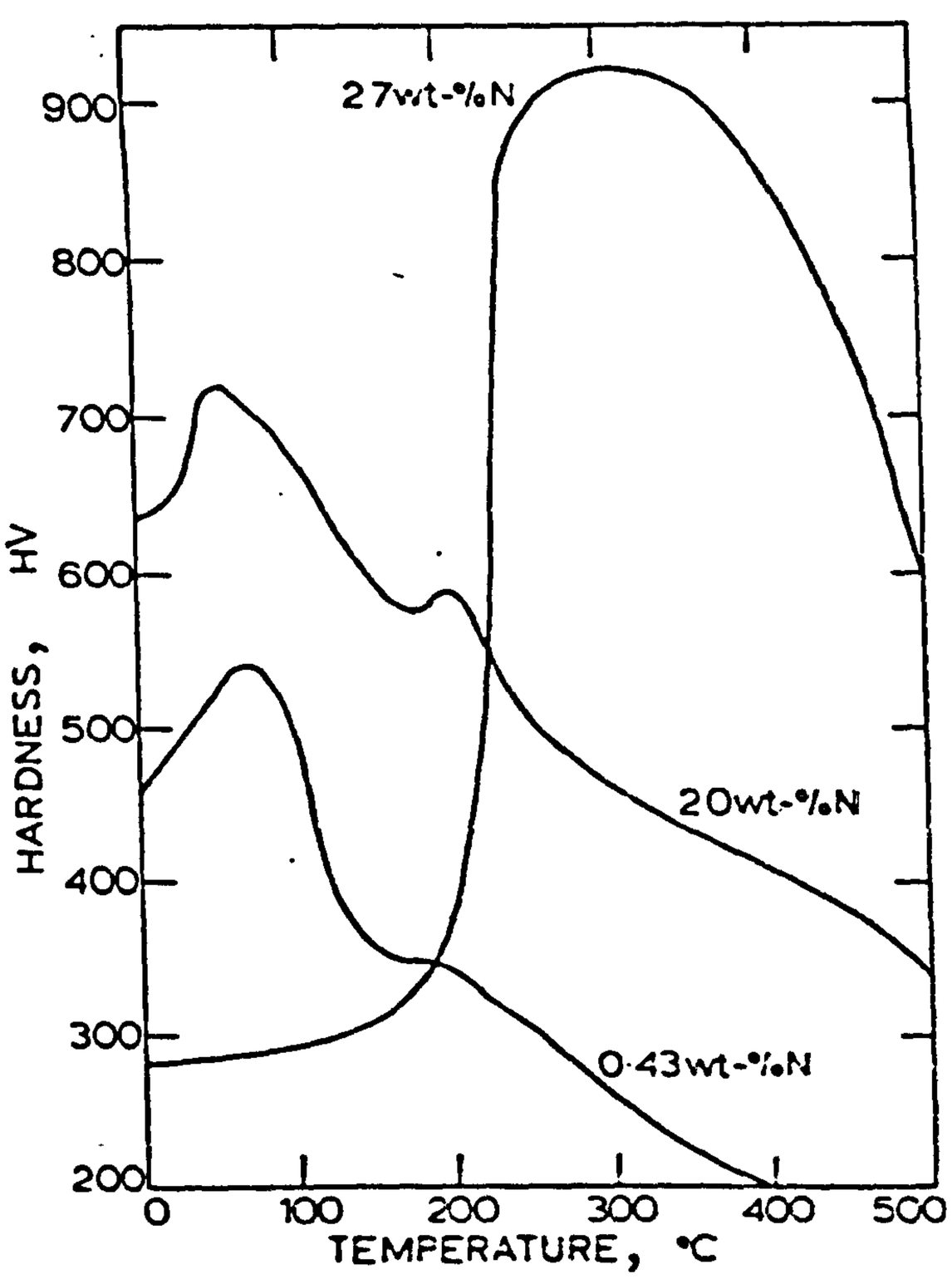
27wt-%N
20wt-%N
0·43wt-%N
HARDNESS, HV
900
800
700
600
500
400
300
200
0 100 200 300 400 500
TEMPERATURE, °C

FIG. 7

VARIATION IN N-POTENTIAL AS A FUNCTION OF NITROGEN CONCENTRATION(1)(35)

FIG.8

IRON - NITROGEN PHASE DIAGRAM(16)

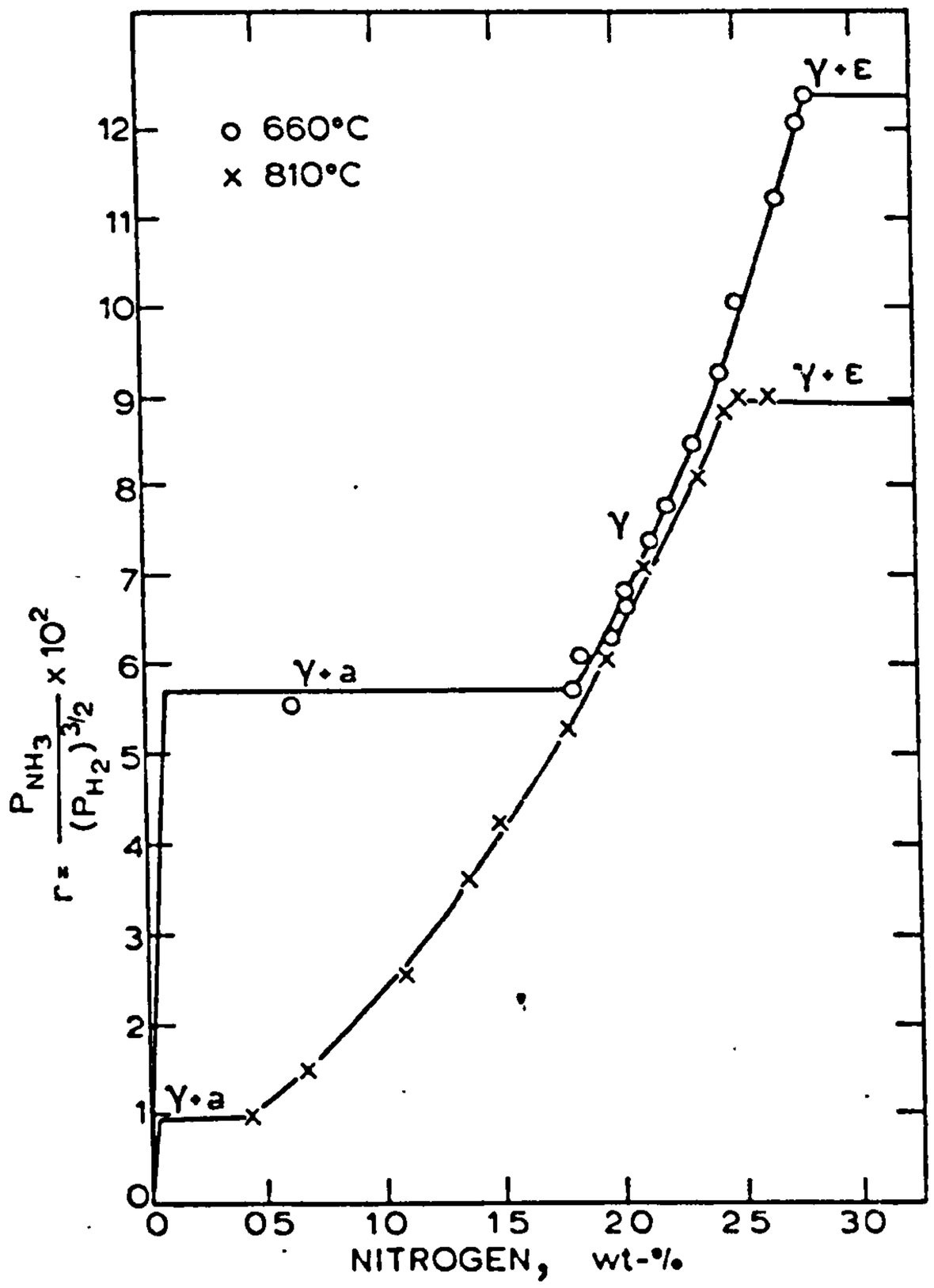
o 660°C
x 810°C
γ + ε
γ + ε
γ
γ + a
γ + a
$r = \frac{P_{NH_3}}{(P_{H_2})^{3/2}} \times 10^2$
0
1
2
3
4
5
6
7
8
9
10
11
12
0
05
10
15
20
25
30
NITROGEN, wt-%

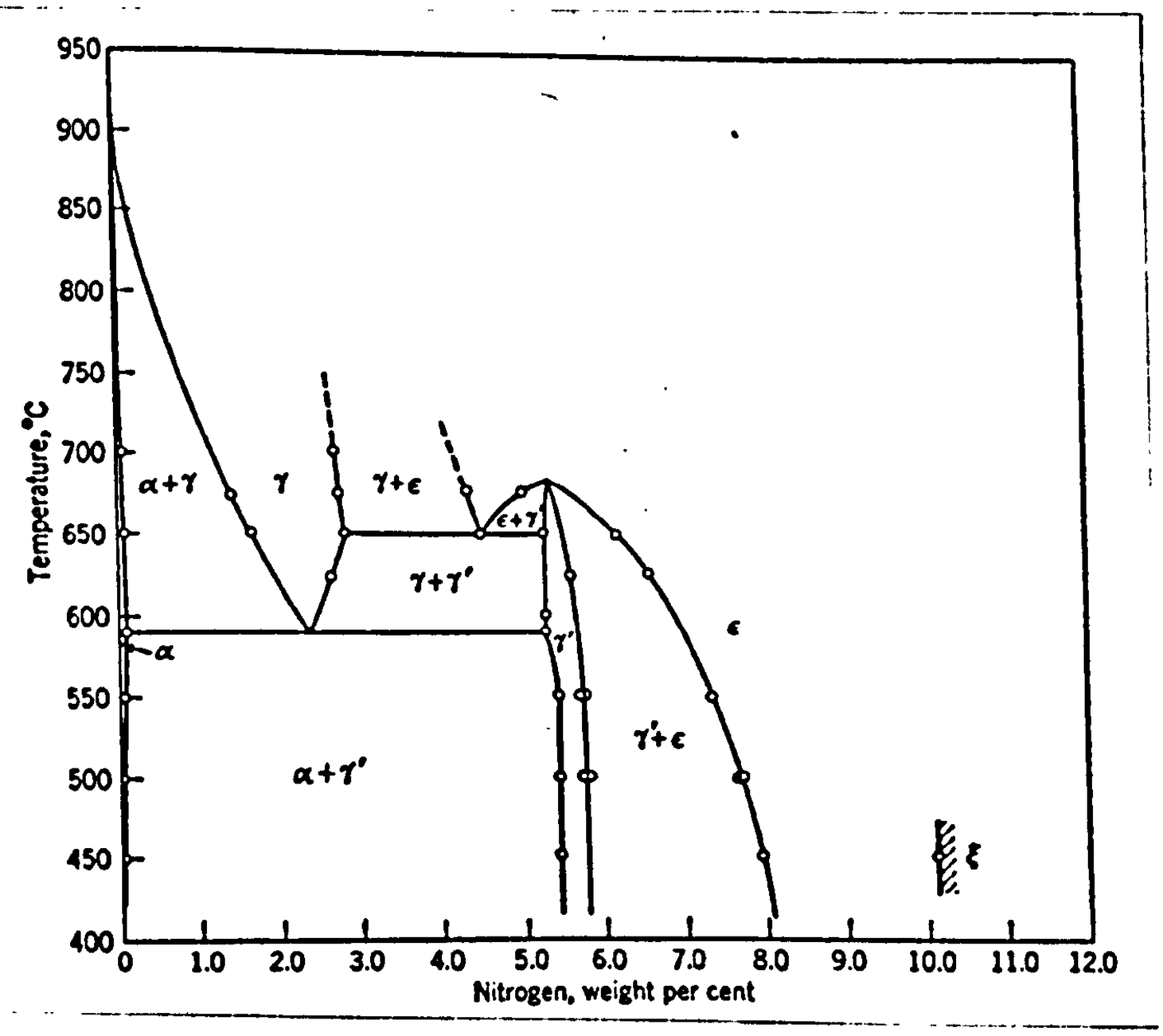
Temperature, °C
950
900
850
800
750
700
650
600
550
500
450
400
α+γ
γ
γ+ε
ε+γ'
γ+γ'
α
γ'
α+γ'
γ'+ε
ε
0
1.0
2.0
3.0
4.0
5.0
6.0
7.0
8.0
9.0
10.0
11.0
12.0
Nitrogen, weight per cent

FIG. 9

IRON - CARBON PHASE DIAGRAM.(37)

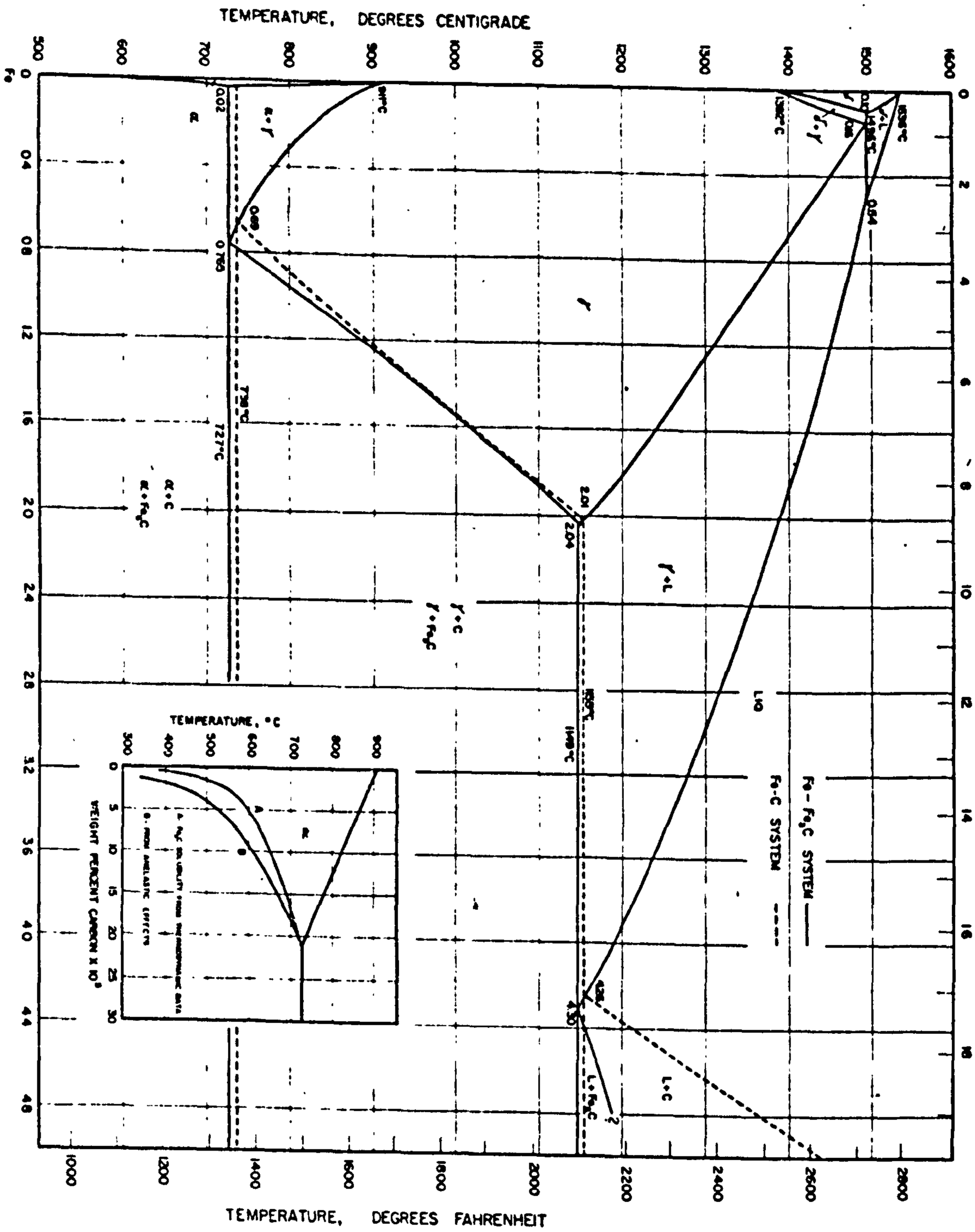
TEMPERATURE, DEGREES CENTIGRADE
ATOMIC PERCENT CARBON
WEIGHT PERCENT CARBON
Fe-Fe3C SYSTEM
Fe-C SYSTEM
TEMPERATURE, °C
WEIGHT PERCENT CARBON X 10³
TEMPERATURE, DEGREES FAHRENHEIT

FIG. 10

RELATIONSHIP BETWEEN CARBON CONTENT IN THIN SHEET AND CARBON DIOXIDE CONTENT IN 'ENDO' GAS DERIVED FROM PROPANE, WITH AND WITHOUT AMMONIA ADDITION.(19)

FIG. 11

CALCULATED RELATIONSHIP BETWEEN THE CARBON POTENTIAL AND CARBON DIOXIDE CONTENT IN 'ENDO' GAS DERIVED FROM PROPANE WITH AND WITHOUT AMMONIA ADDITION.(20)

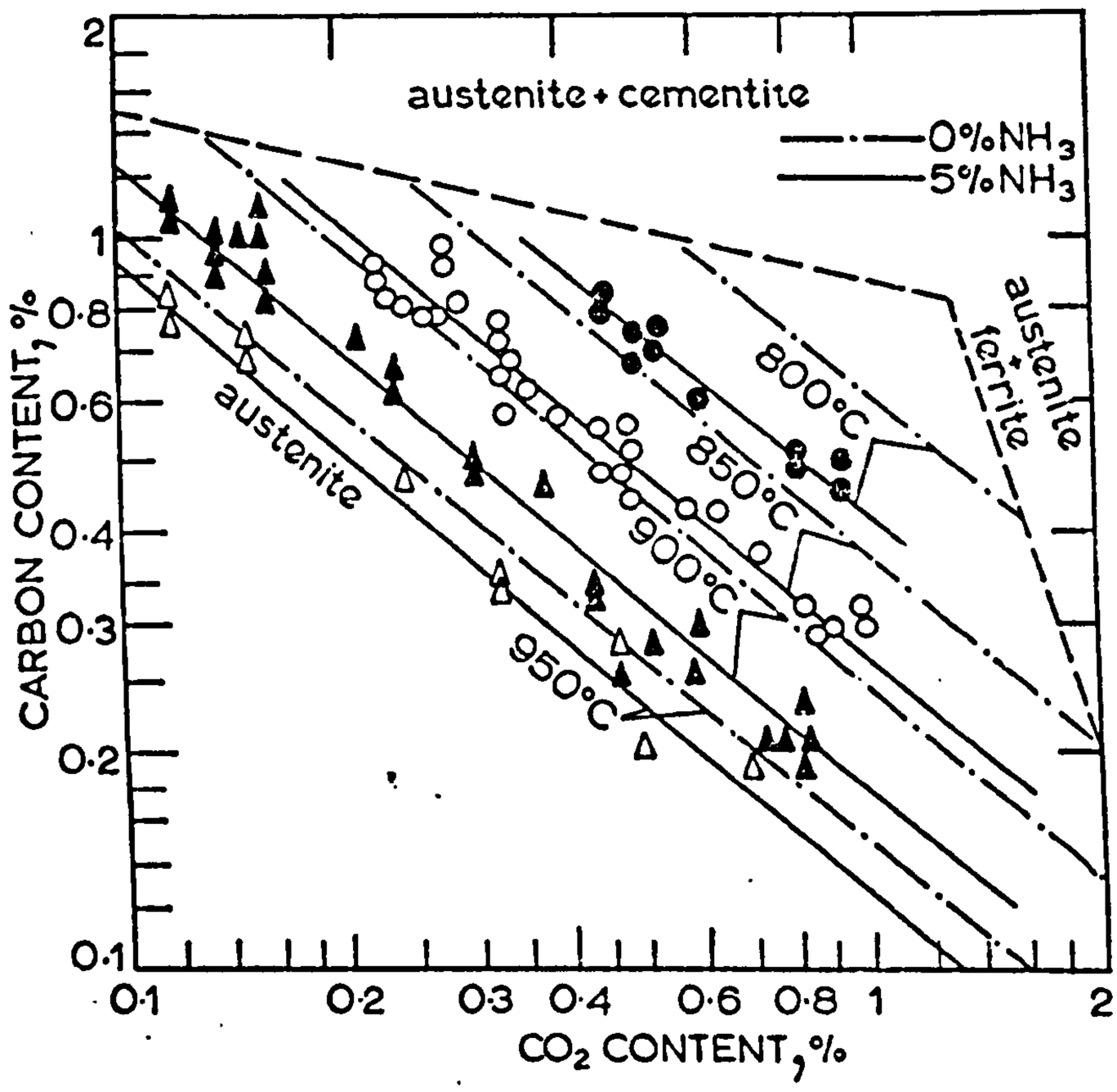
austenite + cementite
0% NH3
5% NH3
800°C
850°C
900°C
950°C
austenite
austenite + ferrite
CARBON CONTENT, %
CO2 CONTENT, %
2
1
0·8
0·6
0·4
0·3
0·2
0·1
0·1
0·2
0·3
0·4
0·6
0·8
1
2

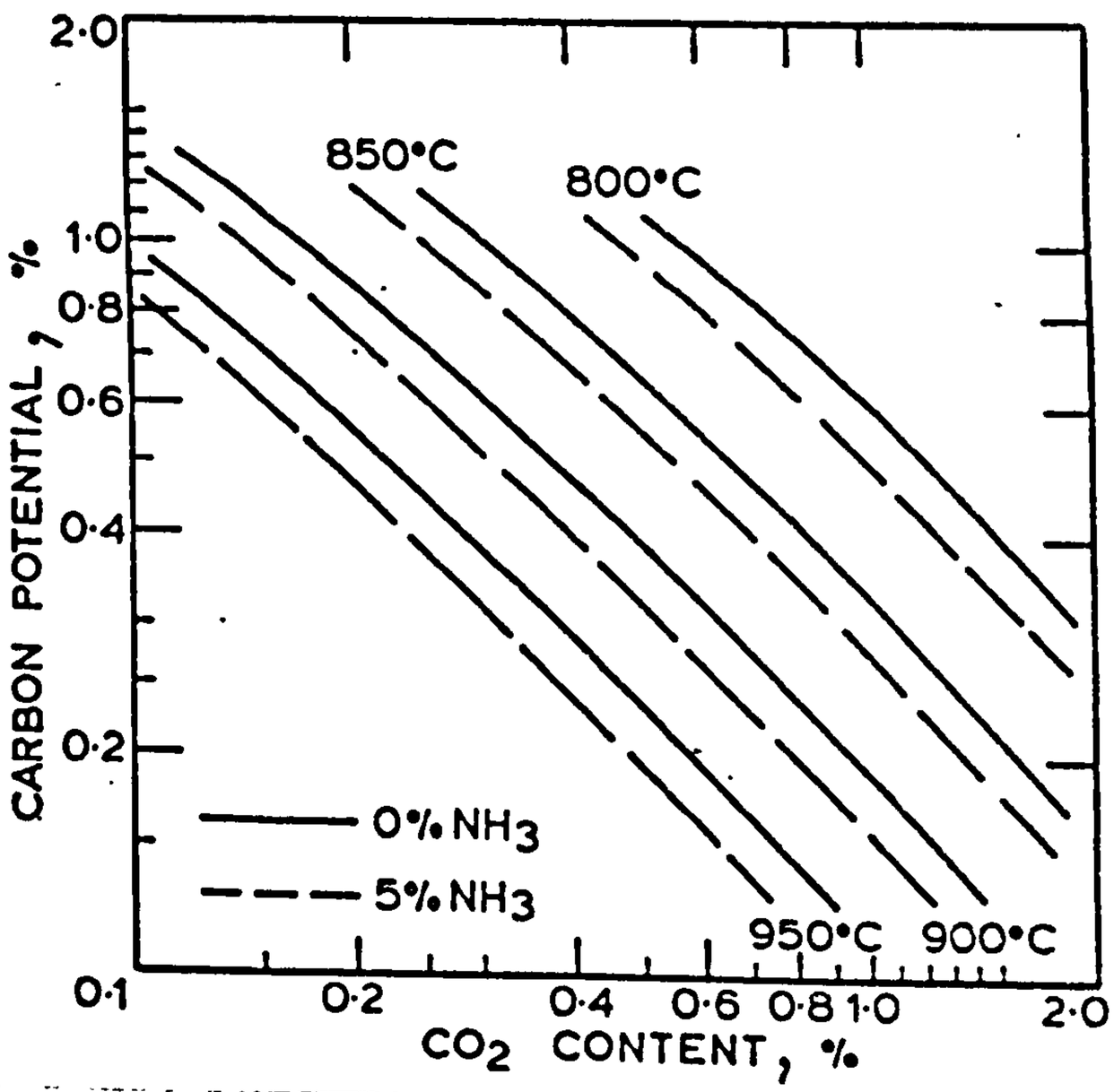
2·0
1·0
0·8
0·6
0·4
0·2
0·1
850°C
800°C
0% NH3
5% NH3
950°C
900°C
CARBON POTENTIAL, %
CO2 CONTENT, %
0·2
0·4
0·6
0·8
1·0
2·0

FIG. 12.

CALCULATED RELATIONSHIP BETWEEN CARBON DIOXIDE CONTENT AND ADDED AMMONIA WITH CARBON POTENTIAL AS PARAMETER; THE CARRIER GAS IS AN 'ENDO' GAS DERIVED FROM PROPANE. (20)

FIG. 13

N-POTENTIAL AS A FUNCTION OF AMMONIA ADDITION AT DIFFERENT TEMPERATURES (53)

FIG. 14

NITROGEN CONTENT OBTAINED IN FOILS CARBONITRIDED AT 870° AS A FUNCTION OF HYDROGEN CYANIDE CONTENT (20)

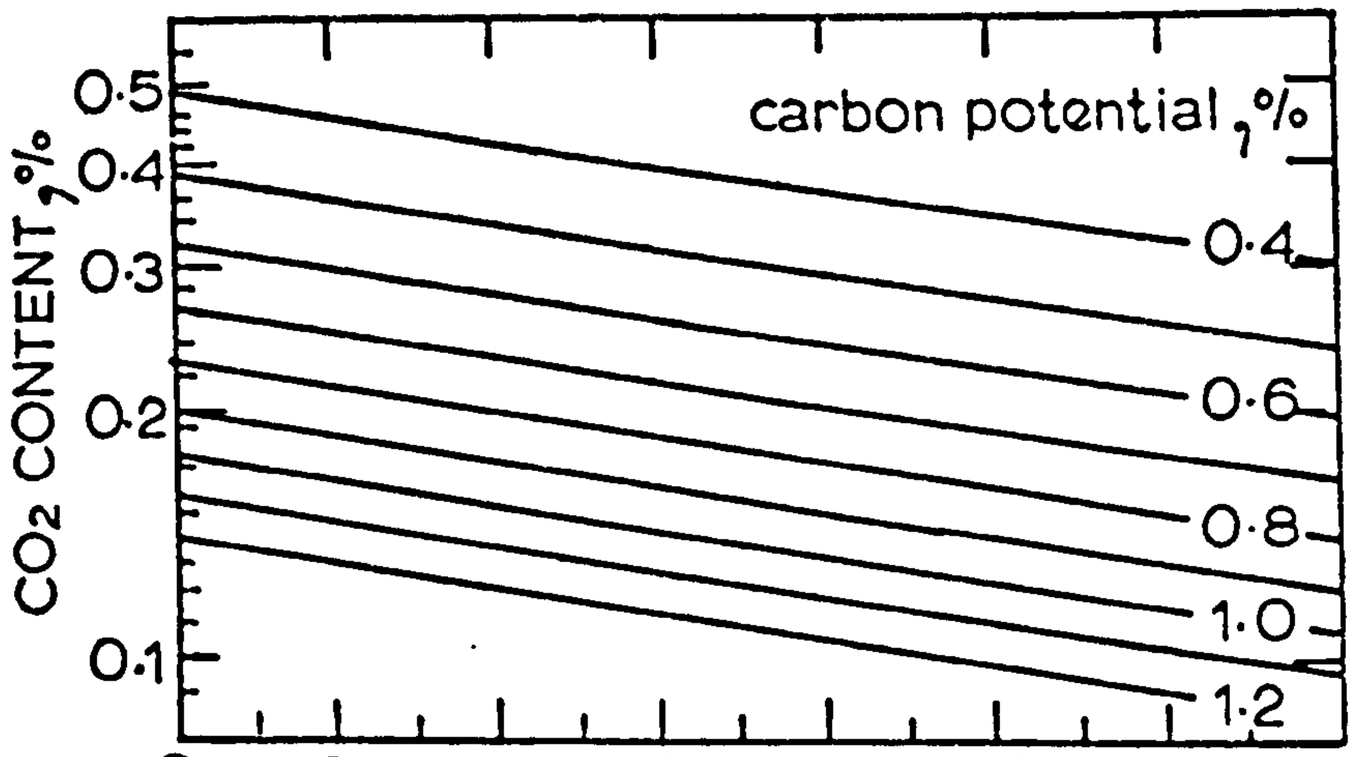

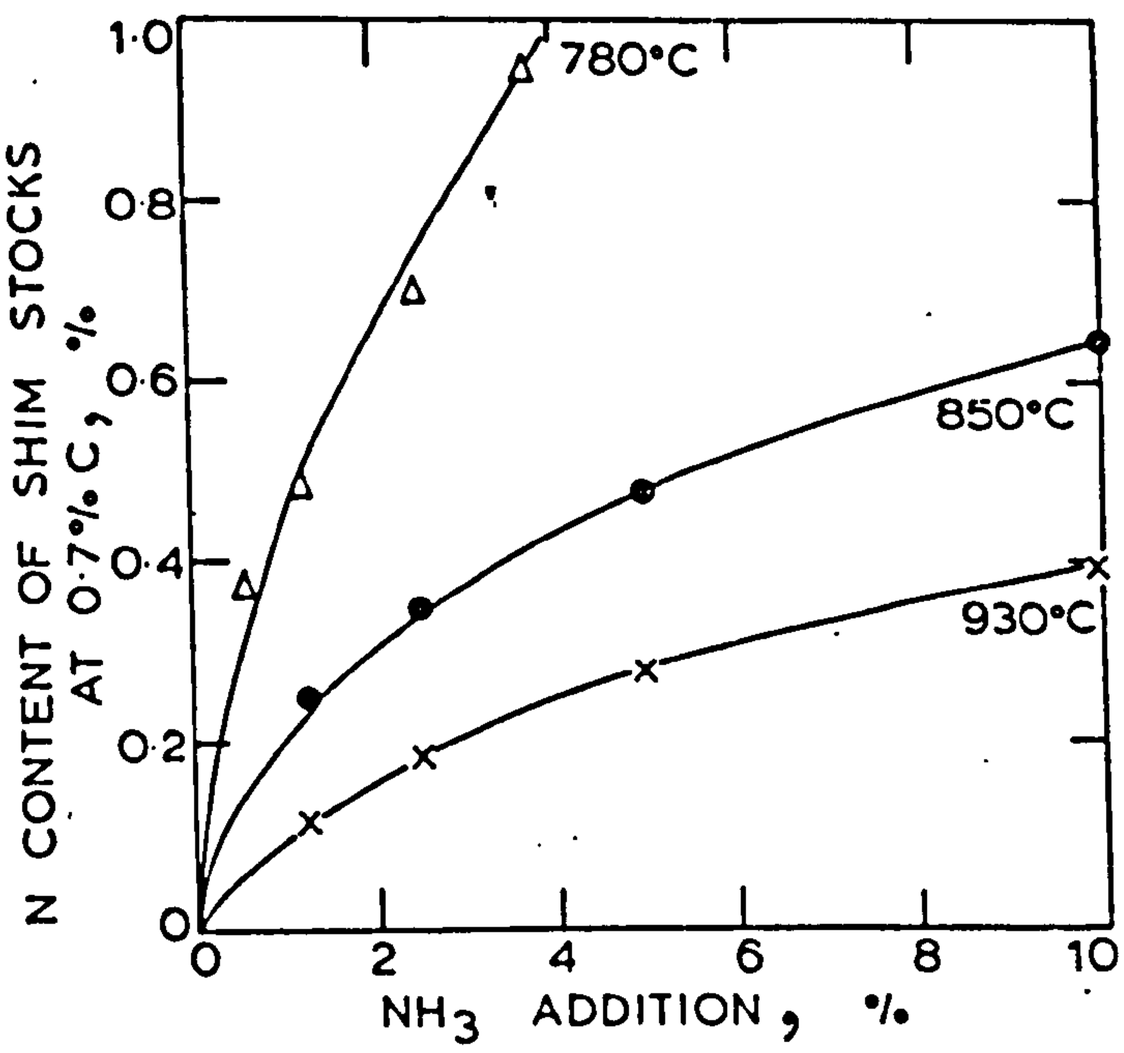

Shim stocks 0·7% C → slowly cooled

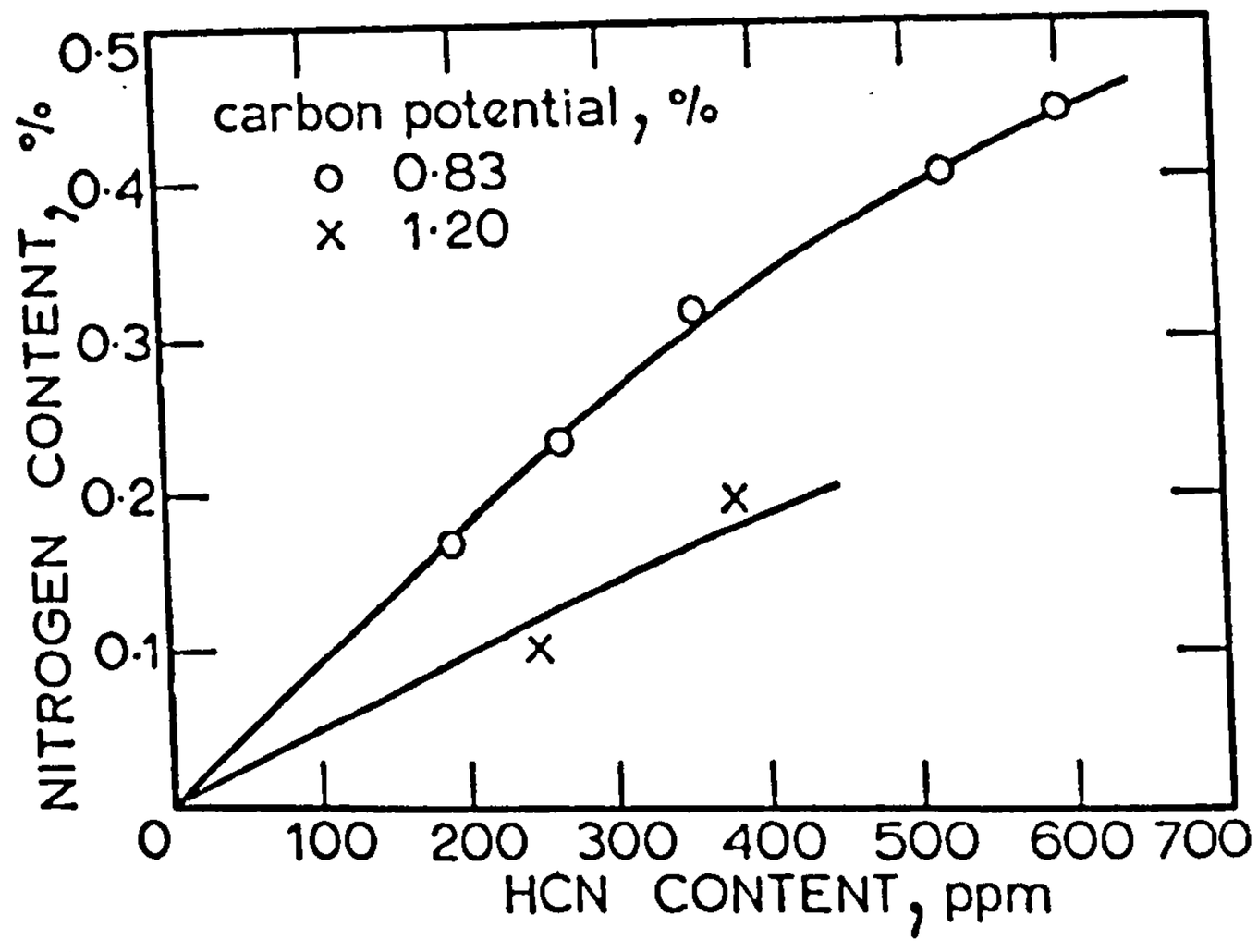

FIG. 15

NITROGEN ACTIVITY IN AUSTENITE IN EQUILIBRIUM WITH A CARBONITRIDING ATMOSPHERE AT 870°C AS A FUNCTION OF THE NITROGEN ACTIVITY OF HYDROGEN CYANIDE; STANDARD STATE NITROGEN GAS OF 1 ATMOSPHERE(20)

FIG. 16

EFFECT OF TEMPERATURE AND MATERIALS ON AMMONIA DECOMPOSITION IN CARBONITRIDING GAS.(58)

FIG. 17

RELATION BETWEEN ACTIVATION ENERGY FOR AMMONIA DECOMPOSITION AND STANDARD HEAT OF OXIDE FORMATION.

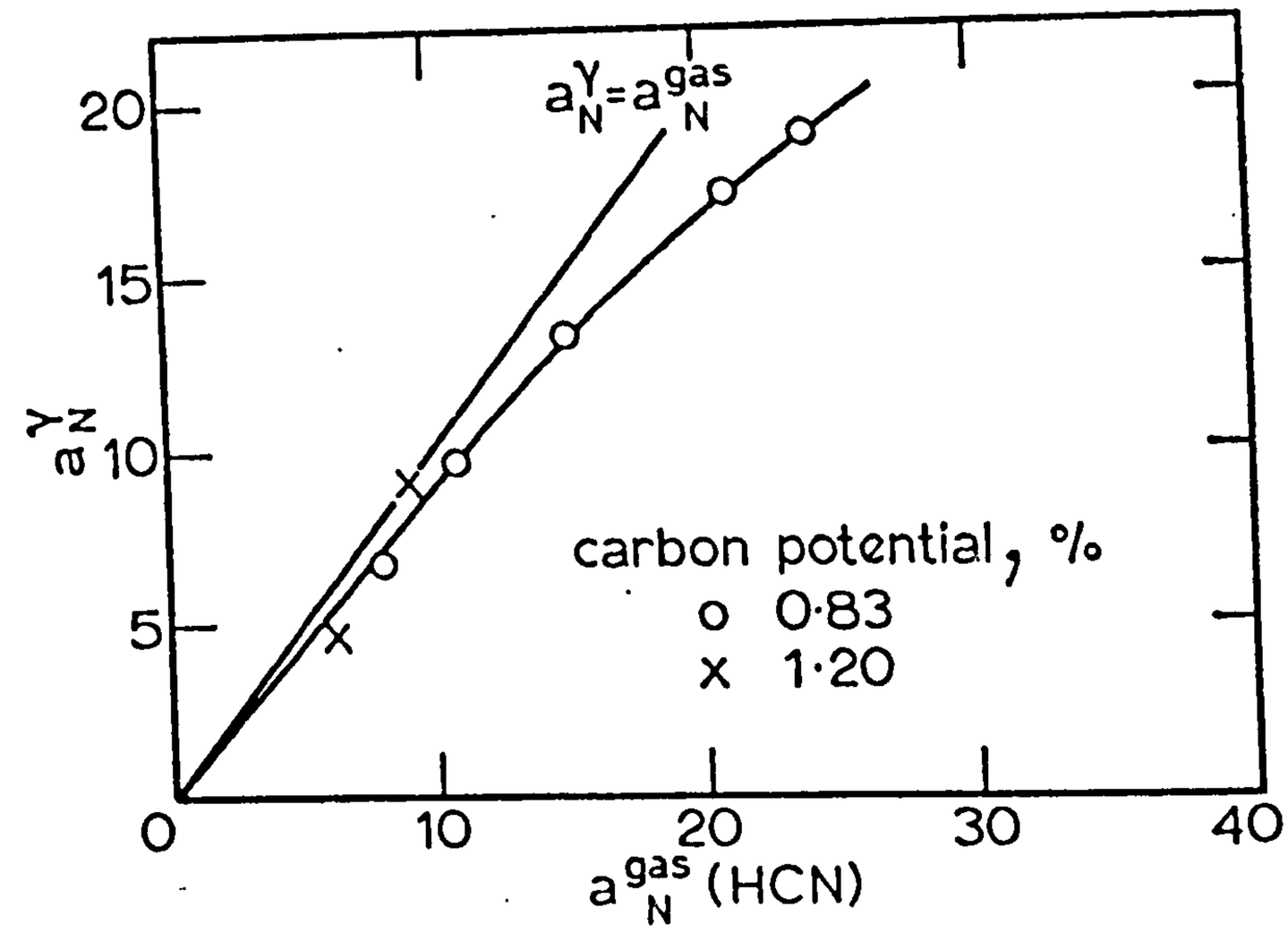
$a_N^{\gamma}=a_N^{gas}$
carbon potential, %
o 0·83
x 1·20
a_N^{γ}
a_N^{gas} (HCN)
0
10
20
30
40
5
15

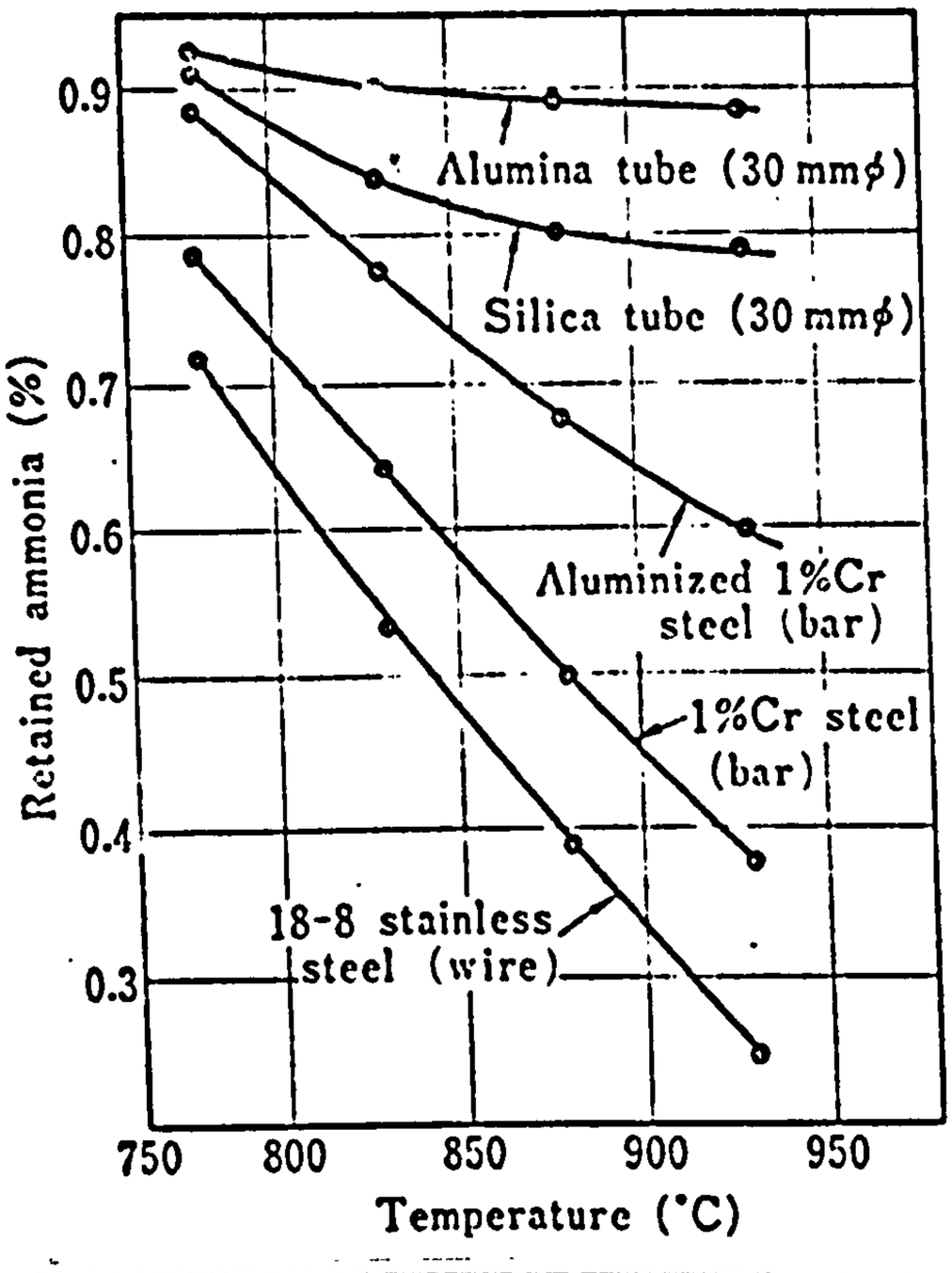
Alumina tube (30 mmφ)
Silica tube (30 mmφ)
Aluminized 1%Cr steel (bar)
1%Cr steel (bar)
18-8 stainless steel (wire)
Retained ammonia (%)
Temperature (°C)
0.9
0.8
0.7
0.6
0.5
0.4
0.3
750
800
850
900
950

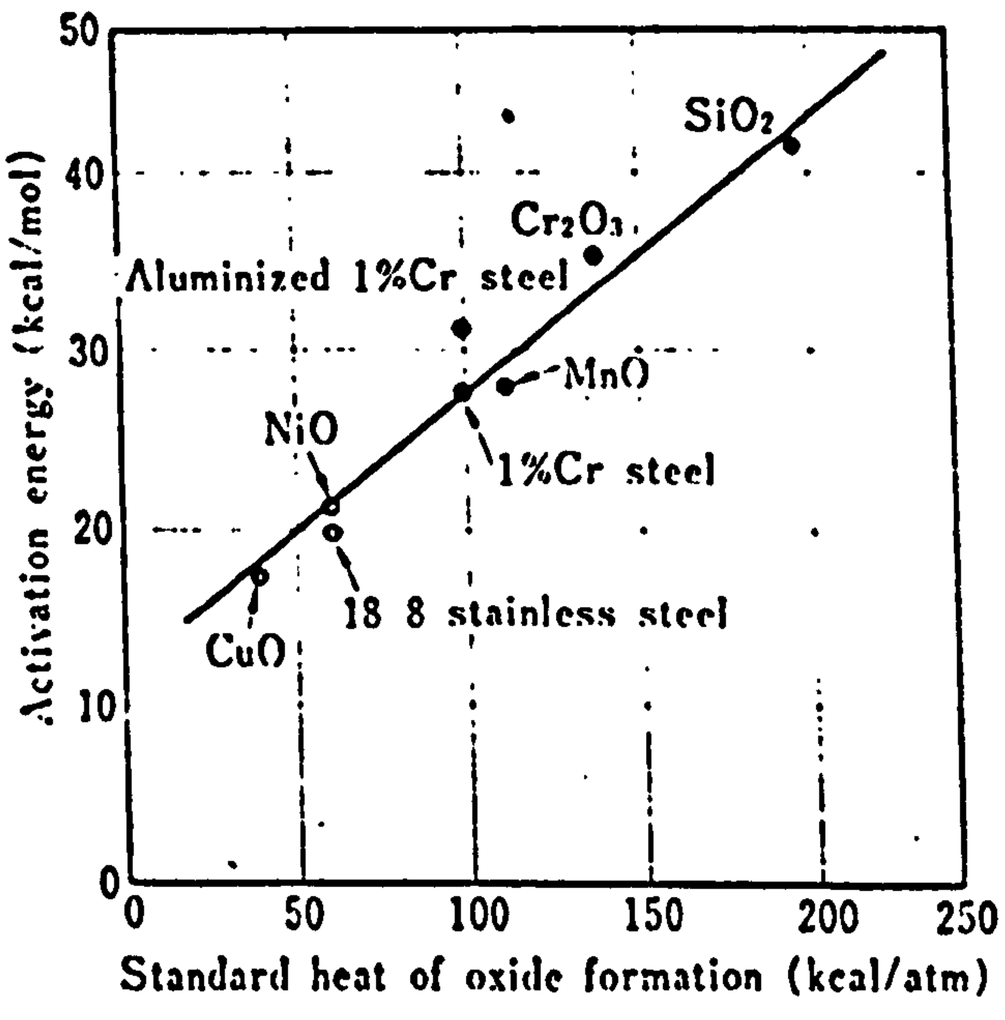
SiO_2
Cr_2O_3
Aluminized 1%Cr steel
MnO
NiO
1%Cr steel
18 8 stainless steel
CuO
Activation energy (kcal/mol)
Standard heat of oxide formation (kcal/atm)
50
40
30
20
10
0
0
50
100
150
200
250

FIG. 18

INFRA-RED GAS ANALYSER WITH DUAL RANGE

AMMONIA METER.

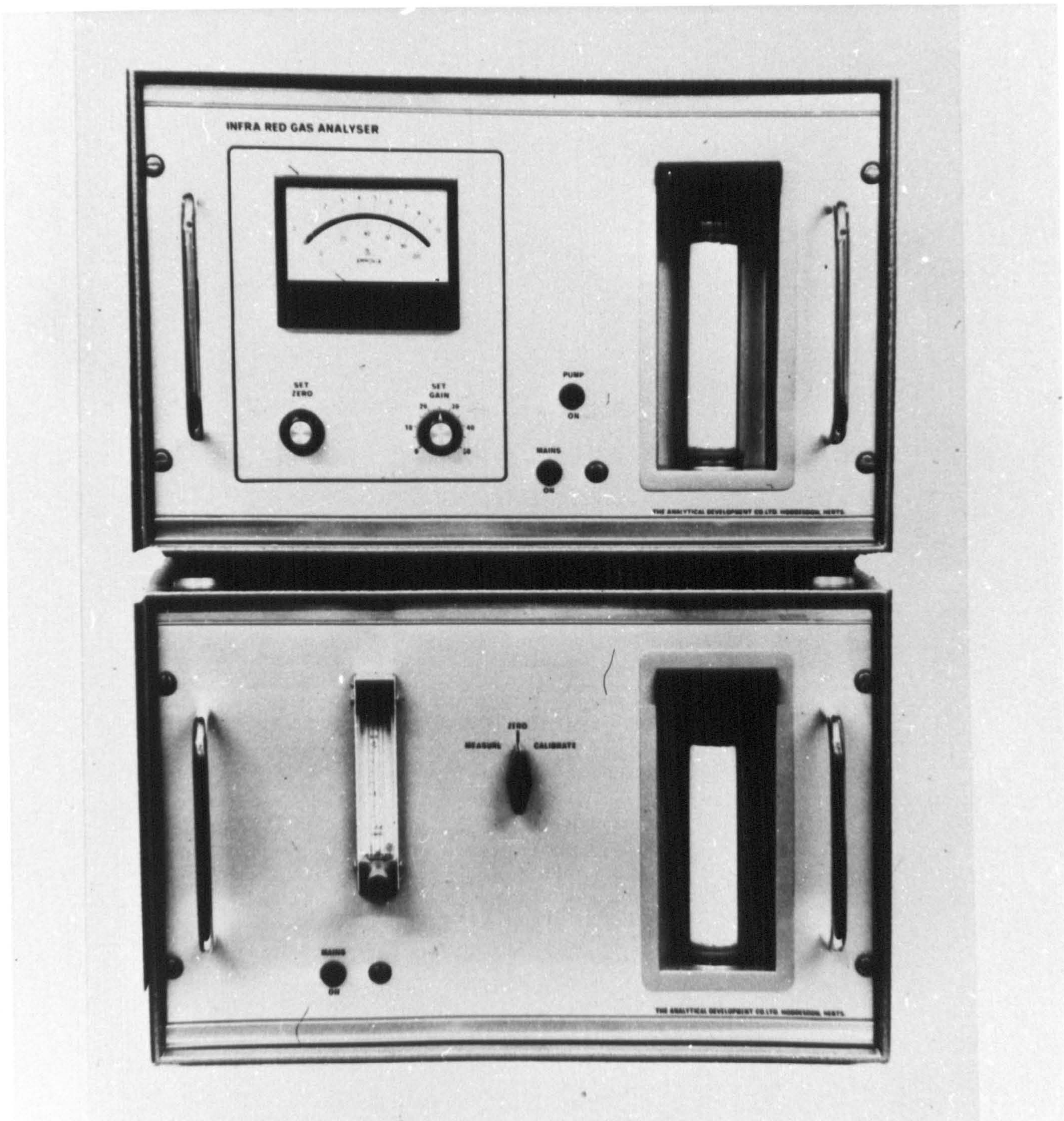
INFRA RED GAS ANALYSER
SET ZERO
SET GAIN
PUMP
ON
MAINS
ON
THE ANALYTICAL DEVELOPMENT CO LTD HODDESDON HERTS
ZERO
MEASURE
CALIBRATE
MAINS
ON
THE ANALYTICAL DEVELOPMENT CO LTD HODDESDON HERTS

FIG. 19

RESISTANCE TO TEMPER SOFTENING OF THE CASE FOR A Ni/Cr STEEL IN THE AS-CARBURISED AND AS-CARBONITRIDED STATE[64]

-16 NC6-

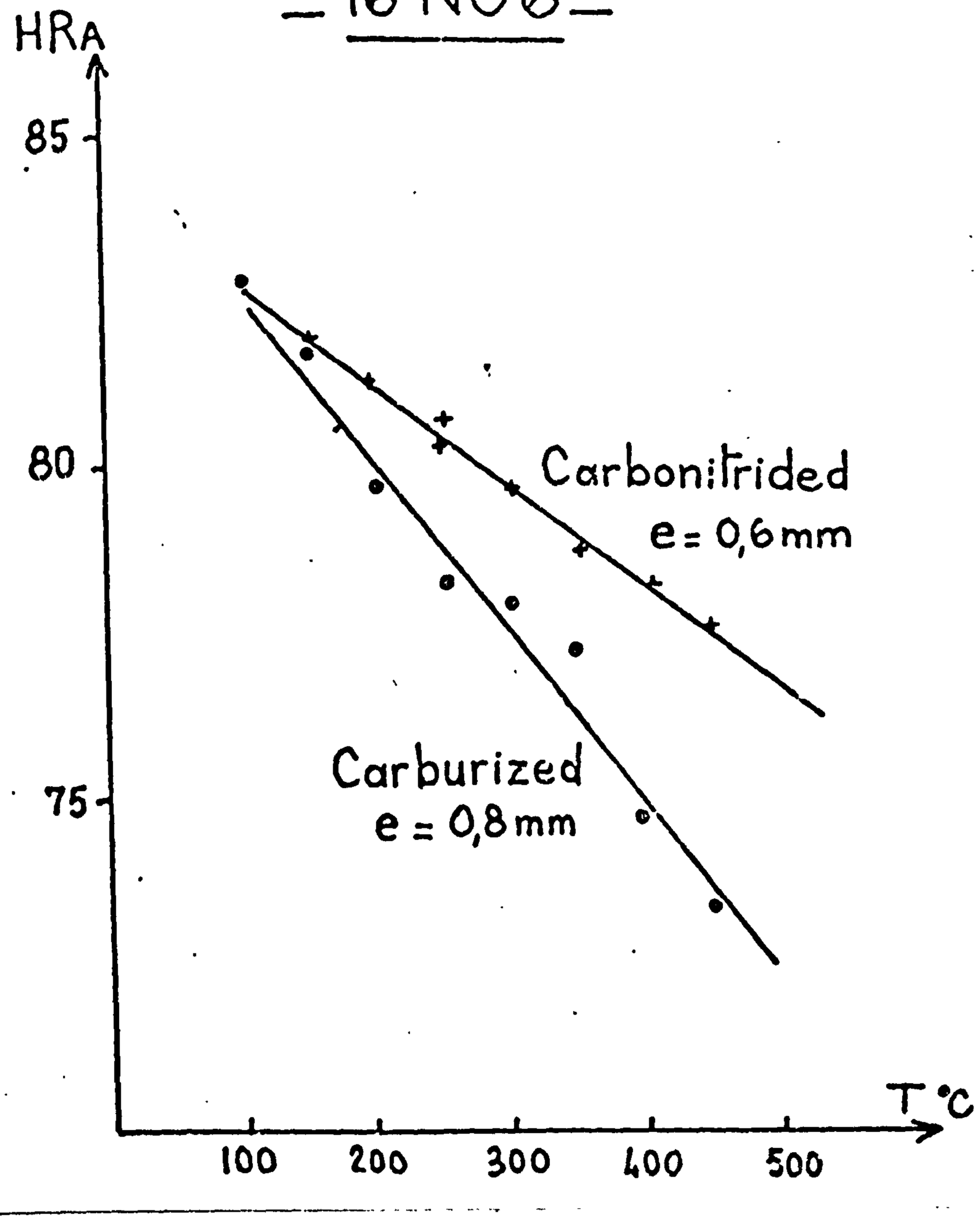
HRA
85
80
75
Carbonitrided
e = 0,6mm
Carburized
e = 0,8mm
T °C
100
200
300
400
500

CHAPTER 3

SCOPE AND AIMS OF THE PRESENT PROJECT

Restrictions on the long term availability of carbonaceous sources for heat treatment atmospheres have led to the investigation and introduction of nitrogen-based carrier gases as alternatives to carrier gases generated, somewhat wastefully, from hydrocarbon gases. A further logical step in the conservation of hydrocarbons in the thermochemical processing sector is to replace carbon by nitrogen as the hardening element in austenitic treatments.; a step which has already been taken industrially, at least in part, with the acceptance of carbonitriding modifications to the carburising process. The complete replacement of carbon by nitrogen however has only been undertaken as a laboratory exercise; this has identified, through various investigations[2,3,35], a number of limitations on the further developments of austenitic nitriding treatments.

These limitations, of which there are many at this stage, include an incomplete appreciation of the physical metallurgy of the austenite phase and its athermal and isothermal decomposition in the iron-carbon-nitrogen system. This matter is further aggravated by the lack of adequate experimental tools to simultaneously analyse for high carbon and nitrogen levels in iron-based materials as a function of depth of penetration into the material.

It is the purpose of the present project to develop suitable electronprobe microanalysis and emission spectrometric analysis techniques for nitrogen and apply these techniques to a study of various aspects of iron-carbon-nitrogen austenite, with a

view to making a contribution to

(a) the technological development of austenitic nitriding treatments,

(b) the understanding of the physical metallurgical kinetics of austenitic thermochemical processing.

The development of these analytical techniques is described in detail in chapter 5, with particular attention being paid to the preparation of suitable standard samples and to the calibration techniques employed. In addition, the development of atmosphere gas analysis systems is described in this chapter, since accurate atmosphere analysis also plays an important role in thermochemical processing.

In chapter 6 previous studies of the austenitic nitriding of pure iron are amplified using these new analytical tools, and extended to study certain restrictions, namely gas void formation, observed by earlier workers.

In chapter 7 the austenitic nitriding process has been applied to iron-carbon alloys in order to investigate the iron-carbon-nitrogen system. Application of the analysis procedures developed in chapter 5 to the problems of determining concentration gradients is also examined. The diffusion of nitrogen in austenite and the extent of the austenite phase field in the iron-carbon-nitrogen system are also examined.

In the final chapter (8), both the scientific and technological developments described in this thesis are summarised, and the way in which future work in this area could possibly be developed

using the same analytical tools is outlined.

CHAPTER 4

EXPERIMENTAL PROCEDURE

4.1 Specimen preparation

4.1.1 Pure Iron

Spectrographically pure Iron (Johnson-Matthey) in the form of strips 75mm x 20mm x 1mm were vacuum annealed for 24 hours at 970°C, and cold rolled to various thicknesses from 0.76mm down to 0.23mm. Interstage vacuum anneals (1 hour at 700°C) were used when deformation reached 50%, and careful inspection was made at each stage for any edge cracking, which was then eliminated by trimming or grinding. When deformation was complete, the strips were again vacuum annealed for 24 hours at 970°C.

4.1.2. Iron-Carbon Alloys

The Fe-C alloys were supplied by the British Steel Corporation in the form of 9.5mm diameter hot-rolled bar. (Analysis of the alloys is shown in table 3) The stock was cut into 150mm lengths and turned down on a lathe to approximately 8.4mm diameter to eliminate any decarburised layers, and then vacuum annealed for 1 hour at 970°C. The stock was then cold rolled longitudinally, until a flat approximately 5mm wide was achieved. Cross rolling was then used to spread the width of the strip to 20mm, occasional longitudinal rolling was used to straighten the strip, and alternate cross rolling and longitudinal rolling was used until the required thicknesses were obtained (0.76mm to 0.23mm). Interstage vacuum anneals (1 hour at 700°C) were used when deformation had reached 50%,

and careful inspection was made at each stage for any edge cracking, which was then eliminated by trimming or grinding. When deformation was complete, the strip was again vacuum annealed for 24 hours at 970°C. Vacuums of better than 10^{-5}mm Hg were used at all times.

4.1.3. Preparation for heat treatment.

Specimens for heat treatment from both the Pure Iron and Fe-C strip were cut on a guillotine to sheets 23mm x 25mm, and a small hole (2.5mm dia.) drilled in the centre of one of the 23mm edges for suspension purposes. The major surfaces of the specimens were polished down to 600 grit finish to

(a) provide a uniform surface and

(b) simulate a typical finish for industrial components.

4.2. Heat treatment furnace.

Fig. 20 shows the heat treatment furnace used, together with its associated gas supply and monitoring apparatus. The flow meters for ammonia, and hydrogen and nitrogen were of the capillary type, the gas flow being directly proportional to the pressure difference across the ends of the capillary. The flowmeters were calibrated in the apparatus to take account of back pressure effects from other gases. Calibrations were performed using a paddle type flow-meter[67], with an accuracy of 0.005 litres. The flowmeter for natural gas was a Meterrate[68] glass float type A, which was calibrated using a 10cc bubble flowmeter. The maximum flowrates attainable in the various flowmeters were

Ammonia	12	litres/hour
Hydrogen	25	" "
Nitrogen	11	" "
Natural Gas	4	" "

Very stable and accurate gas flow control for ammonia, hydrogen and nitrogen was obtained by passing the gases across constant pressure head devices, consisting of a long tube filled with di-n-butyl-pthalate, excess pressure being bubbled off to the atmosphere.

After mixing, the gases were passed into the top of the furnace, exhausted from the bottom and piped away to the atmosphere. Three-way taps were placed in the inlet and exhaust lines, so that the gases could be diverted to an infra-red ammonia analyser. Later in the work, a Packard-Becker type 417 gas chromatograph became available, and suitable sampling ports were inserted in the inlet and exhaust lines, as shown in the figure.

A more detailed diagram of the furnace itself is shown in fig.21. The temperature was controlled in the single winding by an Ether temperature controller with a platinum-platinum/13% rhodium sensor, and switched high/low current in the winding. A hot zone of $\pm 2^{o}C$ was obtained over a distance of 4cm. The specimen was introduced throught the bottom of the furnace and suspended on a platinum hook wired to a 6.4mm dia. Inconel sheathed chromel/alumel thermocouple, suspended in the centre of the silica glass reaction tube. A compression fitting with 'o' rings held the thermocouple in place. Interchangeable Quickfit B34 cones and sockets were used to

enable alternative tops to be fitted. All joints in the apparatus were sealed where necessary with vacuum grease, and a positive pressure from the gas mixtures at all times prevented influx of air. The quench tank was filled with brine solution, covered with a layer of di-n-butyl-pthalate, an oil with very low vapour pressure.

4.3 Heat treatment procedure

The required gas atmosphere mixtures were set on the appropriate flowmeters, and allowed to flow through the apparatus for at least half an hour before treatment. A total gas flowrate of 20 litres/hour, equivalent to a linear flowrate in the furnace of 1 cm/sec, was used to enable sufficient undissociated ammonia to reach the specimen surface at high temperatures[35,56]. Use of the gas chromatograph enabled complex gas mixtures, with natural gas and ammonia, to be readily set. Specimens were thoroughly cleaned and degreased before weighing on a 5 figure analytical balance. The specimen weights averaged 3 gm with a total surface area of approximately 12 cm^2 for the 0.76mm thick specimens. The specimen was introduced into the bottom of the furnace, and placed on the platinum hook, just above the quench tank. With the furnace again sealed to the atmosphere, the ammonia supply, (when used) was turned off and the gas mixture allowed to flush through the apparatus. After 5 minutes flushing, the specimen was raised to the hot zone and after a further 5 minutes, when the specimen had heated up to temperature, the ammonia supply was turned on. After the required time at temperature, the specimen was quickly plunged into the quench tank. When cold,

the specimen was removed from the furnace and thoroughly cleaned and degreased before reweighing.

The ammonia supply was turned off prior to heating up of the specimen to reduce the tendency to form nitride phases during warm-up. Even quite low ammonia contents ($2^{v}/o$) have high nitriding potentials in the temperature range up to $600^{o}C$.

The accurate weighing of the specimens before and after treatment enabled nitrogen contents to be estimated directly in the case of the pure iron specimens and indirectly, if the carbon weight change was known, in the case of the Fe-C specimens.

During treatment, inlet and exhaust gas streams were analysed by the infra-red ammonia meter or by chromatography. Calibration and use of these instruments is discussed in section 5.1.

4.4 Metallographic examination

After treatment and weighing, a small piece was removed from the top of the specimen by a diamond cutting wheel, and cold mounted in Scandiplast resin, to enable a cross section of the specimen to be examined. Mounted specimens were polished on silicon carbide papers to 600 grit, then on diamond impregnated cloth wheels to 1μ or $\frac{1}{4}\mu$ Etching was performed with 2v/o nital, or when necessary 5v/o nital, and examination and photography made on a Reichart microscope. Microhardness measurements were made using a Leitz Miniload tester with 300gm load. Hardnesses of very soft

areas were made with appropriately lighter loads when necessary.

4.5 Bulk chemical analysis for nitrogen.

This was performed using the standard Kjeldahl method (69) of chemical analysis for nitrogen which consists of three steps

(a) Dissolve steel sample in suitable acid to convert nitrogen to an ammonium salt.

(b) React ammonium salt with caustic soda and collect the ammonia gas produced. (This is the Kjeldahl distillation step.)

(c) Titrate the solution obtained in (b) to determine concentration of ammonia and thus nitrogen content of original sample.

The procedure for each step is described in detail below.

4.5.1. Dissolution of sample.

Depending on the estimated nitrogen content of the sample, a small piece, between 0.05gm and 0.3gm, of clean sample is weighed out and transferred to a small pear shaped flask. 20ml of 50% hydrochloric acid is then added to the flask to dissolve the sample. A long reflux air condenser is fitted to the top of the flask to prevent any solution losses. Nitrogen dissolved in the sample is converted by the acid to ammonium chloride.

$$Fe + N + 4HCl = FeCl_3 + NH_4Cl \quad -(29)$$

Dissolution of the sample normally takes several hours and sometimes a little gentle heat is advantageous. When dissolved the solution is then ready for distillation.

4.5.2 Kjeldahl distillation

This distillation technique is that developed by Kjeldahl for determination of nitrogen in organic compounds and is conducted in the apparatus shown in fig.22. A 3 litre glass boiler flask is heated by two 500 watt immersion heaters sheathed in silica. Steam produced in this flask passes through into two distillation flasks via taps which can be opened to the atmosphere, this is necessary when shutting down, to prevent suck back on cooling. Each of the distillation flasks sit in 750 watt mantle heaters. All the heaters can be controlled independently through variacs to vary the rate of distillation. Entry to each of the flasks is by dropping funnel the end of which is below the liquid level. The distilled ammonia is condensed in water cooled condensers and collected in deionised water in the titration flask.

The standard distillation procedure adopted is as follows:
Each distillation flask is half filled with 20% Sodium Hydroxide (Analar grade) solution and the apparatus is steamed for about half an hour to clean and wet all the glass surfaces to ensure elimination of any absorbed ammonia. The water supply to the condensers is switched off during this period, and freedom from ammonia checked with Nessler's reagent before commencing distillation of samples.
The titration flasks are then filled with sufficient deionised water to cover the tip of the delivery tubes. Collection of ammonia under HCl or borax is not necessary according to a recent British Steel Corporation report [70]. The acid solution from the first step is transferred carefully to a distillation

flask and washed in with deionised water, Distillation is then carried out for about 15-20 mins to collect 100-150 ml. of distillate, which is subsequently titrated, while a further 10cc . of distillate is collected to ensure completion of the ammonia separation. The extraction is represented by the reaction

$$NH_4Cl + NaOH = NH_4OH + NaCl \qquad (30)$$

To compensate for any ammonia in the chemicals used a blank test is run on each distillation flask at the beginning and end of a run of nitrogen determinations. Ammonia from $^{N}/_{100}$ Ammonium Chloride solution is distilled and collected, 10ml is used at the start and 20ml at the end of the run, the difference in titration between twice the 10ml result and the 20ml result gives the blank.

4.5.3 Titration with Potassium Di-iodate

Normally $^{N}/_{100}$ Potassium di-iodate is used, but when small quantities of ammonia are involved $^{N}/_{400}$ solution is used. Standard titration methods are used with an automatic burette of 10ml capacity. As the solutions involved are very dilute a special end point indicator is used, consisting of a mixture $0.2^{W}/_{o}$ Methyl Red in $95^{V}/o$ Ethanol and $0.2^{W}/o$ Methylene Blue in $95^{V}/o$ Ethanol, (12 drops of Methyl Red + 6 drops of Methylene Blue are used). The end point is a colour change from green to violet, with the solution almost colourless just before the end point.

4.5.4. Special Precautions in Kjeldahl technique.

Because of the possibility of contamination from ammonia (due to its high affinity for water), all operations are carried out in a clean atmosphere, using only the purest chemicals and

de-ionised water. No greases are used on any glassware and all washings are made with de-ionised water.

4.5.5. Possible modifications to the Kjeldahl technique.

Improved end point determination of the titration can be obtained using photometric determination with indophenol blue[70].

Alternatively the ammonia concentration in the distillate can be measured very accurately with a potentiometric ammonia probe[71] which the makers claim to have a range of detection of 10^{-6}M to 1M for ammonia - equivalent to 0.017mg/l to 17 x 10^{3}mg/l.

Recent work with such a probe has shown excellent results from organic nitrogen determinations using the Kjeldahl digest directly without distillation[72,73]. However no work to date has been published on direct determination of ammonia in strongly metal ion containing solutions.

4.6 Concentration profile analysis of specimens.

Special methods for concentration profile analysis were developed using electron probe microanalysis and emission spectrometer techniques; these are fully described in sections 5.2 and 5.3 respectively.

4.7 X-Ray Diffraction.

Specimens were examined on both Siemens and McLean diffractometers, using Cobalt or Chromium targets with filters of Iron and Vanadium respectively. The McLean instrument was designed

for high precision angle measurement required for residual stress analysis[74], and could therefore be used for lattice parameter measurements. It was therefore possible to estimate the interstitial contents of specimen surfaces using the known relationships for carbon[75] and nitrogen[2,76] austenites and martensites of iron alloys. Lattice parameter measurements were made by point counting to accurately identify the peak angles and then either extrapolating using an appropriate error function[77], or by direct comparison to ferite peaks determined on spectrographically pure iron. Phase identification was made using known relationships and ASTM cards where appropriate.

TABLE 3

ANALYSIS OF IRON-CARBON ALLOYS

C	Mn	Ni	Cr	Si	Mo	P	S	Cu	Al	V	B
0.50	<0.03	<0.03	<0.03	0.03	<0.01	0.003	0.007	<0.02	<0.05	<0.01	0.0001
0.87	"	"	"	"	"	"	"	"	"	"	"
1.07	"	"	"	"	"	"	"	"	"	"	"

Analysis by emission spectrometer.

FIG. 20

LABORATORY HEAT TREATMENT FURNACE
WITH ASSOCIATED GAS SUPPLIES AND
MONITORING APPARATUS.

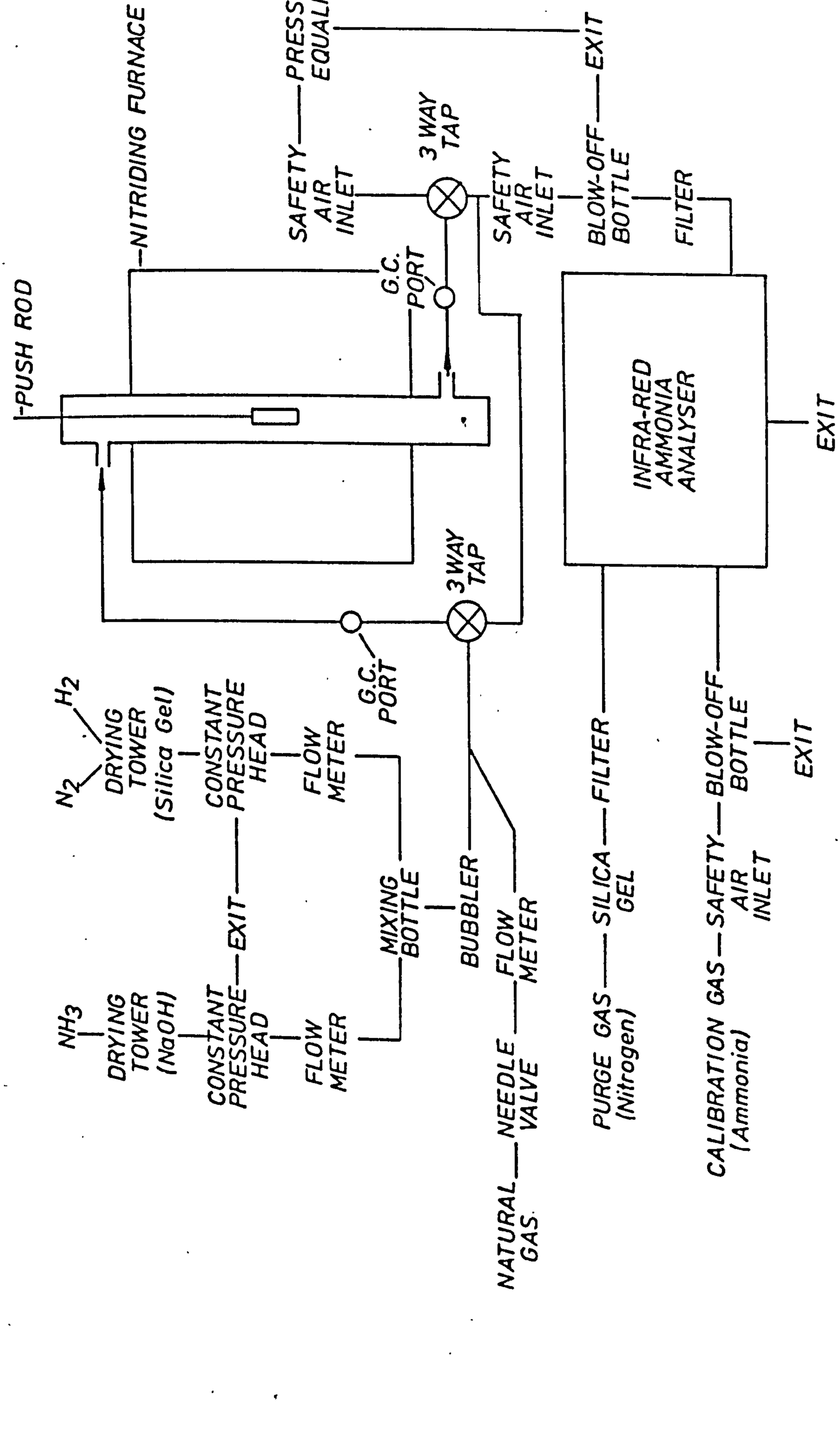
NITRIDING FURNACE
PUSH ROD
N2
H2
DRYING TOWER (Silica Gel)
CONSTANT PRESSURE HEAD
FLOW METER
G.C. PORT
EXIT
MIXING BOTTLE
BUBBLER
FLOW METER
3 WAY TAP
SAFETY AIR INLET
PRESSURE EQUALISER
BLOW-OFF BOTTLE
FILTER
INFRA-RED AMMONIA ANALYSER
EXIT
NH3
DRYING TOWER (NaOH)
CONSTANT PRESSURE HEAD
FLOW METER
NATURAL GAS
NEEDLE VALVE
SILICA GEL
PURGE GAS (Nitrogen)
CALIBRATION GAS (Ammonia)
SAFETY AIR INLET
BLOW-OFF BOTTLE
EXIT

FIG. 21

DETAILED DIAGRAM OF HEAT TREATMENT FURNACE

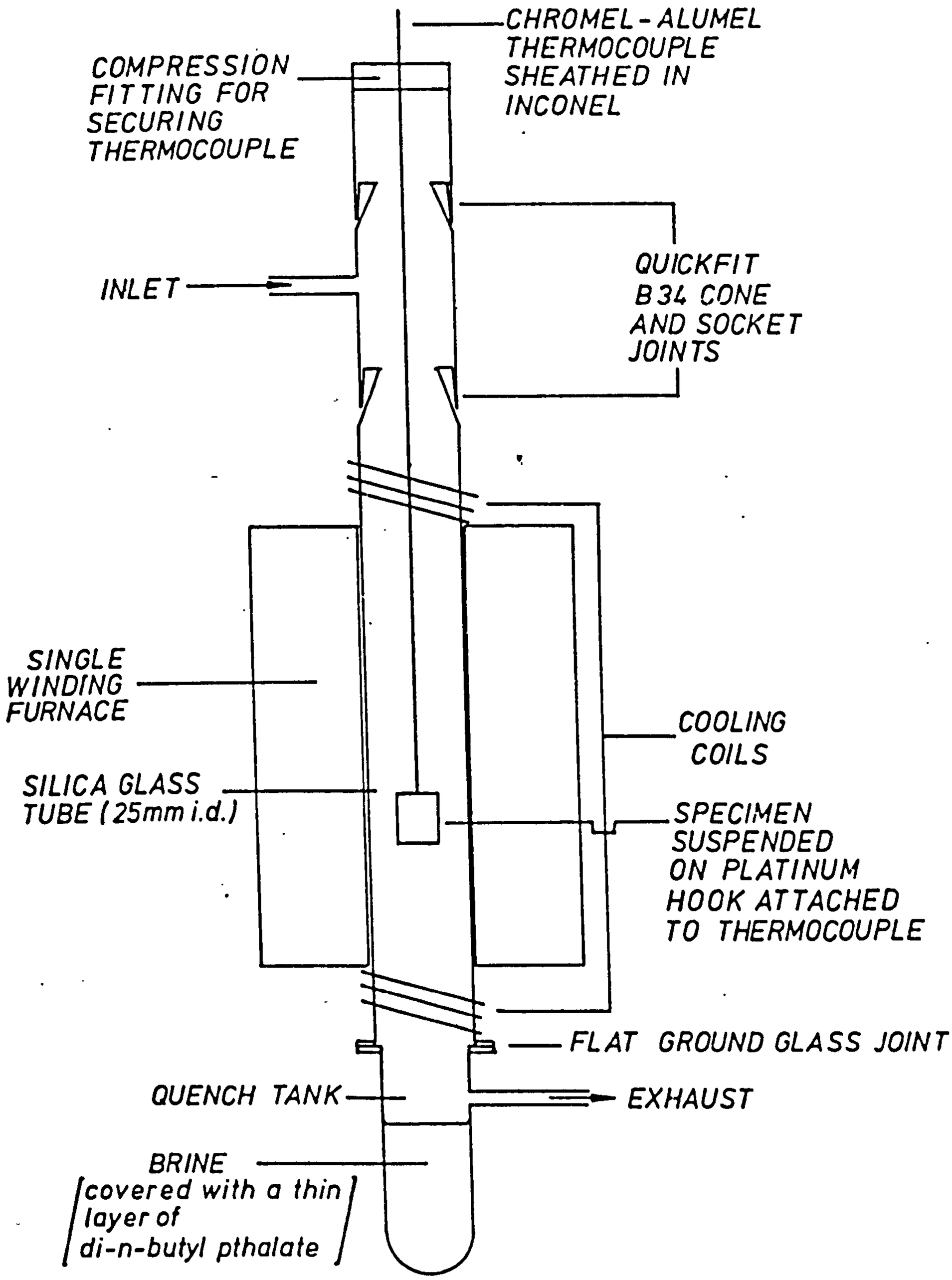
CHROMEL - ALUMEL THERMOCOUPLE SHEATHED IN INCONEL
COMPRESSION FITTING FOR SECURING THERMOCOUPLE
INLET
QUICKFIT B34 CONE AND SOCKET JOINTS
SINGLE WINDING FURNACE
SILICA GLASS TUBE (25mm i.d.)
COOLING COILS
SPECIMEN SUSPENDED ON PLATINUM HOOK ATTACHED TO THERMOCOUPLE
FLAT GROUND GLASS JOINT
QUENCH TANK
EXHAUST
BRINE
(covered with a thin layer of di-n-butyl pthalate)

FIG. 22

STEAM DISTILLATION APPARATUS FOR

KJELDAHL NITROGEN DETERMINATIONS.

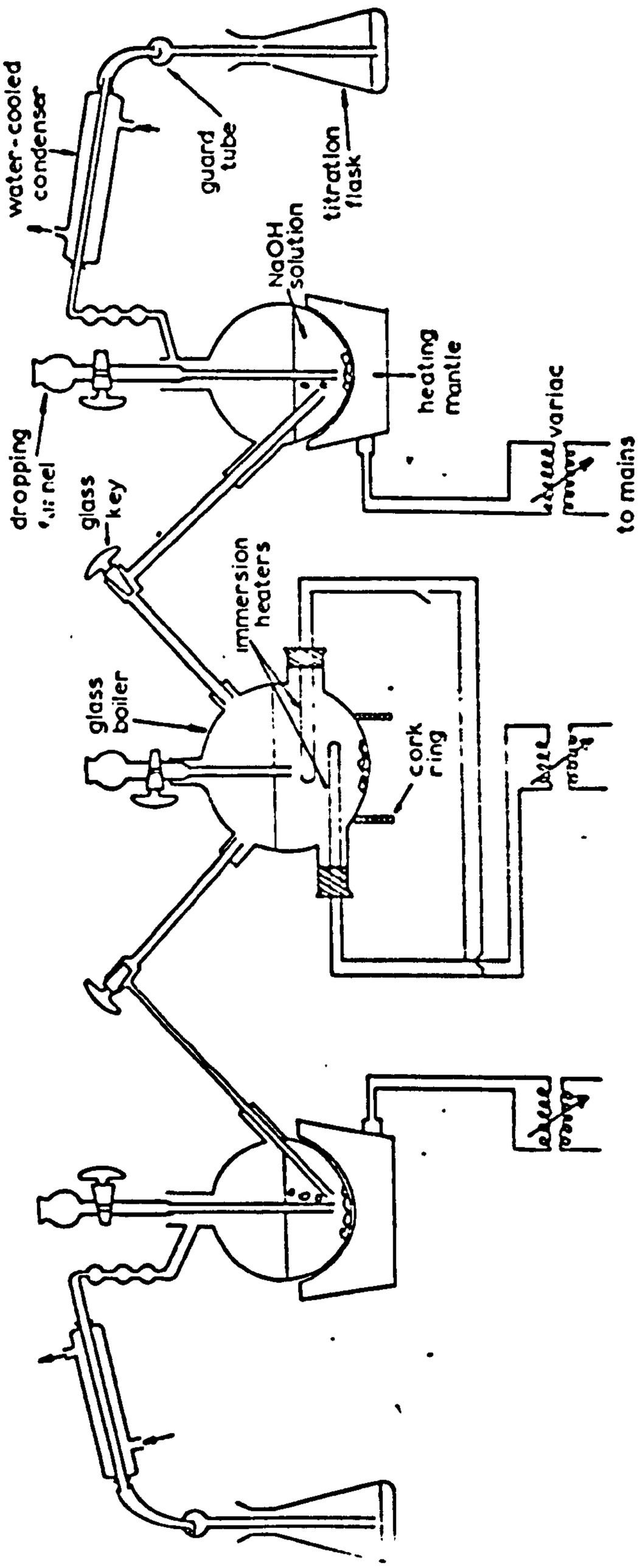

DISTILLATION OF AMMONIA

ARRANGEMENT OF THE APPARATUS FOR THE STEAM

CHAPTER 5

DEVELOPMENTS IN ANALYTICAL TECHNIQUES.

5.1. Methods of Monitoring and control of Ammonia in gas atmospheres.

In reviewing current industrial practice in austenitic thermochemical treatments (section 2.8) it was pointed out that, apart from the dissociation pipette, there were no methods of direct monitoring of ammonia being used by industry. Several possible methods, the alphameter[60], the infra-red analyser[61] and the hot wire resistivity technique[59] had been investigated on a laboratory scale but only the hot wire resistivity technique had been directly applied to austenitic treatments. It was also pointed out in section 2.3.2.4. that advances in gas chromatography were now making the technique attractive for furnace gas monitoring and control.

Against this background, the infra-red analyser because of its already proven potential in atmosphere analysis and gas chromatography because of its great potential for complete furnace gas analysis were chosen for further investigation.

5.1.1. Infra-red gas analysis.

The operating principle of the infra-red analyser is as follows:

An electrically heated filament (fig.23) produces an infra-red source which is split into two collumated beams, which in turn are simultaneously chopped to provide a series of low frequency pulses. The pulses then pass through a pair of cells to a detector. One cell -.the reference cell -

contains a non-infra-red absorbing gas, i.e. high purity nitrogen, while the other cell contains the sample to be analysed. The detector is a cell divided into two by a pressure sensitive diaphragm, one half of which contains a gas which absorbs infra-red radiation. While the analysis cell is free of the gas being analysed, the radiation from each cell will be identical and there will be no effect on the pressure diaphragm. However when a gas mixture to be analysed is admitted to the sample cell, some infra-red radiation passing through the cell is absorbed and so the beams emerging from the cells are of different intensities. Now because the infra-red radiation produces a heating effect in the detector gas, a pressure differential is set up in the cell which is equalised by movement of the sensitive diaphragm. The movement is sensed electronically, amplified and fed directly to a meter usually calibrated directly for the gas to be analysed.

The infra-red analyser can detect all gases, except the elemental gases such as hydrogen, nitrogen and oxygen which do not absorb infra-red radiation. The main gases of interest in gas carbonitriding or austenitic nitriding atmospheres are shown in table 4 together with their infra-red wavelengths[78]. The complete infra-red spectra for these and several other gases are shown in fig.24[79], the atmospheric water vapour spectrum being shown in fig.25[80]. Comparison of the various analytical wavelengths shows that all the gases are fairly well separated and suitable wavelengths can be chosen without too much interference from other gases. In the case of ammonia it can be seen that the infra-red spectrum is always closely associated

with that of water vapour, probably because of its great affinity for water and so care must be taken to eliminate this contaminant if accurate results are to be obtained.

Selectivities of infra-red analysers are better when small quantities of the gases to be analysed are present in a gas mixture. This is because only the strong absorbance bands will be present and hence interference between components will be minimal. This can be seen from fig.24 where curves marked A represent 100^{v}/o of the component and curves B,C, and D represent smaller partial pressures.

5.1.1.1. Calibration of infra-red analysers.

Calibration methods normally used consist of passing gas mixtures of known composition through the analyser to set the zero and full scale deflections of the meter.

5.1.1.2. Sensitivity and limitations of infra-red analysis.

The limits of detection by infra-red gas analysis vary with the gas being analysed, but in the majority of cases detection down to a few ppm is possible.

The infra-red analysis method has the advantage that one component in a gas mixture can be continuously monitored and is therefore suitable for atmosphere control when this component is the controlling variable of the atmosphere e.g. CO_2 in a carburising atmosphere, or NH_3 in a nitriding atmosphere. When several components need to be monitored, then the infra-red method can become uneconomic as individual instruments for the individual components are necessary.

5.1.2. Gas chromatography analysis.

Chromatographic instruments for analysing mixtures of elemental and compound gases normally use a thermal conductivity detector to analyse the constituent gases which are separated by a specially prepared column.

Thermal conductivity is a physical property of an element or gaseous compound which under given conditions is constant but different for each compound. Consequently when a minor component is added to a gas stream, the thermal conductivity of the gas stream changes in proportion to the addition of the minor component (assuming their individual thermal conductivities are different). The thermal conductivity detector (fig.26) consists of a metal block containing four channels each with a heated filament (whose resistance changes with temperature). Two channels are positioned in a reference gas stream through which pure carrier gas always passes. The other two channels are positioned in the gas stream eluting from the chromatograph column. These latter two are on the measuring side and are thus exposed to the carrier gas stream which contains components eluted by the column.

The filaments are connected in a Wheatstone bridge network, being heated by the bridge current. When only carrier gas flows over both sets of filaments, heat is conducted away equally under identical flow conditions and the bridge stays in balance as all resistances are identical.

When a component gas is eluted by the column, the thermal conductivity of the gas stream passing over the measuring filaments changes, increasing or decreasing depending on

whether the component gas has a higher or lower thermal conductivity than the carrier gas. A change in the thermal conductivity changes the rate of heat extraction from the measuring filaments, changes their resistance and throws the bridge out of balance. By connecting a recorder, via amplifiers and attenuators to the output of the bridge a continuous record can be made of the bridge balance. When no component is present in the gas stream a stable base line results, but whenever a component is eluted by the column, a sharp peak is observed with the area under the peak proportional to the amount of component in the gas sample. A typical chromatogram is shown in fig. 27.

The sensitivity of the detector will depend on several factors, the main ones being

(a) Bridge current - affects heat transfer

(b) Detector Temperature - affects temperature difference between filaments and cell walls

(c) Gas flow rates - affects rate of heat transfer

(d) Thermal conductivity difference betesn carrier gas and components to be measured. - affects sensitivity (quantitative)

Normally, for a particular column, Detector temperature and carrier gas flow rates are kept constant and bridge current kept low to extend filament life but increased when necessary to provide sensitivity.

The choice of the carrier gas depends on the components to be detected as sensitivity depends on differences between the carrier gas and the component. The thermal conductivity of

common gases are shown in table 5[81]. As can be seen from the table, hydrogen and helium have the greatest differences between themselves and the common gases, and these two gases are the most widely used carrier gases. Hydrogen is preferred for economy and sensitivity, helium is preferred for safety from explosion hazards. For detection of hydrogen or helium carrier gases such as argon or nitrogen are used.

Separation of gases depends on the column packing material and the temperature of the column. In general an increase in column temperature increases sensitivity and shortens the time required for analysis, but this can also decrease the selectivity as component peaks may then appear very close. Fortunately only a few different packing materials are required to separate virtually all known gases which can make operations relatively straight forward. Widespread publication has been made for column materials to separate gases of interest in heat treatment atmospheres[82,83]. Two columns are required to separate all heat treatment atmosphere gases these can be

(a) Molecular Sieve, separates O_2, N_2, CH_4, CO.

(b) Porous Polymer type (Porapak[84], Chromosorb[85]) separates CH_4, CO_2, NH_3, C_2H_6, C_3H_8, H_2O,

and therefore require two gas samples.

Recent research in chromatography has devised column switching techniques [86-90] which only require one gas sample. Usually the higher molecular weight gases are detected on a Porous Polymer type column and the eluted gases after passing over the measuring filament are then passed into another column

usually a molecular sieve to separate the elemental gases. Complete analysis can take up to 20mins, but analyses for CH_4, CO_2 and NH_3 need only 3-5 mins.

Gas sampling can be performed manually with special gas tight syringes or automatically with special sampling valves, typical sample sizes being 0.5cc to 1cc.

5.1.2.1. Calibration of gas chromatographs.

Calibration of the chromatograph is made by injecting samples of known concentration. Under a given set of operating conditions a component is identified qualitatively by its retention time on the column (see fig.27) and a quanititative assessment is made by relating its peak area (or for very symmetrical peaks, its peak height) to a calibration chart of standards vs peak areas (or peak heights). Samples and standards must be injected onto the column under the same conditions and at the same pressure (normally 1 atmosphere). Suitable standards can be obtained from chromatographic suppliers or made up using an apparatus similar to Averett[91]. Another method of calibration which can be used is the exponential dilution flask[92]. A flask of known volume V_1 is inserted between the inlet to the chromatograph and the carrier gas supply. A known volume V_2 of calibrating gas is injected into the flask, which contains a stirrer to mix the gases, and the concentration of the calibrating gas in the carrier gas stream then decays exponentially according to the following relation

$$\text{Concentration at time } t = V_2 e^{\frac{-ft}{V_1}} \qquad (31)$$

where t = time (secs)

V_1, V_2 = volume (cc)

f = flow rate of carrier gas through flask (cc/sec)

Providing the detector response is linear for the particular calibration gas, deviation from the baseline can then be related on a time basis to composition through the above formula. This technique is often used in reverse to check the linearity of detector response, when calibration has been made by another method.

5.1.2.2. Sensitivity and limitations of gas chromatography. Limits of detection of gases by chromatography depend considerably on operating conditions, but can be in the order of several ppm. As with infra-red analysis best results are usually obtained when measuring impurities in a gas mixture. Increasing the sample size to be analysed can improve the sensitivity, but often, on small bore (3mm diameter) columns, overloading occurs because the sample size is large in relation to the volume of carrier gas passing through the column. The result is often seen in peak spreading of the eluted gases.

Although chromatography can now analyse complex gas mixtures very quickly, it still has not gained widespread use because it is a little more complicated than infra-red analysis and industry prefers to keep monitoring and control methods simple. However it is still possible to use the method in heat treatment plant, particularly when used with automatic sampling devices and electronic integrators to rapidly interpret results. A fully automated chromatograph has been installed to monitor heat treatment plant in Hungary[93], and it is believed that there are now chromatographic installations in this country monitoring heat treatment plant.

5.1.3. Furnace gas analysis procedures

5.1.3.1. Infra-red gas analysis

In the initial part of the work, gas analysis was performed with the ammonia infra-red analyser; the principle of which has been described in section 5.1.1. Some problems with interference from water vapour were experienced, but these could be minimised by the fitting of a drying column of NaOH, just before the analyser inlet. However, these water vapour problems were of particular concern when the analyser was used to measure ammonia levels less than 10v/o. The saturated vapour pressure of water [81] at room temperature ($20^{o}C$) is 17.54mm, equivalent to 2.3v/o of any gas passing over water at this temperature. It is already known from the calibration of the ammonia analyser that 2v/o water vapour interference will give a reading equivalent to 3v/o ammonia on the infra-red analyser. Therefore there can be very serious errors in readings, if even small traces of water vapour are present in the gas stream, or any of the gas lines.

While using the analyser, it was noted that even at relatively high temperatures of heat treatment ($> 750^{o}C$), the dissociation of ammonia was not as great as was expected, in some cases exhaust readings greater than inlet readings were found, due to presence of water vapour. These errors were reduced somewhat by the fitting of the drying column as described above. The manufacturers are now doing design modifications at present commercially confidential to eliminate this water vapour problem.

5.1.3.2. Gas chromatography analysis.

With the acquisition of the Packard-Becker gas chromatograph prospects for very accurate gas analysis were greatly enhanced. Although chromatography has been used for many years for complete gas analysis it has only been in recent years that column packing materials have become available, together with advances in instrumental techniques, to enable rapid (5 min per sample) analyses to be made. The advent of the newer column packing materials such as Porapak[84] and Chromosorb[85] has enabled some of the more difficult-to-separate gases to be analysed. Ammonia is one of these 'difficult' gases, because of its highly polar nature, this results in the molecule 'sticking' to the column packing material, and not being eluted as a sharp peak. Prospects for separating ammonia on a Porapak column were therefore investigated further.

Even with a Porapak column, the problem of 'sticking' still exists to a limited extent. The problem was overcome by raising the temperature of operation of the column (see fig.28), which also reduces the resolution of the column for components which elute close together. This can be seen in the same figure for nitrogen and methane. The problem of 'sticking' was also overcome by a technique known as silylation, which involves coating the column packing material with a special chemical compound which effectively reduces the polarity of the highly polar gases. Comparison of results from coated and uncoated Porapak columns can be seen in fig.29. Using a combination of both methods enabled a compromise solution to be made for good resolution of close peaks and efficient separation of highly polar gases. This solution was therefore adopted for the Packard-Becker chromatograph by using a 9'

Porapak Q column, coated with a tri-methyl-silyl compound, operating at 125°C. Good separation of ammonia can still be made down to 100°C, see fig.28. The standard operating conditions used are also indicated on fig.28. A standard bridge current of 150mA was used to combine good sensitivity with extended filament life. Raising the bridge current to 200mA increased the sensitivity by a factor of 2.64 (see fig.30). Bridge currents up to 300mA were occasionally used to detect low levels of water vapour.

The carrier gas chosen was hydrogen, mainly for economic reasons, but also because it gives the best sensitivity, and the bulk of the sample to be analysed was hydrogen; so it was more convenient and accurate to measure the effective impurities in the sample. Calibration gas mixtures were made using an apparatus similar to Averrett[91] in which a gas tight 500cc container was evacuated by rotary pump, filled to a measured pressure with the gas of interest, and then backfilled to a standardised pressure with hydrogen. Samples were then extracted through a special silicone rubber septum (microsep) with a 0.5cc lockable gas syringe (Precision Sampling Corpn.). Injections into the column were also through microsep septa, and calibration charts of gas composition versus peak height were constructed.

The sampling ports to the furnace were situated as close as physically possible to the inlet and exhaust of the furnace, and fluid (di-n-butyl-pthalate) manometers were also attached to the ports to check the sampling pressure. With a gas flowrate of 20 l/h through the furnace, the actual line pressure was 1.03 atmospheres.

The chromatograph also proved useful in checking the efficiency of the drying column fitted to the inlet of the infra-red analyser. Gas samples, taken before and after the drying column, showed that although water content of the gas stream was reduced, it was not completely removed. Fig.31 compared the true ammonia calibration by chromatography against the apparent ammonia calibration by infra-red, and as can be seen, substantial errors can occur, when the gas stream contains water vapour. Considerable variations in the infra-red readings can occur particularly on the 0 - 10 v/o range, due to variations in water vapour content of the gas stream.

TABLE 4

INFRA-RED WAVELENGTHS OF GASES IN HEAT TREATMENT ATMOSPHERES.

GAS	WAVELENGTH (μ)
CO	4.67*
CO_2	4.3+, 2.8
H_2O	2.8, 5-7, 8-11, 11-15, 16.
NH_3	2.9+, 5.5-7, 8-15, 10.4-10.7
CH_4	2.4, 3.39, 7-8.5+
HCN	3.0, 7.1+, 13-15
H_2	These gases do not absorb infra-red radiation.
N_2	
O_2	

+This indicates preferred analytical wavelengths.

Source - Reference 78.

TABLE 5

THERMAL CONDUCTIVITIES OF COMMON GASES

		Relative to Hydrogen.
Air	60.34[+]	0.139
Ammonia	55.79	0.129
Argon	41.33	0.095
CarbonDioxide	37.61	0.087
CarbonMonoxide	57.86	0.134
Ethane	47.94	0.111
Helium	352.10	0.813
Hydrogen	433.92	1.000
Methane	78.11	0.180
Nitrogen	60.34	0.139
Oxygen	61.58	0.142
Water vapour	40.50	0.094

[+]Units Cal/(sec)(cm^2)(^oC/cm) $x10^{-6}$ at 15.6°C

Source - Reference 81.

FIG. 23

SCHEMATIC OF INFRA RED GAS ANALYSER (61)

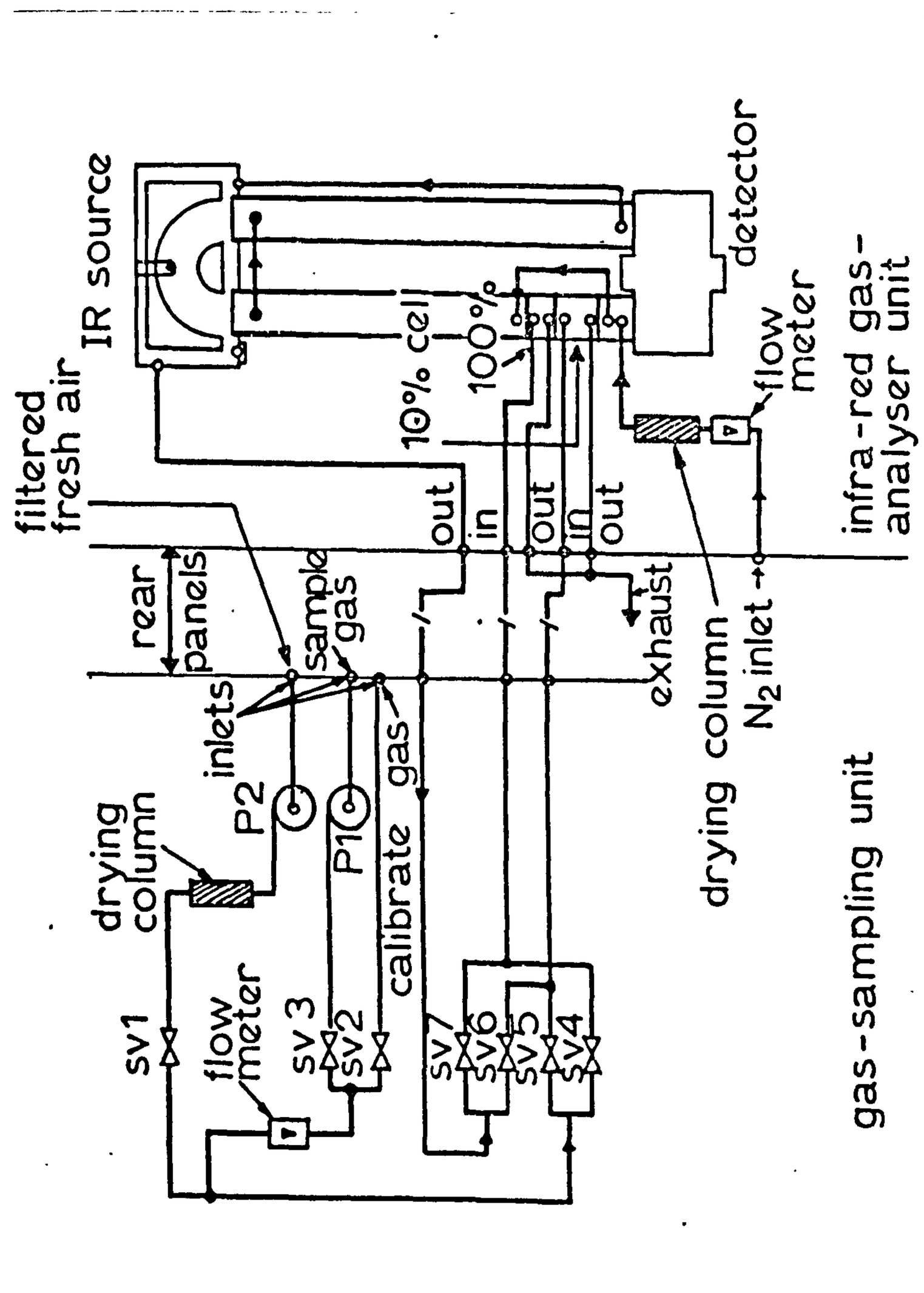
filtered fresh air
IR source
10% cel
100%
detector
flow meter
infra-red gas-analyser unit
rear panels
sample gas
out
in
out
in
out
exhaust
column
N2 inlet
inlets
gas-
drying column
P2
P1
calibrate gas
flow meter
sv1
sv3
sv2
sv7
sv6
sv5
sv4
drying column
N2 inlet
gas-sampling unit

FIG. 24 (a)

INFRA-RED SPECTRA FOR NH_3, CH_4, CO_2 AND CO.(79)

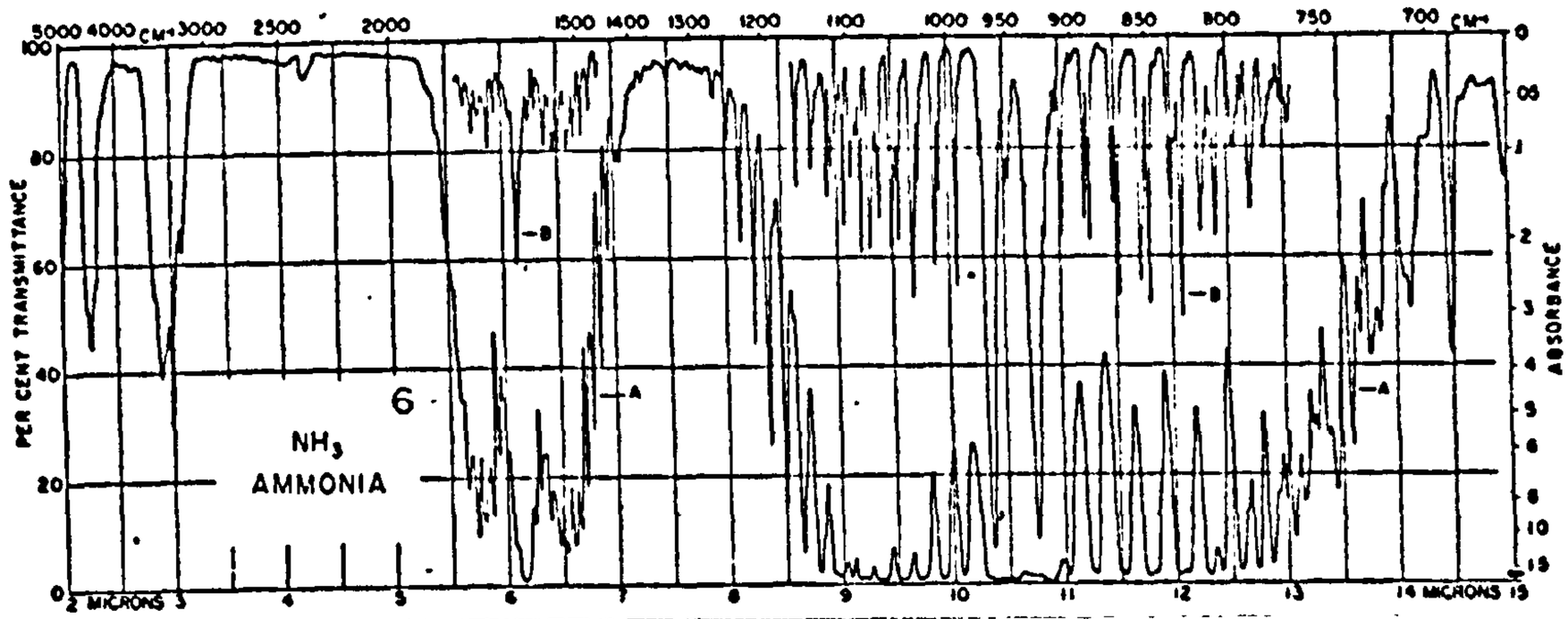
5000 4000 CM-1 3000 2500 2000 1500 1400 1300 1200 1100 1000 950 900 850 800 750 700 CM-1
PER CENT TRANSMITTANCE
ABSORBANCE
6
NH3
AMMONIA
2 MICRONS 3 4 5 6 7 8 9 10 11 12 13 14 MICRONS 15

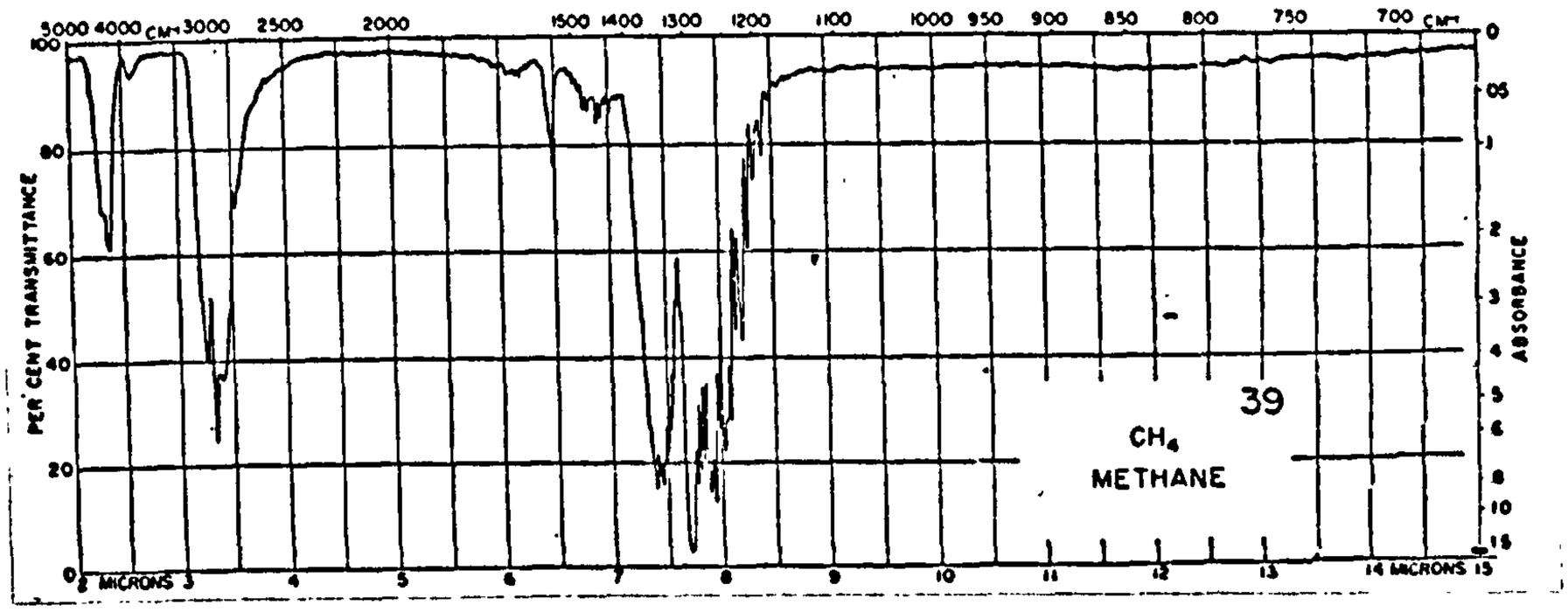
5000 4000 CM-1 3000 2500 2000 1500 1400 1300 1200 1100 1000 950 900 850 800 750 700 CM-1
PER CENT TRANSMITTANCE
ABSORBANCE
39
CH4
METHANE
2 MICRONS 3 4 5 6 7 8 9 10 11 12 13 14 MICRONS 15

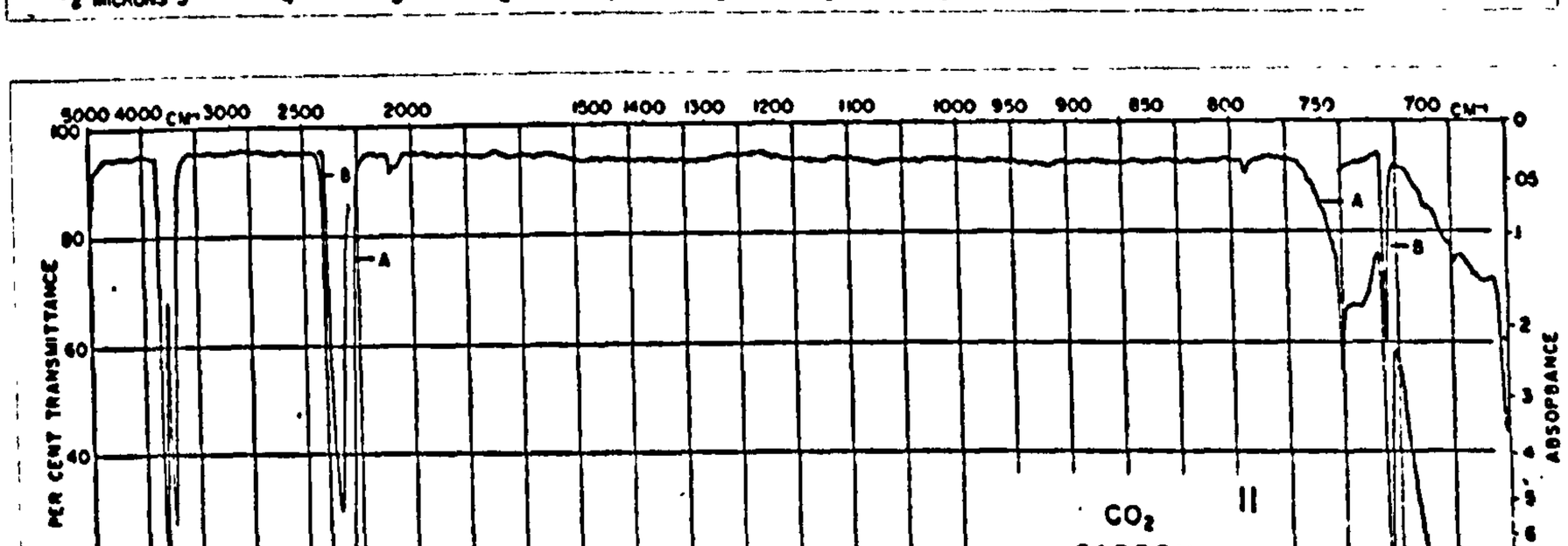
5000 4000 CM-1 3000 2500 2000 1500 1400 1300 1200 1100 1000 950 900 850 800 750 700 CM-1
PER CENT TRANSMITTANCE
ABSORBANCE
A
B
11
CO2
CARBON
DIOXIDE
2 MICRONS 3 4 5 6 7 8 9 10 11 12 13 14 MICRONS 15

5000 4000 CM-1 3000 2500 2000 1500 1400 1300 1200 1100 1000 950 900 850 800 750 700 CM-1
PER CENT TRANSMITTANCE
ABSORBANCE
12
CO
CARBON
MONOXIDE
2 MICRONS 3 4 5 6 7 8 9 10 11 12 13 14 MICRONS 15

FIG. 24 (b)

INFRA-RED SPECTRA FOR C_2H_6, C_3H_8 AND HCN (79)

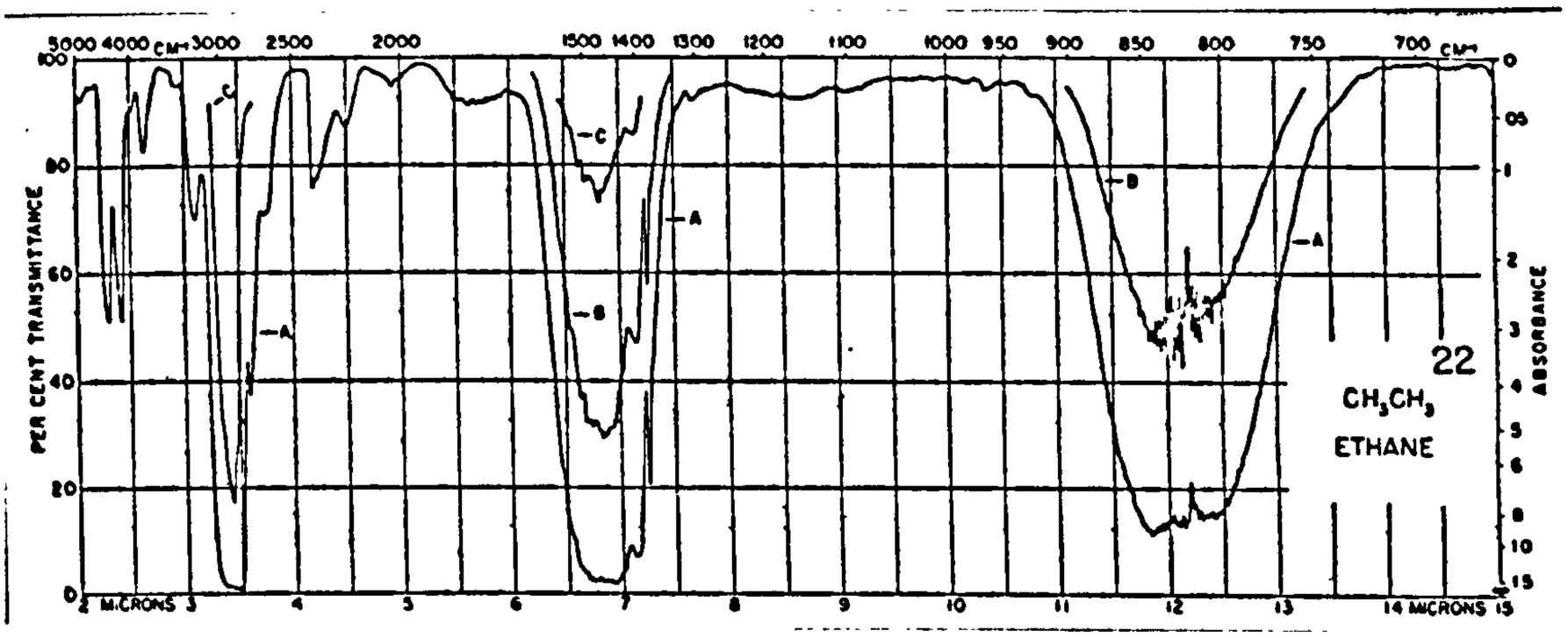
5000 4000 CM⁻¹ 3000 2500 2000 1500 1400 1300 1200 1100 1000 950 900 850 800 750 700 CM⁻¹
PER CENT TRANSMITTANCE
ABSORBANCE
2 MICRONS 3 4 5 6 7 8 9 10 11 12 13 14 MICRONS 15
22
CH₃CH₃
ETHANE

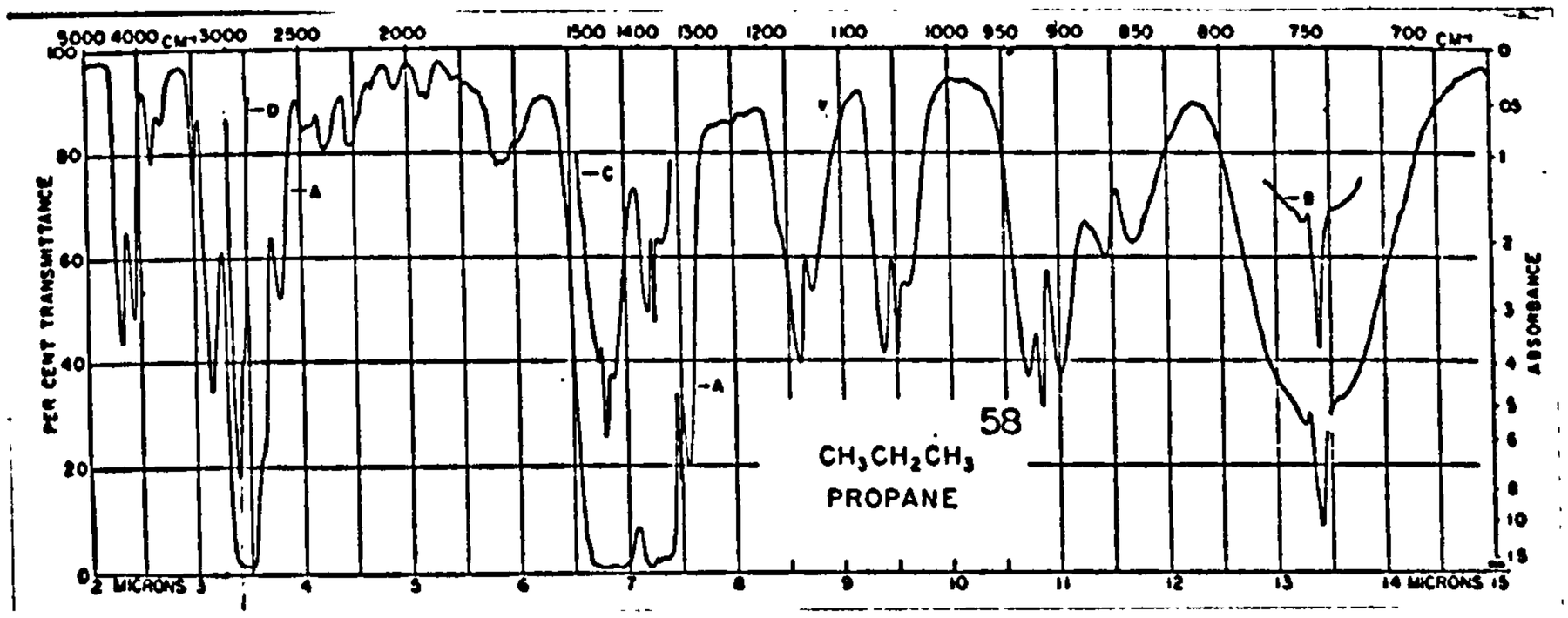
5000 4000 CM⁻¹ 3000 2500 2000 1500 1400 1300 1200 1100 1000 950 900 850 800 750 700 CM⁻¹
PER CENT TRANSMITTANCE
ABSORBANCE
2 MICRONS 3 4 5 6 7 8 9 10 11 12 13 14 MICRONS 15
58
CH₃CH₂CH₃
PROPANE

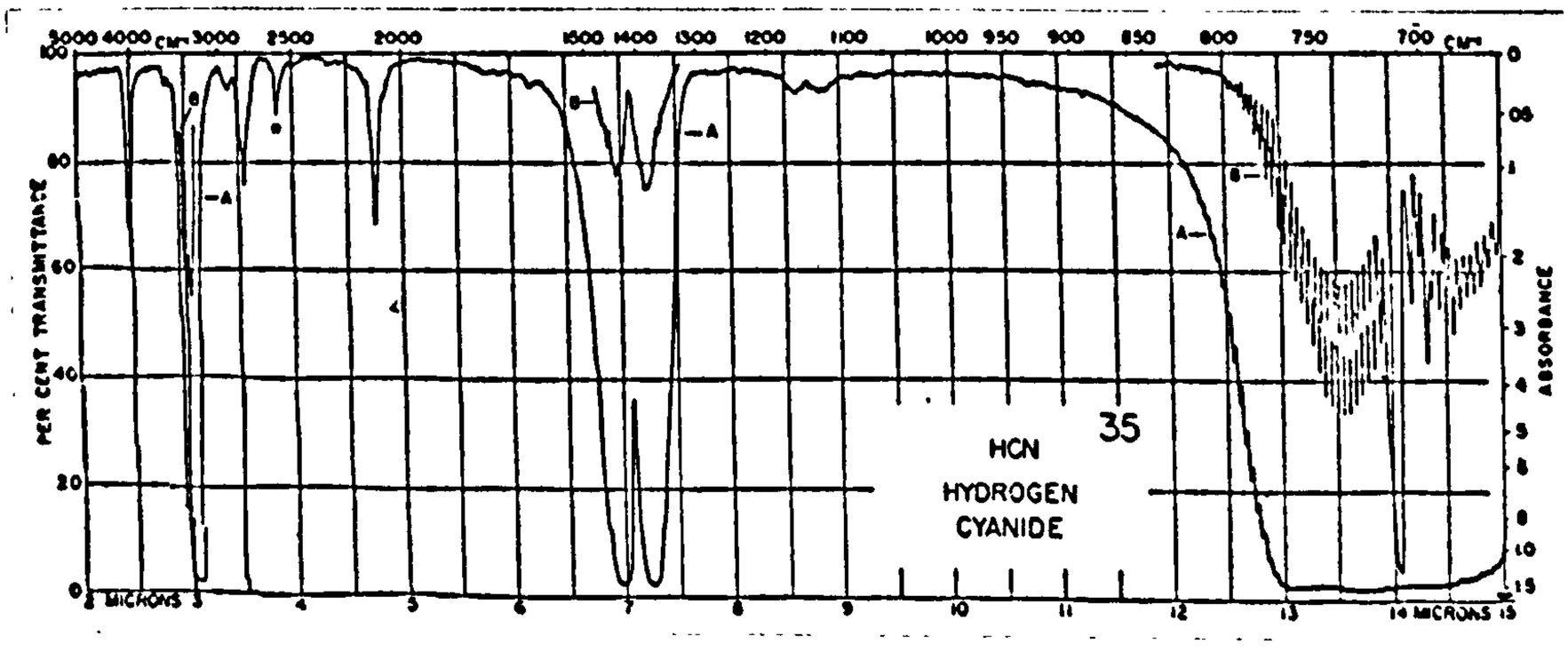
5000 4000 CM⁻¹ 3000 2500 2000 1500 1400 1300 1200 1100 1000 950 900 850 800 750 700 CM⁻¹
PER CENT TRANSMITTANCE
ABSORBANCE
2 MICRONS 3 4 5 6 7 8 9 10 11 12 13 14 MICRONS 15
35
HCN
HYDROGEN
CYANIDE

FIG. 25

INFRA-RED SPECTRUM FOR ATMOSPHERIC WATER VAPOUR(80)

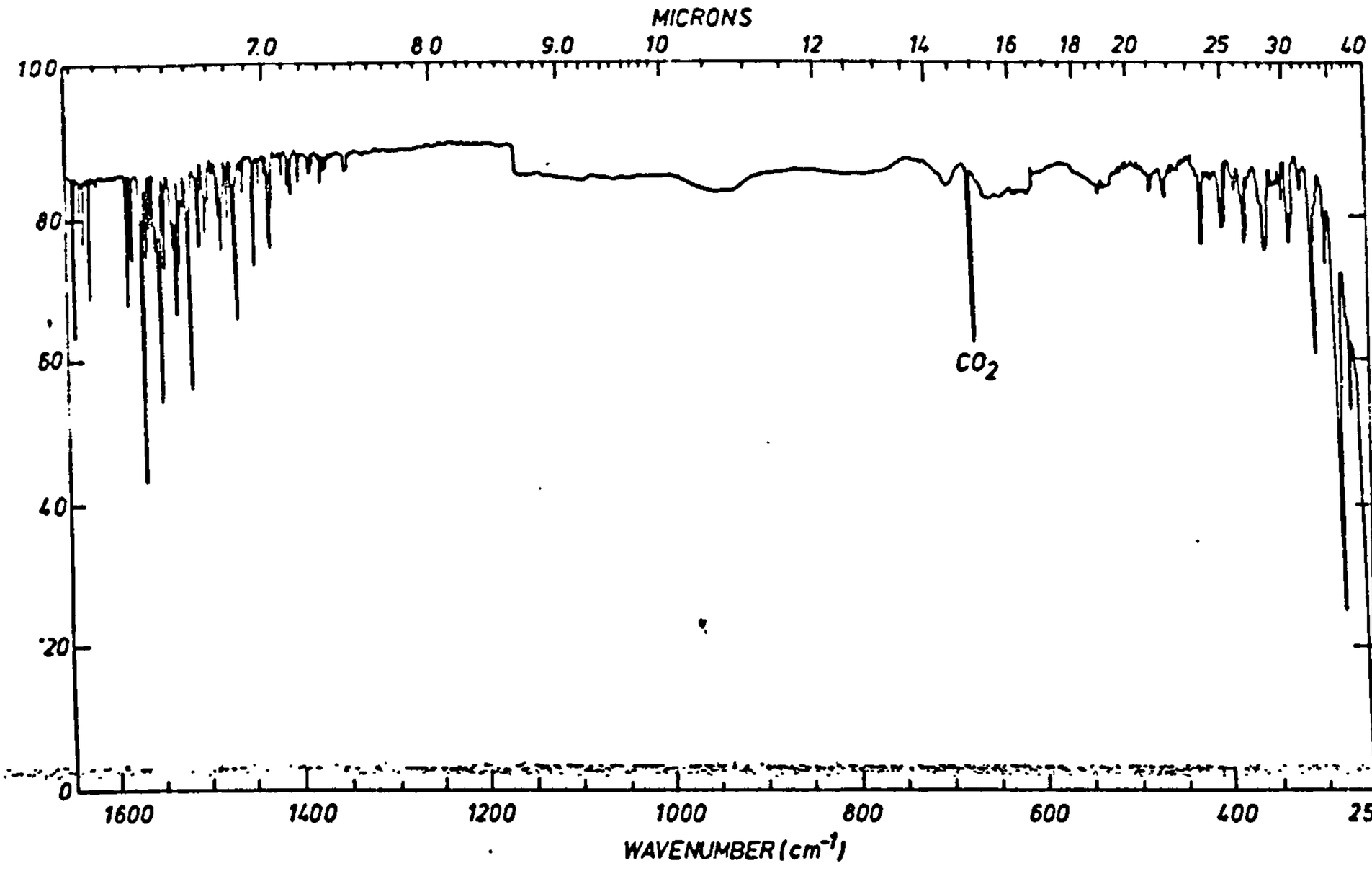
MICRONS
7.0
8.0
9.0
10
12
14
16
18
20
25
30
40
100
80
60
40
20
0
CO_2
1600
1400
1200
1000
800
600
400
250
WAVENUMBER (cm^{-1})

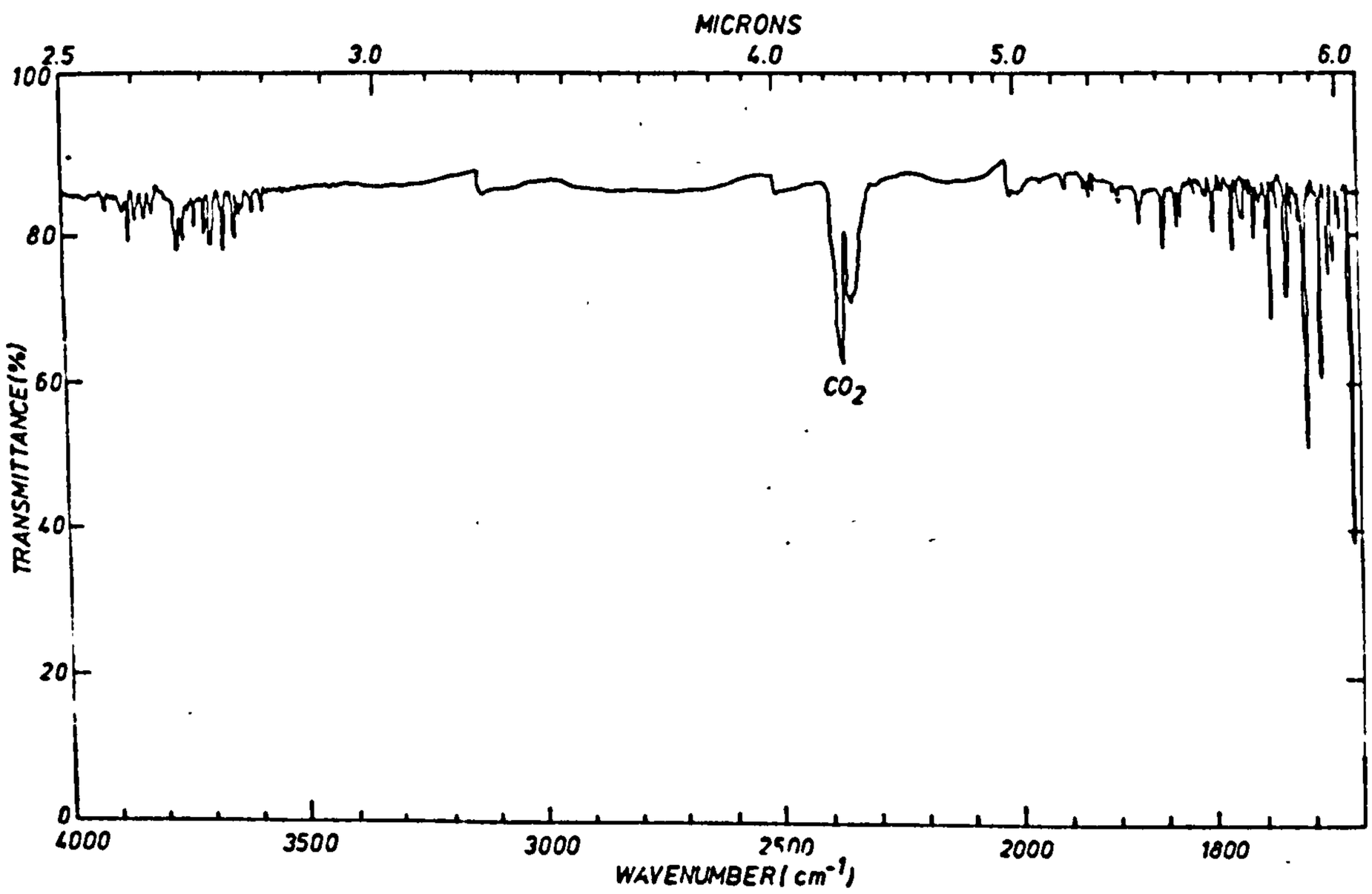
MICRONS
2.5
3.0
4.0
5.0
6.0
100
80
60
40
20
0
TRANSMITTANCE(%)
CO_2
4000
3500
3000
2500
2000
1800
WAVENUMBER (cm^{-1})

FIG. 26

THERMAL CONDUCTIVITY DETECTOR ARRANGEMENT

IN A CHROMATOGRAPH.

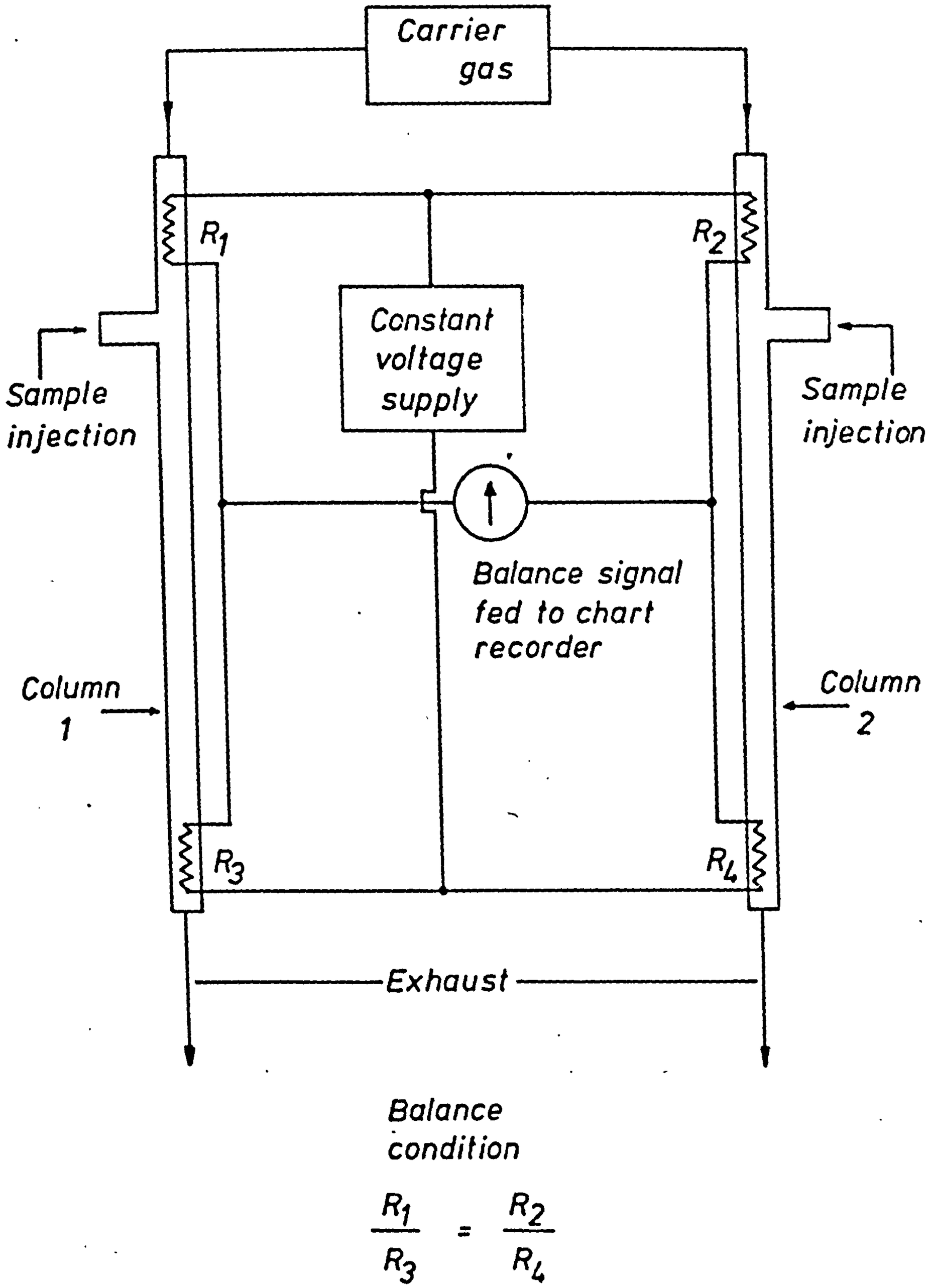

$$\frac{R_1}{R_3} = \frac{R_2}{R_4}$$

FIG. 27

A TYPICAL CHROMATOGRAM OF A GAS MIXTURE.

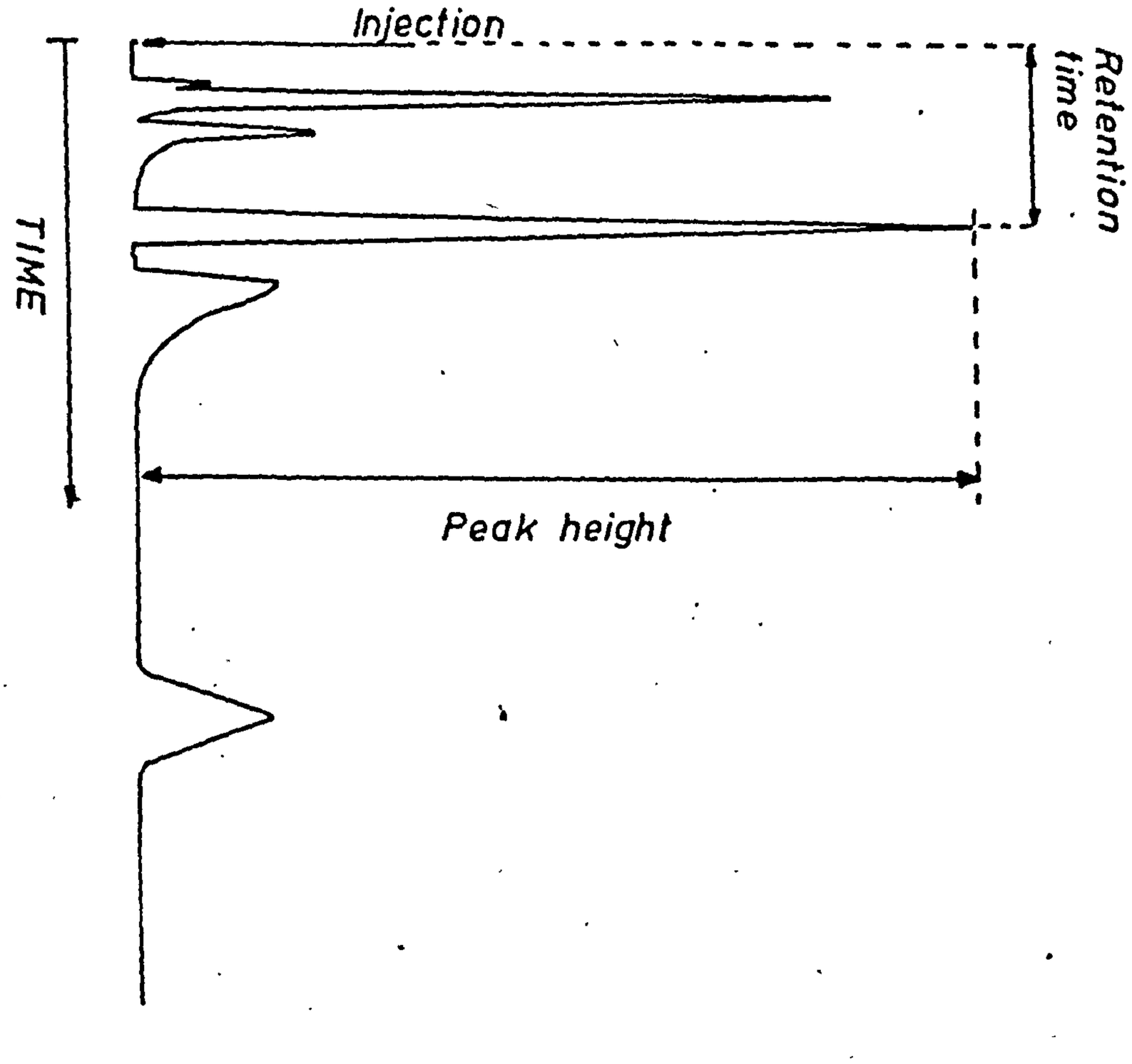
Injection
Retention time
TIME
Peak height

FIG. 28

EFFECT OF COLUMN TEMPERATURE ON RESPONSE OF A COATED PORAPAK Q COLUMN

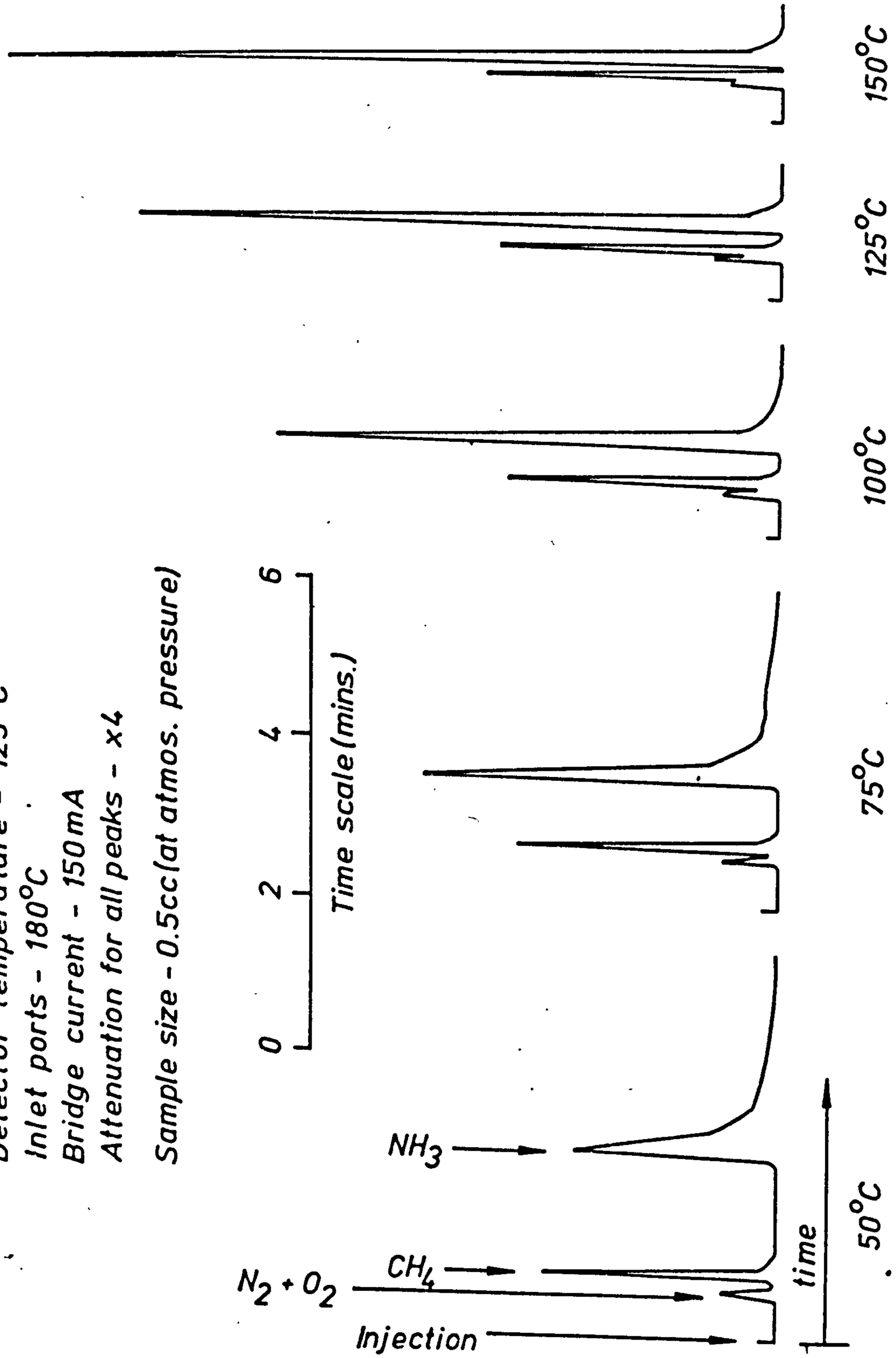
9' coated Porapak Q column (0.125" bore glass)
Hydrogen carrier gas - 17.5cc/min
Column temperature as indicated below
Detector temperature - 125°C
Inlet ports - 180°C
Bridge current - 150mA
Attenuation for all peaks - x4
Sample size - 0.5cc (at atmos. pressure)
0
2
4
6
Time scale (mins.)
NH3
N2 + O2
CH4
Injection
time
150°C
100°C
125°C
75°C
50°C
COLUMN TEMPERATURES

FIG. 29

EFFECT OF COATING OF PORAPAK Q COLUMN ON RESPONSE TO AMMONIA.

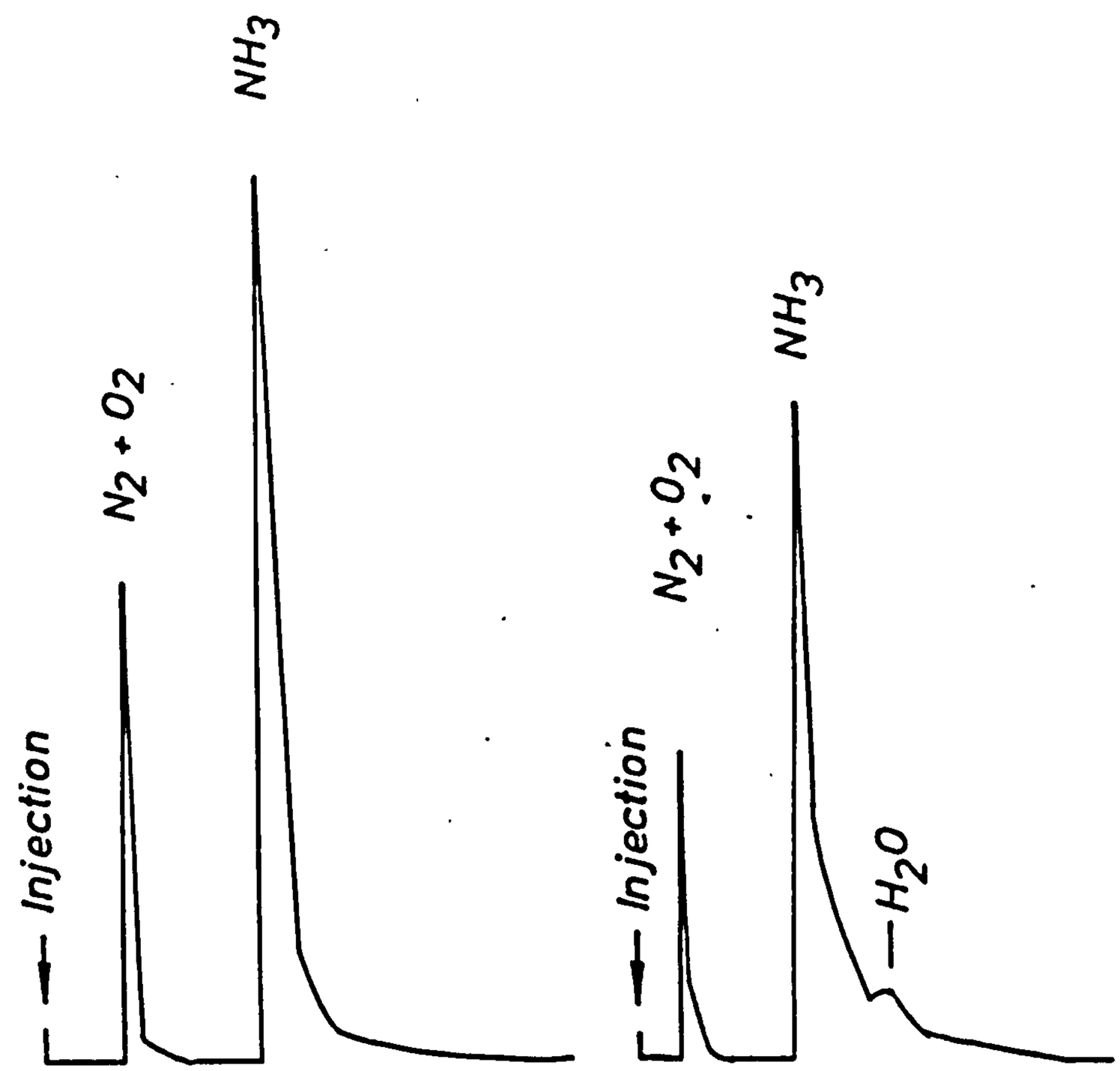

9' coated Porapak Q (glass column)

6' uncoated Porapak Q (stainless steel column)

Hydrogen carrier gas - 17.5cc/min
Column temperature - 75°C
Detector temperature - 150°C
Inlet ports - 150°C
Bridge current - 150 mA
Attenuation for all peaks - x2

Sample size - 0.5cc (at atmos. pressure)

FIG. 30

EFFECT OF BRIDGE CURRENT ON SENSITIVITY OF COATED PORAPAK Q COLUMN TO AMMONIA.

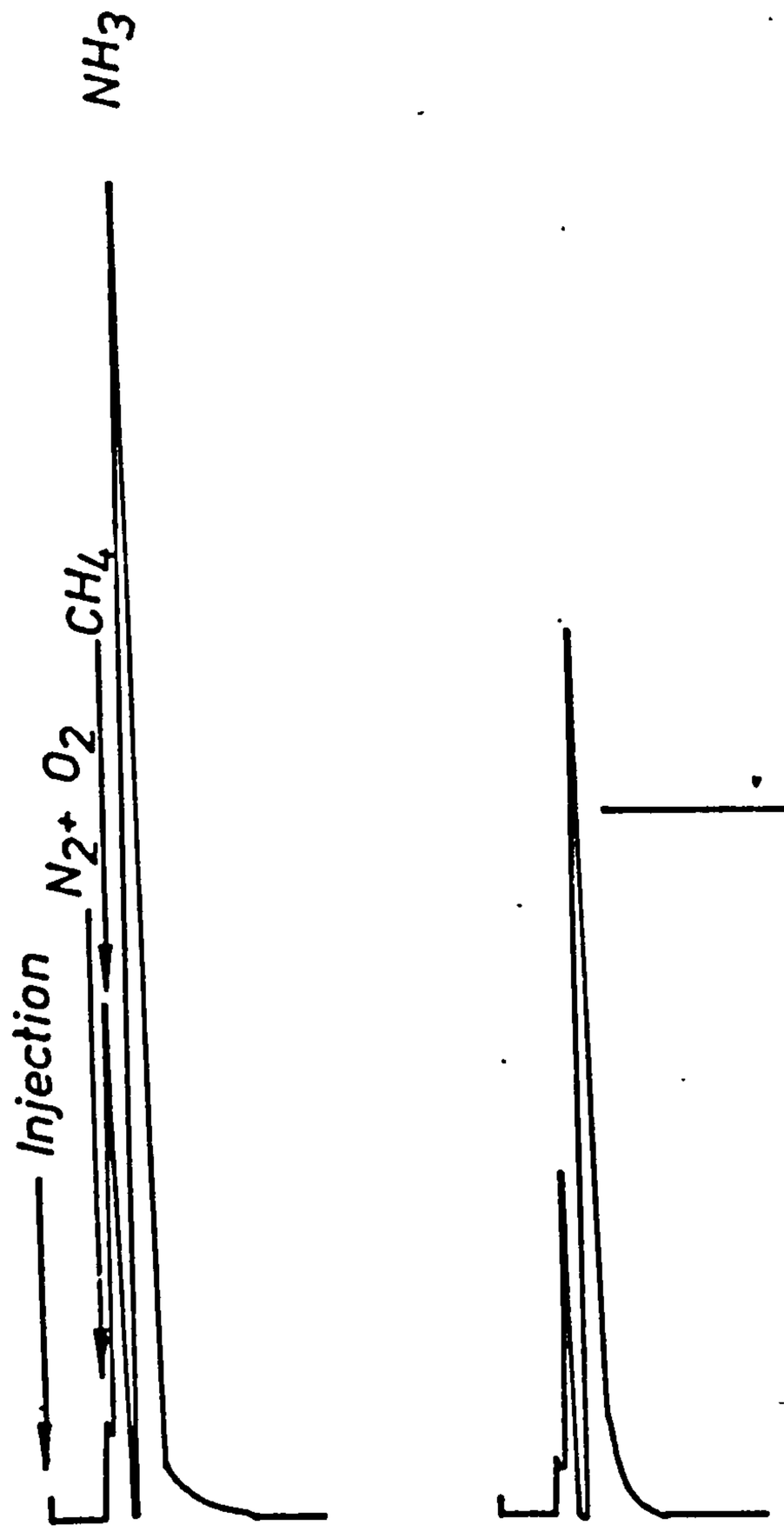

9' coated Porapak Q column (0.125" bore glass)
Hydrogen carrier gas - 17.5cc/min
Column temperature - 150°C
Detector temperature - 125°C
Inlet ports - 180°C

Sample size - 0.5cc (at atmos. pressure)

FIG. 31.

COMPARISON OF AMMONIA LEVELS DETECTED BY CHROMATOGRAPHY AND INFRA-RED GAS ANALYSIS.

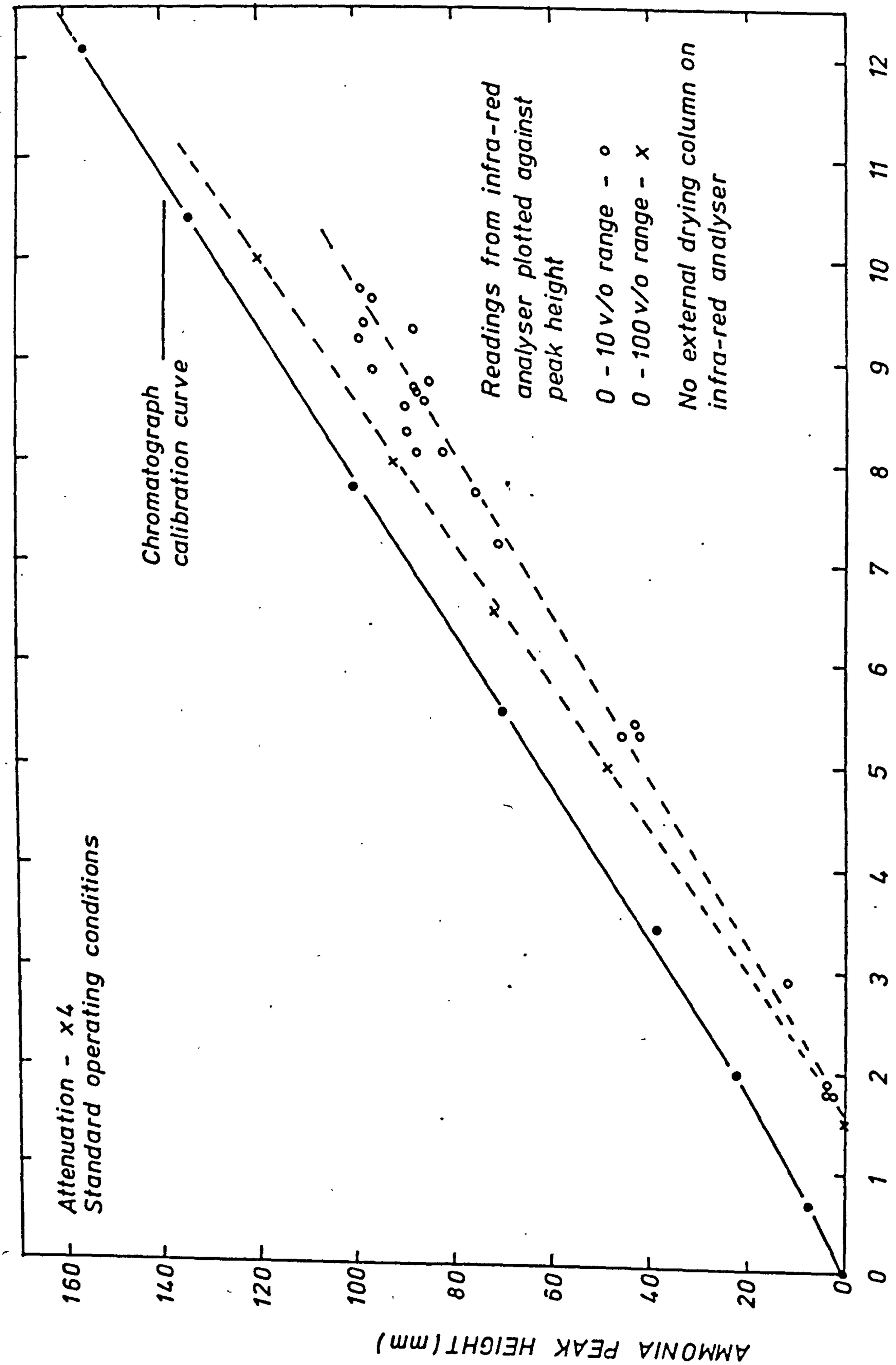
AMMONIA PEAK HEIGHT (mm)
AMMONIA (v/o)
Chromatograph calibration curve
Readings from infra-red analyser plotted against peak height
0 - 10 v/o range - o
0 - 100 v/o range - x
No external drying column on infra-red analyser
Attenuation - x4
Standard operating conditions

5.2 Electronprobe microanalysis for light elements.

The electronprobe microanalyser is a widely accepted tool for critical examination of phase compositions within metallic and non-metallic structures. The vast majority of published work quoting the use of such instruments has been concerned with detection and analysis of heavy elements (atomic number> 10), mainly due to limitations on equipment and experimental technique. In recent years however advances in equipment have been made and it is now possible[93,94] to detect and analyse down to boron (atomic number 4). This section deals with the considerations needed for light element analysis and is primarily concerned with the development of a quantitative method for the microanalysis of nitrogen.

5.2.1. Basis of microanalysis.

Microanalysis is based on X-ray spectrometry, a method of analysis which has been in use for many years and is readily adapted to microanalysis. X-ray spectrometry has been recently reviewed in depth [95] and its principle is illustrated in fig.32. X-radiation from a source unit is directed onto the sample to be analysed and radiation characteristic of the elements within the sample is excited. Part of this polychromatic radiation is selected by either a primary collumator or a source slit and directed onto a flat or curved analysing crystal respectively.

Depending on the 2d spacing of the analysing crystal, characteristic wavelengths (λ) are diffracted through a certain angle (θ) according to the Bragg relationship.

$$n\lambda = 2d \sin\theta \qquad (32)$$

where n is an integer, normally unity.

The diffracted beams at the various θ angles are collected by a detector and fed into an electronic counting system. To satisfy Bragg's law the angles of incidence and reflection must be the same and this is achieved in the spectrometer by simultaneously rotating the analysing crystal and detector.

In microanalysis, the sample is maintained under vacuum and a beam of electrons from a heated tungsten filament at between 10kv and 30kv is directed at right angles to the sample surface, characteristic x-radiation is then emitted from the sample surface and detected as just described. The spectrometer is usually based on system (b) shown in fig. 32 with interchangeable crystals covering a range of 2d spacings. The detector is usually a gas-flow proportional detector with an argon-10% methane mixture as the source gas and calibration by reference to pure element standards or standards of known composition.

5.2.2. Considerations for light element analysis.

5.2.2.1. Instrumental problems associated with low atomic number elements include the fact that the wavelength varies as the reciprocal of the square of the atomic number, so that to detect each element below atomic number 9 requires almost a doubling of the wavelength capability of the spectrometer, the wavelengths of the K spectra for such elements is shown in table 6. Special analysing crystals with large 2d spacing have now been developed to detect the long wavelengths, table 7, but some of the other problems must also be considered.

(a) as the atomic number decreases the depth of penetration of excited X-Rays also decreases dramatically such that penetration is only in the order of 1μ for atomic number 6, requiring the specimen standards to be very homogeneous.

(b) with low atomic number elements absorption is very high so that conventional detector windows are too thick to allow the radiation to pass. Consequently special thin windows, usually of polypropylene, in the order of 2000 to 10000 Å thick have been developed. These windows are now available as standard equipment on modern electronprobe microanalysis equipment(96,-98)

5.2.2.2. Calibration procedures.

Conventional microanalysis of the heavy elements relies on comparison of X-ray intensities of the element of interest in a matrix with X-ray intensities of the pure element - if available. Various correction procedures are required for very accurate analysis to compensate for absorption and atomic number effects of the element of interest in a particular matrix. Many models have been developed for these procedures and are fully detailed in a review by Martin and Poole(99); obviously the accuracy of these corrections depend on the availability accurate correcting data.

One of the major difficulties in applying such models to the analysis of light elements is that many of the mass absorption coefficients for the light elements are either unknown or are very inaccurate. With the advent of the new generation of electronprobe microanalysers specifically designed for light element analysis, attempts are now being made to determine the mass absorption coefficients for the light

elements. A recent paper by Scott [100] outlines some of the difficulties in applying these correction models to analysis of light elements and this is elaborated in more detail by Love etal[101,102] for oxygen using new data for mass absorption coefficients[103]. They concluded initially[101] the full Philibert model[104] provided the nearest approximation, but later[102] suggest that the Bishop model [105] is better. A modified correction model has also been investigated by Ruste and Gantois[106] with promising results.

As an alternative to using correction methods, it is possible to use a set of standards of known composition to cover the range of interest. It is necessary to use an identical matrix for the standards as that used in the specimen to be examined if accurate results are required. This type of procedure has been used successfully for carbon analysis in plain carbon and alloy steels[107-110], where it is relatively easy to produce homogeneous Fe-C standards.

Up to the present time no standards for nitrogen (solid solution in iron)are available; the only standards available being compounds such as boron nitride and silicon nitride.

5.2.2.3. Operational and experimental

Several further considerations are necessary before embarking on light element analysis.

(a) Absorption of radiation from light elements excited in a heavy element matrix is very high, so that it is necessary to reduce the standard operating voltage in the microprobe from 25kv to 10kv in order to reduce the penetration of the

electron beam. Thus excitation depth is very small and only a small portion of the excited radiation is absorbed. The effect of different operating voltages on the intensity of Oxygen K_α from various oxides can be seen in fig.3(100)

(b) Emitted X-ray intensities from light elements are low compared to heavy elements, so that it is necessary to increase the beam current by a factor of 3 or more compared with that normally used for heavy elements. This normally increases the spot size of the beam impinging on the specimen.

(c) Particularly when analysing for carbon, contamination must be minimised, by eliminating deposits of carbon on the specimen surface during preparation and more importantly eliminating contamination within the instrument. Even under vacuums of 10^{-5}mm Hg inside the specimen chamber it is still possible to have hydrocarbon vapour present from backstreaming diffusion pump oil. This can deposit on the specimen surface and be broken down to free carbon under the action of the electron beam. Various techniques are used from reducing the possibility of this contamination (1) using a minute gas jet (argon or nitrogen) to blow over the specimen surface(108) or more commonly (2) a 'cold finger'(107, 110-112) cooled by liquid nitrogen is placed adjacent to the specimen as a preferential site for oil vapour deposition. Commercial instruments designed for light element analysis are normally equipped with a cold finger attachment. (3) A further possibility is to improve the vacuum to the order of 10^{-7}mm Hg or better, but this is much more expensive and can only really be justified if the instrument is to be continually employed on light element work. T1 Research labs are (113) currently building an EMMA instrument (electron microscope and microanalyser) based on the better vacuum system.

(d) The surface to be analysed must be prepared as flat as possible to reduce errors due to absorption. Modern microanalysers use a higher take off angle for X-rays (35^{o}) to try to reduce these errors. Heavy etching can interfere with accurate detection of intensities, as well as etchants which contain an element which is being analysed.

Suitable analysing crystals for light element detection have already been shown in table 7, these are all artificially grown crystals based on fatty acid groups[114]. The most commonly used crystal is lead stearate, mainly because of its wide availability, but the larger 2d spacing crystals are becoming increasingly popular because of their increased selectivity. Some of these new crystals are reported to have better peak to background ratios than stearate for some elements[114].

5.2.3. Calibration procedure for light elements.

Because of the complexities of correction procedures and their inherent errors already explained in section 5.2.2.2., it was decided to base the calibrations for light elements on standards of known composition. Even this method has its drawbacks particularly in the case of nitrogen in iron where no standards existed and no attempts had been made to devise methods of producing standards. A calibration procedure for carbon based on the standards method has already been developed[107].

5.2.3.1. Calibration standards for nitrogen in iron.

High nitrogen contents ($> 0.03^{w}/o$) cannot be achieved in iron

by simple equilibration of iron with nitrogen gas, instead the ammonia decomposition reaction must be used[16]. A method of relating the nitrogen potential of this reaction to the nitrogen content of such a reacted sample has been developed by previous research in the department[2,35,115] and is also discussed further in chapter 6. Suitable standards and calibration procedure for (a) nitrogen in solid solution in iron (up to 2.47^{w}/o) and (b) nitrogen in compound form with iron (up to 12^{w}/o have been made using modifications to previously published procedures[116] and these are now described.

5.2.3.1.1. Standards for nitrogen in solid solution in iron.

Because of difficulties in obtaining homogeneous standards by nitriding of pure iron (further discussed in chapter 6) some standards were produced by a modified method involving simultaneous nitriding and decarburising of iron-carbon alloys (this is further discussed in chapter 7).

Table 8 shows the standards prepared for nitrogen in solid solution in iron and preparation conditions explained below.

The alloys in the form of 25 x 23 x 0.75 mm strip were nitrided under the conditions shown in table 8, standard no.5 was taken from the work of Farnell[3]. The nitrogen contents were checked by weight change, Kjeldahl analysis and emission spectrometry. Pieces from standards 1-4 were mounted edge on in Scandiplast resin, whilst standard no. 5 was mounted flat on an aluminium block. All the standards were carefully polished to 1 μ finish and thoroughly cleaned and degreased with carbon tetrachloride.

Standard no.6 for the limit of solubility of nitrogen in austenite at 780°C[35] was prepared as follows. A piece of spec-pure iron was nitrided for several hours at 780°C in $20^{v}/oNH_3/H_2$ and then quenched. Due to the high nitriding potential, ϵ-nitride was formed on the surface, in equilibrium with austenite containing $2.47^{w}/oN$[35] in the layer immediately below the nitride. The ϵ-nitride was carefully polished off the surface on a 1 μ wheel, leaving austenite containing $2.47^{w}/oN$ at the surface. The absence of ϵ-nitride and the presence of austenite of this composition was checked by X-ray diffraction using the data of Jack[76] and Bell[2]. This standard was mounted flat on an aluminium block.

5.2.3.1.2. Calibration results for nitrogen in solid solution in iron.

The standards were examined in a JEOL JXA50A instrument fitted with an anticontamination cold finger. The two spectrometers of the instrument were set up for light element analysis with myristate and stearate analysing crystals. Full operating details for microanalysis are given in table 9.

The calibration procedure followed is a standard precision microanalysis method whereby spot counts are made on various parts of the specimen under standardised operating conditions. With light element analysis, count rates are considerably lower than with heavy elements and so extended count times are necessary to allow, a reasonable number of counts to be accumulated. Normally a 100 second count time was used resulting in a minimum of ~2000 counts being accumulated for very low nitrogen levels.

Some initial experiments showed that the count rate was directly proportional to the specimen absorbed current, so that to take account of any variations in specimen current due to instrument drift, all count rates were normalised and expressed as cps/μA. To be strictly accurate, the normalisation should be made with respect to the actual electron beam current, as absorbed current varies with the average atomic number of the specimen[117]. However it is impractical to make this measurement, and normally absorbed current is used. The advantage with using absorbed current on the JEOL instrument, is that it can be readily measured and fed into the computor store attached to the instrument.

The count rates obtained from each of the standards are shown in table 10, with the computed means and standard deviations. These results are then plotted against nitrogen content of the standard in fig.34. A very good fit was obtained for the myristate crystal, but there was a lot of scatter obtained in the results from the stearate crystal. As calibrations were carried out simultaneously, one must discount variations due to the standards and conclude that they are due to the particular spectrometer and counting circuit.

The calibrations for both crystals show slight deviation from linearity. Two explanations for this deviation are possible, in addition to that of experimental scatter; these are (a) that nitrogen K_α radiation is absorbed in the specimen as nitrogen content increases (b) a possible shift in the K_α peak due to changes in bonding with increase in nitrogen content, although this would normally be expected to occur with iron-nitrogen compounds.

A large deviation from linearity in the calibration of a direct electron excitation X-ray spectrometer - the Betaprobe[118-120] - has been shown for nitrogen by Brand[121]. An O.H.M. crystal (octadecyl hydrogen maleate d = 31.68Å) was used to detect nitrogen in $NaNO_3$/graphite mixtures and the nitrogen count rate was shown to increase significantly with increase in nitrogen content of the mixture. This however is the opposite deviation to that observed in fig.34. It is most likely in Brand's work[121] that at low nitrogen levels, the nitrogen K_α radiation is absorbed by the graphite in the mixture, - present for conduction purposes - and the rate of absorption decreases with decreasing amount of graphite present.

This effect is particularly relevant to determination of nitrogen in iron and iron-carbon base alloys, because of the presence of carbon from both contamination and in solid solution. With light element detection, the cold finger is permanently employed to minimise contamination problems. Where contamination has been purposely allowed to build up, very little change has been found in the nitrogen count rate. No effect of dissolved carbon in amounts normally contained in steels has been found, e.g. standard no.3. containing $0.42^{w}/_{o}N$ and $1.0^{w}/_{o}C$ and standard no.4 containing $0.63^{w}/_{n}N$ and no carbon both lie on the same calibration lines. In addition counts for base nitrogen have been made on the three different carbon content alloys used in this work and virtually identical count rates were obtained, the very slight difference observed is due to the fact that the Fe-C alloys will contain some nitrogen picked up during melting and processing, a normal level to be expected is about 0.005%.

It has also been found that the position of the calibration curve shifts relative to the base line from day to day, so that it is necessary to check calibration standards during each period of operation. Fortunately the curve is almost linear and so it is only necessary to check several standards. It was originally thought that variations in counter gas flow rate could cause the calibration shift, but experiments showed that variations in flow rate between 0.3 l/h and 1.5. l/h had an insignificant effect on count rate.

The most likely explanation is that the shift is due to changes in vacuum in the system from day to day. Vacuum changes are particularly relevant to light element radiation, because different absorption rates can occur. It has been found that when using the instrument under the standard conditions described following a period of use without the cold finger, then calibration curve lies in position A (fig.35), whereas after a day's operation under standard conditions, the calibration moves to position B, and remains there with extended use of cold finger. It is therefore recommended that the cold finger should remain in continuous use in the instrument; this will maintain the best vacuum and also prevent deposition of the oil vapours on the X-ray counter window, which could cut down transmission of X-rays.

In this experiment the stearate crystal was used and the PHA settings altered to those normally used for the myristate crystal. A calibration much closer to that of myristate was obtained and in general use there has been much less scatter in results. This is advantageous as in normal use the instrument is set up with only one spectrometer for light element analysis and this

contains the stearate crystal.

5.2.3.1.3. Extension of Calibration for Iron-nitrogen compounds.

Whilst the primary interest of the project was to develop a microanalysis method for nitrogen levels normally encountered in carbonitriding or austenitic nitriding, it was a relatively simple exercise once a suitable operating procedure was developed to extend the calibration to the known limit of the Fe-N phase diagram.

The following standards were prepared to extend the calibration;

No.7 Fe-5.9^{w}/oN. This is the composition of the stoichiometric γ' nitride Fe_4N and was produced on the surface of pure iron strip by nitriding in 40^{v}/oNH_3/H_2 at 515^{o}C for 24 hours. The presence of Fe_4N was verified by X-ray diffraction. The specimen was mounted flat on an aluminium block and the surface used without any preparation apart from cleaning.

No.8 ϵ - carbonitride This compound is non-stoichiometric and was produced on the surface of pure iron strip by gaseous nitrocarburising in 50^{v}/oNH_3/50^{v}/o Endothermic (carburising) atmosphere at 570^{o}C for 3 hours. A 20μ thick layer of the compound is formed on the surface, previously being shown by microanalysis traces to be reasonably uniform in nitrogen content and chemically analysed to contain 8.25 $\pm$ 0.15^{w}/oN[122]. A cross section of this standard was used, polished but unetched.

No. 9 ϵ-nitride. This compound is also non-stoichiometric and was produced on the surface of pure iron strip by nitriding in 80^{v}/oNH_3/H_2 at 520^{o}C for 48 h. These conditions were designed to give an ϵ-nitride near to its terminal composition Fe_2N (11^{w}/oN at 520^{o}C[123]). The specimen was mounted flat on an aluminium block and the surface was used without any

preparation apart from cleaning. X-ray diffraction showed that the compound contained at least 9^{w}/oN with reference to Jack's data [123].

5.2.3.1.4. Calibration results for iron-nitrogen compounds.

Using the same operating conditions as for nitrogen solid solution standards, countrates were obtained for nitrogen contents up to 12^{w}/oN, these are shown in table 11 and the calibration is shown in fig.36. A high degree of confidence can be placed on the calibration up to 8.25^{v}/oN which is linear. If the calibration is extended to the ϵ-nitride compound, assuming linearity then the estimated nitrogen content is 10.2^{w}/o. Some degree of error can be expected on this compound as there is quite likely to be a composition gradient through the compound layer[123]. Because of the X-ray voltage used (35kv), penetration of the layer by the X-ray beam occurred, evidenced by occurrence of ferrite peaks on the diffractometer trace, and so only a mean estimate of the composition of the layer can be obtained. In the case of the electron beam in the microanalyser, a 10kv source is used and the penetration is much less, thereby indicating a high composition at the outermost parts of the compound layer.

The count rate from the nitrocarburised specimen (standard no.7) indicates that the presence of carbon in the compound layer (up to 2.5^{w}/o) has no effect on absorption of nitrogen K_{α} radiation. A count rate was also determined for ferrite just below the surface of the compound layer. The nitrogen content is estimated at 0.08^{w}/o from the phase diagram at this temperature and the result readily fits the calibration for nitrogen in solid solution in iron (fig.34).

In section 5.2.3.1.2. it was noted that changes in average atomic number (Z) can affect the specimen absorbed current. This effect was suggested by Heinrich[117] as a method of analysing binary alloys provided atomic number differences were large. Using Heinrich's data [117], the variation in absorbed current for average atomic numbers of a series of Fe-N binary alloys (table 12) is shown to be small. This small variation over short atomic number changes is also confirmed by the data of Harris etal[124], who used the method to analyse oxygen levels in Tantalum oxides where large changes in average atomic number were necessary to obtain accuracy.

Using standard no. 8 the absorbed current was monitored in changing from the ϵ-carbonitride compound layer ($Z \simeq 24$) to the ferrite layer ($Z = 26$); no measureable change was found, confirming the above data.

5.2.3.2. Calibration standards for carbon in iron. Following the techniques used by previous workers[107-110], a series of homogeneous Fe-C standards were made from the alloys used throughout the work (table 3). The alloys in the form of specimens 25 x 23 x 0.76 mm, were heat treated for 1 h at 850°C in vacuum and quenched into oil. Pieces from each alloy together with a piece of spec-pure iron were mounted together in cross section in Scandiplast resin and prepared metallographically to a 1μ finish.

5.2.3.2.1. Calibration results for carbon in iron. Using the stearate crystal, count rates were obtained from each of the standards in the unetched condition, table 13, and the

resulting calibration is shown in fig. 37, the standard microanalysis conditions are also shown on the figure.

The linear calibration confirms that obtained by previous workers[107-110] and linearity has also been shown to exist up to Fe_3C composition ($6.67^{W}/oC$) confirming the work of Kolhaas[110] and Anderson [125].

Problems with contamination build-up are experienced when analysing for carbon. This contamination can be minimised by careful specimen preparation, it is also important that when a specimen is mounted in a plastic resin, not to move the beam onto the resin, as carbon is released due to localised melting. Even when all precautions possible are taken, and after extended use of cold finger, contamination build-up is still experienced, but the rate is much lower than that obtained without the cold finger in use. With no cold finger, the contamination rate is approximately $2^{W}/oC/min$, reduced to approximately $0.15^{W}/oC/min$ with the cold finger.

Even so there was still an appreciable build-up of carbon when analysing for low carbon levels. This contamination rate should be further cut down by fitting a liquid nitrogen baffle to the diffusion pump.

5.2.4. Examples of the use of the calibrated microanalyser. As was previously mentioned the primary interest in the micro-analyser was to develop a calibration method to determine nitrogen in solid solution in iron. Because of the very low count rates, accurate nitrogen levels ($<3^{W}/o$) can only be determined by the point counting method developed in this work.

An example of profile determination by this method is shown in fig. 38 where the nitrogen profile of a piece of nitrided pure iron strip has been determined.

Analysis was started at least 10 μ from the free edge to prevent burning of the mounting compound, and to avoid any problems associated with bevelling of edges during specimen preparation. The nitriding potential used was sufficient to form an austenite phase which penetrates into the ferrite matrix. The shape of the diffusion profile obtained being characteristic of a compositionally dependent diffusion coefficient[126]. An average D_γ^N value of $1.8 \times 10^{-8} cm^2/sec$ calculated from this data compares with a value of $5.7 \times 10^{-9} cm^2/sec$ extrapolated from the data of Grieveson and Turkdogan[127]. Because of the relatively large spot size used, the composition at the actual austenite/ferrite interface is difficult to determine, but values very close to the phase composition limit of $0.46^w/_oN$ are obtained.

For large nitrogen contents and other interstitial contents, continuous profile analysis can be made by moving the specimen under a stationary beam by means of the stepping motors attached to the instrument specimen stage. Such profiles have been determined for nitrogen, carbon and oxygen in the compound layers of EN32 material which has been treated under various nitrocarburising heat treatments[128]. These profiles are shown in fig.39, all countrates were converted using the previously determined calibrations, in addition oxygen was referenced against count rates determined on heavily oxidised iron with the three oxides FeO, Fe_2O_3 and Fe_3O_4, sulphur was referenced against an FeS_2 standard.

The relative performace of the myristate and stearate crystals at high and low nitrogen levels was checked by simultaneous continuous profile determination of nitrogen on the gaseous nitrocarburised standard (no.8). The result is shown in fig.40 the standard operating conditions set out in table 9 being used for both sets of results (fig.39 and fig.40.). The specimen scan rate was 10μ/min traversing from inside the compound layer towards the outside of the specimen to avoid disturbing the mounting compound. The results in fig.40 show that the myristate crystal has a better peak to background ratio than the stearate crystal, but the performance of the stearate crystal can be improved by using the same PHA settings as for myristate.

TABLE 6

WAVELENGTHS OF LOW ATOMIC NUMBER ELEMENTS.

Atomic No.	Element	Wavelength (Å)
9	F	18.31
8	O	23.71
7	N	31.60
6	C	44.00
5	B	67.00

TABLE 7

CRYSTALS FOR LIGHT ELEMENT DETECTION

Crystal.	Chemical Formula	Spacing (2d Å)	Wavelength Range Å	Element Range K	L
Myristate	$M(C_{14}H_{27}O_2)_2$	79	18 - 71	B_5-F_9	Cl_{17}-Mn_{25}
Stearate	$M(C_{18}H_{35}O_2)_2$	98	22 - 89	B_5-O_8	S_{16} -V_{23}
Lignocerate	$M(C_{24}H_{47}O_2)_2$	125	26 - 113	Be_4-N_7	P_{15}-Se_{21}
Cerotate	$M(C_{26}H_{51}O_2)_2$	137	31 - 124	Be_4-N_7	S_{14}-Ca_{20}
Melissate	$M(C_{30}H_{59}O_2)_2$	156	35 - 141	Be_4-C_6	S_{14}-K_{19}

M = bivalent cation e.g. Ba, Pb.

TABLE 8

EPMA STANDARDS FOR NITROGEN IN SOLID SOLUTION IN IRON

Standard No.	Nitrogen (w/o)	Alloy	Temperature (°C)	Atmosphere	Time (h)	Thickness (mm)
1	0	Spec Pure Fe	——— UNTREATED ———			0.75
2	0.11	Fe-0. 83%C	930	$5\%NH_3/H_2$	8.3	"
3	0.42	Fe-0. 5%C	845	$20\%NH_3/3\%CH_4/H_2$ (a)	21	"
4	0.63	"	811	$5\%NH_3/H_2$	24	"
5	1.10	Spec Pure Fe	780	$4\%NH_3/H_2$	4	0.1
6	2.47 (b)	" " "	"	$20\%NH_3/H_2$	2	0.75

(a) Methane used for back-up carbon potential, giving 1% carbon in centre of alloy.

(b) see text

All specimens quenched in brine from treatment temperature.

TABLE 9

DETAILS OF JXA-50A MICROANALYSER OPERATING CONDITIONS.

Accelerating voltage	10KV
Specimen Current	0.08 μA

Pulse Height Analyser (ORTEC)	Myristate	Stearate
GAIN	32 x 4	16 x 4
WINDOW	2.5 Volts	2.0 Volts
LOWER LEVEL	0.5 Volts	0.5 Volts
MODE	DIFFERENTIAL	DIFFERENTIAL

Counter.	Gas filled proportional 10%CH_4/Argon flowing at 1.41/h
Window	Grid supported 2000Å thick polypropylene - 1mm slit.
Voltage	1700

TABLE 10 (a)

COUNT RATES FOR NITROGEN IN SOLID SOLUTION IN IRON.

Standard	Absorbed Current ($x10^{8}$A)	Count Time (sec)	Counts Accumulated		cps/μA	
			Myristate	Stearate	Myristate	Stearate
	7.80	100	2063	2896	265	371
	"	"	2129	3330[x]	273	427[x]
	"	"	2079	2849	266	365
	7.90	"	2177	2868	276	363
	"	"	2171	3039	275	385
1	8.00	400	9247	12097	289	378
	7.90	100	2227	2988	282	378
O^{W}/oN	8.00	"	2252	2881	282	360
	"	"	2258	2961	282	370
	"	400	8704	11542	272	361
	"	800	17265	22807	270	356
	"	100	2126	2835	266	354
	"	"	2089	2814	261	352
	"	"	2109	2867	264	358
	"	"	2132	2889	267	361
	8.10	"	2133	2798	263	345
	"	"	2087	2767	258	341
	"	"	2095	2875	259	355
	"	"	2265	2884	280	356
	"	"	2175	2963	269	366
	"	"	2150	2916	265	360
	"	400	8577	11571	265	357
			Mean		270.4	361.5
			Std. dev.		8.48	10.66

[x] NOT INCLUDED IN AVERAGE.

TABLE 10 (b)

COUNT RATES FOR NITROGEN IN SOLID SOLUTION IN IRON

Standard	Absorbed Current ($\times 10^{-8}$A)	Count Time (sec)	Counts Accumulated		cps/μA	
			Myristate	Stearate	Myristate	Stearate
	7.40	100	2189	3040	296	411
	7.50	"	2186	3106	291	414
	"	"	2232	3017	298	402
	"	"	2215	3008	295	401
	"	"	2196	3031	293	404
	"	400	8775	11913	293	397
	7.30	100	2127	2857	291	391
	"	"	2130	2918	292	400
2	7.20	"	2015	2979	280	414
	"	"	2058	2817	286	391
0.11 W/oN	"	"	2109	2850	293	396
	6.80	400	8290	11519	305	423
	6.70	100	1978	2664	295	398
	6.60	"	1932	2580	293	391
	6.70	"	1877	2648	280	395
	6.50	"	1933	2595	297	399
	"	"	1873	2548	288	392
	7.55	"	2162	2923	286	387
	"	"	2136	2762	283	366
	"	"	2133	2781	283	368
	7.60	400	8830	11705	290	385
	7.50	"	8658	11246	289	375
		Mean			290.8	395.5
		Std. dev.			6.13	14.09

TABLE 10 (c)

COUNT RATES FOR NITROGEN IN SOLID SOLUTION IN IRON

Standard	Absorbed Current ($\times 10^{8}$A)	Count Time (sec)	Counts Accumulated		cps/μA	
			Myristate	Stearate	Myristate	Stearate
	8.50	100	2835	3357	334	395
	"	"	2813	3499	331	412
	"	"	2770	3543	326	417
	"	"	2906	3401	342	400
3	8.65	800	22890	27485	331	397
$0.42^{W}/_{oN}$	8.70	100	3012	3539	346	407
	"	"	2907	3600	334	414
	"	"	2991	3547	344	408
			Mean		336.0	406.3
			Std. Dev.		7.15	8.14

TABLE 10 (d)

COUNT RATES FOR NITROGEN IN SOLID SOLUTION IN IRON

Standard	Absorbed Current ($\times 10^{-8}$A)	Count Time (sec)	Counts Accumulated		cps/μA	
			Myristate	Stearate	Myristate	Stearate
	8.60	100	3065	4010	356	466
	"	"	3040	3936	353	458
	"	"	3162	3949	368	459
	"	"	2996	3768	348	438
	"	"	2919	3917	339	455
4	8.20	"	3656[x]	3831	446[x]	467
0.63[w]/oN	"	"	3031	3844	370	469
	"	"	2902	3812	354	465
	"	400	11888	15026	362	458
	8.00	100	2927	3715	366	464
	7.90	"	3035	3756	384	475
	"	"	3010	3696	381	468
	"	"	2866	3906	363	494
	"	"	2874	3730	364	472
	"	"	2842	3569	360	452
	7.80	"	2728	3371	350	432
	"	"	2785	3528	357	452
	"	"	2797	3528	359	452
		Mean			360.8	460.9
		Std. dev.			11.27	13.88

[x]Not included in average.

TABLE 10 (e)

COUNT RATES FOR NITROGEN IN SOLID SOLUTION IN IRON

Standard	Absorbed Current ($x10^{8}$A)	Count Time (sec)	Counts Accumulated		cps/μA	
			Myristate	Stearate	Myristate	Stearate
5 $1.1^{W}/_{oN}$	8.30	100	3581	4023	431	485
	"	"	3566	4078	430	491
	"	"	3619	4024	436	485
	8.00	"	3479	4044	435	506
	8.10	"	3514	3978	434	491
	8.00	400	13966	15946	436	498
			Mean		433.7	492.7
			Std.dev.		2.58	8.12

TABLE 10 (f)

COUNT RATES FOR NITROGEN IN SOLID SOLUTION IN IRON

Standard	Absorbed Current ($\times 10^{-8}$ A)	Count Time (sec)	Counts Accumulated		cps/μA	
			Myristate	Stearate	Myristate	Stearate
	8.00	100	4853	5105	607	638
	7.90	"	4790	5067	606	641
	"	"	4998	5346	633	677
	"	"	4945	5209	626	659
	"	"	4639	5021	587	636
	"	"	4691	4965	594	628
6	8.00	"	4810	5106	601	638
2.47 w/o N	"	"	4640	5110	580	639
	"	"	4627	4905	578	613
	"	"	4607	4858	576	607
	"	"	4780	5035	598	629
	"	"	4754	5169	594	646
	7.80	"	4802	5190	616	665
	7.70	400	18843	19997	612	649
	"	100	4367	4754	567	617
	"	"	4342	4748	564	617
	"	"	4396	4675	571	607
	7.60	400	18930	20117	623	662
			Mean		596.3	637.1
			Std. dev.		20.95	20.18

TABLE 10 (g)

COUNT RATES FOR NITROGEN IN SOLID SOLUTION IN IRON

Standard	Absorbed Current ($x10^{8}$A)	Count Time (sec)	Counts Accumulated		cps/μA	
			Myristate	Stearate	Myristate	Stearate
Iron	6.70	100	1867	2560	279	382
Ferrite in Nitrocarburised 0.08 w/oN	6.50	"	1761	2502	271	385
	"	"	1868	2429	287	374
	"	"	1829	2507	281	386
	5.95	400	7078	9761	297	410
	7.90	"	2251	3003	285	380
	"	"	2263	3038	286	385
	"	"	2293	3028	290	383
			Mean		284.5	385.6
			Std. dev.		7.75	10.57

TABLE 11 (a)

COUNT RATES FOR NITROGEN IN IRON UP TO $12^{w}/o$

Standard	Absorbed Current ($x10^{8}A$)	Count Time (sec)	Counts Accumulated Stearate	cps/μA Stearate
No.7 γ' Nitride $5.9^{w}/oN$	7.70	40	2850	925
	"	"	3401	1104
	"	"	3079	1000
	7.60	"	2910	957
	7.50	"	3248	1082
	"	"	3317	1106
	7.30	100	7404	1014
	7.10	"	7238	1019
	7.20	"	7539	1047
	7.00	"	7709	1101
	7.80	"	8408	1078
			Mean	1039
			Std. dev.	61.85.

TABLE 11 (b)

COUNT RATES FOR NITROGEN IN IRON UP TO 12^{W}/o

Standard	Absorbed Current ($x10^{8}$A)	Count Time (sec)	Counts Accumulated		cps/μA	
			Myristate	Stearate	Myristate	Stearate
No. 8 ∈ - Carbonitride $Fe_{2-3}(CN)$ 8.25^{W}/oN	5.70	20	1556	1397	1365	1225
	5.60	200	13936	13543	1244	1209
	"	"	14005	13760	1250	1229
	7.60	"	17484	16238	1150	1068
	5.60	20	1521	1432	1358	1273
	"	"	1512	1414	1350	1205
	"	"	1481	1398	1322	1180
	"	"	1484	1320	1325	1179
	"	"	1396	1349	1246	1204
	"	"	1413	1408	1262	1128
	"	"	1426	1317	1273	1137
	"	"	1431	1270	1278	1141
			Mean		1285.3	1181.5
			Std. dev.		62.00	55.36

TABLE 11 (c)

COUNT RATES FOR NITROGEN IN IRON UP TO 12^{W}/o

Standard	Absorbed Current ($x10^{8}$A)	Count Time (sec)	Counts Accumulated		cps/μA	
			Myristate	Stearate	Myristate	Stearate
	8.50	100	14605	13716	1718	1614
	"	"	13421	12461	1579	1466
	"	"	12942	13746	1523	1617
	8.70	"	13004	13489	1495	1550
	"	"	12931	13631	1486	1567
	"	"	12764	13399	1467	1540
	8.80	"	12778	13745	1452	1561
	"	"	14986	12761	1703	1450
	"	"	14639	12806	1663	1455
	"	"	14121	13433	1605	1526
	"	"	14592	14516	1658	1650
	"	"	14266	14788	1621	1680
	8.60	"	14044	11439	1633	1330
	8.65	"	14264	13192	1649	1525
	8.60	"	13483	14279	1568	1660
	"	"	14993	14076	1743	1638
	8.10	"	13129	11636	1621	1437
	7.60	"	11591	11760	1525	1547
	7.70	"	10785	10678	1401	1387
	7.80	"	11298	12999	1448	1667
	"	"	12545	11555	1608	1481
	8.40	"	12686	12341	1510	1469
	"	"	13724	13678	1634	1628
			Mean		1578.7	1541.0
			Std.dev.		94.10	95.38

No. 9 ∈ - Nitride Fe_2N 11.14^{W}/o N

TABLE 12

AVERAGE ATOMIC NUMBER (Z) AND COMPARATIVE ABSORBED CURRENTS FOR A SERIES OF Fe-N ALLOYS.

	Z	ABSORBED CURRENT^{+} x 10^{8}	
Pure Fe	26.00	7.29	for z = 26
Fe - $1^{W}/_{oN}$	25.81		
Fe - $2^{W}/_{oN}$	25.62		
Fe - $5^{W}/_{oN}$	25.05	7.37	for z = 25
Fe - $10^{W}/_{oN}$	24.10	7.46	" " " 24

$^{+}$ Based on an absorbed current of 7.13 x 10^{-8}A on a Nickel standard (z = 28)[117]

TABLE 13(a)

EPMA STANDARDS FOR CARBON IN IRON

Standard	Absorbed Current ($x10^{-8}$A)	Count Time (sec)	Counts Accumulated Stearate	cps/μA Stearate
Pure Fe. $0^{W}/_{oC}$	7.15	40	951	333
	"	"	1114	389
	"	"	873	305
	7.18	"	999	348
	7.15	"	963	336
	"	"	900	314
	"	"	1057	370
	4.40	"	1025	582
	4.38	"	641	366
	"	"	666	381
	4.35	"	591	339
	"	"	724	416
	"	"	607	349
	"	"	576	331
	"	"	604	347
	"	"	533	306
	"	"	652	375
	"	"	571	328
	"	"	521	300
			Mean	347.0
			Std. dev.	31.0

TABLE 13 (b)

EPMA STANDARDS FOR CARBON IN IRON

Standard	Absorbed Current ($x10^{8}$A)	Count Time (sec)	Counts Accumulated Stearate	cps/μA Stearate
Fe- 0.5^{W}/oC.	6.98	40	1386	497
	"	"	1445	518
	"	"	1413	506
	"	"	1352	485
	"	"	1551	556
	"	"	1417	508
	4.35	"	923	530
	"	"	808	464
	4.38	"	988	565
	4.40	"	924	524
	"	"	908	516
	4.43	"	909	513
	4.45	"	927	520
			Mean	515.5
			Std. dev.	26.6

TABLE 13 (c)

EPMA STANDARDS FOR CARBON IN IRON

Standard	Absorbed Current ($x10^{-8}$A)	Count Time (sec)	Counts Accumulated Stearate	cps/μA Stearate
Fe - 0.87 W/oC	7.05	40	1853	656
	"	"	1790	634
	"	"	1750	620
	"	"	1890	670
	"	"	1751	620
	4.50	"	1215	675
	4.53	"	1289	712
	4.55	"	1175	646
	"	"	1211	666
	4.58	"	1259	689
		Mean		658.8
		Std. dev.		29.8

TABLE 13(d)

EPMA STANDARDS FOR CARBON IN IRON

Standard	Absorbed Current ($x10^{-8}$A)	Count Time (sec)	Counts Accumulated Stearate	cps/μA Stearate
Fe - 1.06 w/o C	6.95	40	1873	673
	"	"	1962	706
	"	"	1939	697
	"	"	1940	697
	"	"	1970	708
	4.50	"	1335	740
	"	"	1270	705
	"	"	1292	717
	"	"	1293	717
	"	"	1238	687
		Mean		704.7
		Std. dev.		18.3

TABLE 13 (e)

EPMA STANDARDS FOR CARBON IN IRON

Standard	Absorbed Current ($x10^{-8}$A)	Count Time (sec)	Counts Accumulated Stearate	cps/μA Stearate
Fe - 1.07% C	7.0	40	2155	769
	"	"	2051	732
	"	"	1995	712
	"	"	2061	736
	"	"	2037	728
	4.53	"	1332	737
	4.55	"	1253	688
	"	"	1303	716
	"	"	1408	774
	"	"	1400	770
		Mean		736.2
		Std. dev.		28.0

FIG. 32

GEOMETRY OF CONVENTIONAL X-RAY SPECTROMETERS[95]

(a) FLAT-CRYSTAL SYSTEM

(b) CURVED-CRYSTAL SYSTEM.

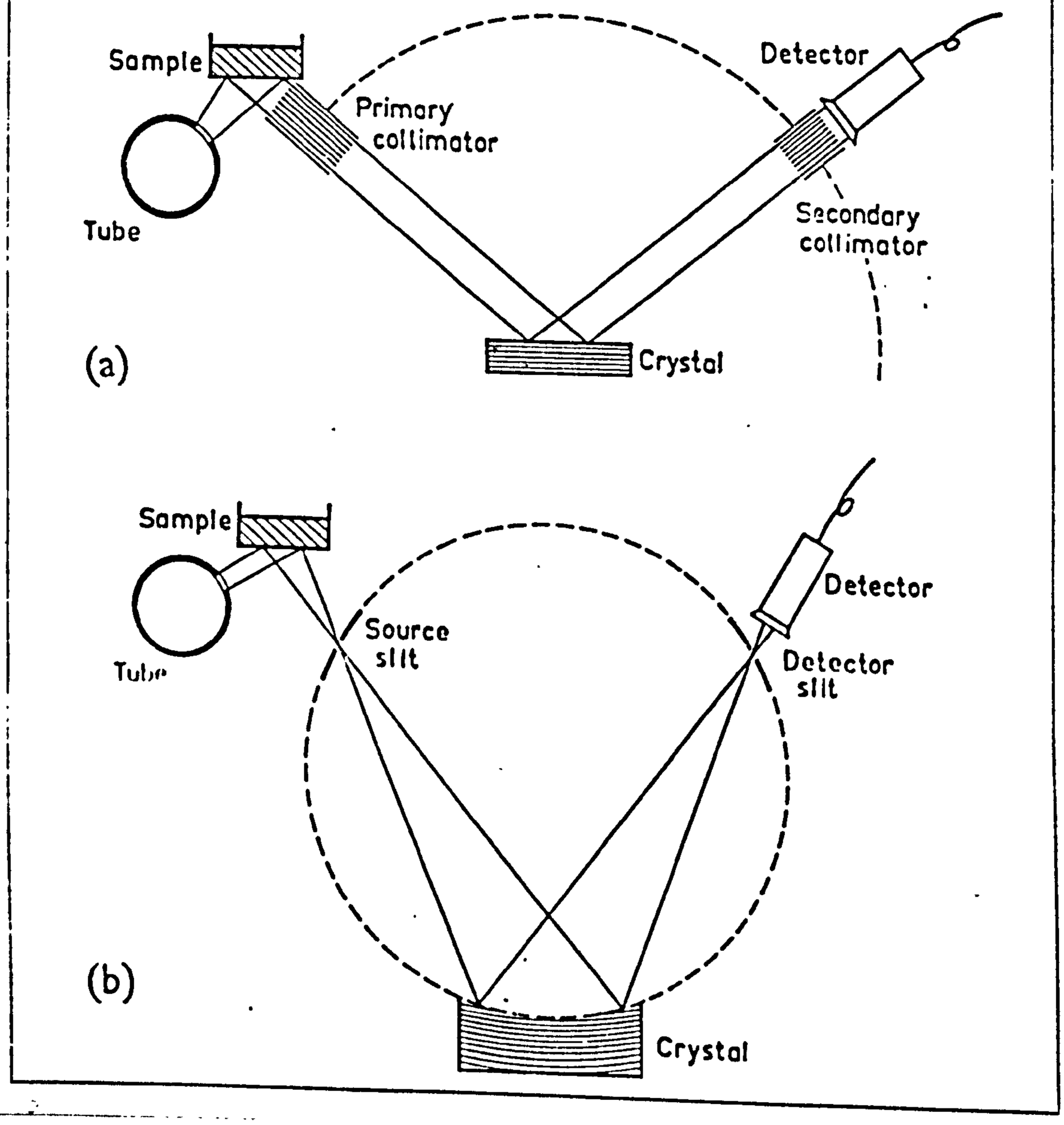
Sample
Primary collimator
Detector
Tube
Secondary collimator
Crystal
(a)
Sample
Source slit
Detector
Tube
Detector slit
Crystal
(b)

FIG. 33

VARIATION OF OXYGEN K_α X-RAY INTENSITY WITH PROBE VOLTAGE FOR DIFFERENT OXIDES (100)

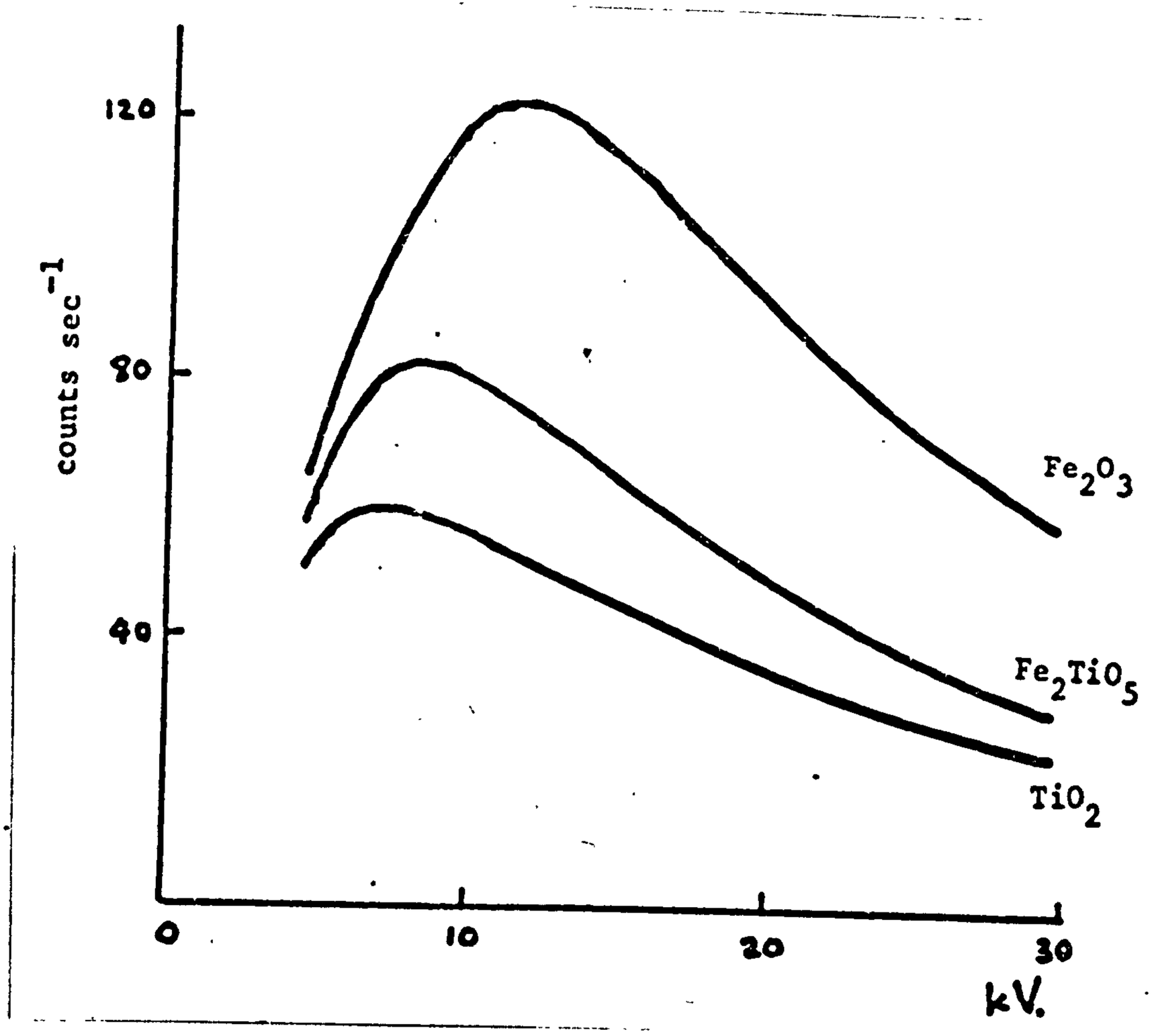
120
80
40
counts sec^{-1}
Fe_2O_3
Fe_2TiO_5
TiO_2
0
10
20
30
kV.

FIG. 34

CALIBRATION OF JXA-50A MICRO ANALYSER FOR NITROGEN IN SOLID SOLUTION IN IRON.

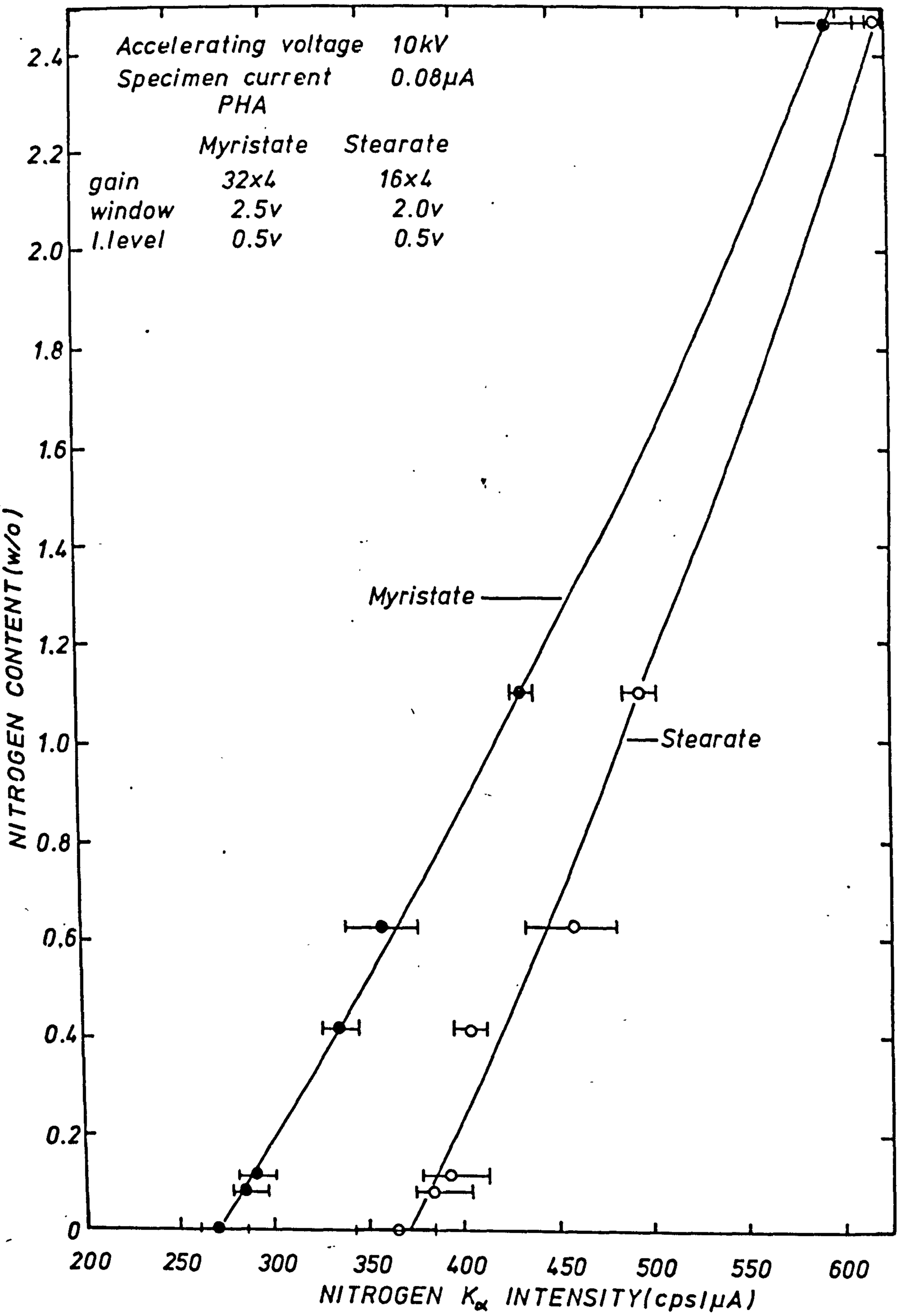
Accelerating voltage 10kV
Specimen current 0.08μA
PHA
Myristate Stearate
gain 32x4 16x4
window 2.5v 2.0v
l.level 0.5v 0.5v
Myristate
Stearate
NITROGEN CONTENT (w/o)
2.4
2.2
2.0
1.8
1.6
1.4
1.2
1.0
0.8
0.6
0.4
0.2
0
200
250
300
350
400
450
500
550
600
NITROGEN Kα INTENSITY(cps/μA)

FIG. 35.

SHIFT OF NITROGEN CALIBRATION WITH USE OF COLD FINGER.

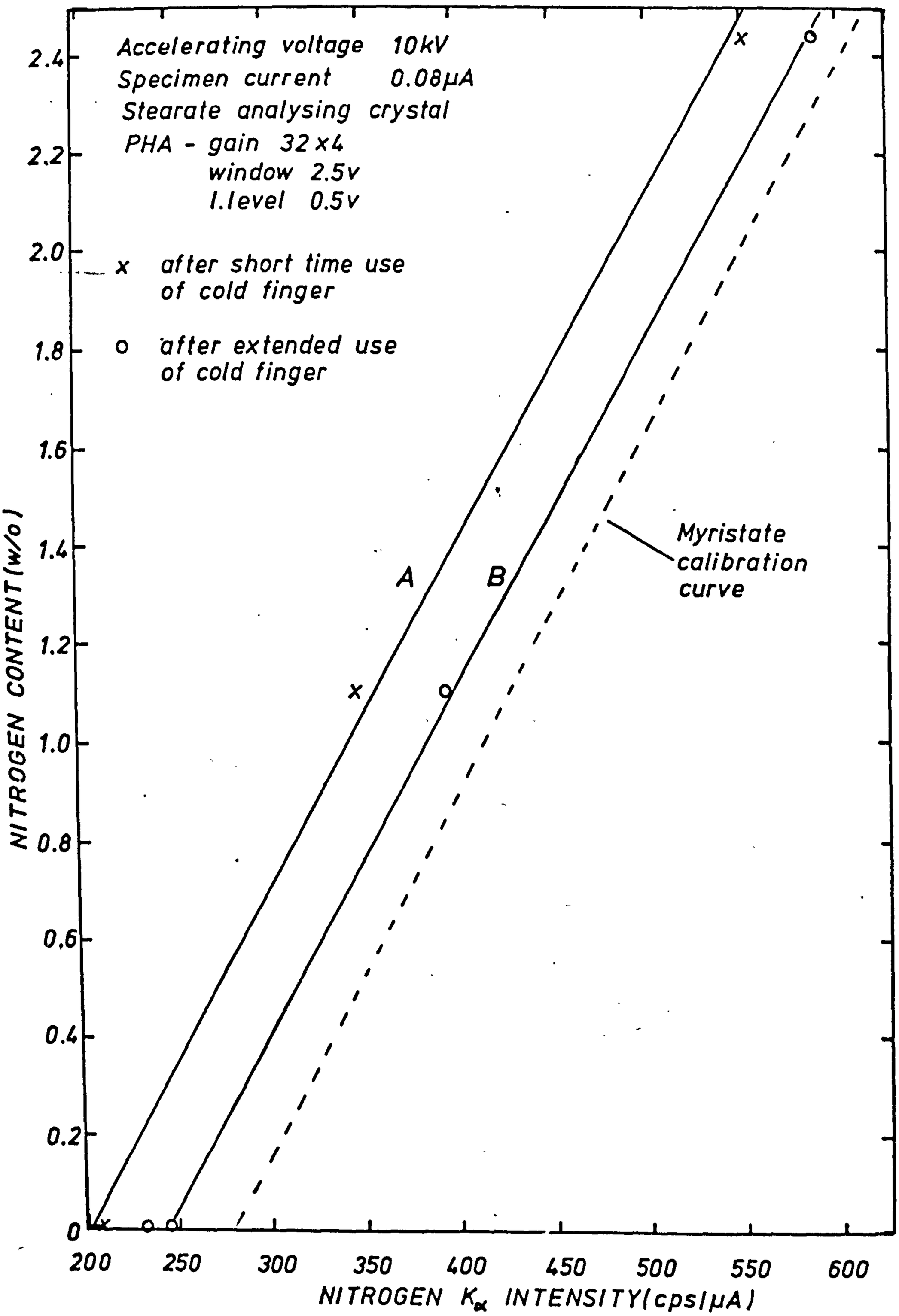
Accelerating voltage 10kV
Specimen current 0.08μA
Stearate analysing crystal
PHA - gain 32x4
window 2.5v
l.level 0.5v
x after short time use of cold finger
o after extended use of cold finger
A
B
Myristate calibration curve
NITROGEN CONTENT (w/o)
NITROGEN Kα INTENSITY (cps/μA)
2.4
2.2
2.0
1.8
1.6
1.4
1.2
1.0
0.8
0.6
0.4
0.2
0
200
250
300
350
400
450
500
550
600

FIG. 36 (a)

CALIBRATION OF JXA-50A MICROANALYSER FOR NITROGEN IN IRON UP TO 12^{W}/o.

Stearate Crystal(116)

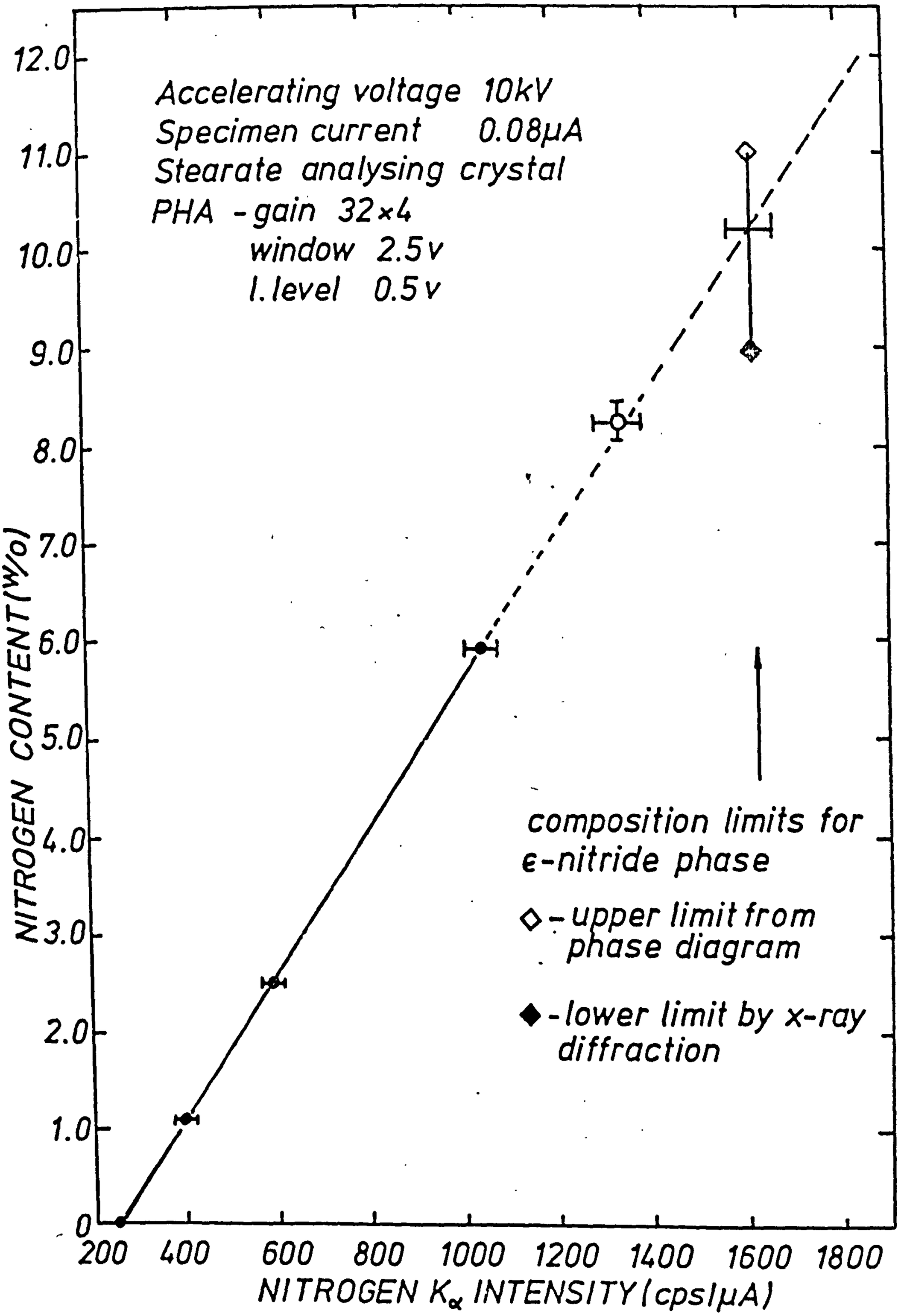
Accelerating voltage 10kV
Specimen current 0.08μA
Stearate analysing crystal
PHA - gain 32×4
window 2.5v
l. level 0.5v
NITROGEN CONTENT(W/o)
12.0
11.0
10.0
9.0
8.0
7.0
6.0
5.0
4.0
3.0
2.0
1.0
0
composition limits for ε-nitride phase
◇ - upper limit from phase diagram
◆ - lower limit by x-ray diffraction
200
400
600
800
1000
1200
1400
1600
1800
NITROGEN Kα INTENSITY (cps/μA)

FIG. 36 (b)

CALIBRATION OF JXA -50A MICROANALYSER FOR NITROGEN IN IRON UP TO 12 W/o.

Myristate and Stearate Crystals

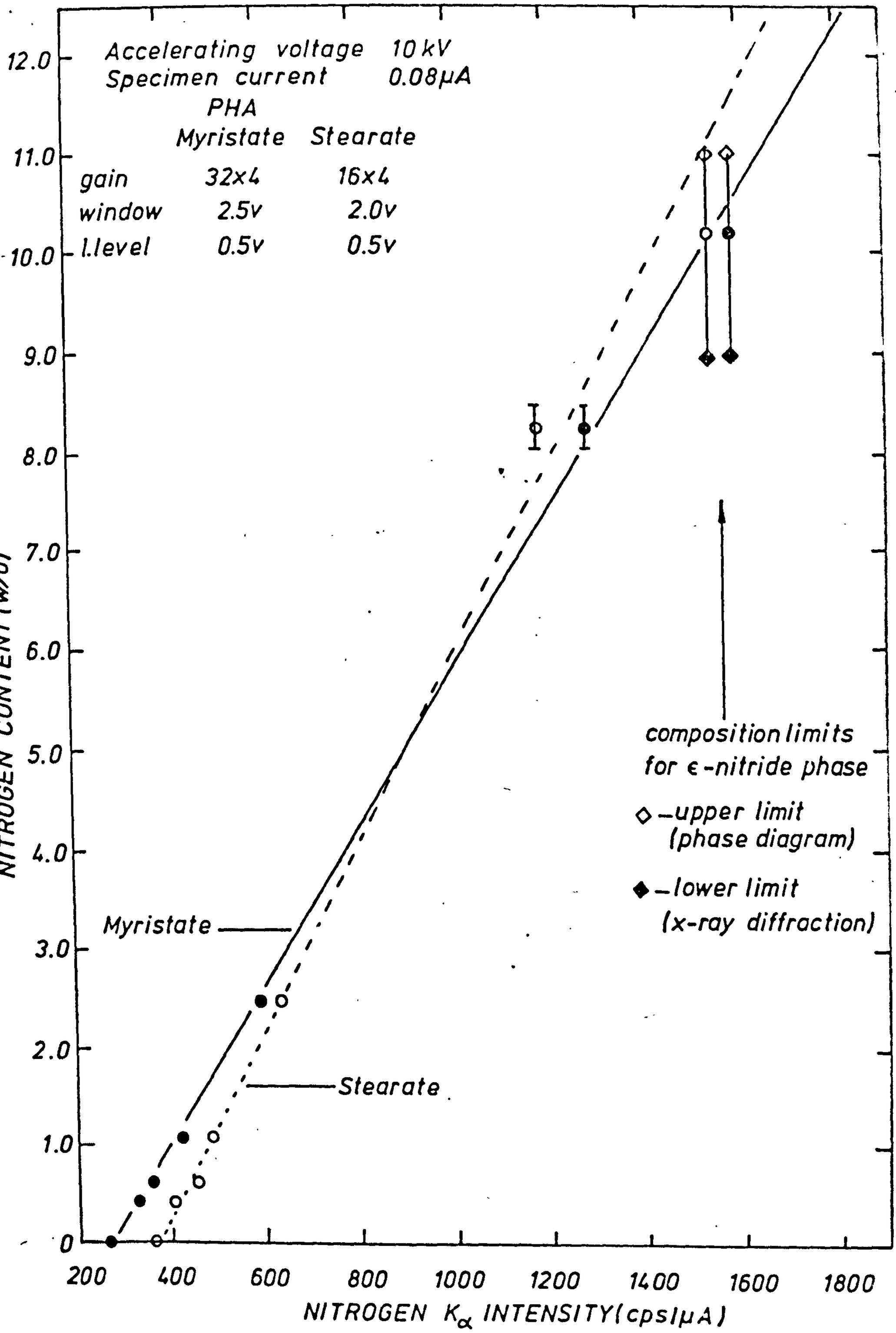
Accelerating voltage 10 kV
Specimen current 0.08μA
PHA
Myristate Stearate
gain 32x4 16x4
window 2.5v 2.0v
l.level 0.5v 0.5v
NITROGEN CONTENT (w/o)
12.0
11.0
10.0
9.0
8.0
7.0
6.0
5.0
4.0
3.0
2.0
1.0
0
Myristate
Stearate
composition limits
for ϵ-nitride phase
◇ –upper limit
(phase diagram)
◆ –lower limit
(x-ray diffraction)
200
400
600
800
1000
1200
1400
1600
1800
NITROGEN Kα INTENSITY (cps/μA)

FIG. 37

CALIBRATION OF JXA-50A MICROANALYSER FOR CARBON IN IRON UP TO 7 W/o.

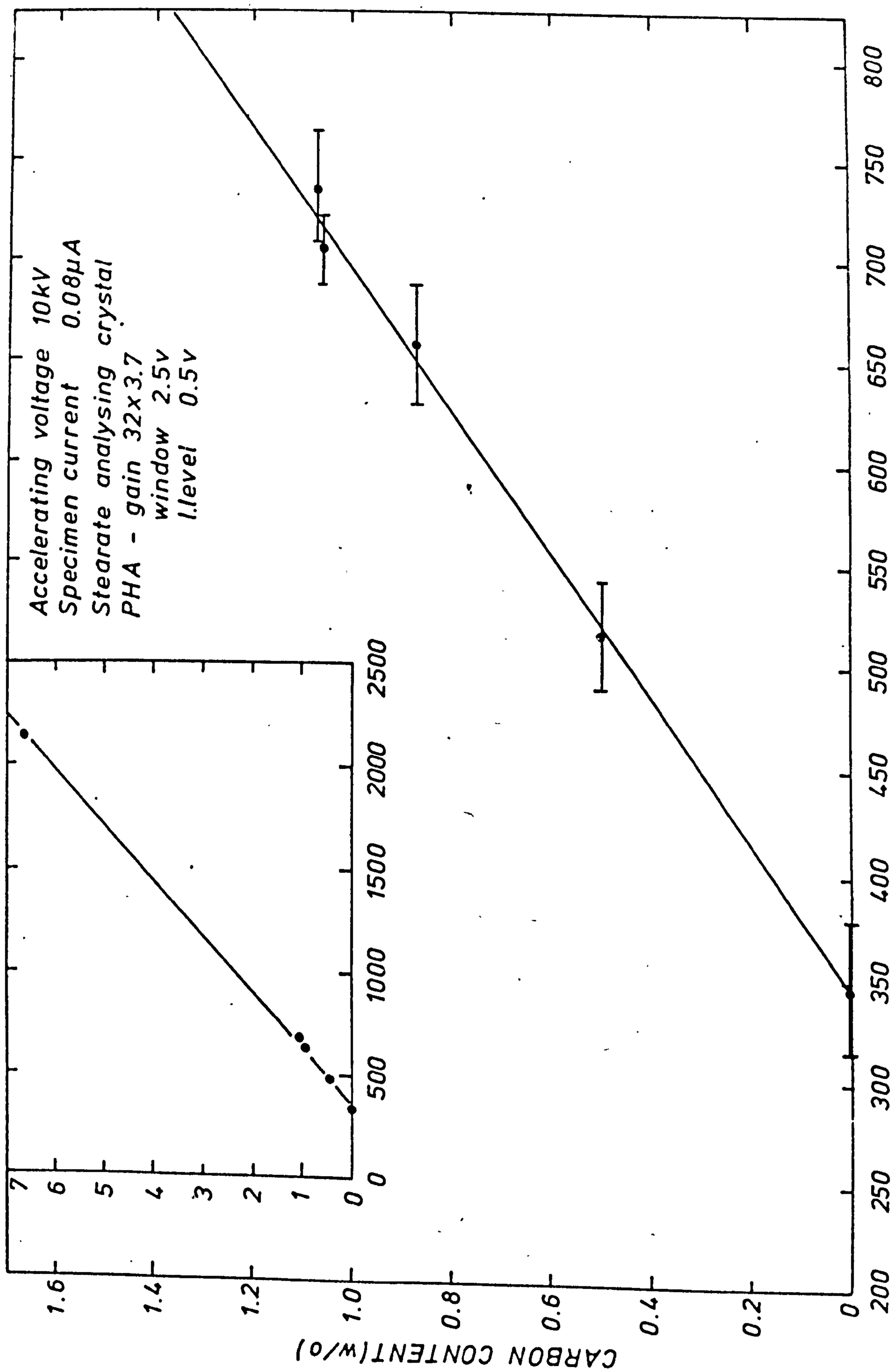
Accelerating voltage 10kV
Specimen current 0.08μA
Stearate analysing crystal
PHA - gain 32x3.7
window 2.5v
l.level 0.5v
CARBON Kα INTENSITY (cps/μA)
CARBON CONTENT(w/o)
0
200
250
300
350
400
450
500
550
600
650
700
750
800
0
500
1000
1500
2000
2500
0
1
2
3
4
5
6
7
0.2
0.4
0.6
0.8
1.0
1.2
1.4
1.6

FIG. 38.

NITROGEN PROFILE IN NITRIDED PURE IRON
AS DETERMINED BY EPMA SPOT COUNT METHOD.(116)

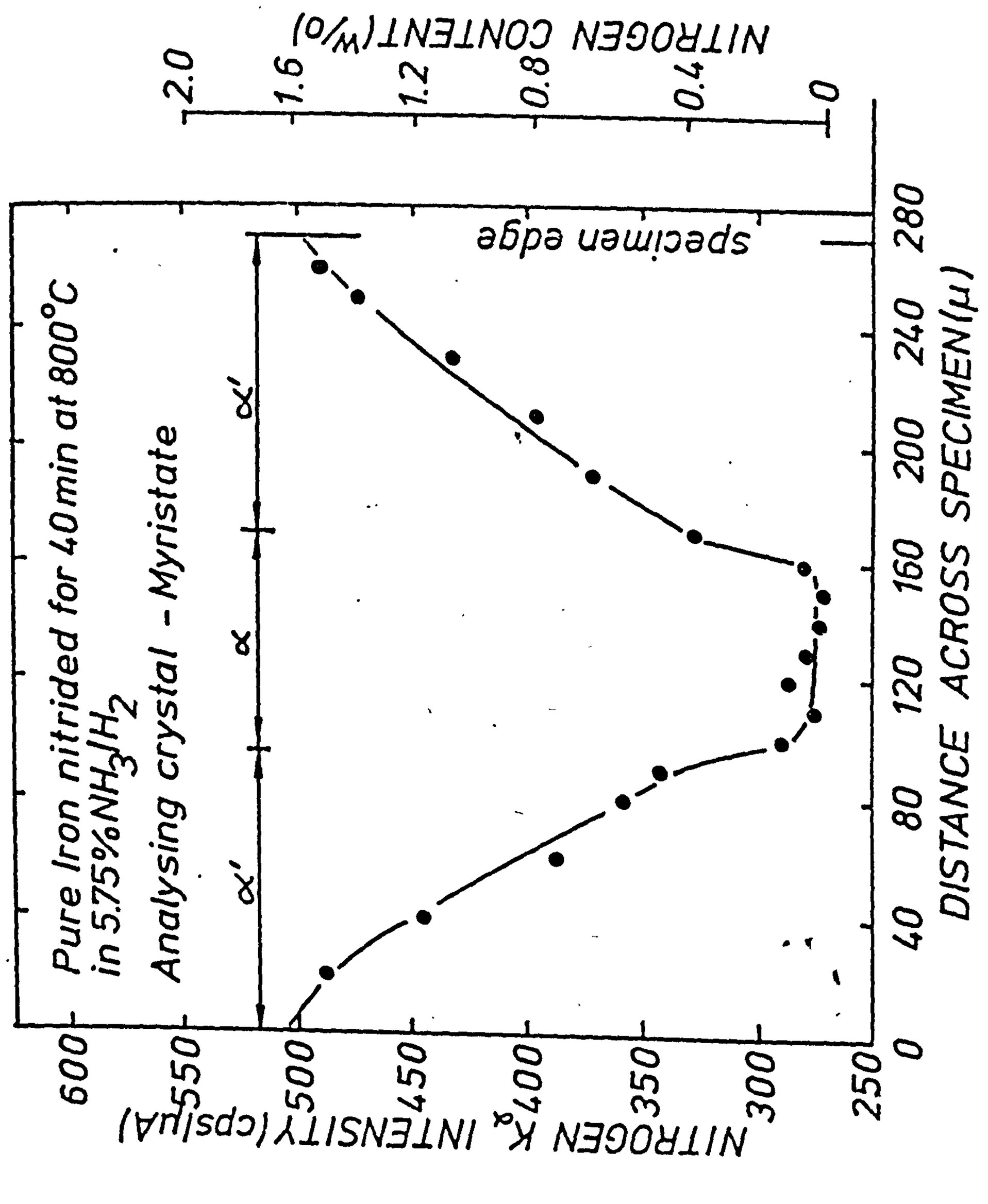
NITROGEN CONTENT (W/O)
2.0
1.6
1.2
0.8
0.4
0
Specimen edge
Pure Iron nitrided for 40 min at 800°C
in 5.75% NH_3/H_2
Analysing crystal - Myristate
α'
α
α'
600
550
500
450
400
350
300
250
NITROGEN K_α INTENSITY (cps/μA)
0
40
80
120
160
200
240
280
DISTANCE ACROSS SPECIMEN (μ)

FIG. 39

CONCENTRATION PROFILES THROUGH THE COMPOUND LAYERS ON EN32 PRODUCED BY FERRITIC NITROCARBURISING TREATMENTS AS DETERMINED BY CONTINUOUS PROFILE ANALYSIS.(128)

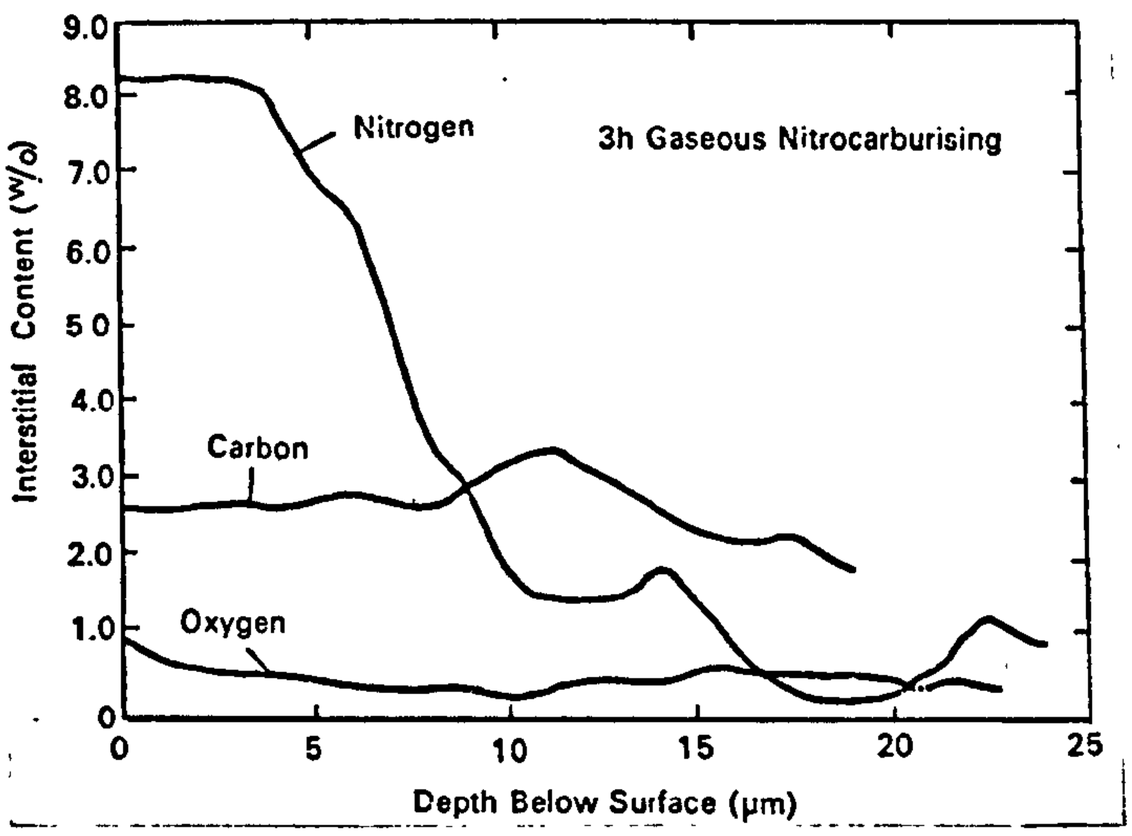
Interstitial Content (W/o)
9.0
8.0
7.0
6.0
5 0
4.0
3.0
2.0
1.0
0
Nitrogen
3h Gaseous Nitrocarburising
Carbon
Oxygen
0
5
10
15
20
25
Depth Below Surface (μm)

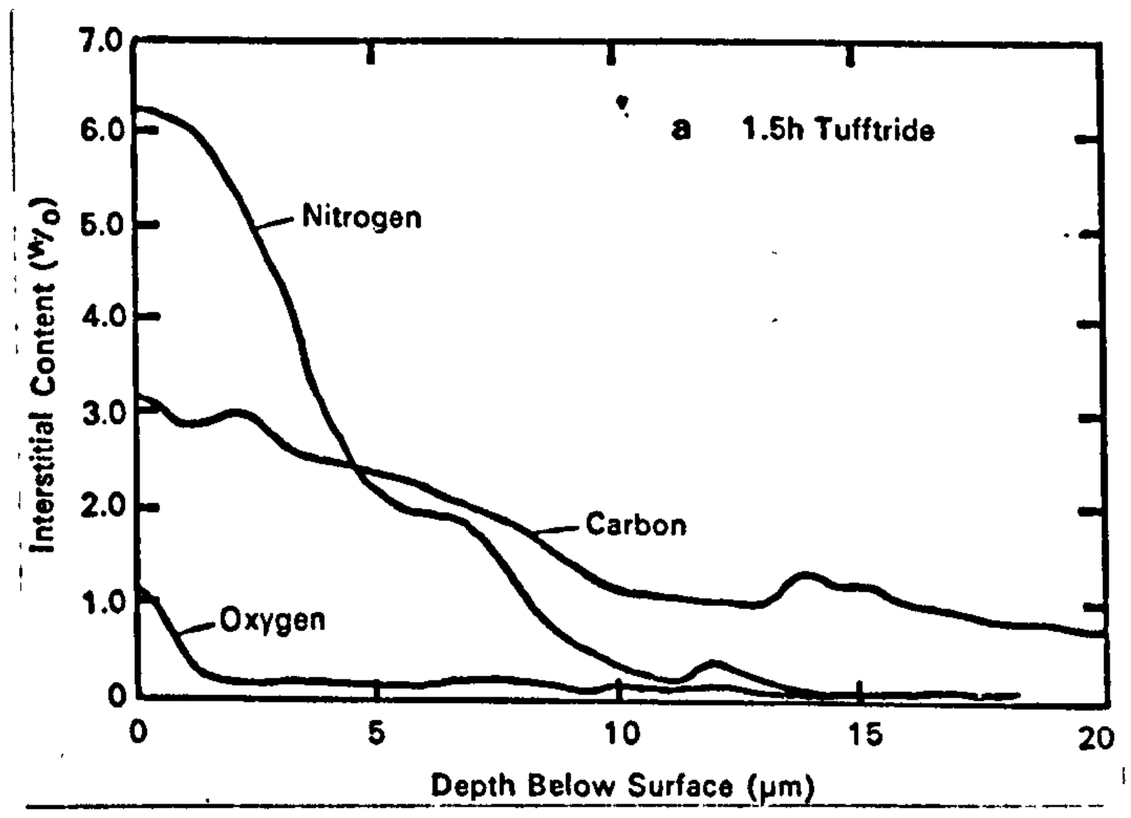
Interstitial Content (W/o)
7.0
6.0
5.0
4.0
3.0
2.0
1.0
0
a 1.5h Tufftride
Nitrogen
Carbon
Oxygen
0
5
10
15
20
Depth Below Surface (μm)

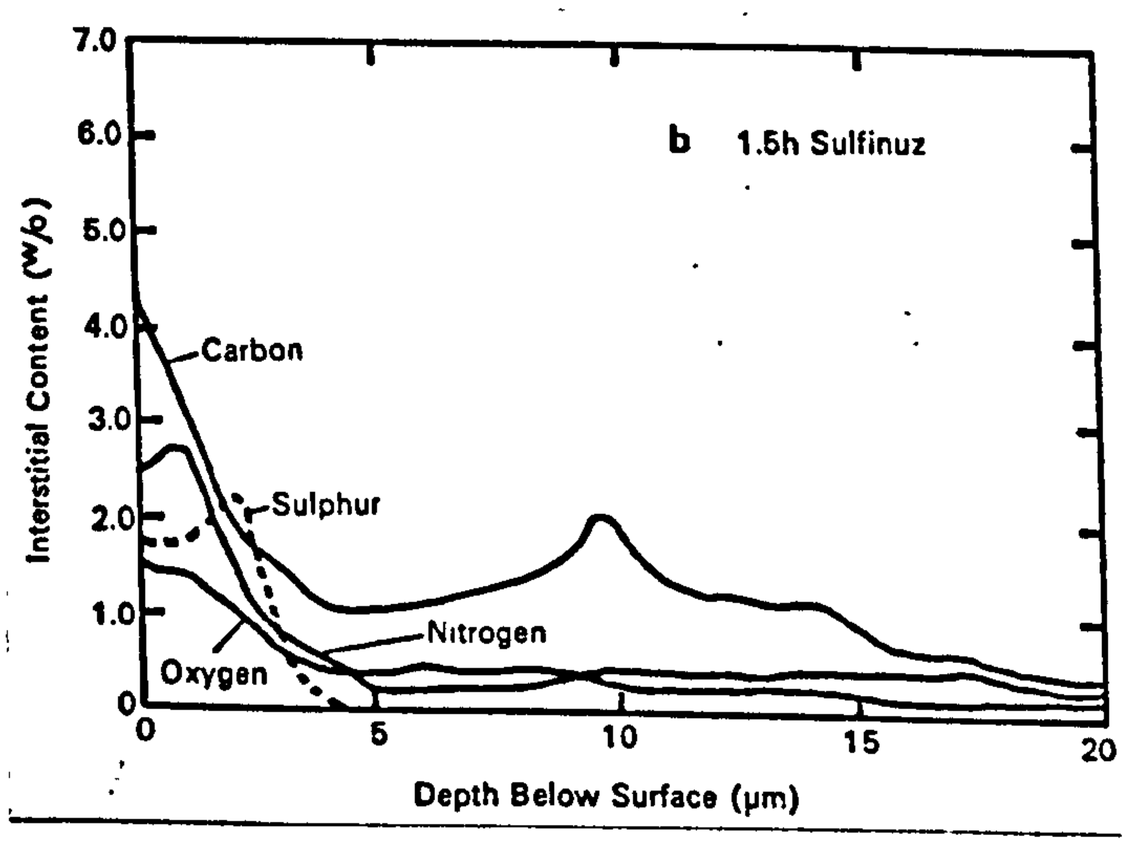
Interstitial Content (W/o)
7.0
6.0
5.0
4.0
3.0
2.0
1.0
0
b 1.5h Sulfinuz
Carbon
Sulphur
Nitrogen
Oxygen
0
5
10
15
20
Depth Below Surface (μm)

FIG. 40

RELATIVE RESPONSE OF MYRISTATE AND STEARATE CRYSTALS TO NITROGEN K_α ON A GASEOUS NITROCARBURISED PURE IRON SPECIMEN.

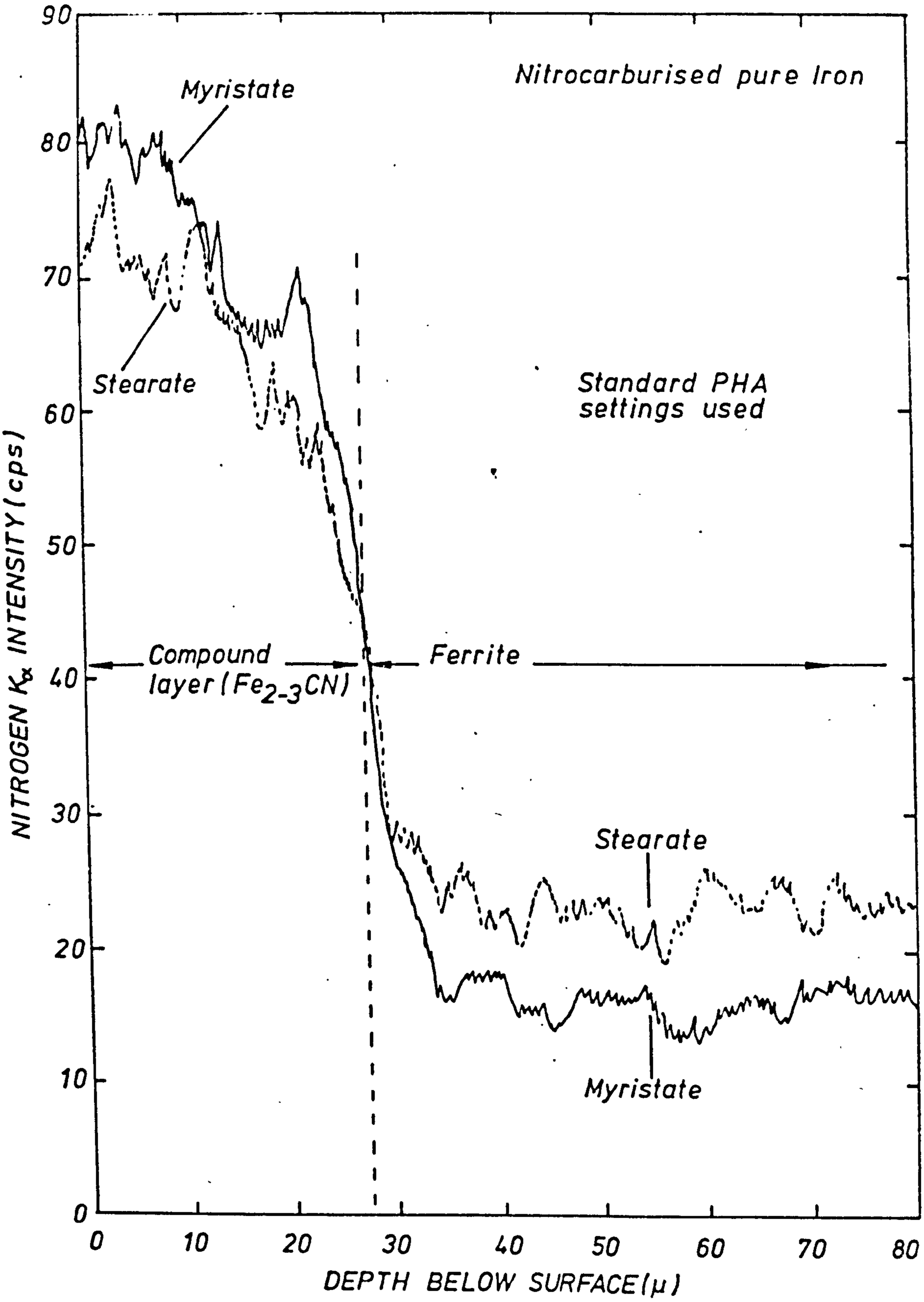
Nitrocarburised pure Iron
Myristate
Stearate
Standard PHA settings used
Compound layer ($Fe_{2-3}CN$)
Ferrite
Stearate
Myristate
NITROGEN K_α INTENSITY (cps)
DEPTH BELOW SURFACE (μ)
0
10
20
30
40
50
60
70
80
90

5.3. Determination of nitrogen by emission spectrometry.

For many years the only recognised method of nitrogen analysis in steels has been the modification of the Kjeldahl organic nitrogen analysis[69], this method has been described in detail in section 4.5. The main drawback to this method is the long time required for analysis and its inherent sources of error. In recent years, the method has been superceded somewhat by vacuum fusion methods[129,130] in which the specimen is rapidly heated and melted under vacuum to evolve all dissolved gases which can then be detected by volumetic or electrical methods. Whilst this method has the advantage of rapidity, about 5 minutes, it requires complete destruction and rather expensive equipment for just the one gas.

Other developments in physico-chemical analysis methods have produced the well known emission spectrometers, marketed under trade names such as Quantovac[96] and Polyvac[131], which are capable of rapid simultaneous analysis of most elements present in steels and other alloys. These instruments have found extensive use in steel works and mass production lines where rapid analysis of batches is essential. Such an instrument if capable of being calibrated for nitrogen in steel would provide an excellent tool for both research and production work as complete destruction of the sample is not necessary and the method could be adapted to concentration profile analysis of cases in surface hardened components.

5.3.1. Principles of emission spectrometry.

If a sample is volatilised and atomised and a fraction of the

free atoms raised to an excited state by an electrical discharge, radiation is emitted from this discharge dependent on the composition of the volatilised sample. Dispersing this radiation through a suitable diffraction grating then splits the total radiation into line spectra whose distribution and intensity depend qualitatively and quantitatively respectively on the composition of the sample. This is the basis of all emission spectrometry techniques, and the technique has the advantage that all elements which are present in a sample will give rise to line spectra such that complete analysis is possible from just one spark. An excellent review of the theory and origin of line spectra in emission spectrometry is given in reference 132.

The commercial instruments available in the U.K. working on this principle, (the Quantovac and Polyvac) are classed as direct reading emission spectrometers. Fig. 41 shows the physical setup of a Quantovac instrument.

The sample to be analysed can be solid, liquid or gaseous, but it is more usual to use solid samples. When using solid samples a flat ground surface is used (minimum size is $^{5}/_{8}$" dia.). The sample is placed over an orifice to a chamber which is subsequently evacuated and filled with Argon. Within this chamber is an electrode normally silver, which is used to spark volatilise and atomise the sample. The energy emitted from this discharge is in the form of a light beam which passes through the condensing lens and into the spectrometer which is normally kept under vacuum. (Any gas however may be used to fill the spectrometer.) Inside the spectrometer the light beam is directed onto a concave diffraction grating which

splits the beam into its component wavelengths. A typical grating has a focal length of 1 metre and a ruling of ~ 2000 lines mm^{-1} with dispersion of 4.6 Å/mm. The diffracted beam then appears as a series of varying intensity lines along the focal length plane of the spectrometer grating. The elements are characterised by the positions of the lines on this plane and required element lines are isolated by secondary slits positioned on this plane. Typical slit widths are in the range 40 - 75μ. Behind each slit is a photomultiplier tube which then converts the light signal into an electrical impulse directly proportional to the intensity of the beam. This impulse is used to charge a capacitor for a period of 5 to 40 seconds to produce an integrated voltage which is then accurately measured for each element. By ratioing each reading to the major constituent in the sample high accuracy can be obtained. Obviously direct analysis can only be made by reference to known standards, and it is normal for calibration charts for each element to be drawn up so that unknown voltages can be directly converted to an accurate analysis. Instruments with built-in computer facilities perform this automatically and a complete analysis can be printed out in less than 3 mins, the most recent Quantovac instrument, model 80[96] is capable of producing complete analysis for up to 60 elements in that time.

Although direct reading emission Spectrometers are the most widely used and known instruments because of their rapid analysis time, it is possible to obtain more accurate results by recording the line spectra photographically on suitably equipped instruments known as spectrographs. In this situation standards are not normally required, because measurement of

image density on a photographic plate with a microdensitometer reduces this density to a quantitative function called the exposure index, which can be thought of as characteristic to the photographic emulsion used. Once this has been determined from a series of known intensities, intensity ratios of all spectral lines on the emulsion can be determined. Because of the wavelength sensitivity of photographic emulsions, the emulsion should be calibrated as near to the lines of interest as possible.

Even greater accuracy of analysis can be obtained in spark emission instruments which dispense with the spectrometer and use a mass spectrometer in its place.

Analysis for nitrogen is possible using emission spectrometers, however the actual spectrometer must be operated under vacuum or inert atmosphere, as the nitrogen emission line exists below 2000Å

At present time there are only a few instruments in the U.K. with capability for detection for the nitrogen emission line. This deficiency is probably due to lack of knowledge of the significance of high nitrogen levels in steel and the lack of a suitable calibration method. Vauxhall Motors, Ellesmere Port have a Quantovac with facility for nitrogen detection, and offered its use in preparing a suitable calibration method because of their interest in using the instrument as a quality control tool for carbonitriding processes.

5.3.2. Calibration of emission spectrometers.

The normal method of calibration for elements is by sparking standards of known composition, and plotting the resulting voltage obtained against the composition of the standard to form a calibration curve, for example carbon in iron as in fig.42. As can be seen, the calibration is not linear but is a power curve function; this is characteristic of most elements analysed. It is relatively easy to construct calibration curves for all the common elements which exist in iron because very good homogeneous standards can be obtained. However in the case of nitrogen in iron, standards are only available for extremely low concentrations, usually less than 0.01^{w}/o, because high nitrogen content alloys cannot be made by conventional metal melting techniques.

A method of producing homogeneous Fe-N alloys was reported by Atkinson et al[115], which involved the controlled nitriding, in NH_3/H_2 mixtures of pure iron wire up to 0.25mm thick and foil up to 0.1mm thick. Fe-N alloys with nitrogen contents up to 2.6^{w}/o could be produced by this method, and this range appeared to be suitable for the range of nitrogen contents which could conceivably be used in carbonitriding and nitriding treatments.

5.3.3 Specimen thickness considerations.

Prior to attempting calibration of the instrument, it was necessary to determine the minimum thickness of material which could be satisfactorily sparked on the Quantovac.

Although a typical spark penetration depth is between 50 and 75μ, enough material is required behind the spark point to

conduct away heat produced by the spark action. Trials of materials with thicknesses just greater than the maximum spark depth showed that 'burn through' of the spark occurred, often due to the fact that the material was not completely flat after manufacture. When thin material is being analysed, a large backup weight (either carbon steel, or copper) is clamped over the material to maintain the seal of the spark chamber and also to conduct heat away from the specimen. Errors which could be introduced by 'burn through' are (a) pick-up of elements in the backup weight, resulting in an average analysis of the specimen and the backup weight. (b) Loss of sensitivity and accuracy due to air leaks on puncturing the specimen, even a large weight could not always maintain crinkled specimens flat during analysis.

Specimen thickness needed to be increased to 0.25mm before satisfactory sparking without 'burn through' could be achieved; the advantage with the greater thicknesses is that specimen heat up is at an acceptable level. It was therefore decided to use a minimum thickness of 0.25mm for all specimens analysed on the instrument.

As the majority of the work quoted in reference 115 was performed with 0.1mm sheet, it was therefore necessary to re-examine conditions under which homogeneous specimens could be produced in 0.25mm sheet. Unfortunately, homogeneous specimens of Fe-N alloys could not be produced in this thickness sheet because of phenomena associated with the metastability of the iron-nitrogen system; this is fully described in section 6.3 - 6.4.

Consequently an alternative calibration method needed to be developed and is now described.

5.3.4. Weight change calibration method for nitrogen.

During the nitriding operation of Fe-C alloys in addition to nitrogen diffusing into the steel surface, carbon also diffused out, due to the decarburising action of hydrogen in the gas mixture. After a period of treatment the concentration profiles within the specimen can be represented as shown in fig.43(a). If the assumption is made that the only species changing during the reaction are carbon and nitrogen, then the following relationships can be derived. Plotting the nitrogen profile in terms of the Quantovac voltage, the carbon profile in actual composition and the weight change as an average concentration throughout the specimen, the profiles now shown in figs. 43 (b), (c), and (d) represent the state of the distribution of carbon and nitrogen in the specimen.

The areas under the curves, area x, y and z, then represent the total nitrogen gain, the total carbon loss and the total weight change respectively.

For zero weight change Area x = Area y (33)

For +ve " " Area x = Area y + Area z (34)

For -ve " " Area x = Area y - Area z (35)

by conservation of mass.

The total nitrogen gain can therefore be expressed in terms of a weight percentage and providing that the difference between voltage readings for nitrogen at the surface and at the centre of the specimen is small (because actual calibration,

may not be linear) a calibration point for the average voltage reading through the profile can thus be obtained.

For differences between surface and centre voltage readings, the nitrogen content can be expressed as a percentage of the area which would exist under a completely homogeneous profile and extrapolated to give the content of a completely homogeneous profile corresponding to Q'_v (fig. 43 b)

$$\text{Hence} \quad Q'_v = \frac{x}{x_1} \, (y + z)\%N \qquad (36)$$

The accuracy of the method will depend on the following factors

(1) Accurate determinations of the areas under curves, the error will decrease as the area increases.

(2) Consistency of base carbon level in all specimens used.

(3) Assumption that only carbon and nitrogen are involved in the gas transfer reactions.

5.3.5. Experimental.

Calibration points were obtained using this technique from the concentration profiles determined on a series of Fe-0.5^{W}/oC specimens after nitriding under various conditions. The concentration profiles were determined by a layer analysis method as follows.

A heat treated specimen was cleaned and its thickness accurately measured with a vernier micrometer. The cleaned surface was then sparked in the Quantovac instrument, and voltage readings(Q) proportional to the carbon content and nitrogen contents obtained. The impression of the spark was then removed by careful

grinding on a precision surface grinding machine and the thickness remeasured. Typical depths of penetration of the spark were 50 - 75μ. The cleaned surface was then resparked, and the operation repeated until readings up to halfway through the specimen were obtained. Because thin specimens (0.75mm) were used, it was necessary to hold the specimens with large thin sheets of steel on a magnetic chuck when grinding.

The spark produces an average analysis of the volume of material actually sparked, and this average will be attributed to a depth somewhere in the layer sparked.

The geometry of the spark profile was examined and shown to approximate to a cone, and therefore the average analysis will be attributed to a plane parallel to the base bisecting the cone into two equal volumes. It can readily be shown that this plane is 1/5th of the height of the cone away from the base. All measurements in the layer analyses are therefore corrected for this factor, before plotting out the profiles.

Actual carbon contents were obtained from existing calibration data. The profile curves were then plotted out as in fig.43 on axes such that 1cm = 10Ω volts = 0.05^{w}/o C = 0.001" (25.4μ). Table 14 shows the nitriding treatments used for the calibration specimens together with the calibration data obtained from equation 36. Several specimens were analysed chemically for nitrogen to compare with the weight change method, the results (table 15) indicate that the method appears to overestimate the chemically determined nitrogen content by up to 0.15^{w}/o.

Some completely homogeneous nitrogen standards with nitrogen contents up to $\sim$ 0.6^{w}/o were produced by long time nitriding of 0.75mm Fe-C alloy strip. The conditions used are shown in table 16, and their homogeneity was checked using the layer analysis method just described. The resulting profiles are shown in fig. 44. Nitrogen content was determined by both weight change and chemical analysis methods, with good agreement at low nitrogen levels, but discrepancies at the high nitrogen level. The mean Quantovac voltage for each profile is assigned to the nitrogen content determined.

Further calibration points at high nitrogen levels have been obtained by making use of specimen nos. 15, 16, and 17 (see chapter 6) in the following way. Although the specimens are not homogeneous, they do possess a nitrogen gradient as checked by microanalysis. It is also possible to approximate to such a concentration profile knowng the surface and overall nitrogen content of the specimen If C_1, C_2, and C_3 represent the surface, the centre and the average nitrogen contents respectively, then assuming a linear slope between surface and centre (fig.45) the following relationship holds.

$$C_3 = C_2 + \tfrac{1}{2}(C_1 - C_2)$$

$$= \frac{(C_2 + C_1)}{2} \qquad (37)$$

It is already known that (a) the Quantovac spark penetrates between 50 and 75 μ into the specimen surface and (b) the average analysis relates to a distance of 1/5th spark depth, therefore a spark voltage on the surface relates to an average analysis between 10 and 15u below the surface.

The surface concentrations can be estimated from the nitriding potential and by extrapolation of microanalysis profiles and these are shown in table 17 for specimens 15, 16 and 17. Using the values determined by microanalysis, together with weight gains in equation 37, the nitrogen levels corresponding to depths 15μ below the surface were obtained; these are shown in table 18.

5.3.6. Final calibration curve and discussion.

Using all the data from tables 14, 16, 18 and fig. 44 a calibration curve (fig.46) has been plotted and the curve drawn as a best fit to the points.

One might challenge the weight change method on the grounds that it should always overestimate the nitrogen content because a linear relationship between Q_v and $^w/_o$ nitrogen is assumed. However in many cases, this linearity is assumed only over short ranges of Q_v and can be regarded as valid. In addition, chemical determination of nitrogen is at best 3% accurate. Normally vacuum fusion methods overcome this difficulty, but table 15 shows that the weight change method overestimates the vacuum fusion determined nitrogen content. The specimens in table 15 were particularly chosen to represent different types of nitrogen profile, with specimens C and F representing steep nitrogen profiles whereas specimens S and 171 are virtually homogeneous, yet both sets of specimens overestimate nitrogen by the weight change method by similar amounts. An error would be involved in the weight change method if species other than carbon or nitrogen were involved in the reaction. The only possibilities are hydrogen and oxygen; hydrogen can be

discounted because of its low weight and no traces of oxygen have been found by microanalysis.

The most accurate part of the curve is up to about 1.4^{W}/o nitrogen, mainly due to the number of data points available and it is below this nitrogen level that most present interest lies.

5.4 Summary of Analysis Methods.

As a result of the extensive work described in this chapter, the following methods of analysis are available

(a) Furnace gas analysis for ammonia - this can be done by infra-red gas analysis, providing suitable precautions are taken to eliminate or allow for water vapour, and by gas chromatography. In both cases repeatability should be better than 1%. The limit of detectability for ammonia in gas chromatography can be below 100ppm; in the case of infra-red, this depends on the instrument but can be as good as if not better than gas chromatography.

(b) Electron micro-probe analysis for light elements - in particular for nitrogen in iron, a method was developed which could detect levels as low as 0.08^{W}/o and as high as 12^{W}/o with an accuracy in the order of 2%.

(c) Emission spectrometric analysis for nitrogen - a method was developed for calibration to allow nitrogen levels up to 2.5^{W}/o in iron to be determined with an accuracy in the order of 3%

Method (a) should prove useful for monitoring and control of ammonia in commercial heat treatment atmospheres. Methods (b) and (c) provide useful tools for research and industry

in the analysis of nitrogen in heat treated components . In particular method (c) is an excellent quality control tool now used in the monitoring of nitrogen in carbonitrided automobile components; the method also provides simultaneous analysis of all elements in the component.

TABLE 14

DETAILS OF SPECIMEN HEAT TREATMENT AND SUBSEQUENT DATA FOR CALIBRATION OF QUANTOVAC BY WEIGHT CHANGE METHOD.

Specimen No. (a)	Heat Treatment Time (h)	Temp (°C)	Atmosphere.	Area under Profile Curves (CM^2) Nitrogen	Carbon Loss	Weight Change	Calculated Nitrogen Content. %	Estimated Nitrogen in Homogeneous spec.	Equiv. Voltage Reading	V.surf - V.centre
A	1	748	$5^{v}/oNH_3/H_2$	66.25	13.50	+66.51	0.273	1.601	350	266
B	4	"	" " "	137.50	48.00	+94.65	0.479	1.307	337	230
C	15.5	"	" " "	183.68	111.00	+85.24	0.657	1.074	286	135
D	1	780	" " "	59.75	16.75	+54.66	0.236	1.315	305	221
E	8	"	" " "	142.38	75.75	+69.54	0.476	0.842	250	130
F	16.3	"	" " "	185.23	116.50	+81.57	0.658	0.882	250	70
G	1	811	" " "	74.50	25.25	+58.50	0.279	1.152	290	206
H	4	"	" " "	69.25	45.25	+18.44	0.220	0.618	217	105
I	16	"	" " "	185.48	133.10	+50.48	0.627	0.762	239	40
J	2	845	$2,5^{v}/oNH_3/H_2$	57.00	47.15	- 1.71	0.186	0.395	184	74
K	2	"	$5^{v}/oNH_3/H_2$	68.50	55.00	+12.86	0.227	0.485	183	76
L	4	"	" " "	83.63	80.05	+ 6.83	0.293	0.525	186.	88
M	8	"	" " "	108.20	106.35	- 6.04	0.332	0.473	187	47
N	2	780	$20^{v}/oNH_3/H_2$	136.75	42.25	+135.95	0.608	1.661	340	256
O	2	"	10 " " "	122.25	37.75	+126.60	0.548	1.646	331	247
P	2	"	$2.4^{v}/oNH_3/H_2$	55.00	33.50	+22.97	0.197	0.847	252	168
Q	8	"	10 " " "	158.68	83.30	+115.24	0.668	1.095	260	120
R	2	"	$20^{v}/oNH_3/N_2$	124.75	31.50	+128.83	0.524	1.555	327	243
S	19.6	845	$5^{v}/oNH_3/3^{v}/oCH_4/H_2$	144.25	-177.50	+302.10	0.415	0.548	212	42
T	19.5	"	40 " " " "	144.63	-177.35	+333.43	0.533	0.823	238	71
U	1.2	"	$10^{v}/oNH_3/1.1^{v}/oCH_4/H_2$	102.30	2.15	+105.48	0.367	0.956	267	172
V	4	"	" " " " "	153.66	-2.48	+167.79	0.586	0.828	239	69
W	4	"	5 " " " " "	129.33	-7.70	+135.07	0.435	0.626	212	67
X	15		$5^{v}/oNH_3/H_2$	144.00	140.00	+0.87	0.486	0.631	214	39

(a) All specimens were 25 x 23 x 0.75 mm coupons of Fe-0.5 w/o C. steel.

TABLE 15

NITROGEN CONTENTS DETERMINED BY CHEMICAL ANALYSIS AND WEIGHT CHANGE METHODS.

SPEC. NO	NITROGEN w/o CHEMICAL		WEIGHT CHANGE.
	Vacuum Fusion	Kjeldahl	
C	0.510		0.657
F	0.530		0.658
S	0.345		0.415
171	0.520	0.544	0.674

TABLE 16

HOMOGENEOUS Fe-N ALLOYS PRODUCED BY THROUGH NITRIDING OF Fe-C ALLOYS

Specimen	Alloy	Temp. (°C)	Atmosphere	Time(h)	Specimen Weight Change (%)	Weight Change	Nitrogen w/o Chem. Analysis. Kjeldahl	Vacuum	Fusion
171	Fe-0.5%C	811	5v/oNH_3/H_2	23.75	+0.174x	0.674	0.544	0.515	0.520
172	"	930	" " "	15.00	-0.358x	0.142	--	--	--
173	Fe-1.07%C	"	2.5v/o" "	8.00	-0.827	0.085	0.096	0.087	0.091
174	Fe-0.87%C	"	5.0v/o" "	8.33	-0.729	0.100	0.114	0.105	0.110
176	"	"	0.5v/o" "	17.50	-0.823x	0.047	0.057	0.053	0.053

x completely decarburised.

FIG. 41

THE LIGHT SPECTROMETER IN A TYPICAL EMISSION SPECTROMETER (QUANTOVAC 80). (96)

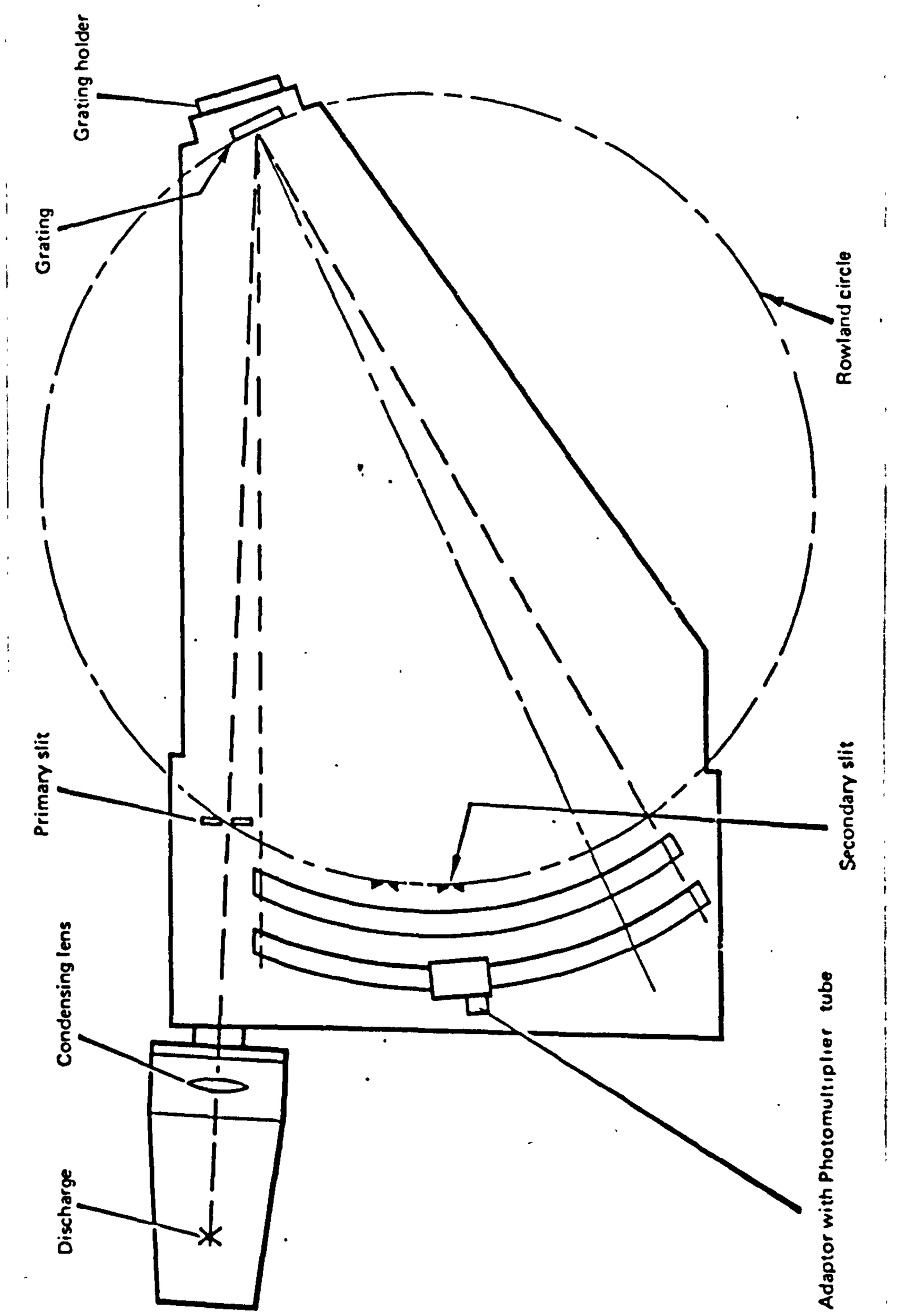
Grating holder
Grating
Rowland circle
Primary slit
Secondary slit
Condensing lens
Discharge
Adaptor with Photomultiplier tube

FIG. 42

CALIBRATION FOR CARBON IN IRON.

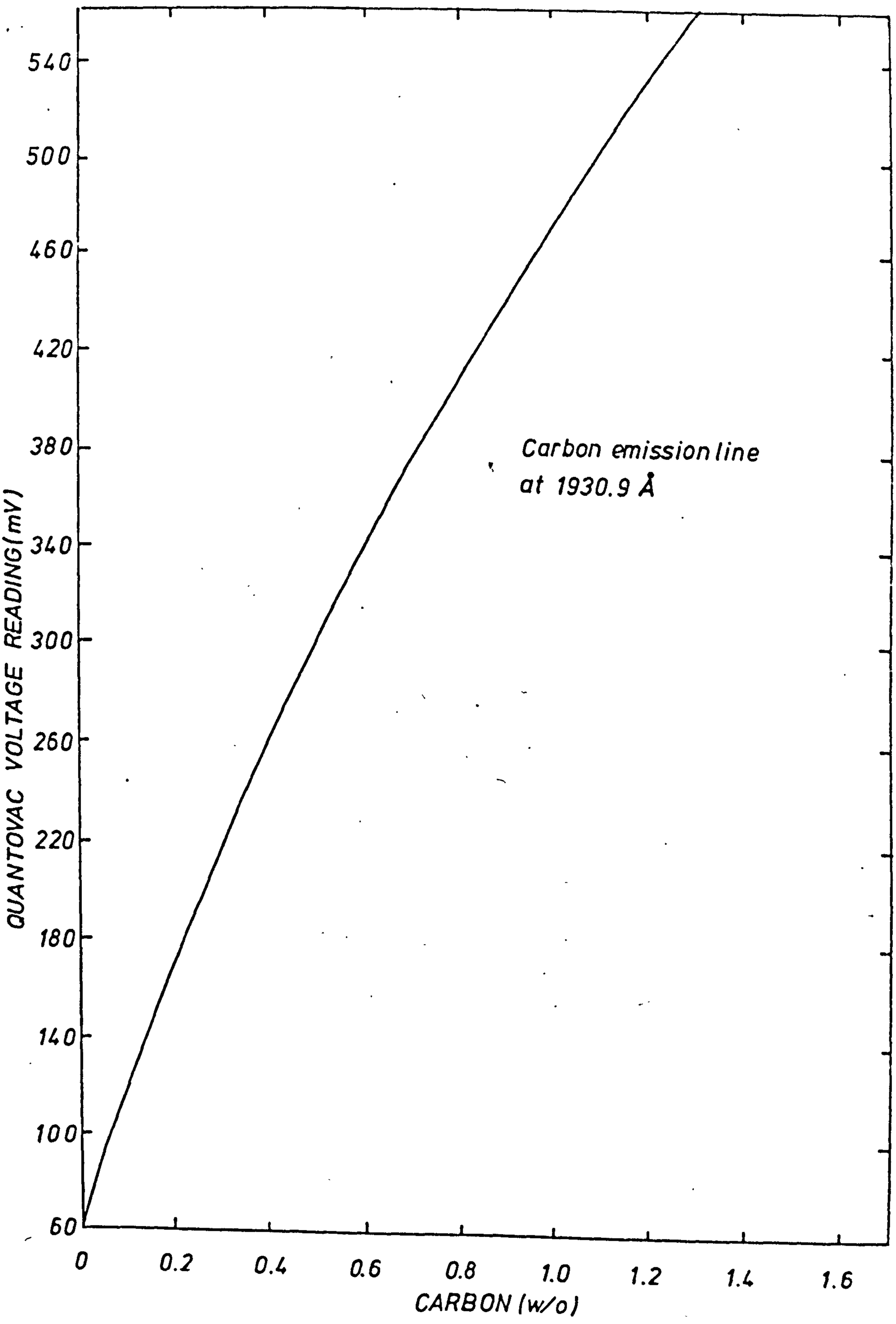
540
500
460
420
380
340
300
260
220
180
140
100
60
QUANTOVAC VOLTAGE READING (mV)
Carbon emission line
at 1930.9 Å
0
0.2
0.4
0.6
0.8
1.0
1.2
1.4
1.6
CARBON (w/o)

FIG. 43

PRINCIPLE OF WEIGHT CHANGE CALIBRATION METHOD.

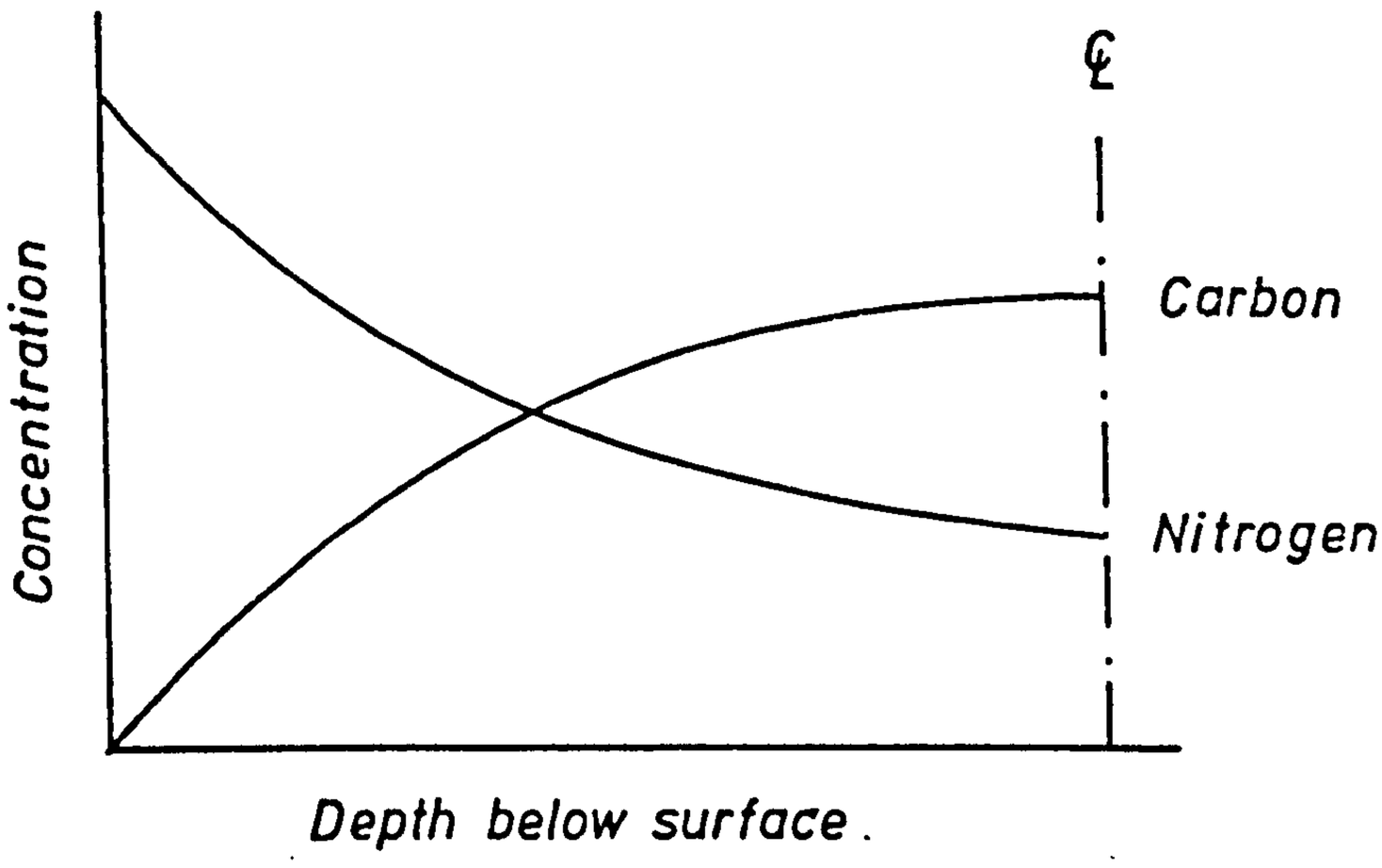
Concentration
℄
Carbon
Nitrogen
Depth below surface.

(a)

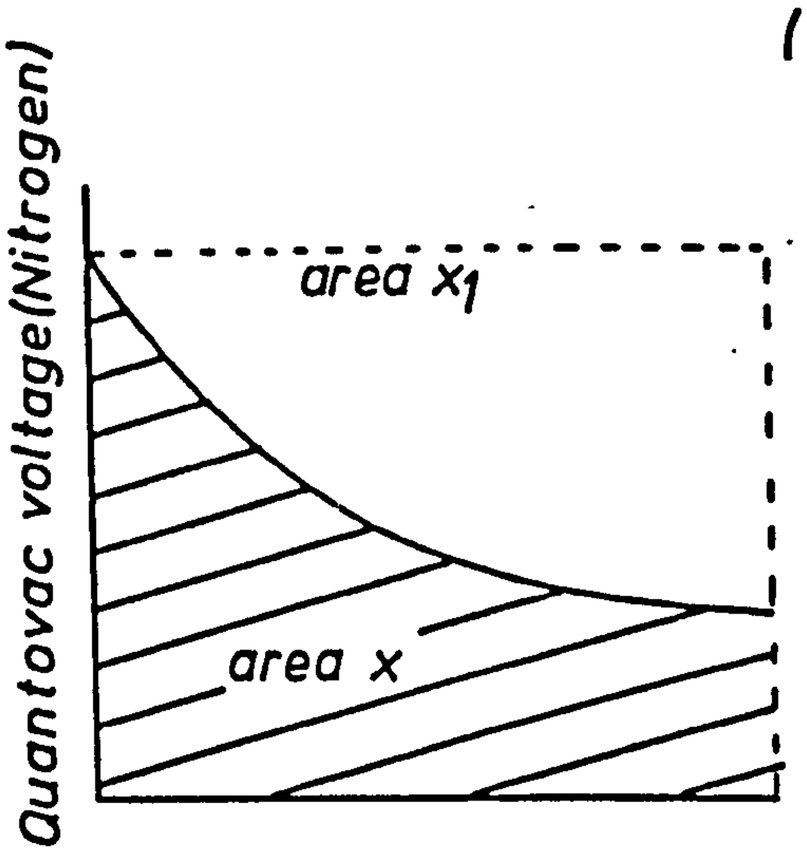
Quantovac voltage(Nitrogen)
area x_1
area x

(b)

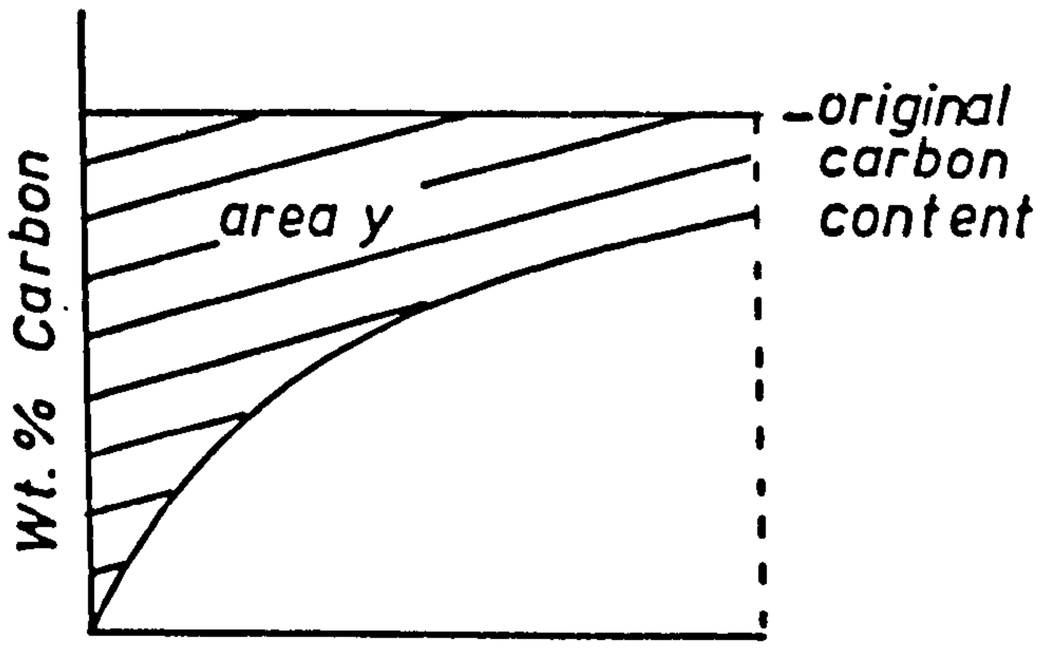
Wt.% Carbon
area y
original carbon content

(c)

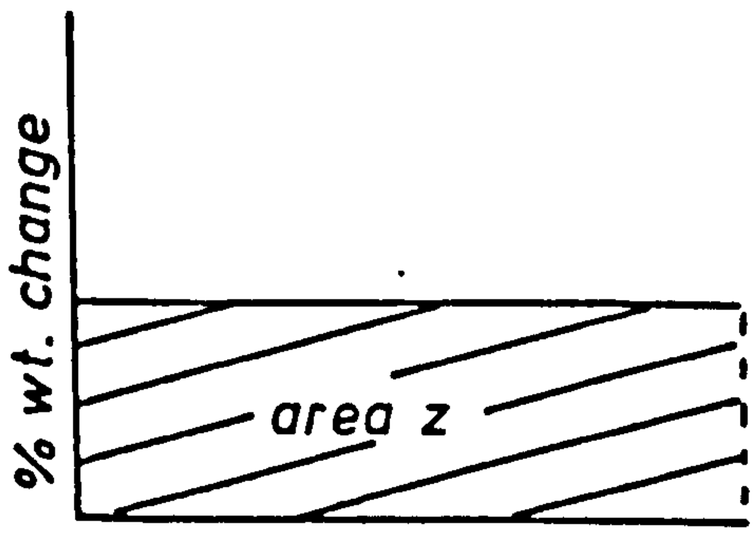
% wt. change
area z

(d)

FIG. 44

NITROGEN VOLTAGE PROFILES DETERMINED ON HOMOGENEOUS IRON-NITROGEN ALLOYS.

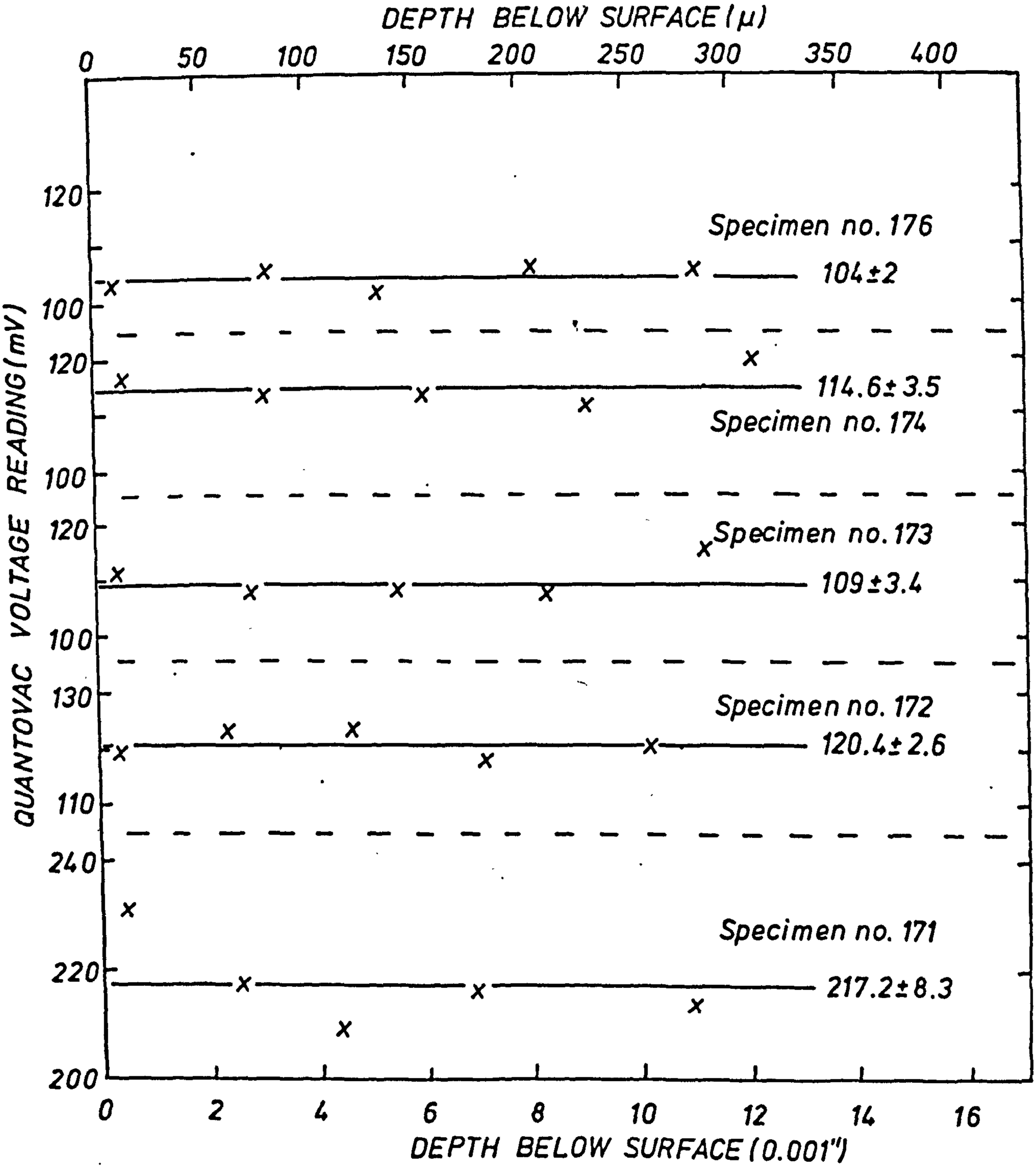
DEPTH BELOW SURFACE (μ)
0
50
100
150
200
250
300
350
400
QUANTOVAC VOLTAGE READING (mV)
120
100
120
100
120
100
130
110
240
220
200
Specimen no. 176
104±2
Specimen no. 174
114.6±3.5
Specimen no. 173
109±3.4
Specimen no. 172
120.4±2.6
Specimen no. 171
217.2±8.3
0
2
4
6
8
10
12
14
16
DEPTH BELOW SURFACE (0.001")

FIG. 45

LINEAR CALIBRATION REPRESENTATION OF CONCENTRATION.

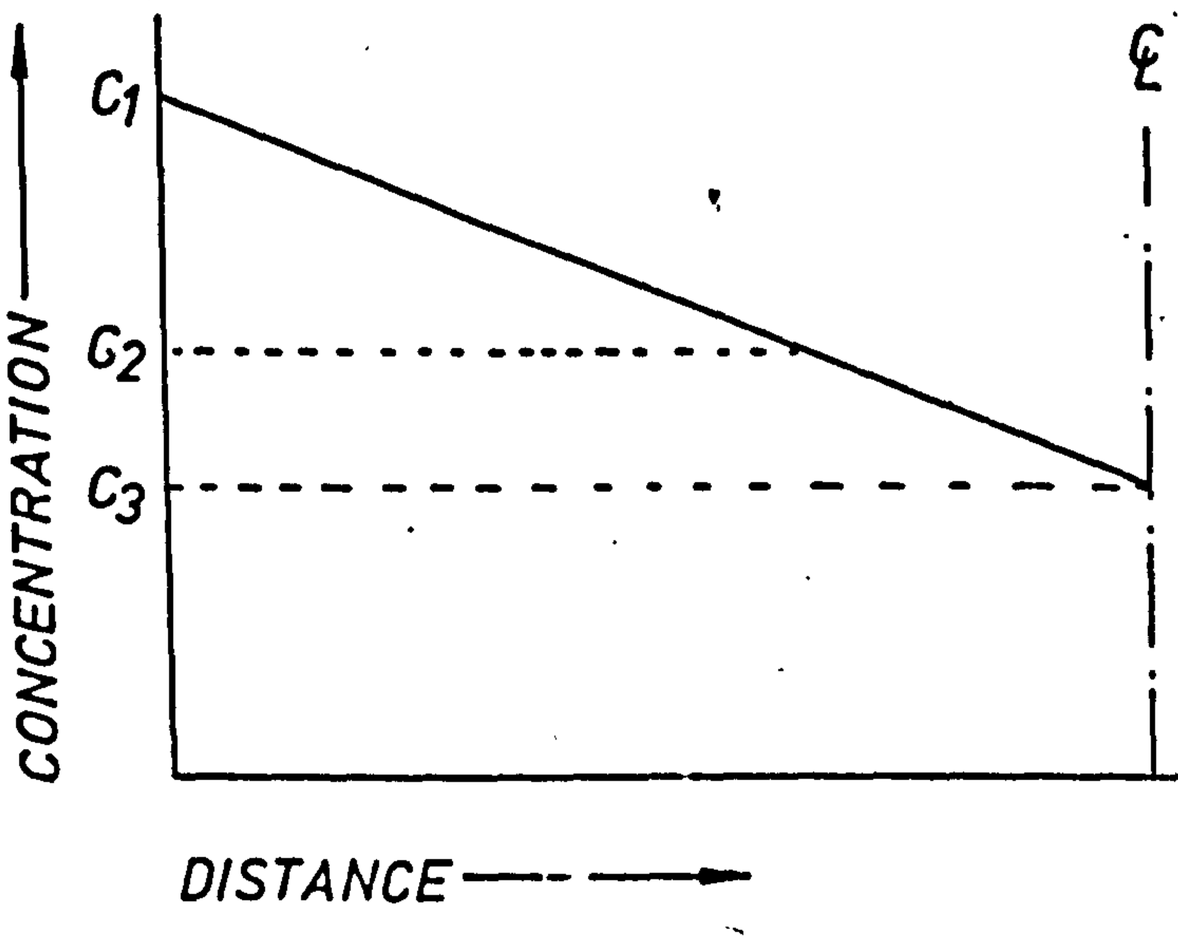
C_1
C_2
C_3
℄
CONCENTRATION
DISTANCE

FIG. 46

CALIBRATION FOR NITROGEN IN IRON ON

QUANTOVAC EMISSION SPECTROMETER.

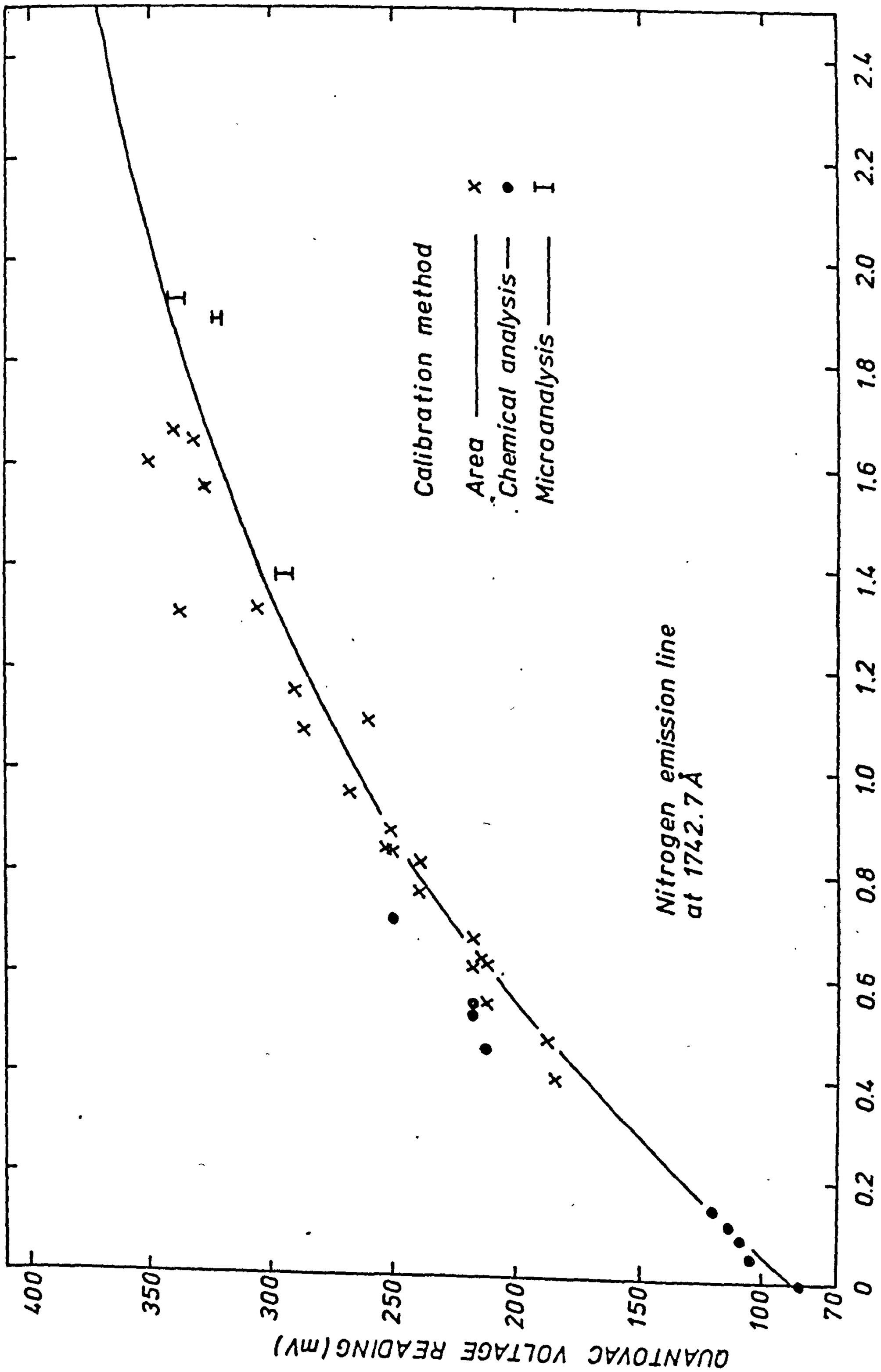
Calibration method
Area
Chemical analysis
Microanalysis
Nitrogen emission line at 1742.7 Å
NITROGEN (w/o)
0.6
0.8
1.0
1.2
1.4
1.6
1.8
2.0
2.2
2.4
0
0.2
0.4
QUANTOVAC VOLTAGE READING (mv)
400
350
300
250
200
150
100
70

CHAPTER 6.

AUSTENITIC NITRIDING OF PURE IRON.

6.1. INTRODUCTION

In chapter 2 it was seen that one of the reported major limitations of increasing nitrogen in solid solution, during gas carbonitriding, was the formation of grain boundary precipitates and voids at inlet ammonia levels greater than $10^{v}/_{o}$[40, 63, 64]. Although instinctively, it might appear that presence of such precipitates should adversely affect mechanical properties, in particular ductility, there are reports that this is not the situation in practice[133]. Consequently potential advantages, outlined earlier, of high levels of nitrogen in solid solution, may well be forthcoming.

The purpose of this chapter is to investigate austenitic nitriding of pure iron, up to nitrogen levels corresponding to its limit of solubility in austenite, with the aid of the new analytical tools, whose developments have been described in chapter 5.

6.2 Theory of Austenitic Nitriding.

In low temperature ($\sim 500^{o}C$) nitriding operations using Ammonia gas, Darken[16] showed that the amount of nitrogen taken up by the specimen was related to the partial pressure of ammonia in the gas atmosphere, through the equilibrium constant of the ammonia decomposition reaction

$$NH_3 \rightleftharpoons N_{(\text{in Fe})} + {}^3/_2H_2 \qquad (23)$$

$$K = \frac{a_N \cdot (pH_2)^{3/2}}{pNH_3} \qquad (26a)$$

$$r = \text{nitriding potential.} = a_N = \frac{K \cdot pNH_3}{(pH_2)^{3/2}} \qquad (26b)$$

In high temperature nitriding ($>$ 650°C), thermal decomposition of ammonia becomes significant, and modification to the above expression must be made to relate directly to amount of nitrogen taken up by the specimen.

Atkinson [35] derived the following expression for r

$$r = \frac{pNH_3(\text{outlet})}{\left[1 - \frac{(pNH_3(\text{inlet}) + pNH_3(\text{outlet})}{2}\right]^{3/2}} \qquad (27)$$

which takes into account thermal decomposition. The volume expansion due to extra Hydrogen from the decomposition reaction is neglected but the error involved is less than 0.05% in the values of r. This equilibrium relationship has beem used as monitor to the production of homogeneous Fe-N alloys[115]. It was initially planned to use this method for the production of standards for the Quantovac instrument, however this did not prove possible due to phenomena associated with the metastability of the iron-nitrogen system. The theory behind homogeneous nitriding will now be described and then its practical problems will be elaborated.

Consider part of the Fe-N phase diagram (fig.47a) above the eutectoid temperature. At a temperature T_1, there are limiting compositions to the $\alpha/\gamma + \alpha$ and $\gamma + \alpha/\gamma$ phase fields indicated by C_1 and C_2 respectively, and a homogeneous γ alloy will only result at a composition $C_3 > C_2$. Atkinson et al[115] showed that a specific nitriding potential exists corresponding to a specific composition as

shown in fig. 7 and 47(b) and to achieve a homogeneous γ alloy, r_a must be exceeded.

The concentration profiles corresponding to nitriding at a potential r_b are shown in fig. 47 (c - f) in respect to time. The diffusion equations covering the situation up to t_3 are rather complex and are given by Jost[134]; they are as follows.

$$C_2 - C_1 = \frac{(C_3 - C_2)\exp(-y^2)}{y\sqrt{\pi}\ \mathrm{erf}\, y} - \frac{(C_1 - C_0)\exp(-\phi/y2)}{y\sqrt{\pi\phi}\,(1 - \mathrm{erf}\sqrt{y\phi})} \qquad (38)$$

$$y = x / 2\sqrt{D_\gamma t} \qquad \phi = D_\gamma / D_\alpha$$

D_γ, D_α, - diffusion coefficients of nitrogen in austenite and ferrite respectively

Other notations as in fig. 47.

This diffusion situation can be simplified considerably for significant values of x at temperatures well above the eutectoid temperature, because $D_\alpha \gg D_\gamma$ and $C_1 - C_o$ is very small, so the equation reduces to

$$C_2 - C_1 = \frac{(C_3 - C_2)\exp(-y^2)}{y\sqrt{\pi}\ \mathrm{erf}\, y} \qquad (39)$$

The equation can be solved numerically very easily if C_1, C_2 and C_3 are known, by plotting values of $\exp(-\gamma^2)$ and $\frac{C_2 - C_1}{C_3 - C_2} \times \gamma\sqrt{\pi}\,\mathrm{erf}y$ against γ. The intersection of the two lines gives the solution in terms of γ. If D is known, then the advancement of the interface x with time can be calculated. Alternatively a known value of D_α can be used to solve equation (38) if supreme accuracy is required.

Apply this to the nitriding of a 0.25mm thick piece of Pure Iron at 800°C, at a potential just greater than that required

to obtain γ phase, the time to reach the centre can be calculated numerically as above using $D\gamma = 5.73 \times 10^{-9} cm^2/sec$ obtained from the data of Grieveson and Turkdogan [127]. Values of C_1 and C_2 obtained from the Fe-N phase diagram[16,35] are 0.038 and 0.462 respectively. The calculated times for various values of C_3 are shown in table 19, and clearly show that the surface concentration has a significant effect on the rate of advance of the γ/α interface. Once the advancing interfaces meet then equation (39) no longer applies and the diffusion equations for a thin plate must be applied[135], these are

$$\frac{\bar{C} - C_1}{C_f - C_1} = 1 - \frac{4}{\pi} \sum_{v=0}^{\infty} \frac{(-1)}{(2v+1)} \cdot e^{\frac{-D\pi^2 t(2v+1)}{l^2}} \cdot \cos \frac{(2v+1)\pi x}{l} \qquad (40)$$

where $\bar{C}$ = composition at any point x

C_1 = initial composition

C_f = Surface composition

v = integer

l = thickness of specimen (cm)

D = Diffusion coefficient (cm^2/sec)

t = time (sec)

or

$$\frac{M_t}{M_\infty} = 1 - \sum_{v=0}^{\infty} \frac{8}{(2v+1)^2\pi^2} \cdot e^{\frac{-D\pi^2 t(2v+1)}{l^2}} \qquad (41)$$

where Mt = weight of specimen after time t.

M_α = weight of specimen after infinite time

for long diffusion times (appreciable build up of diffusing substance in centre of specimen) the equations reduce to

$$\frac{\bar{C} - C_1}{C_f - C_1} = 1 - \frac{4}{\pi} e^{\frac{-D\pi^2 t}{l^2}} \cdot \cos \frac{\pi x}{l} \qquad (42)$$

$$\frac{M_t}{M_\infty} = 1 - \frac{8}{\pi^2} e^{\frac{-D\pi^2 t}{l^2}} \qquad (43)$$

The solution for the complete nitriding situation is therefore complex and is best solved in the following manner. (A) Calculate time required to produce homogeneous specimen, assuming all diffusion is in single phase austenite, using equation 43. This time is independent of surface composition, and only depends on the specific accuracy of the homogeneous specimen. The specific accuracy represents the percentage difference between the intended composition and the actual composition. Table 20 shows the calculated times for various accuracies and different thickness specimens at 750°C, 800°C and 850°C using known D_{γ}^{N} values. Equation (43) is transformed to the following to make the calculation.

$$t = -\frac{l^2}{\pi^2 D} \cdot \ln\left[\frac{\pi^2}{8}(1 - M_t/M_\alpha)\right] \qquad (44)$$

(B) Calculate using equation (42) the time required to reach the $\gamma/\gamma + \alpha$ boundary composition at the centre of the strip for various surface concentrations. These are shown in table 21.

$$t = \frac{-l^2}{\pi^2 D} \cdot \ln\left[\frac{\pi}{4}\left(1 - \frac{(\bar{c} - c_i)}{(c_f - c_i)}\right)\right] \qquad (45)$$

Then total time required to produce homogeneous specimen is

$$t_{(\text{Table 7})} + (t_{\text{Table 8}} - t_{\text{Table 9}}) \qquad (46)$$

e.g. a 0.25mm thick specimen at 800°C
to 1% specific accuracy.

time = 4.12h + (13.50 - 2.73)h = 14.89 h (Surface con 1.0%)

2.60h + (13.50 - 1.93)h = 14.29 h (" " 1.5%)

6.3 Initial Experiments.

To check these calculations, specimens of ~0.3mm thick pure iron strip were nitrided at 800°C for relatively short times to

monitor the movement of the γ/α interface. An inlet gas mixture of $5.75^{v}/o$ NH_3/H_2 was used, giving an exhaust level of $3.7^{v}/oNH_3$ by infra-red analysis and an r value of 4×10^{-2} (see equation 27). According to Atkinson et al[115], this r value would give a surface potential of $1.5^{w}/o$ nitrogen (see fig.7).

The results (table 22) indicate that the γ/α interface moves considerably faster than the above calculations indicate. A possible explanation for this large discrepancy between calculated and experimental results is the compositional dependence of the diffusion coefficient, similar to that found with carbon in γFe[136]. This was confirmed by determination of the nitrogen profile by microprobe analysis (fig.48) showing the type of profile which Crank[135] predicts for compositional dependent diffusion coefficients.

Using the data from specimen 14 (table 22) and assuming a surface concentration of 1.5% and a γ/α boundary concentration of 0.462%, a diffusion co-efficient was calculated using equation 39, resulting in a D_{γ}^{N} value of $1.83 \times 10^{-8} cm^2/sec$ over 3 times greater than that estimated from Grieveson's data[127].

Using this value of D_{γ}^{N} just determined, the recalculated time for meeting of the γ/α interface is 1 hour (confirmed by the through nitriding of specimen 15). The estimated nitrogen content at the centre of specimen 15 is $0.68^{w}/o$, this has been calculated as follows.

Time to reach 0.462%N in centre by equation 41 = 37 min.

" " " " " " " " 39 = 1 h.

Time lag = 23 min.

Equivalent time to be used for Specimen 15 in calculating concentration at centre using equation 42 is actual time 80 min - time lag 23 min = 57 mins. Using this equivalent time, an estimated nitrogen concentration of $0.68^{w}/o$ at the centre is obtained, this is confirmed by microprobe analysis, see fig.48

The estimated time to reach 1% homogeneity calculated from the revised D_{γ}^{N} of 1.83×10^{-8} cm^2/sec is 5.31h for a 0.27mm thick specimen, approximately three times faster than the original estimate. However treating a specimen for this time period did not produce a homogeneous specimen, but surprisingly resulted in a smaller weight gain ($0.55^{v}/o$) than the 80 minute specimen, and in addition the specimen was severely blistered. The resulting microstructure was martensite and ferrite.

Further specimens were nitrided for short times using different gas mixtures (table 23), and through nitriding was achieved in less than 1 hour confirming the faster diffusion rates, the resulting microstructures are shown in figs 49-51. Again increasing the treatment time to that required for a homogeneous specimen produced a similar result to that just described, with a smaller weight gain and considerable amounts of ferrite in the structure. For example specimen 19 was treated for $6\frac{1}{2}$h at $800^{o}C$ in a $12.7^{v}/o NH_3/H_2$ producing a weight gain of only $0.75^{w}/o$ and a badly blistered specimen with a microstructure shown in fig.52.

It became clear from these initial investigations that there could be considerable problems with long time nitriding operations and further investigation into the blistering and denitriding phenomena was warranted.

6.4 Further investigations into void formation during long time nitriding.

Additional pure iron specimens of different thicknesses were nitrided under a variety of conditions. In the first instance, thin specimens (0.1mm) were nitrided at 845°C for rapid through nitriding, table 24 shows the results obtained.

For specimens 20, 22 and 27 the nitriding potentials used would give surface potentials $\geq$ 1.3%(see fig.7). By Grieveson's diffusion data [127], the calculated through nitriding and homogeneous nitriding times are 7 mins and 60 mins respectively. However, it has already been shown (section 6.3) that diffusion is in fact about three times faster than these calculated times, and therefore all three specimens should be homogeneous. Metallographic examination shows that this is not true; fig 53 shows that the relevant microstructures exhibit variations in structure, particularly that of specimen 27, which consist of martensite, ferrite, possible grain boundary nitrides and considerable gross porosity resulting in considerable blistering. From these observations it would appear that blistering is not directly related to treatment time, but more likely to be indirectly related through either

(a) specimen thickness or

(b) nitriding potential/surface nitrogen level.

At the lower nitriding potential (specimens 37-40), a similar oscillation in weight change was observed. Assuming a surface nitrogen potential of 0.35% (the $\gamma + \alpha/\alpha$ boundary occurs at $0.25^{w}/oN$), through nitriding would be expected in 48 mins, using Grievesons data [127], the extended time is due to lower surface potential. However, metallographic examination shows through nitriding in only 15 mins in parts of specimen 37 (fig. 54 (a)) again confirming the faster diffusion rate for nitrogen. All traces of ferrite are not removed until between 30 and 60 mins treatment time (fig.54(b)-(d)) but continued treatment results in reappearance of ferrite. This series of experiments therefore suggests that void formation is independent of nitrogen potential and nitrogen level in solid solution, and is therefore related to specimen thickness.

To confirm this, nitriding of thicker (0.38mm) specimens was carried out at 845°C (table 25). The average penetration of the γ/α interface represents D_{γ}^{N} values of 2.52×10^{-8} and $2.38 \times 10^{-8} cm^2 sec^{-1}$ respectively for specimens 34 and 35, compared with Grievesons[127] value of $1.22 \times 10^{-8} cm^2 sec^{-1}$. Long time exposure (specimen 33) resulted in a structure (shown in fig 55) exhibiting large pools of ferrite, most of which are ellipsoidal, with a crack-like defect at the axis. Close examination of the γ/α boundary at the edges of the ellipses revealed not a plane interface but an extremely jagged one, suggesting that the α phase was 'eating into' the γ phase (fig.56). Further examination of specimen 35 revealed similar conditions existing at some γ/α interfaces. In specimens nitrided at different potentials (table 26) for long times, structures similar to that shown in fig. 55 were observed (fig.57), in all cases some form of defect being associated with the

ferrite in the centre of the structures.

It can therefore be concluded that void formation and associated ferrite reversion only occurs after completion of through nitriding, but before complete homogeneity can be established. Clearly, if the phenomena only occurs at this stage, there should be no detrimental effect in the surface hardening of heavy sections in industrial processing. However, because the phenomena is interesting from the physical metallurgical viewpoint, still further consideration will be given to void formation during production of homogeneous specimens.

6.4.1. Experimental investigation of blistering.

It was therefore decided to monitor the ferrite reversion effect by a series of kinetic specimens. Pureiron specimens 0.27mm thick were nitrided in $8.54^{v}/oNH_3/H_2$ mixtures at $710^{o}C$, the resulting nitriding potential being equivalent to a surface potential of 2.42^{w}/onitrogen (see fig.7). Table 27 shows the results obtained, the kinetic weight change curve being shown in fig.58.

Using the γ/α interface penetration data from specimen 184, a value of $4.86 \times 10^{-9} cm^2 sec^{-1}$ for D_{γ}^{N} was obtained. This value of D_{γ}^{N} was then used to calculate a theoretical weight gain curve as follows. Using equation (39), the γ/α interface penetrationwas calculated for times up to through nitriding - 5.5h, the weight gain was then estimated by the method illustrated in fig.59. For times $>$ 5.5h equation (43) was used with a

corrected time value, as time to reach 1.0$\overset{W}{\%}$N ($\gamma/\gamma + \alpha$ boundary composition) inthe centre by nitriding in single phase γ (equation 42 and 43) is only 3.5h compared with 5.5h for γ interface penetration. Therefore to calculate the weight gain for 7h, equation 43 is used with t = 5h. (i.e. $t = t_{Actual} - 2h$). The calculated curve is also shown on fig. 58. A step occurs in the calculated curve where the equations change, this is due to the fact that the method of fig.59 implies some compositional dependence of diffusion coefficient whereas equation (43) does not. This difficulty cannot readily be overcome.

It can be seen that the sudden loss of nitrogen does not occur until some 1.5h after complete penetration of the γ/α interface has occurred. Assuming that denitriding occurs in a planar interface (similar to decarburisation), times for various states of denitridation can be calculated using equation (38), assuming the nitrogen content to be constant at the surface with values for D_{γ}^{N}, D_{α}^{N} 5×10^{-9} and 5×10^{-7} cm^2/sec respectively. The calculated times for 50, 100 and 130μ thickness of ferrite are 21, 83 and 141 mins respectively. The observed penetration of γ in the 8.5h specimen is a maximum of 25 - 30μ, indicating a denitrided ferritic layer of $\sim$ 100μ after 1.5h which agrees extremely well with these calculations. The actual γ penetration is not planar but concave, as was shown in previous specimens which have denitrided from the centre. This would indicate the possible existence of sinks or defects randomly distributed along the centre of the specimen. The ferrite structure is also columnar indicating that denitriding has in fact taken place; during nitriding the ferritic structure is equiaxed amd the interface planar. Parts of the specimen show very little

penetration of γ, this would not necessarily suggest a faster diffusion of nitrogen through ferrite, but more likely that the sink for nitrogen gas is nearer the surface and not in the centre of the specimen (defects have been observed away from the centre).

For the longer treatment time of 16 h, similar γ penetration and nitrogen weight gain are observed. This suggests that an equilibrium is set up between the rate of supply of nitrogen to the γ interface, penetrating into α, and the rate of denitriding, through α penetrating into γ. The same denitriding phenomena is observed at lower temperatures (~ 660°C).[74]

Several investigations have been made of the penetration of austenite into ferrite in the Fe-N system [137-139], but none have investigated complete penetration and subsequent effects. Grozier[137] however refers to equilibrium weight gains obtained in 0.05mm strip, and Atkinson et al[115] report homogeneous nitriding in strips 0.1mm thick. Blistering phenomena was occasionally observed by Atkinson and Bell[140], but no investigation was ever undertaken.

6.5. Proposed Model for Void Formation.

These findings have lead to the following hypothesis.

During nitriding defects, as yet unspecified, are formed in the overlapping diffusion profiles. At such a defect, a possible sink for gas phase constituents exists, analogous to the formation of gas phases in nuclear irradiated materials[141]. As the Fe-N system is metastable with regard to the gas phase, the

presence of a defect within the structure constitutes a pressure release point, at which nitrogen atoms can recombine to form nitrogen gas. Once formed, bubbles do not redissolve and their only release is by swelling and bursting at a free surface[141]. Nitrogen gas void formation is therefore a viable proposition. Because the situation is such that a γ interface is progressing into an α matrix, the rate of penetration of the interface depends on the diffusion of nitrogen through austenite. But D_{α}^{N} is at least two orders of magnitude faster than D_{γ}^{N} and so nitrogen atoms presented at the γ/α interface can be readily removed by diffusion through ferrite. Once a defect exists as a gas sink, then nitrogen atoms in ferrite will move towards the sink to form gas, depleting the existing ferrite, which in turn replenses itself by removing nitrogen from the advancing γ/α interface. Because of the large differences between D_{γ}^{N} and D_{α}^{N}, nitrogen can be removed from the γ/α interface faster than it can diffuse from the surface to the γ/α interface, and consequently the γ/α interface reverses towards the outside of the specimen.

As the γ/α interface recedes, the build up in gas pressure inside the voids can become sufficient to cause yielding of the bulk of the specimen probably by creep. Considering the metastable equilibrium between nitrogen in solid solution in ferrite and the solubility of nitrogen gas at 1 atmosphere pressure, an estimate at the pressure within a void can be made using Sievert's law - the solubility of a diatomic gaseous element in a metal is proportional to the square root of the pressure.

The solubility nitrogen in ferrite at 800°C and 850°C is 0.029 and 0.0165 w/o respectively, the solubility of nitrogen gas at 1 atmosphere pressure in ferrite at these temperatures are 2.535×10^{-3} and 3.048×10^{-3} w/o respectively. Applying Sieverts law, the resulting gas pressures due to nitrogen in solid solution are 131 and 29.3 atmospheres for 800 and 850°C respectively, equivalent to 1.34 and 0.30 kg/mm^2 respectively. Considering the effect of temperature on the volume of gas released, these pressures would be at least 5.26 and 1.23 kg /mm^2 Recent hot hardness results on various phases in steel[142] give hardnesses of approximately 10kgf/mm^2 for ferrite at temperatures greater than 800°C, and hardnesses of 25 and 20 kgf/mm^2 for austenite at temperatures of 800 and 850°C respectively. It is not inconceivable therefore that the internal gas pressures developed can cause creep and yielding in iron at these temperatures.

6.6 Conclusions.

(1) Calculation of diffusion coefficients for nitrogen in austenite from γ/α interface penetration data has produced a value up to 3 times larger than currently accepted data. This has been linked to the compositional dependency of D_γ^N.

(2) Investigations of void formation has evolved a model which attributes the phenomena to the intersection of advancing austenite/ferrite interfaces in through nitriding of pure iron.

(3) An important inference from (2) is that the surface hardening of heavy sections with high nitrogen content cases should not suffer from gas voids.

TABLE 17

SURFACE NITROGEN CONTENTS OF NITRIDED PURE IRON SPECIMENS.

Specimen No.	Time (h)	Temp. (°C)	Atmosphere	r value x10^2	Surface Nitrogen (w/o) From Fig.7	Surface Nitrogen (w/o) By EPMA
15	1.33	800	5.75 v/o NH_3/H_2	4	1.5	1.55
16	1.50	"	17.35 v/o " "	9.5	2.5(a)	2.00
17	1.00	"	11.44 v/o " "	9.3	2.4	2.10

(a) Surface Nitride Precipitation.

TABLE 18

CALIBRATION DATA FOR QUANTOVAC FROM NITRIDED PURE IRON SPECIMENS

Specimen No.	Quantovac Spark Readings (MV)	Nitrogen Content (w/o)
15	295, 290	1.38
16	324, 320	1.88
17	336, 341	1.92

TABLE 19.

CALCULATED TIMES FOR γ/α INTERFACE TO REACH CENTRE OF 0.25mm THICK PURE IRON STRIP AT 800°C FOR VARIOUS SURFACE CONCENTRATIONS.

SURFACE CONCENTRATION C_3	($^W/_{oN}$)	TIME (h)
	0.48	90
	0.75	6.74
	1.00	4.12
	1.50	2.60

Using a value of $D_\gamma^N = 5.73 \times 10^{-9} cm^2/sec$ (127)

TABLE 20.

CALCULATED TREATMENT TIMES FOR SPECIFIC ACCURACIES OF HOMOGENEOUS SPECIMENS.

Specific Accuracy.	Temperature (°C)	$\ln\left[\frac{\pi^2}{8}\left(1-\frac{M_t}{M_\infty}\right)\right]$	Time required for various thicknesses. (h)				
			0.1	0.25	0.38	0.50	0.75 mm
10%	750	-2.0926	2.85	17.82	41.16	71.27	160.35
	800	"	1.03	6.42	14.84	25.70	57.82
	850	"	0.44	2.77	6.40	11.09	24.94
1%	750	-4.3952	5.99	37.42	86.46	149.69	336.80
	800	"	2.16	13.50	31.18	53.97	121.43
	850	"	0.93	5.82	13.45	23.29	52.38

D_γ^N values used (127)

750	2.066×10^{-9} cm^2/sec
800	5.73×10^{-9} " "
850	1.328×10^{-8} " "

TABLE 21

CALCULATED TIMES TO REACH 0.462 $^{W}/_{oN}$ AT CENTRE OF 0.25mm THICK PURE IRON STRIP AT 800°C FOR VARIOUS SURFACE CONCENTRATIONS

SURFACE CONCENTRATION $^{W}/_{oN}$	TIME (h)
0.48	11.17
0.75	3.80
1.00	2.73
1.50	1.93

Using a value of $D_{\gamma}^{N} = 5.73 \times 10^{-9} cm^2/sec$ (127)

TABLE 22

NITRIDING OF 0.27mm PURE IRON STRIP AT 800°C

CONSTANT POTENTIAL.

Specimen No.	Treatment Time (min)	Atmosphere	Wt.Gain (%)	γ/α interface penetration (μ)
13	5	5.75^{v}/oNH_3/H_2	0.124	20
14	40	" " "	0.797	110
15	80	" " "	0.970	through nitrided

TABLE 23.

NITRIDING OF 0.27mm PURE IRON STRIP AT 800°C

VARYING POTENTIAL.

Specimen No.	Treatment Time (min)	Atmosphere	Wt.Gain (%)	γ/α interface penetration
16.	90	17.35 v/o NH_3/H_2	1.47	through nitrided
17	60	11.44 " "	1.51	
18	80	" " "	1.40	
19	6.5h	12.71 " "	0.75	α' with random α structure and cracks.

TABLE 24

NITRIDING OF 0.1mm PURE IRON STRIP AT 845°C

Specimen No	Ammonia in Atmosphere (v/o) Inlet	Exhaust.	r x 10^2	Time	Weight Gain (%)	Structure
20	9.1	3.0x	3.3	30min	1.00	α'
22	"	3.25x	3.6	60 "	0.73	α '
27	"	4.50x	5.0	21.5h	1.37	α' + α + blisters
37	2.5	1.0	1.0	15min	0.23	α' + α
32	"	"	"	30min	0.25	α' + α at g.b
36	"	"	"	60 "	0.33	α'
38	"	"	"	2 h	0.12	α' + α at g.b.
39	"	"	"	4 h	0.19	" " "
40	"	"	"	8 h	0.78	α' + nitrides, cracks

x Original readings by infra-red meter.

Corrected by chromatography.

TABLE 25

NITRIDING OF 0.38mm PURE IRON STRIP AT 845°C

- CONSTANT POTENTIAL.

Specimen No	Ammonia in Atmosphere (v/o) Inlet	Exhaust	$r \times 10^2$	Time (h)	Weight Gain (%)	Structure	γ/α penetration
34	2.5	1.0	1.0	1	0.13	$\alpha' + \alpha$	80μ
35	"	"	"	2	0.14	$\alpha' + \alpha$	110μ
33	"	"	"	16	0.50	α' with large pools of α and blisters	-

TABLE 26

NITRIDING OF 0.38mm PURE IRON STRIP AT 845°C

- VARYING POTENTIAL.

Specimen No.	Ammonia in Atmosphere (v/o) Inlet(a)	Time (h)	Weight Gain (%)	Structure
29	5.0	16	0.29	α with large pools of α and blisters.
30	"	65.2	0.29	
28	9.1	17.1	0.39	
31	15.0	18	0.31	

(a) infra-red analyser not available for measurements, inlet analysis from flowmeter - later confirmed by analyser.

TABLE 27

NITRIDING OF 0.27mm PURE IRON STRIP AT 710°C

- CONSTANT POTENTIAL.

Specimen No	Ammonia in Atmosphere (v/o) Inlet	Exhaust	r x 10^2	Time (h)	Weight Gain (%)	Structure	γ/α penetration
184	8.54	7.92	9.0	4	1.49	α' + α	115μ
186	"	7.70	8.7	6	1.89	α'	through nitrided
187	"	"	"	7	1.93	α' + α	"
185	"	"	"	8.5	0.42	α' rim with α and blisters	
183	"	7.00	7.8	16	0.48		

FIG. 47

PRINCIPLE OF HOMOGENEOUS NITRIDING.

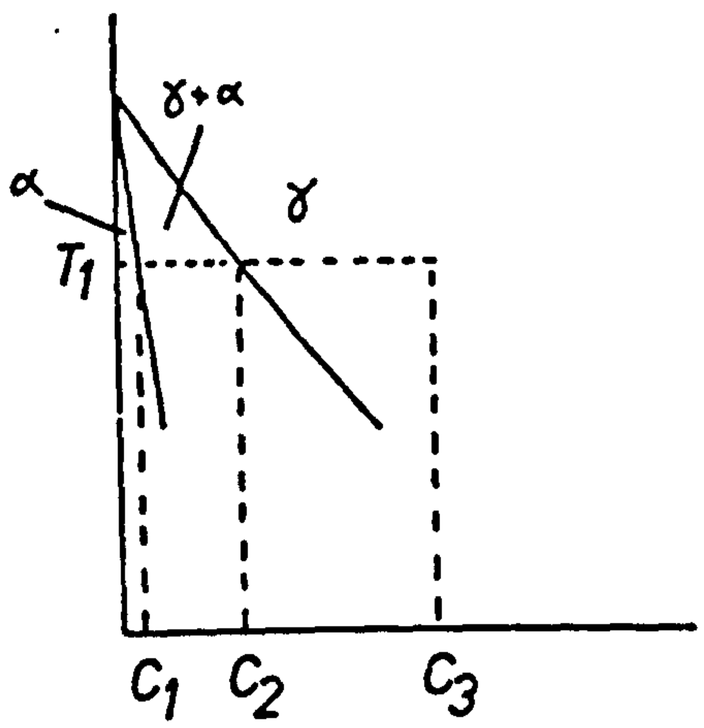

(a)

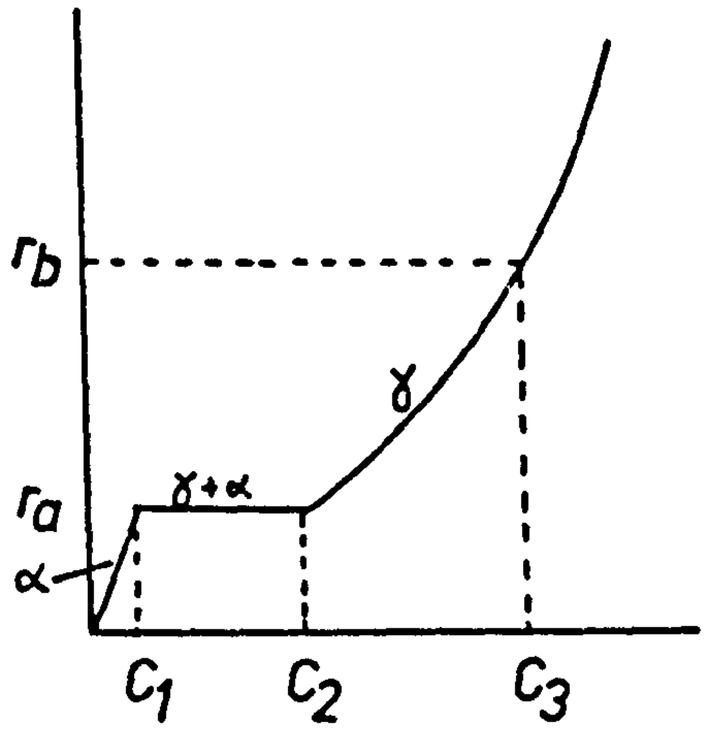

(b)

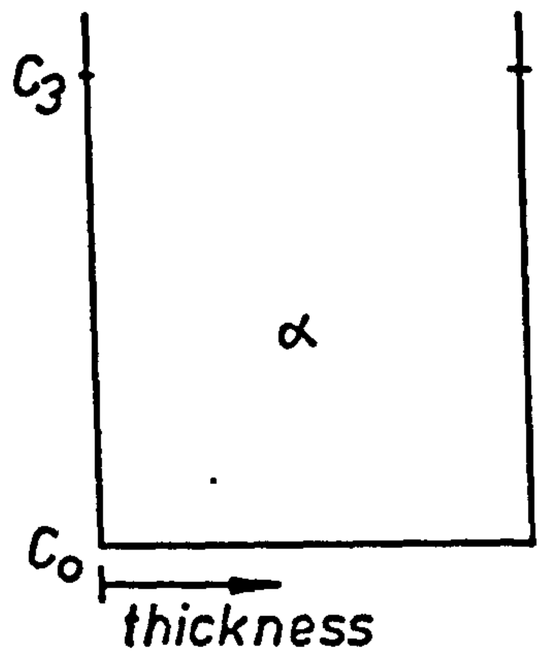

$t_1 = 0$

(c)

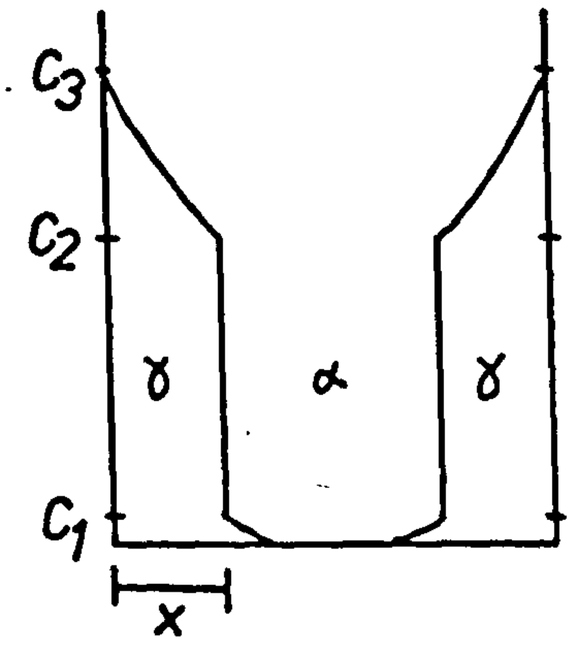

$t_2 > 0$
$< t_3$

(d)

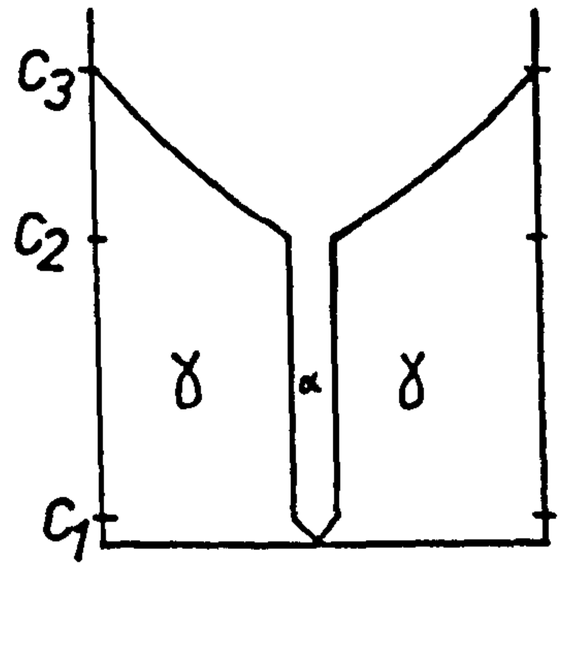

$t_3 \gg t_2$

(e)

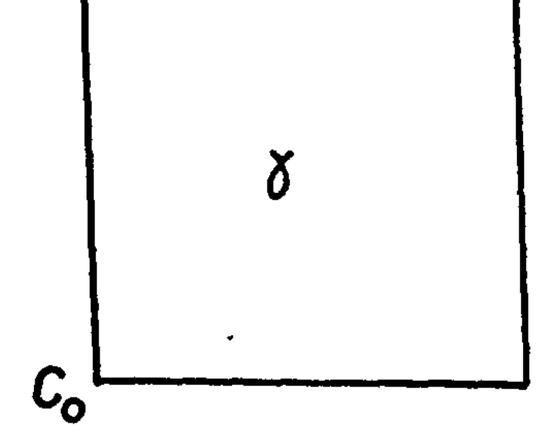

$t_4 \gg t_3$

(f)

FIG. 48

NITROGEN CONCENTRATION PROFILE ON SPECIMEN NO.15 AS DETERMINED BY EPMA.

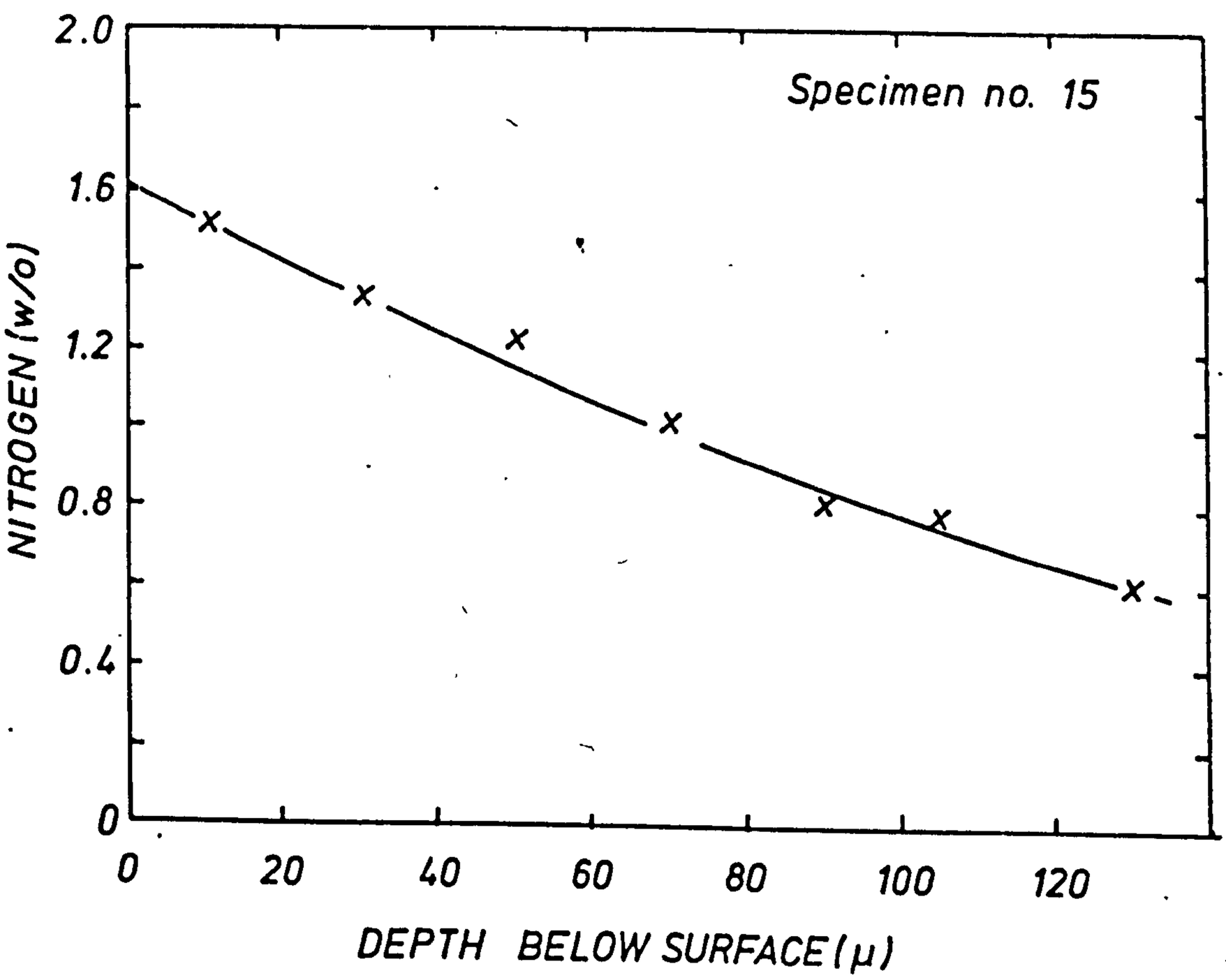
Specimen no. 15
NITROGEN (w/o)
2.0
1.6
1.2
0.8
0.4
0
0
20
40
60
80
100
120
DEPTH BELOW SURFACE (μ)

FIG.'49 SPECIMEN NO. 16

0.27mm THICK PURE IRON NITRIDED AT 800°C FOR 90 MIN. IN 17.35^{v}/oNH_3/H_2, ETCHED IN 2 ^{v}/o NITAL.

MAG. x200

FIG. 50 SPECIMEN NO. 17

0.27mm THICK PURE IRON NITRIDED AT 800°C FOR 60 MIN IN 11.44^{v}/oNH_3/H_2, ETCHED IN 2^{v}/o NITAL.

MAG. x200

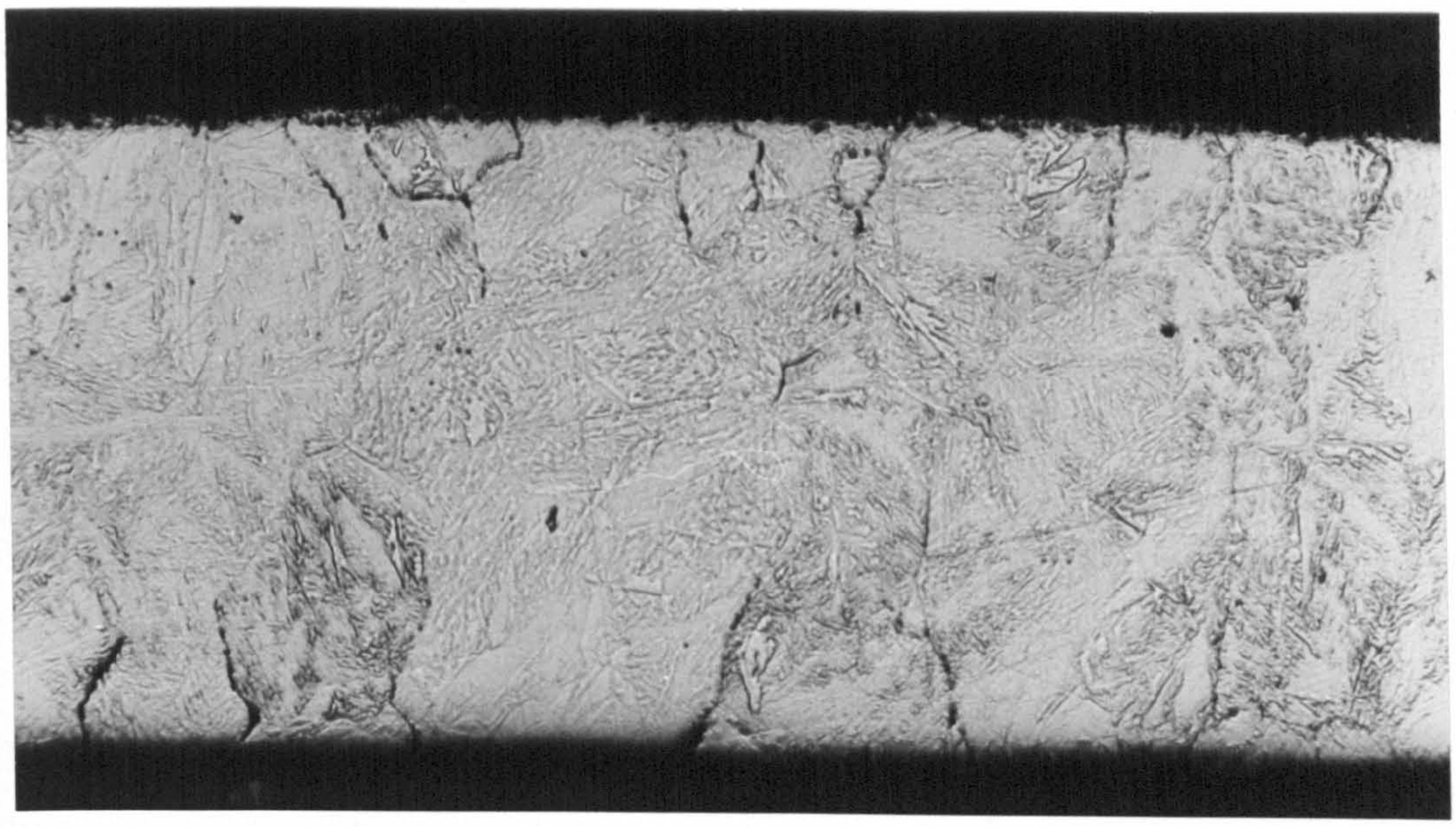

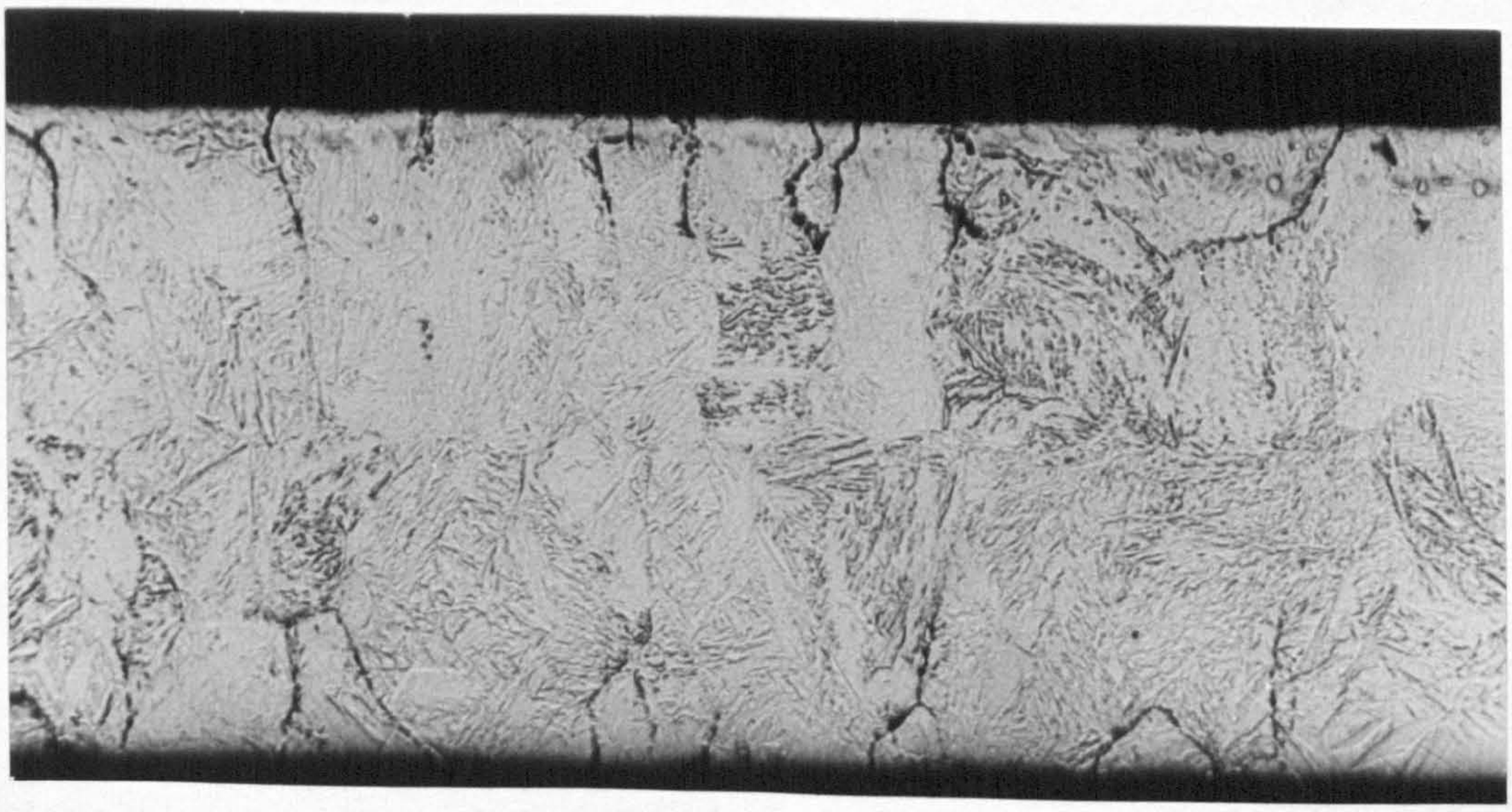

FIG. 51 SPECIMEN NO. 18

0.27mm THICK PURE IRON NITRIDED AT 800°C FOR 80 MIN IN 11.44^{v}/oNH_3/H_2, ETCHED IN 2^{v}/o NITAL.

MAG. x200

FIG. 52 SPECIMEN NO. 19

0.27mm THICK PURE IRON NITRIDED AT 800°C FOR 6.5h IN 12.71^{v}/oNH_3/H_2, ETCHED IN 2^{v}/o NITAL.

MAG. x200

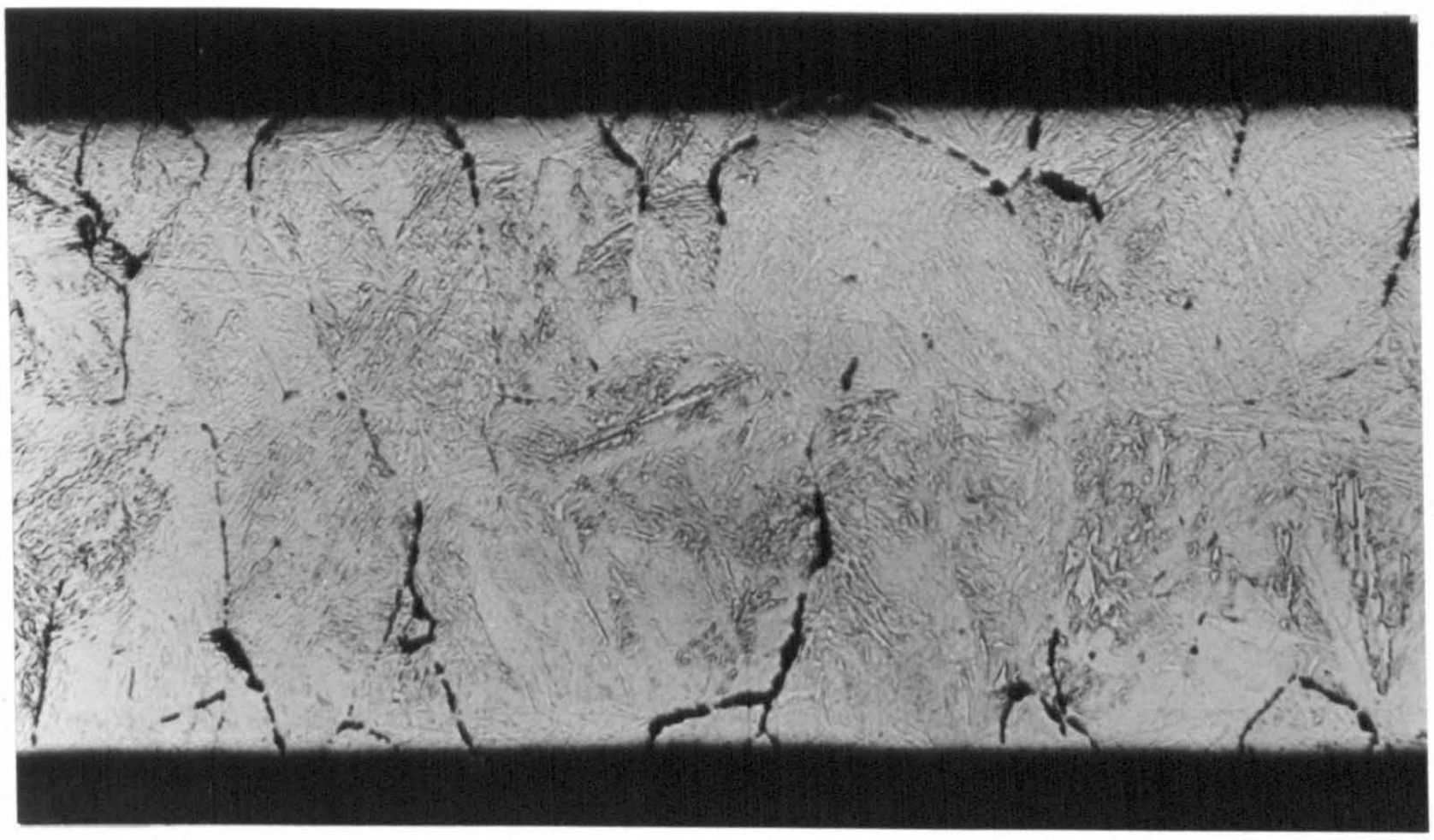

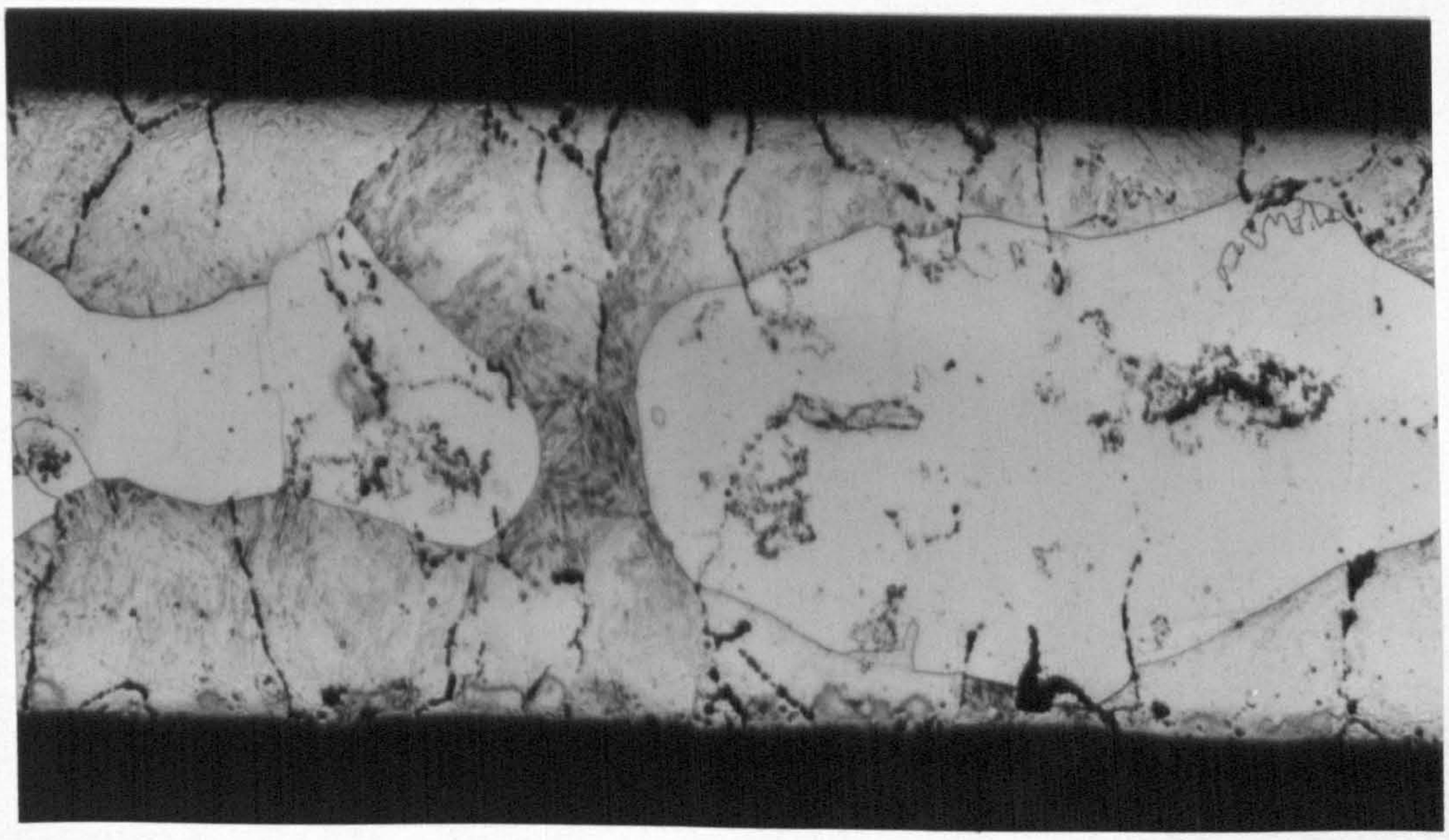

FIG. 53a SPECIMEN NO. 20

0.1mm THICK PURE IRON NITRIDED AT 845°C FOR 30 MIN IN 9.1^{v}/oNH_3/H_2, ETCHED IN 2^{v}/o NITAL.

MAG. x440

FIG. 53b SPECIMEN NO. 22

0.1mm THICK PURE IRON NITRIDED AT 845°C FOR 60 MIN IN 9.1^{v}/oNH_3/H_2, ETCHED IN 2^{v}/o NITAL.

MAG. x900

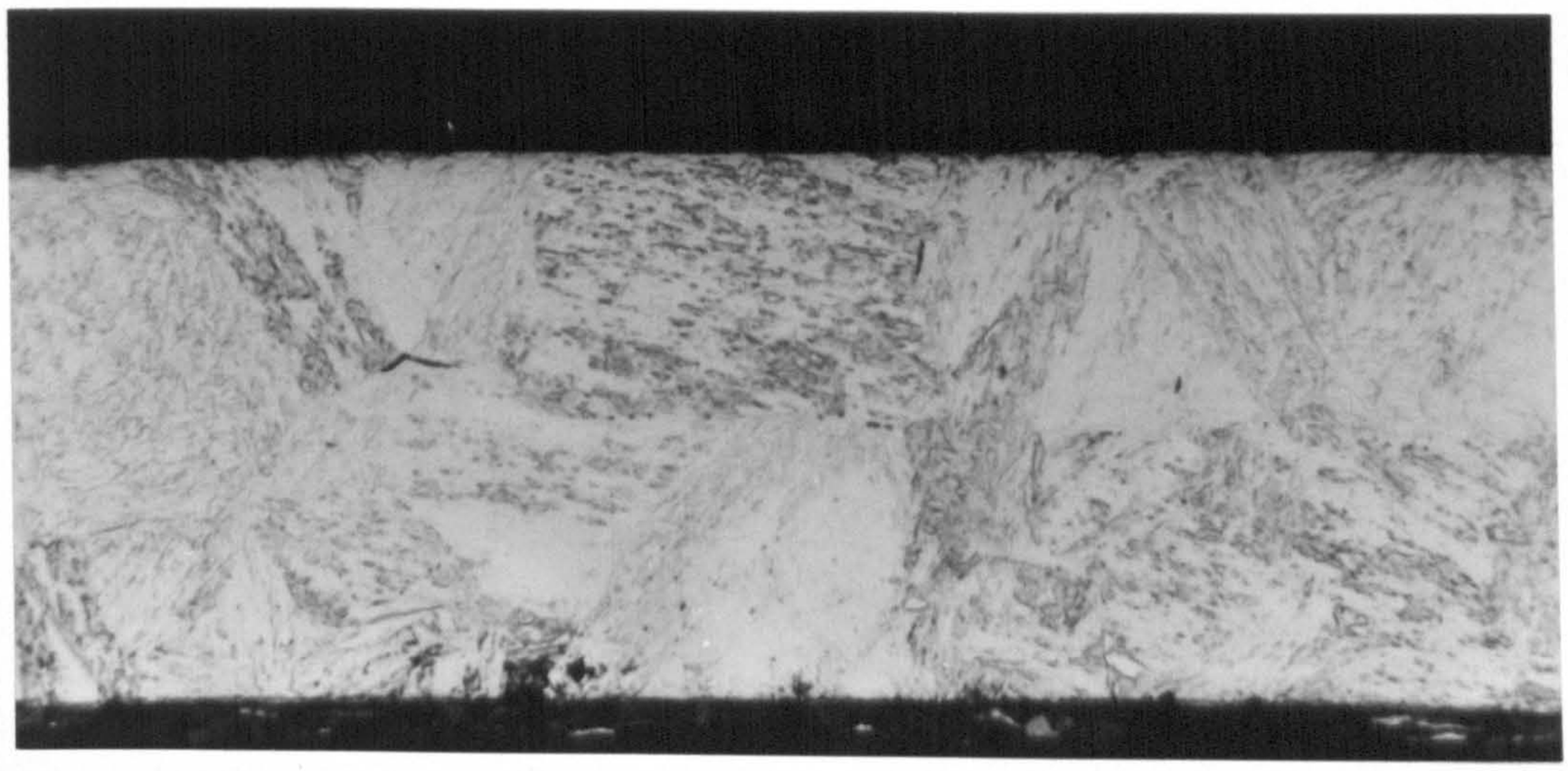

FIG. 53c SPECIMEN NO. 27

0.1mm THICK PURE IRON NITRIDED AT 845°C FOR 21.5h IN 9.1^{v}/oNH_3/H_2, ETCHED IN 2^{v}/o NITAL.

MAG. x300

FIG. 53d SPECIMEN NO. 27

AS FIG 53c, SAME MAGNIFICATION.

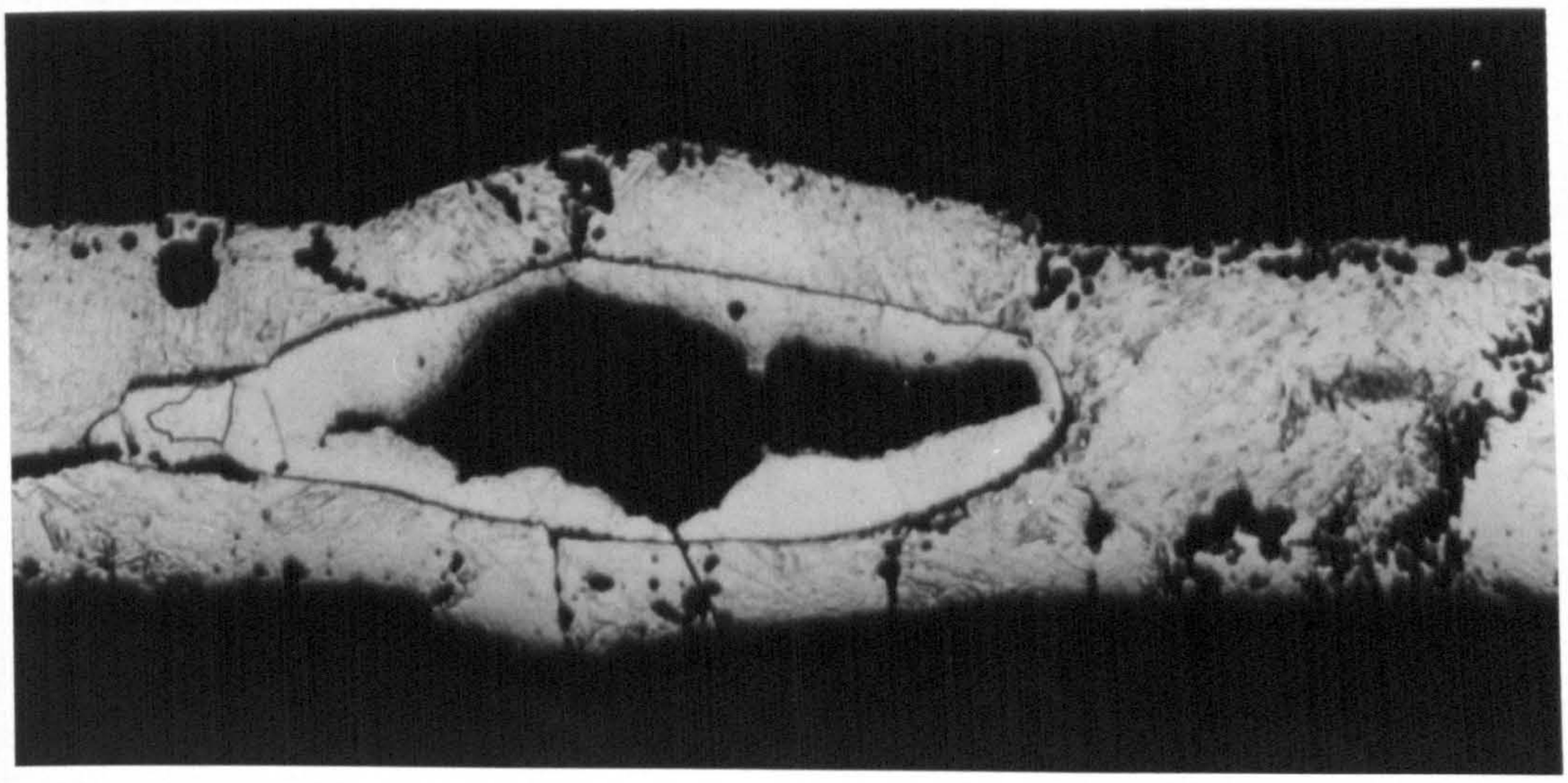

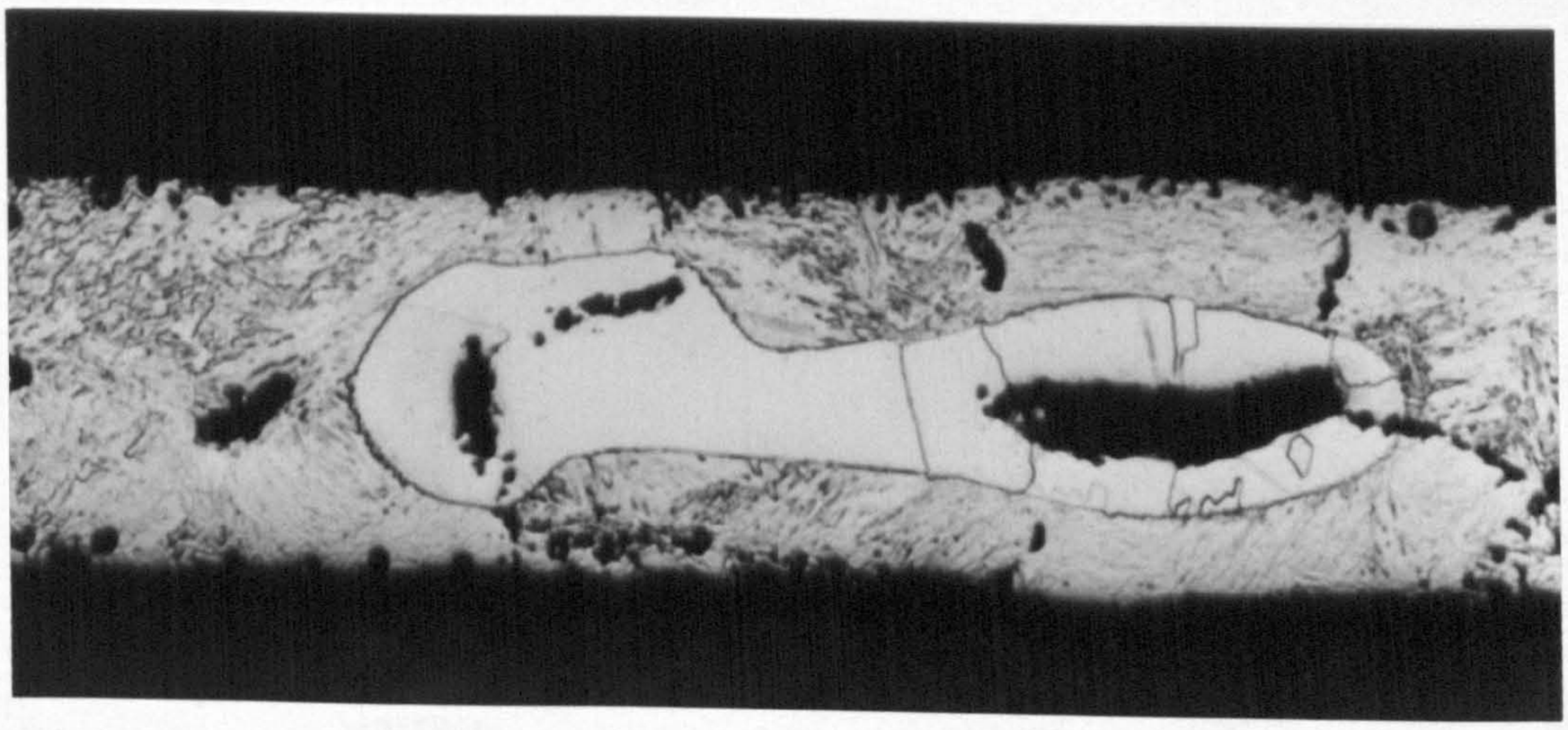

FIG. 54a SPECIMEN NO. 37

0.1mm THICK PURE IRON NITRIDED AT 845°C FOR 15 MIN IN 2.5^{v}/oNH_3/H_2, ETCHED IN 2^{v}/o NITAL.

MAG. x800

FIG. 54b SPECIMEN NO. 36

0.1mm THICK PURE IRON NITRIDED AT 845°C FOR 60 MIN IN 2.5^{v}/oNH_3/H_2, ETCHED IN 2^{v}/o NITAL.

MAG. x800

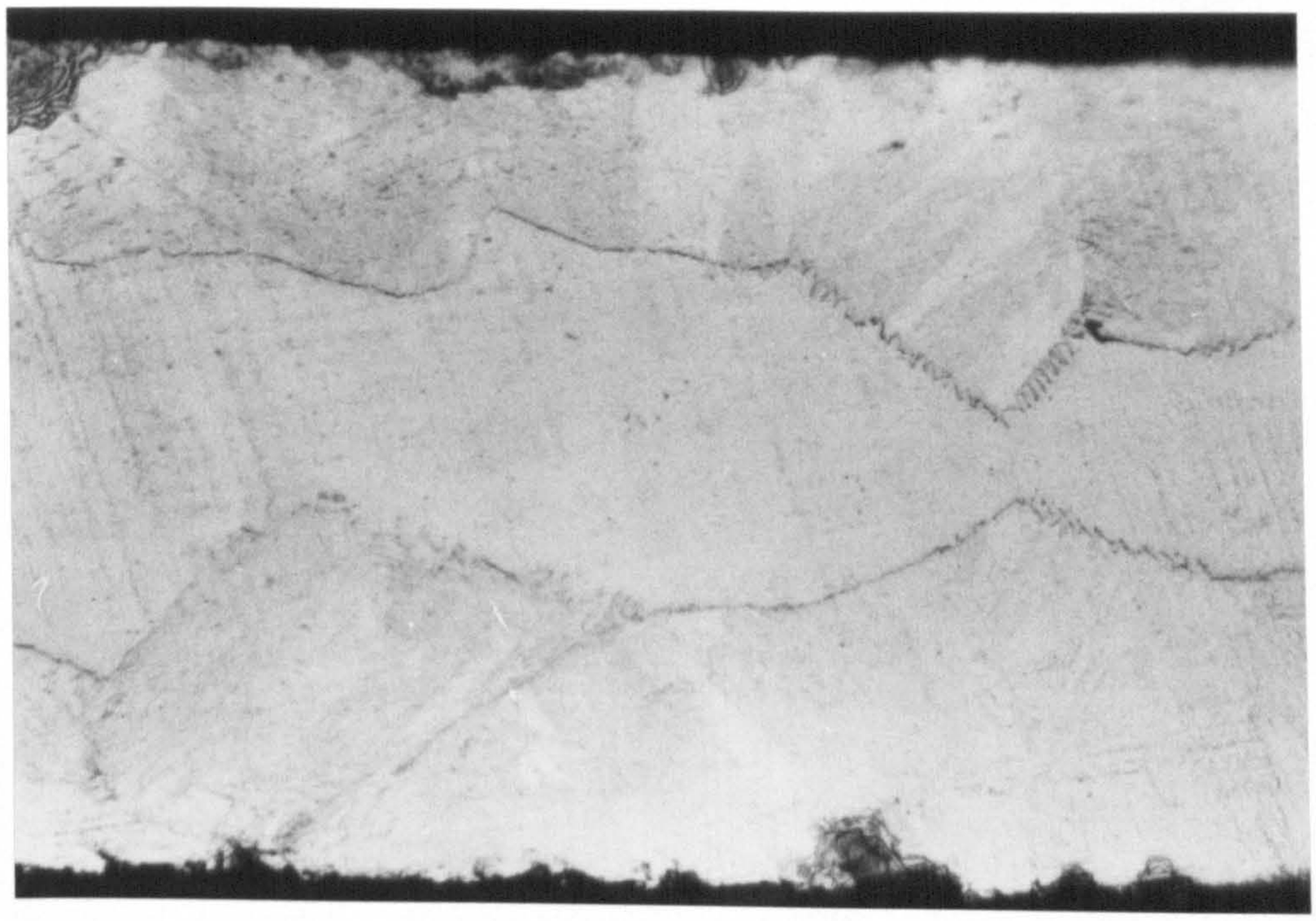

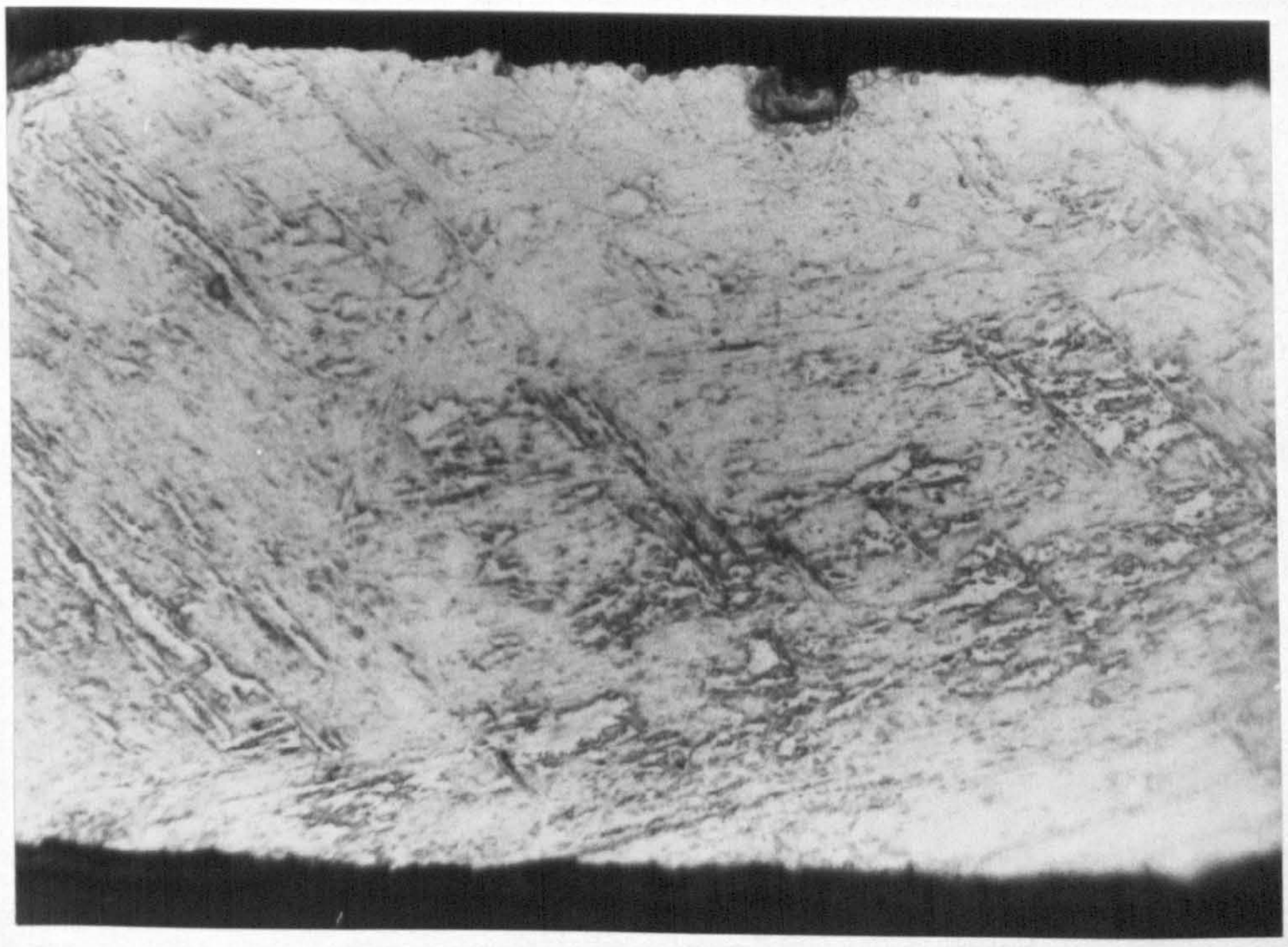

FIG. 54c SPECIMEN NO. 38

0.1mmTHICK PURE IRON NITRIDED AT 845°C
FOR 2h IN 2.5^{v}/oNH_3/H_2, ETCHED IN
2^{v}/o NITAL.
MAG. x800

FIG. 54d SPECIMEN NO. 40

0.1mm THICK PURE IRON NITRIDED AT 845°C
FOR 8h IN 2.5^{v}/oNH_3/H_2, ETCHED IN
2^{v}/o NITAL.
MAG. x800

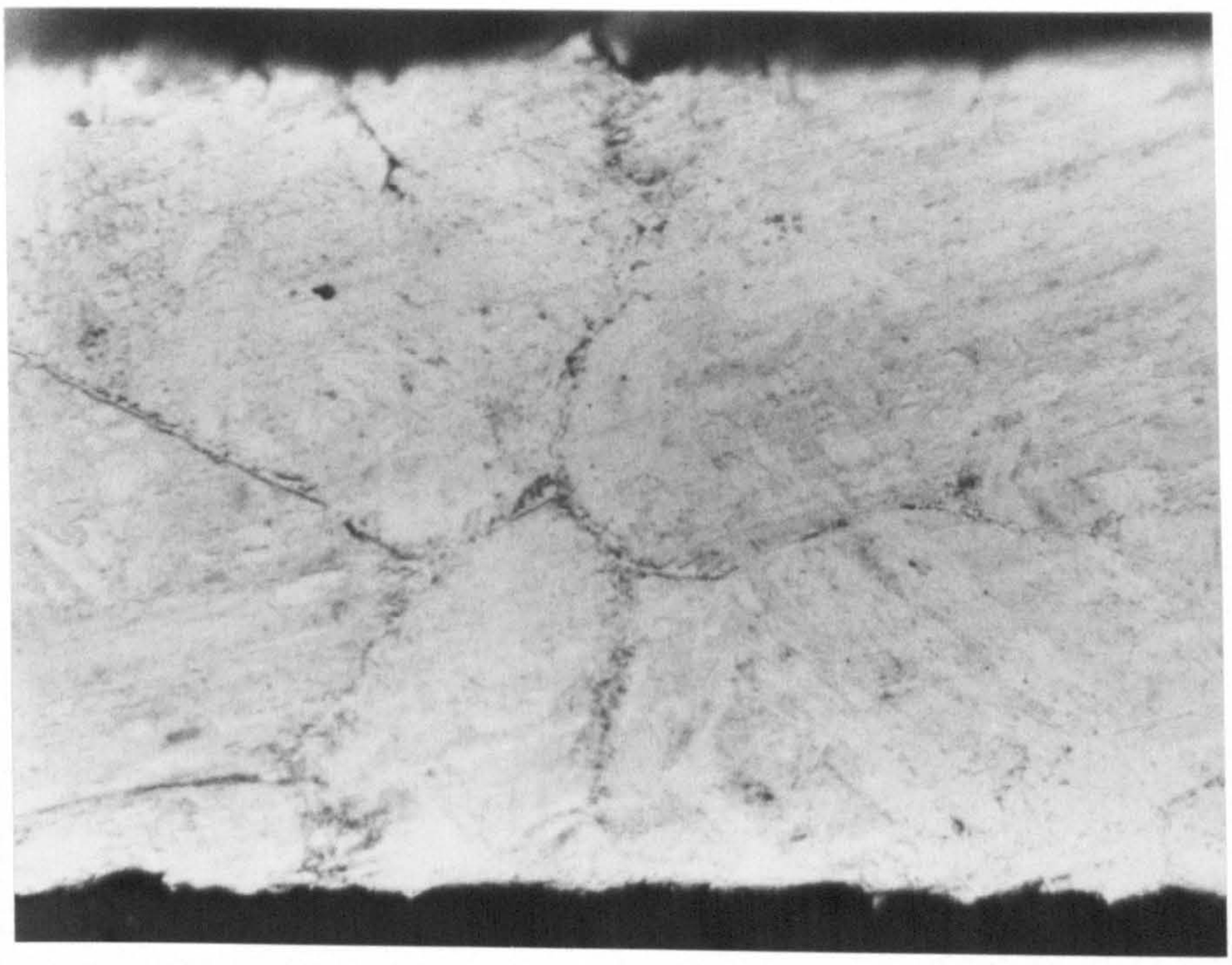

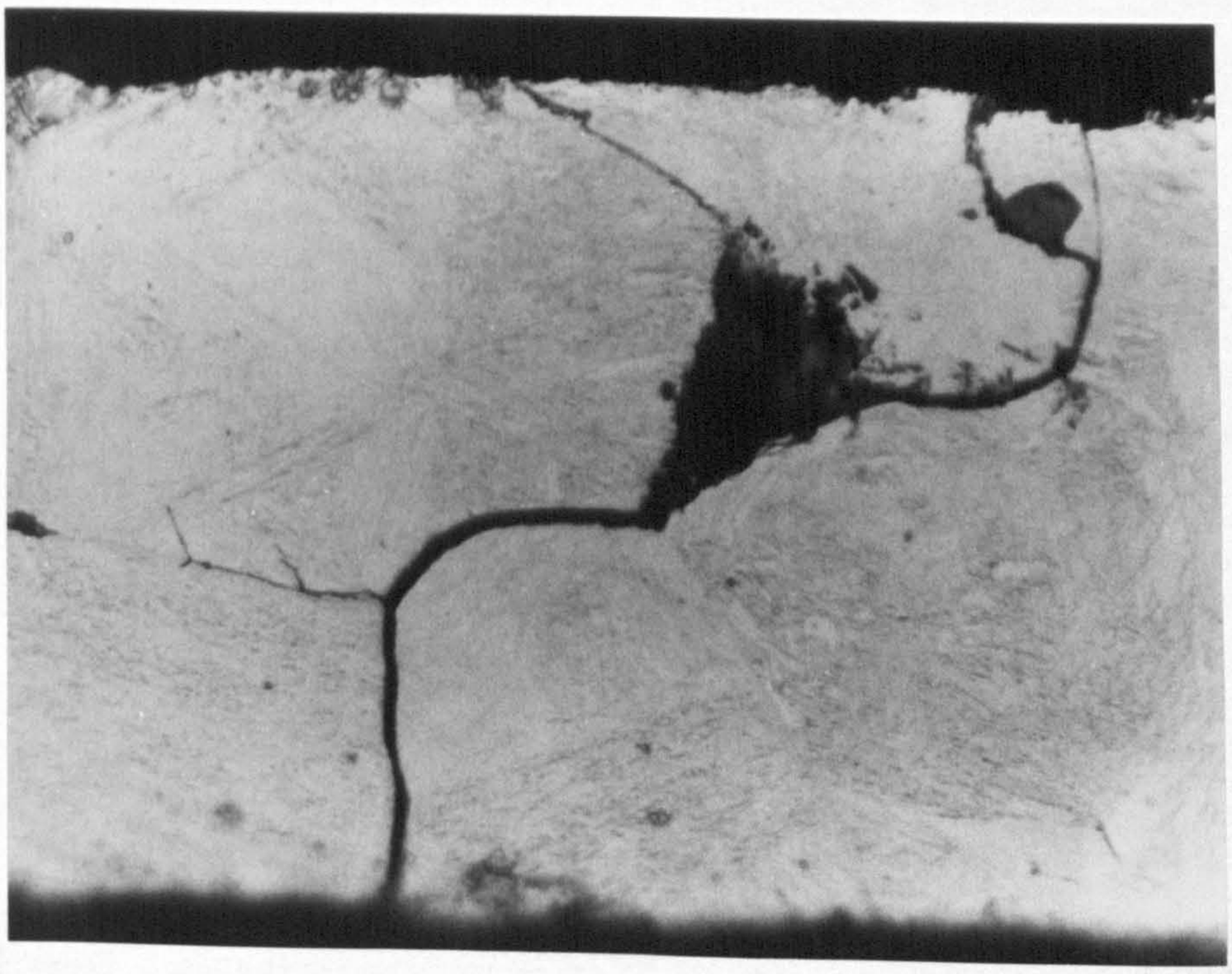

FIG.. 55 SPECIMEN NO. 33

0.38mm THICK PURE IRON NITRIDED AT 845°C FOR 16h IN 2.5^{v}/oNH_3/H_2, ETCHED IN 2^{v}/o NITAL.

MAG. x250

FIG. 56 SPECIMEN NO. 33

AS ABOVE, SHOWING THE FERRITE PHASE EATING INTO THE AUSTENITE PHASE (TRANSFORMED TO MARTENSITE ON QUENCHING).

MAG. x800

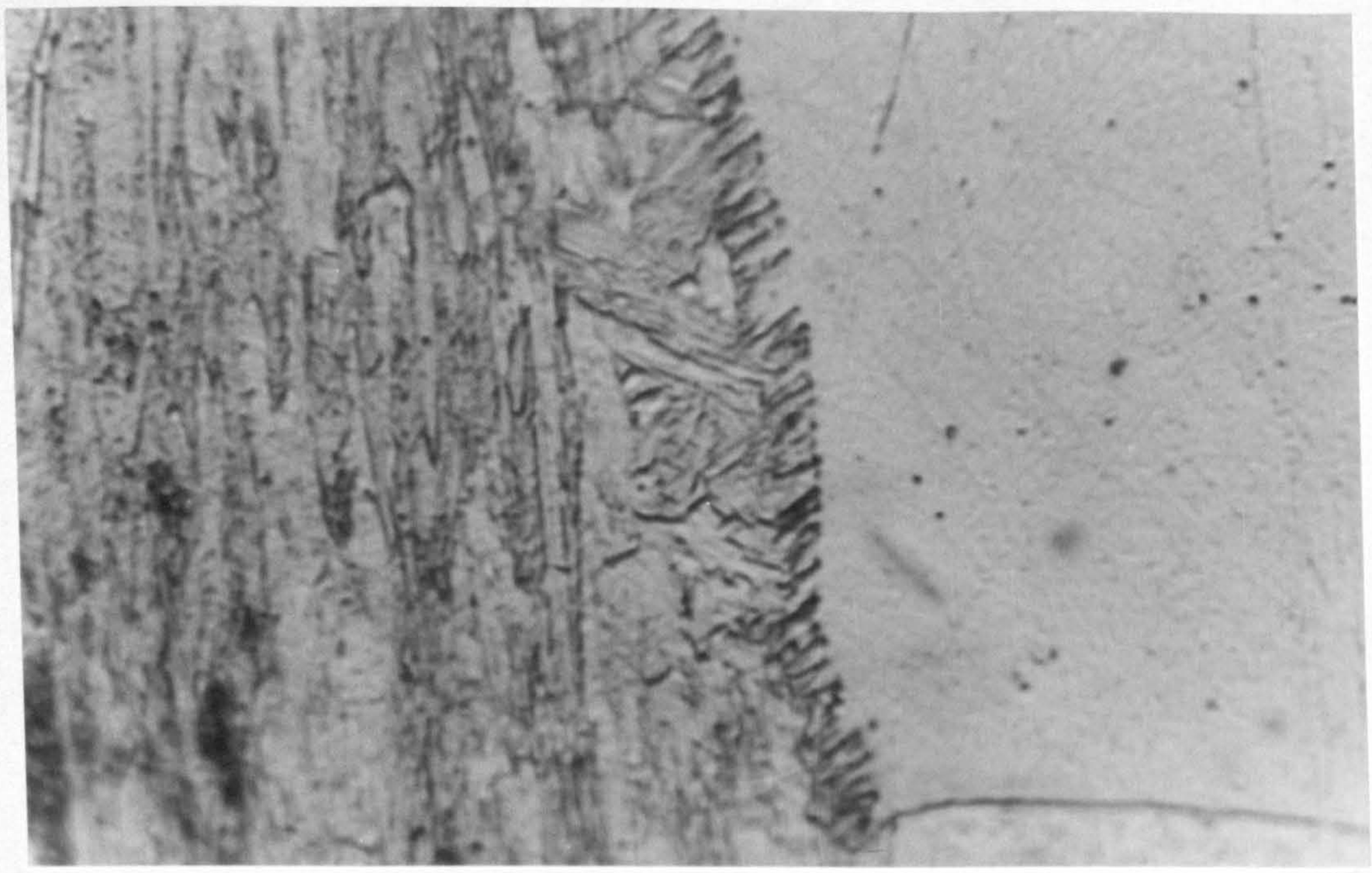

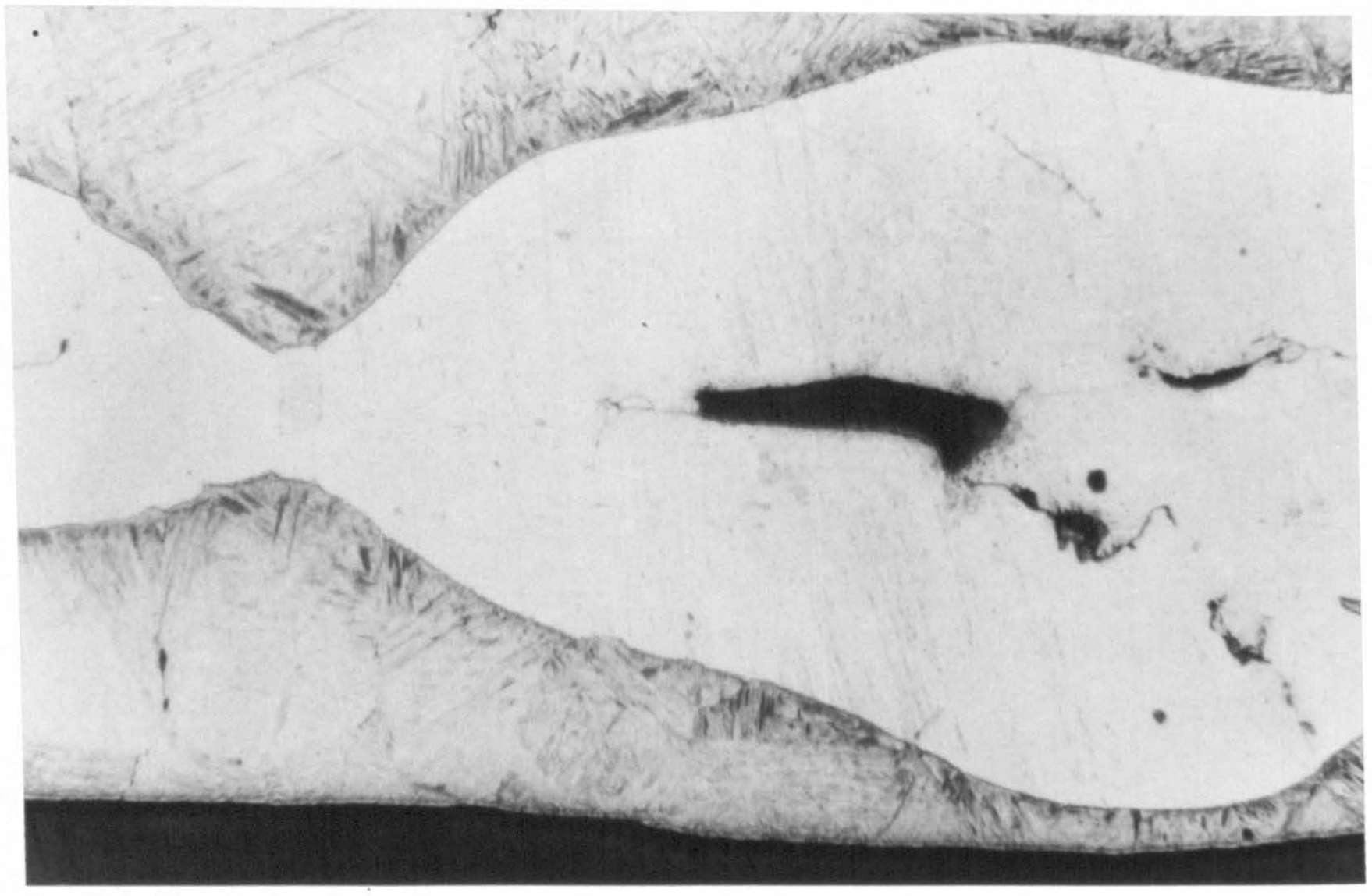

FIG.' 57a SPECIMEN NO. 29

0.38mm THICK PURE IRON NITRIDED AT 845°C FOR 16h IN 5^{v}/oNH_3/H_2, ETCHED IN 2^{v}/o NITAL.

MAG. x250

FIG. 57b SPECIMEN NO. 30

0.38mm THICK PURE IRON NITRIDED AT 845°C FOR 65.2h IN 5^{v}/oNH_3/H_2, ETCHED IN 2^{v}/o NITAL.

MAG. x100

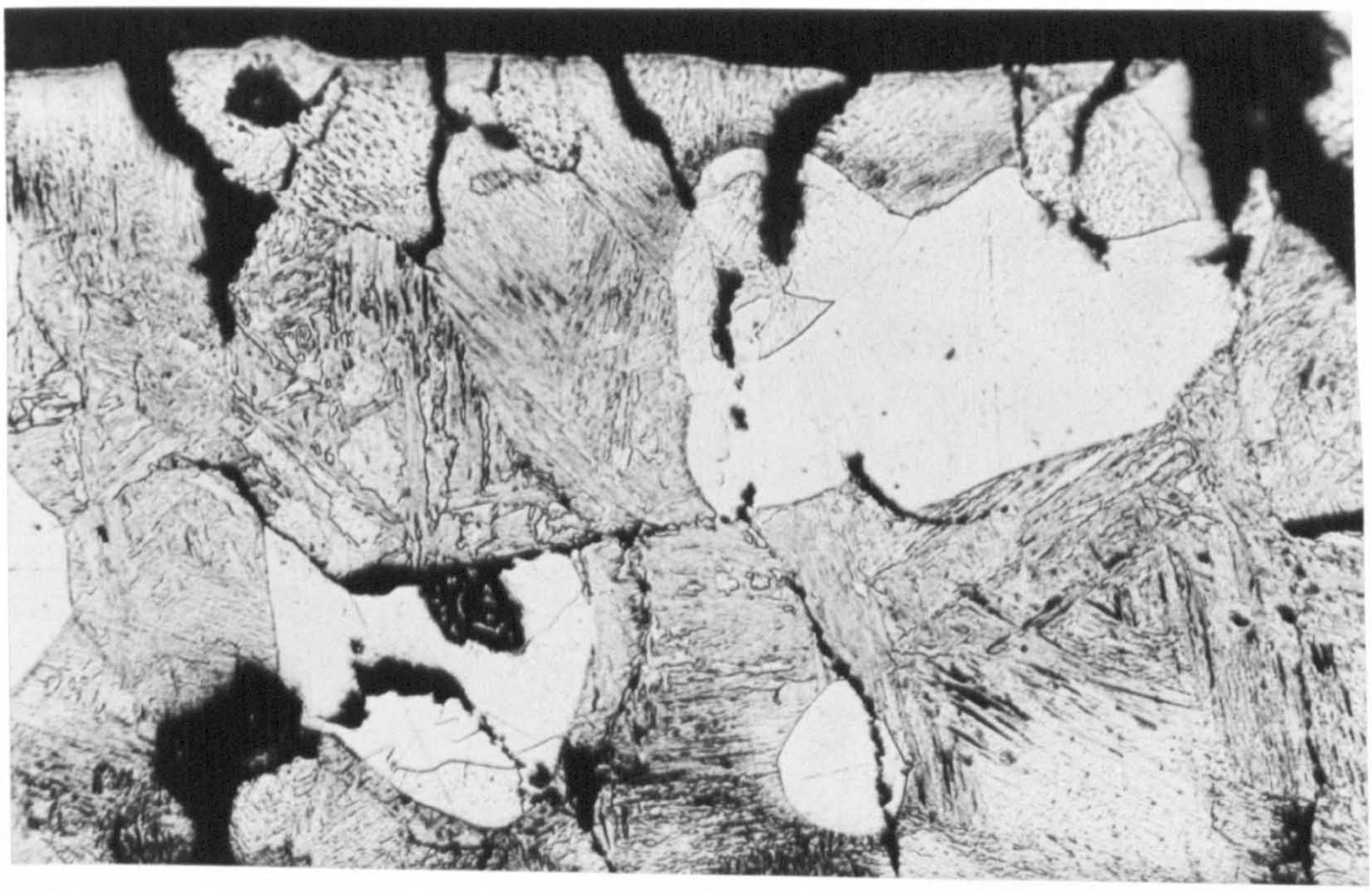

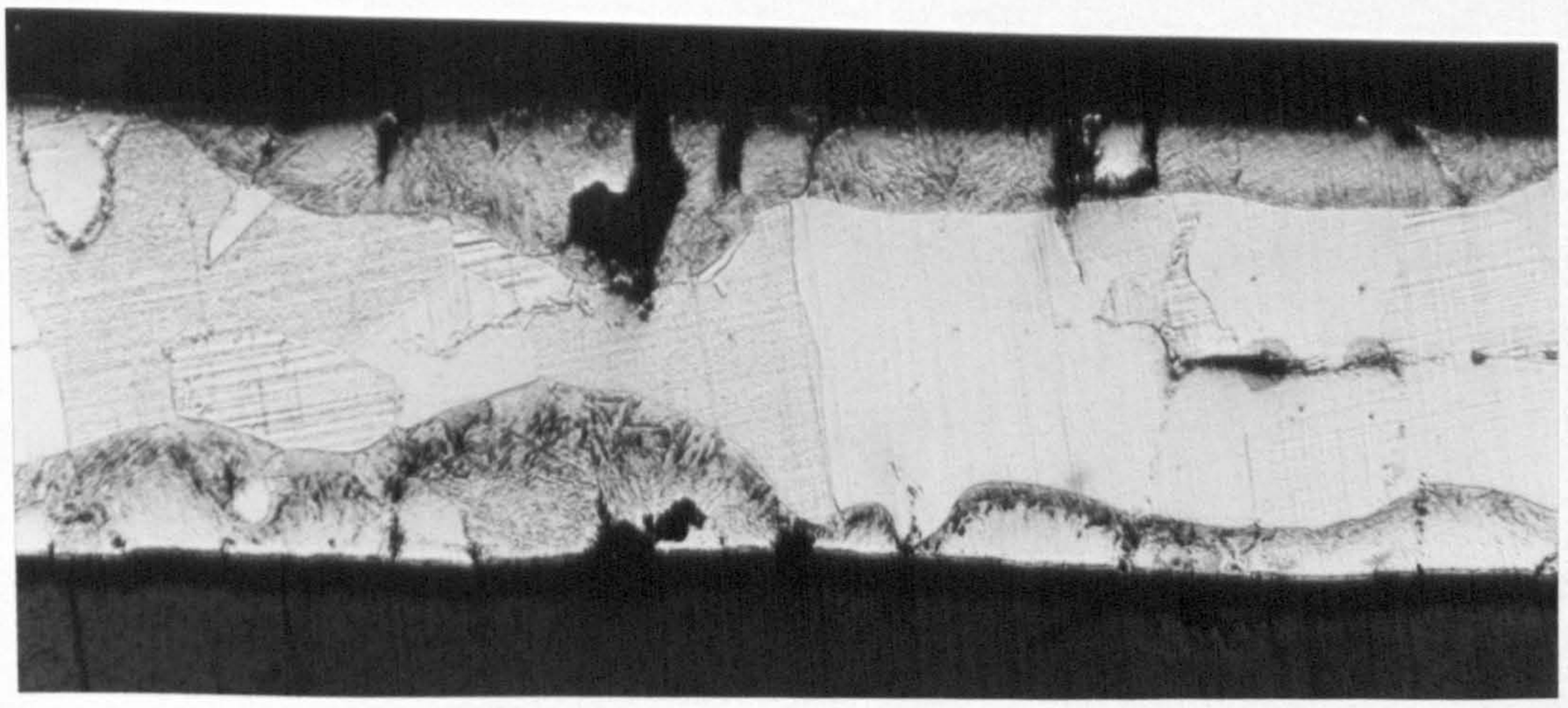

FIG. 57c SPECIMEN NO. 28

0.38mm THICK PURE IRON NITRIDED AT 845°C FOR 17.1h IN 9.1^{v}/oNH_3/H_2, ETCHED IN 2^{v}/o NITAL.

MAG. x450

FIG. 57d SPECIMEN NO. 31

0.38mm THICK PURE IRON NITRIDED AT 845°C FOR 18h IN 15^{v}/oNH_3/H_2, ETCHED IN 2^{v}/o NITAL.

MAG. x100

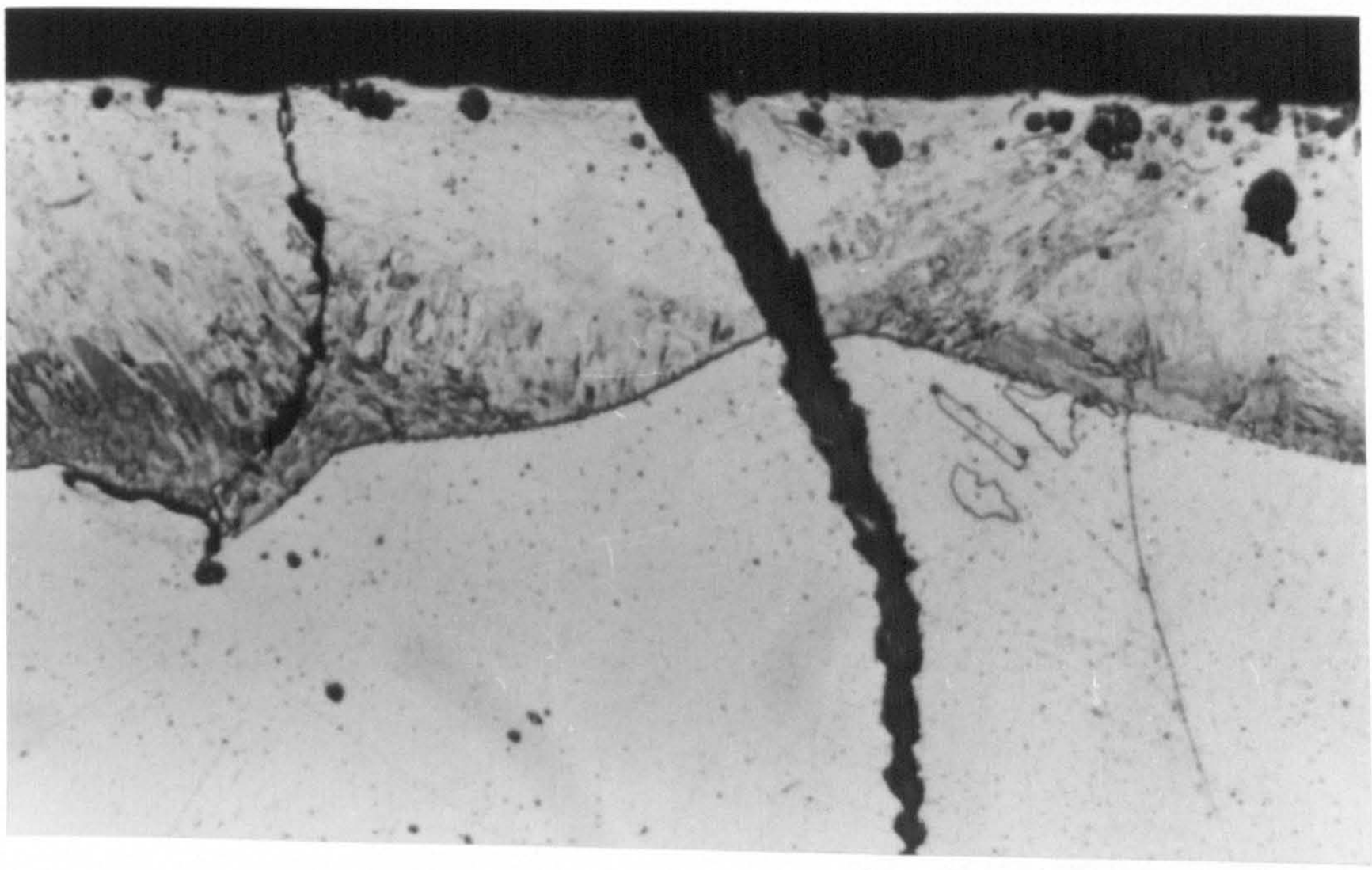

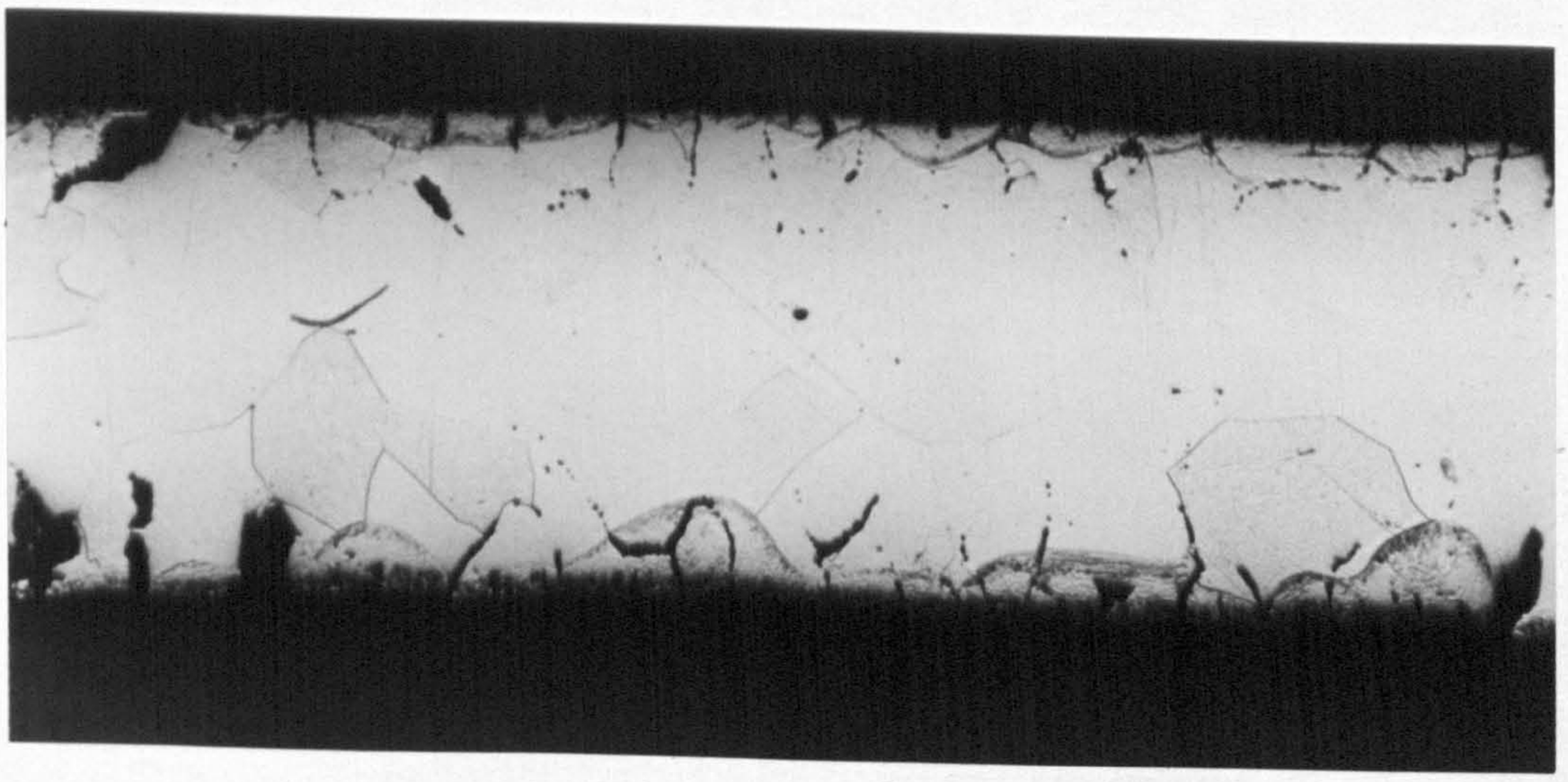

FIG. 58

WEIGHT CHANGE OF 0.27mm THICK PURE IRON NITRIDED AT 710°C IN 8.5$^{v}/_{o}NH_3/H_2$ AS A FUNCTION OF TEMPERATURE.

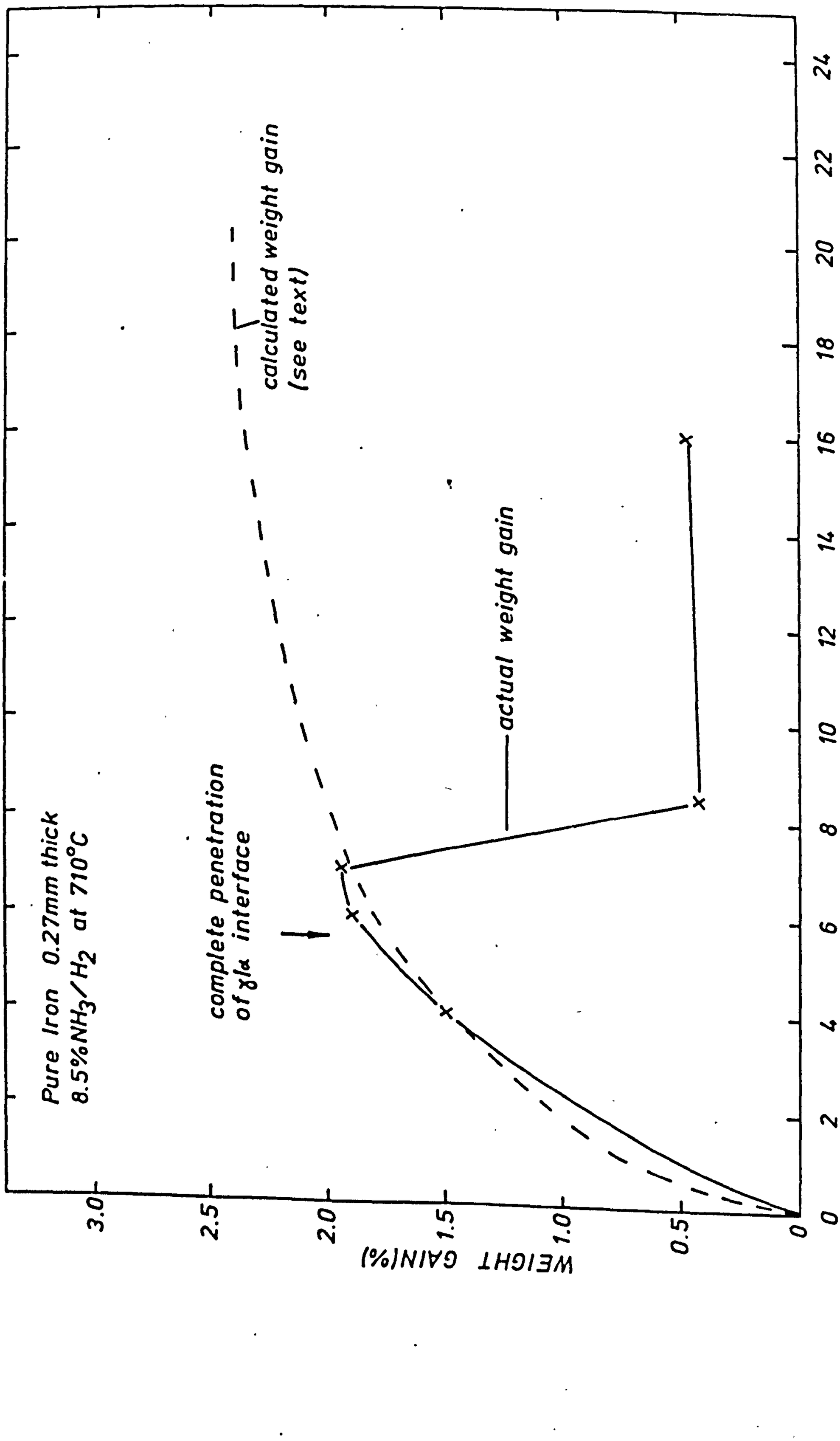
Pure Iron 0.27mm thick
8.5%NH3/H2 at 710°C
complete penetration
of γ/α interface
actual weight gain
calculated weight gain
(see text)
WEIGHT GAIN(%)
TIME OF TREATMENT(h)
0
0.5
1.0
1.5
2.0
2.5
3.0
2
4
6
8
10
12
14
16
18
20
22
24

FIG. 59

ESTIMATION OF WEIGHT GAIN BY MEASUREMENT OF γ/α INTERFACE PENETRATION.

℄

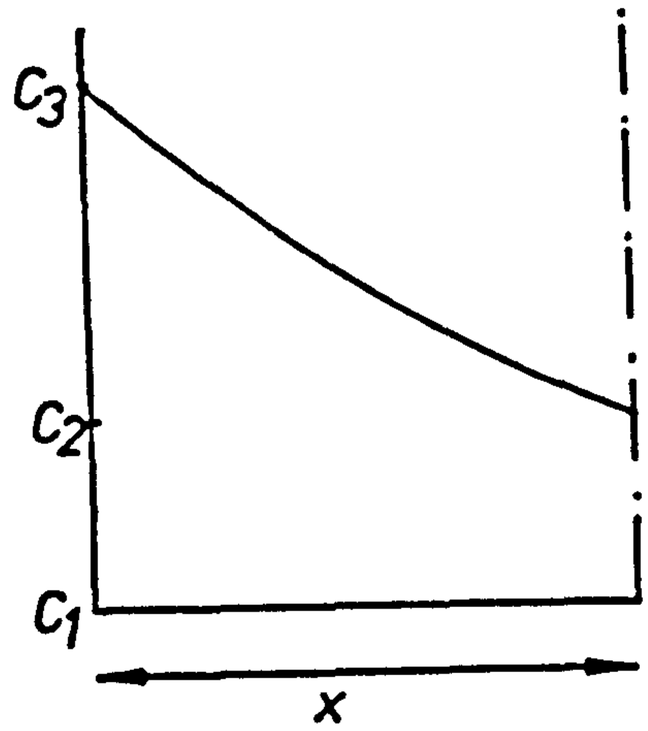

Average weight gain

$$= C_2 + \left[\frac{C_3 - C_2}{2}\right] \qquad (a)$$

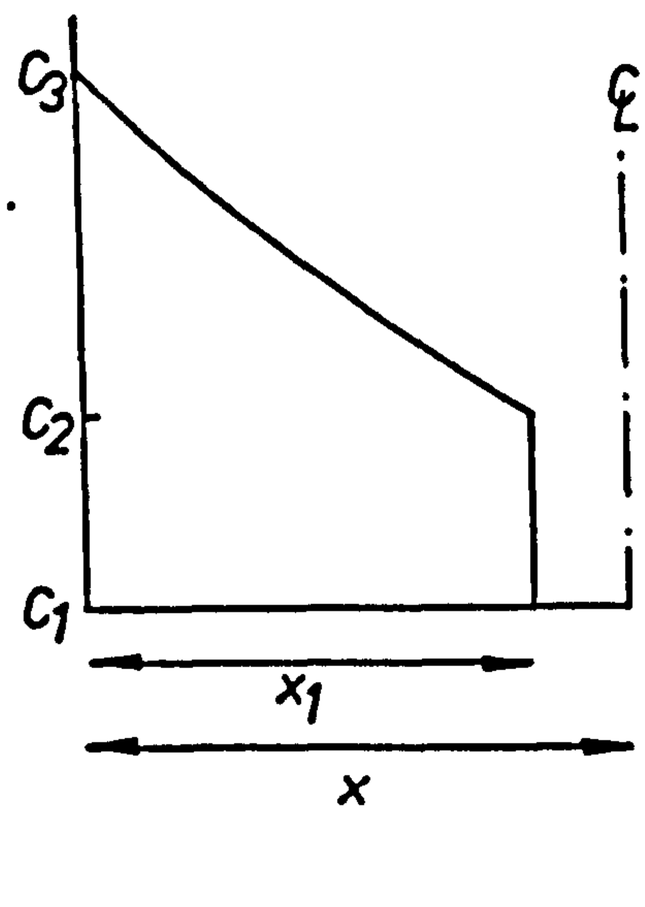

Average weight gain

$$= \frac{x_1}{x} \times \left[C_2 + \left(\frac{C_3 - C_2}{2}\right)\right] \qquad (b)$$

where $C_1 = 0$ or *original weight content of specimen*

CHAPTER 7

AUSTENITIC NITRIDING OF IRON-CARBON ALLOYS

7.1 INTRODUCTION

For the development of an austenitic nitriding process, or for an extension of the range of interstitial nitrogen in solid solution in the carbonitriding process it is clearly necessary to consider the nitridation of iron-carbon alloys. Three iron-carbon alloys (table 3) were selected for detailed kinetic analysis over the temperature range 748°C to 845°C, which is of interest in carbonitriding treatments. The specimens after treatment were analysed using the techniques developed and described in chapter 5. These experiments yielded a considerable amount of new data of particular relevance to

(a) the interaction effects of carbon and nitrogen in solid solution
(b) the diffusion of carbon and nitrogen in austenite
(c) an extension of the Fe-C-N ternary phase diagram.

7.1.1. Experimental and Results

Some preliminary experiments were performed with the Fe-0.5^{w}/oC alloys at 845°C. At this temperature the alloy is fully austenitic and therefore represents a rather different situation to that in chapter 6, where the advancing austenite interfaces consumed the ferrite matrix and, as was seen, led to the nucleation and formation of nitrogen gas voids when the diffusion profiles overlapped. The nitriding conditions for a series of thin (0.1mm thick) specimens are given in table 28, together with the structural and compositional data obtained by metallo-

graphy and Quantovac analysis respectively. Because of the thin section size employed, 'burn-through' occurredand hence absolute carbon and nitrogen levels are not available, but still a number of important observations can be made. Firstly, there was no evidence during the nitriding cycle of any void formation or blistering, even after long treatment times. In addition, a more or less complete decarburisation of the specimen took place thus yielding an essentially homogeneous iron-nitrogen alloy.

The observation of decarburisation accompanying the nitridation arises due to the presence of hydrogen[143-146] and the absence of a background carbon potential in the heat treatment atmosphere, and the effect was examined in more detail using 0.2mm and 0.75mm thick specimens. The 0.2mm specimens were used to confirm the simultaneous decarburising and nitriding effects; the nitriding conditions employed and the results obtained are given in table 29. It can be seen that although absolute carbon levels once again were not obtained due to 'burn-through', complete decarburisation (zero carbon Q_v 62, fig. 42) did not occur under the conditions prevailing.

The 0.75mm specimens were used to establish the decarburisation rate in pure dry hydrogen. This was done metallographically after treatment at 780°C. Table 30 shows the extent of ferrite penetration for various treatment times. The calculated penetrations for thin plate specimens, using known diffusion data indicate that the reaction is not diffusion controlled[136,147] thus confirming the results of Turkdogan and Martonik[143] and Grieveson[146] who have shown that it is necessary to use wet hydrogen to obtain diffusion controlled decarburisation.

Following these preliminary experiments, a series of 0.75mm thick iron-carbon alloys were nitrided in a constant inlet nitriding atmosphere of $5^{v}/o$ NH_3/H_2 (tables 31 - 33). Treatment temperatures between 748°C and 845°C were employed for periods up to 24h. At the lower treatment temperature it was estimated from known data[115] that surface nitrogen contents of ~ $1.8^{w}/o$ N would be obtained at this inlet ammonia level; this was anticipated to be sufficient to saturate the γ phase already containing the higher carbon levels ($1.07^{w}/o$). At the higher temperatures increased thermal dissociation of the ammonia would lower the effective nitriding potential and hence a more restricted uptake of nitrogen could be anticipated.

The kinetic curves obtained at the four temperatures from the series of treatments are shown in figs. 60 -63, weight changes being expressed in terms of mg/cm^2 to correct for any differences in surface areas between specimens. Although the shape of most of the curves is similar to that to be expected from diffusion of a single species into a thin plate[148], the situation is in fact morecomplicated. As has already been indicated, due to a lack of background carbon potential, decarburisation will occur simultaneously with nitriding. Hence the curves represent the net weight change between nitrogen absorption and carbon desorption. Detailed analysis of these kinetic curves is difficult without being able to relate composition profile curves and metallographic structures to the curves. Hence 1, 4, and 16h specimens were analysed for carbon and nitrogen by emission spectrometry using the layer analysis technique described in section 5.3.5. and all specimens were examined metallographically. The actual composition profiles obtained are shown in figs 64-75

which were produced using the calibration data given in figs.42,46. These profile curves represent a significant amount of data on the Fe-C-N system which will be discussed under several general headings.

7.2. DISCUSSION

7.2.1. Simultaneous Decarburisation and Nitridation Effects.

It is often assumed in decarburisation studies, particularly with a single phase system, that the surface carbon content is zero[149]. Yet from figs. 64 - 75 it can be seen that although the surface carbon level decreases with increasing nitriding time, the surface carbon level is not zero during the initial stages of reaction. In fact the situation would appear to be the same as that reported by Leutgöb and Trenkler[150] and Malik[151] on the decarburisation of Fe-C and Fe-C-X alloys under conditions where simultaneous scaling took place.

By measuring the area under the carbon concentration profile curves, it is possible to determine the carbon weight loss of the specimen. These values have been computed for all specimens shown in figs. 64 - 75, and the rate of carbon loss with time is shown in figs. 76, 77 and 78 for the Fe-0.5^{w}/oC, Fe-0.87^{w}/oC and Fe-1.07^{w}/oC alloys respectively. As might be expected the highest decarburisation rate occurs with the highest carbon alloy at any particular temperature, and the decarburisation rate increases with increase in temperature. In turn, as is shown later, this means that if carbon loss is to be avoided during austenitic nitriding a higher carburising potential would have to be provided at the higher carbon contents. In industrial practice it may not be necessary to prevent decarburisation,

but detailed consideration of this point is outside the scope of the present project.

Consideration of the concentration profile curves(figs 64-75) shows that both treatment time and original carbon content affect the surface nitrogen content of the nitrided specimens. It is particularly apparent that the surface nitrogen content drops dramatically in the initial period of treatment, and there would appear to be some link with decarburisation rate.

Examining the situation of nitriding a plain carbon steel from a theoretical viewpoint; the nitriding potential is provided by the NH_3/H_2 gas mixture, where the ammonia component catalytically decomposes on the specimen surface as follows:

$$NH_3 \rightleftharpoons N_{in\ Fe} + 3/2\ H_2 \qquad (23)$$

In addition, because there is no backup carbon potential in such an atmosphere, carbon can be lost from the steel surface by the reaction[143,145]:

$$C + 2H_2 \rightleftharpoons CH_4 \qquad (47)$$

These two reactions must therefore be interlinked by virtue of the common reactant gas hydrogen.

It is known that the rate of decarburisation of steels in dry hydrogen is proportional to the partial pressure of hydrogen in the gas mixture[143,145]. Therefore any increase in the production of hydrogen through equation 23 will increase the decarburisation rate, and any decrease in the decarburisation rate would effectively increase the hydrogen in the atmosphere through equation 47 and cause equation 23 to move to the left, decreasing

the amount of nitrogen transferred to the steel surface. The question immediately arises as to which reaction is the controlling influence, or whether some other factor affecting both reactions has a controlling.influence.

The decarburisation rate in dry hydrogen is reported to be linear on thin specimens[145], whilst in this work decarburisation rate was not linear in the initial period of treatment, see figs 76-78. This fact would suggest that there is an additional factor influencing the decarburisation rate in the initial preiod. In all cases, the initial decarburisation rate is higher, sometimes considerably, than the later steady state conditions of linear decarburisation rate. This would imply that the NH_3/H_2 - metal surface equilibrium takes some time to reach a steady state; initially being at a high potential (producing a high decarburisation rate) and then dropping to a lower potential (producing a lower decarburisation rate under equilibrium conditions). What causes such an imbalance in gas/metal surface equilibrium is uncertain.

However, Grieveson[145] also points out that decarburisation rate is a linear function of carbon content at carbon contents below about 0.5$^{w}/o$. One could therefore argue that the high initial rate of decarburisation is due to the relatively high carbon content in the specimen; once significant decarburisation has taken place then the rate would fall due to a lowering of the carbon content of the specimen. The high initial rate of decarburisation would allow for a high nitrogen potential as previously described, with a lowering of the potential as the decarburisation rate decreased. This explanation would seem

more logical, especially in view of the fact that the nitriding potential when nitriding pure Iron in NH_3/H_2 atmospheres does not appear to change significantly during a treatment cycle. In addition the same nitriding potential when applied to both pure Iron and an Iron-Carbon alloy will give a similar surface nitrogen concentration initially, but after extended treatment the.Iron-Carbon alloy has a lower nitriding potential and hence lower surface nitrogen content. This should not be expected if one considers that the Iron-Carbon alloy decarburises itself during treatment to become in effect an Iron-Nitrogen alloy.

One must then consider whether any carbon-nitrogen interaction takes place within the metallic structure to alter or limit the equilibrium nitrogen level attainable. Some interaction was observed when Fe-0.5^{w}/oC specimens were nitrided for the same treatment time and at the same temperature at different nitriding potentials; inlet gas mixtures of 20^{v}/o, 10^{v}/o and 2.4^{v}/oNH_3/H_2 for a 2h treatment were used, and the resultant profiles are shown in fig. 79. These profiles clearly show that carbon and nitrogen contents at any position along the profile are interlinked; when the nitriding potential is raised the rate of decarburisation is also raised, even though the amount of hydrogen available for decarburisation could be reduced. A feasible explanation of the variation in decarburisation rate can be linked to concentration dependency of the diffusion coefficient, (see section 7.2.2.) When there is a high nitriding potential, a high interstitial content in the surface and subsurface region causes a higher rate of diffusion of carbon to the surface than when there is only a low interstitial content in these regions.

Confirmation of carbon-nitrogen interactions was obtained when some further nitriding experiments were performed, with an attempt to maintain a constant carbon potential. The backup carbon potential was obtained by the CH_4/H_2 reaction in the form of natural gas added to the NH_3/H_2 gas stream. These experiments were performed at 845°C and the required methane level to maintain equilibrium with the various carbon content steels at this temperature was calculated from the following equation(6):

$$K = \frac{1}{A} \cdot \frac{pCH_4}{(pH_2)^2} \qquad (48)$$

where $$\log_{10}K = \frac{8370}{T} - 5.77 \qquad (49)$$

A = activity of carbon in Iron
= equilibrium carbon content / maximum solubility of carbon at temperature T

T = °Rankine

The required methane levels being 1.1, 1.9 and 2.3^{v}/o for carbon contents of 0.5, 0.87 and 1.07^{w}/o respectively, no account being taken of the effect of ammonia on the reactions at treatment temperature (chemical interaction and dilution due to thermal dissociation). Table 34 shows the treatment conditions and specimen weight changes which can be directly compared with the plain nitrided specimens (fig. 63). The required gas compositions were set up by flowmeters and checked by chromatography prior to insertion of specimens into the furnace.

By comparison with fig. 63, it can be seen that there are substantially greater weight gains when the backup carbon

potential is provided. Concentration profiles of the specimens were determined by the layer analysis method (section 5.2.5.); specimen 163 however was not examined due to unacceptable distortion. The resultant profiles are shown in figs. 80 - 83, and exhibit remarkable carbon profile curves. The carbon concentration profiles are not flat as one might expect from a constant backup potential, and most of them show a maximum in carbon content just ahead of the advancing nitrogen profile curve. This type of phenomena has previously.been noted for diffusion of phosphorus into Fe-0.4^{w}/oC alloy[152], and more recently by Jack[153] in ferritic nitriding and Bell and Roe[128] in various nitrocarburising processes.

It would appear at first sight in figs. 80 - 83 that decarburisation has taken place, but close inspection of the carbon profiles and measurement of the enclosed areas under the concentration profile curves shows that the overall change in carbon content of the specimens is negligible. What in fact appears to have happened is that a redistribution of carbon within the specimen has taken place, because there is effectively no outlet for carbon at the free surface of the specimen. The advancing nitrogen rich interface appears to displace carbon atoms towards the centre of the specimen, suggesting possibly that carbon atoms are occupying preferred sites when the nitrogen atoms are entering the lattice.

It has previously been noted that in all the kinetic work in the nitriding of Fe-C specimens, surface nitrogen contents under specific nitriding conditions decreased as the time of treatment increased. This phenomena is shown specifically in figs. 84-86,

the data being taken from the concentration profiles shown in figs. 64 -75. The most noticeable change occurs during the first few hours of treatment and might suggest a surface equilibrium phenomena. Chromatographic records of treatments were examined for any appreciable changes in gas compositions which might reflect this. Fig. 87 shows the variation of exhaust ammonia level with time of treatment for two specimens nitrided under conditions which yielded the most appreciable surface nitrogen changes. Although the exhaust ammonia level does fall, it does so very gradually over the 24h period and there are no abnormal variations in the first stages of treatment.

When methane was used as a background carbon potential, the ammonia level in the exhaust fell much more rapidly with increase in treatment time, see fig. 88, with a significant drop in effective nitriding potential, yet there was a small increase in the surface nitrogen content (fig. 83). The exhaust methane level varied insignificantly during the same treatment time.

7.2.2. Compositional Dependence of D_{γ}^{N}

Because of the structural, thermodynamic and other similarities of carbon and nitrogen in iron-based systems[2,3,35], it is highly likely that their diffusion behaviour is similar and in fact there have been numerous reports of such similarities particularly in binary systems[127,136,147,154,155]. It is highly probable that the observed interactions in the ternary Fe-C-N system reported in section 7.2.1. which take place are due to a compositional dependency of D; due to the combined interstitial content at any position along the composition

profile. In this section possible variations of D_γ^N will be considered.

To date, no information has been published on the concentration dependency of D_γ^N, however there is data available concerning the concentration dependency of D_γ^C. Early work by Harris[156] for steady state diffusion of carbon in austenite produced the following relationship (a linear relationship was assumed by Harris from the data);

$$D_\gamma^C = D_o\{ 1 + 2.15 \times {}^{W}/_{oC} \} \qquad (50)$$

Wells and Mehl[157] had also investigated steady state diffusion of carbon in austenite and found the relationship:

$$D_\gamma^C = D_o\{ 1 + 0.9^{W}/_{oC} \} \qquad (51)$$

Their work on the non-steady state[136] shows a linear dependency over short ranges, but D_γ^C increases rapidly as concentration approaches a phase boundary. Simple mathematical expressions do not fit the experimental data, but expressions of the type $D = D_o e^{kc}$ and $D = D_o(1 - kc)^{-1}$ can be shown to fit reasonably well to the curves, see fig. 89. In these formula k is a constant, c is the ratio of concentration at any point along the profile to the surface concentration and D_o is the diffusion coefficient at a zero concentration of diffusing substance.

With the data available from the kinetic work and concentration profiles, it is possible to make estimates of the diffusion coefficient of nitrogen in Fe-C-N austenite. Ideally the situation should be regarded as ternary diffusion and although recent advances have been made in methods for more readily determining ternary diffusion coefficients[158-160], they are not readily

adaptable to the problem in question, mainly due to the very restricted range of carbon and nitrogen compositional variations.

It is therefore proposed to simplify the problem and treat the situation as diffusion in the two separate binary systems Fe-N and Fe-C, because of the similarities of these systems. Even in the simple binary systems the position is further complicated by the phenomena of changing surface concentrations with increase in treatment time, as discussed in section 7.2.1. This applies to both carbon and nitrogen in the case of nitriding of plain carbon steels. However by considering, in the first instance only the short time treatments, a reasonably good comparison can be made between alloy compositions and temperature of treatment.

A further advantage in considering the short time treatments is that the semi-infinite model of diffusion into a surface can be applied[135], for which Crank[126,161] has computed profiles due to a variety of compositionally dependent diffusion coefficients. Therefore some direct comparisons can be made with Crank's data, and the concentration dependency of D_γ^C and D_γ^N compared.

Concentration dependency equations for diffusion coefficients are based on a diffusion coefficient D_o which expresses the diffusion of a species at effectively zero concentration. In an attempt to fit data for experimental profiles, use has been made of existing D_γ^N data[127] for very low nitrogen contents to provide a value of D_o. Fig. 90 shows the fit obtained against experimental data for several expressions of compositionally

dependent diffusion coefficients. An extremely good fit is obtained for the expression $D = 4 \times 10^{-9} \cdot e^{1.61c}$, the fit only deviating at a position below the surface where the total interstitial level changes abruptly. The value of $D_o = 4 \times 10^{-9}$ is taken from Grieveson's data[127] extrapolated to the appropriate temperature. The experimental data was taken from specimen 62 (fig. 79) with a high surface nitrogen content and low surface carbon content. Similar behaviour has been observed where an equivalent total interstitial profile has been obtained by raising the surface carbon level using a background carbon potential and lowering the surface nitrogen level (fig. 91). In this case the experimental data was obtained from specimen 160 (fig. 80). This would tend to confirm that the interaction between carbon and nitrogen in iron lattices is due to a concentration effect.

A limitation in trying to fit experimental profiles to curves from Crank's computations[126,161] is that the latter are based on formula in which D is related to relative compositions, rather than absolute compositions; i.e. in the formula $D = D_o e^{kc}$ or $D = D_o(1 - kc)^{-1}$, c represents the ratio of the concentration at any point along the profile to the surface concentration. This is fine for situations where the surface concentration does not vary between experiments as was the case in Crank's work - solvents diffusing into plastics - where the surface concentratio.. is always 100% of the diffusing substance. But where differing surface concentrations are used, the formula needs constant modification to take account of the different surface concentrations which affect the variable c.

A further complication is the fact that the occasionally observed variations of D with composition, e.g. carbon in iron (fig. 89) do not fit readily to simple formula over the range of variation; probably a complex power series might be more appropriate.

Nevertheless, in spite of these complications, the general principle of fits to computed concentration dependent D curves has been shown (figs. 90,91). The extensive calculation of curves for each of the diffusion profiles shown in figs. 64-75 has not been attempted for some of the reasons just given. However, diffusion coefficients have been calculated using a combination of

(a) the standard error function formula for specimens satisfying the semi-infinite condition, and

(b) the thin specimen formula for other specimens where an appreciable buildup of diffusing substance has occurred in the centre of the specimen.

These formula are described by Crank for thin specimens in terms of the mass of substance absorbed or desorbed[135] as follows;

for short times (equivalent to semi-infinite media)

$$\frac{M_t}{M_\infty} = 2(Dt/l^2)^{1/2}\left[\frac{1}{\sqrt{\pi}} + 2\sum_{v=1}^{\infty}(-1)^v \, i\,\mathrm{erfc}\,\frac{vl}{\sqrt{Dt}}\right] \qquad (52)$$

for long times (where appreciable buildup in the centre of the specimen has occurred)

$$\frac{M_t}{M_\infty} = 1 - \sum_{v=0}^{\infty}\frac{8}{(2v+1)^2\pi^2}\cdot e^{\frac{-D(2v+1)^2\pi^2 t}{4l^2}} \qquad (53)$$

The same notation is used for symbols as for equations 40 and 41 in section 6.2. except that in this case l represents the specimen half thickness. Crank has published solutions to these equations in the graphical form of $\frac{M_t}{M_\infty}$ vs $\sqrt{\frac{Dt}{l^2}}$ (148).

The D values obtained can only be regarded as a weighted mean representing a value at some point along the concentration profile curve. In cases where the surface concentration has dropped with increasing treatment time, the surface concentration appropriate to that particular specimen is used in the formula, rather than the original surface concentration; only a small error is likely. The same criteria is used in the calculation of D values from decarburisation curves, when initially the surface carbon level may not be zero.

The masses absorbed in the case of nitrogen and desorbed in the case of carbon have been computed from the areas under the concentration profile curves, and the relevant D values computed using Crank's solutions just described(148). The calculated data is shown in table 35 for the kinetic specimens nitrided in 5^v/o NH_3/H_2, table 36 for specimens nitrided at 845^oC with a background carbon potential, and table 37 for specimens nitrided under different potentials at 780^oC.

The variation of D values, averaged for each temperature, with base carbon content and temperature are shown in fig. 92 for D_γ^N and fig.93 for D_γ^C using the data from table 35. The calculated D_γ^N values are greater than published data(127,154) on low nitrogen content alloys, indicating significant compositional dependency as previously implied from calculated curves (figs. 90

and 91). In the case of D_{γ}^{C}, these values are less than published data[136] and it can be implied from this that the decarburisation reaction is not diffusion controlled; this is to be expected bearing in mind the relatively dry gas mixtures used (see section 5.2.1.).

From fig. 92 it would appear that increase in base carbon content of the specimen increases D_{γ}^{N} over the temperature range investigated, except at 845°C where a cross-over has occurred. As the temperature increases through the range, the values determined in this work converge on those of established data. This is almost certainly due to a decrease in nitriding potential from a constant composition gas mixture with increasing temperature, causing greater thermal dissociation of ammonia and hence reducing the compositional dependency of D_{γ}^{N}.

Further confirmation of compositional dependency was obtained from calculation of D_{γ}^{N} from the profiles obtained at 780°C (fig 79.) under different nitriding potentials, see table 37.

The data obtained for D_{γ}^{N} has a similar variation with temperature to that of the established data[127,154] which again leads to the conclusion that the deviation from the established data must be due to compositional dependency.

In the case of D_{γ}^{C}, although similar variation with temperature is shown (fig. 93), a slightly different situation arises, as D_{γ}^{C} is shown to reach a maximum for the $0.87^{W}/oC$ specimen and decrease for the $1.07^{W}/oC$ specimen. This could be due to the fact that the $1.07^{W}/oC$ specimens were not always completely

austenitic, containing some Fe_3C. Malik[151] has shown that decarburisation from carbide containing structures is slower than from austenitic structures.

An important observation was made from specimen 91 (table 37). Here the specimen was nitrided in an ammonia atmosphere diluted by nitrogen. This made very little difference to D_γ^N, but lowered D_γ^C effectively reducing the decarburisation rate, compare with specimen 62. This is important in the industrialisation of austenitic nitriding, because dilution with hydrogen might be viewed with some scepticism from the safety viewpoint. This result shows that dilution with nitrogen gives a similar performance, but detailed study of the behaviour of nitrogen diluted atmospheres was beyond the scope of the project.

7.2.3. Limits of the γ Phase Field in the Fe-C-N System.

Although isotherms of the ternary Fe-C-N system have been established by Naumann and Langenscheid[49] at temperatures in the range 500°C to 700°C, there are none available delineating the austenite phase field at higher temperatures. Since such data is clearly of value to austenitic thermochemical processing, it was decided to undertake a restricted study of the Fe-C-N system to establish the austenite phase limits over the range of temperatures employed in the present studies.

Specimens of 0.75mm Fe-0.5^w/oC strip were heat treated in $NH_3/CH_4/H_2$ gas mixtures, in which a constant CH_4 level of 3^v/o was maintained. By previous calculations, this level of CH_4 should be more than sufficient to saturate austenite at the treatment temperature and theoretically precipitate carbide

compounds. A treatment time of approximately 20h was used to ensure that equilibrium conditions would be met. Table 38 shows the resultant weight changes from a range of NH_3 additions to the gas mixture. Carbon and nitrogen concentration profiles determined by layer analysis as previously described (section 5.3.5.) for the $5^v/o$, $20^v/o$ and $40^v/o$ NH_3 additions are shown in figs. 94 - 96 respectively. All three specimens show a constant carbon level of about $1^w/o$ in the centre of the specimen, the nitrogen level at the centre however would appear to fall slightly with increasing NH_3 level; no immediate explanation is available.

At the surface of the specimens there is extensive networks of what appear to be grain boundary precipitates. An attempt was made to analyse these using the calibrated microprobe, however this was not completely successful on a quantitative basis, mainly due to the large spot size required and the uncertainty of having solvent-free grain boundary networks (solvent is present from cleansing hydrocarbons such as carbon tetrachloride and alcohol). However when the electron beam was traversed across whole grains from the outer to the inner surface of the specimens carbon and nitrogen countrates showed little or no deviation, indicating a constant carbon and nitrogen content in the single phase regions. By comparison of the microstructures with the determined concentration profiles(figs. 94 -96) , it can be seen that uniformity of the profiles occurs where the specimen is free of grain boundary precipitates. It has already been indicated that the single phase region has a constant composition, so that the peaks in composition as indicated by layer analysis must be due to the presence of the precipitates. These precipitates are

almost certainly compounds of the $Fe_{2-3}CN$ type. By relating the area under the composition profiles where these compounds are present to their volume in the microstructure in these regions this can be shown; enrichments locally of carbon and nitrogen are greater than $2.7^{w}/o$ from such calculations. The amount of precipitate appears to increase with increase in the NH_3 level in the gas mixture, and at the $20^{v}/o$ level large islands of Fe_3C can occasionally be seen.

Using all specimens on which concentration profiles had been determined, metallographic examination was performed to determine the phases present. By comparison of the metallographic specimen with the corresponding concentration profile determined by layer analysis, the structure at each analysis layer could be determined. Ternary isotherms at the four temperatures investigated were then constructed using this data and are shown in figs. 97 - 100 for the temperatures 748°C, 780°C, 811°C and 845°C respectively. There is only a small amount of data for structures containing high combined interstitial levels of carbon and nitrogen; when attempts were made to produce such structures, the maximum nitrogen level attainable appeared to be limited as has just been seen in specimens such as those in figs. 94 - 97. This may well be due to the metastable equilibrium of structures containing high interstitial levels of elements whose normal state is gaseous.

7.3 Conclusions

(1) Using an approach based on weight change kinetics, the diffusion coefficient of nitrogen in austenite at a fixed carbon level has been shown to be compositionally dependent. This variation is similar to that already known for carbon in austenite. The variation can be approximately represented by the expression $D_\gamma^N = D_o e^{1.61c}$; where D_o is the diffusion coefficient at effectively zero nitrogen content, and c is the ratio of the nitrogen concentration at any point along the concentration profile to the surface nitrogen concentration.

(2) Average D_γ^N values computed from weight change kinetics have been shown to have a similar temperature dependency to that shown by Grieveson and Turkdogan[127], namely $D = D_o e^{\frac{-40,260}{RT}}$. The D_γ^N values obtained are up to three times larger than those extrapolated from reference 127, and this is reflected in the D_o values of 2.5 and 3.0 obtained for Fe-0.5^w/oC and Fe-1.07^w/oC alloys, compared with a value of 0.91 from reference 127. The variation in D_o from existing data is due to compositional dependency of D_γ^N and justifies the use of data from reference 127 as the base D_o value in equations for the calculation of concentration gradients based on compositionally dependent diffusion coefficients.

(3) Following from (2), D_γ^N at fixed nitrogen levels increases with increase in base carbon level and indicates the approximate interchangeability of carbon and nitrogen in their effect on the diffusion coefficient.

(4) During austenitic nitriding of iron-carbon alloys in

ammonia/hydrogen mixtures, decarburisation takes place due to the presence of hydrogen and the lack of a carburising potential. The decarburisation effect is not diffusion controlled and also surface carbon levels in the initial stages are not zero, an assumption often made in decarburisation studies of single phase systems.

(5) By providing a background carbon potential with methane, decarburisation during austenitic nitriding can be prevented. In this case a constant carbon concentration profile is not obtained, although there is no overall change in carbon level in the specimens. Instead, a build-up of carbon ahead of the advancing nitrogen interface is observed, an effect only previously noted in ferritic nitriding and nitrocarburising treatments.

(6) At fixed nitriding potentials, the surface nitrogen level in nitrided iron-carbon alloys decreases dramatically in the initial stages of treatment. This phenomena can be related to decarburisation effects which occur simultaneously.

(7) Extensive determination of the iron-carbon-nitrogen ternary system at high temperatures was not possible, due to the rapid thermal decomposition of ammonia. Nevertheless, the austenite phase limits in the range 748°C to 845°C have in part been delineated.

TABLE 28

NITRIDING OF 0.1mm Fe - 0.5$^{w}/_{o}$C STRIP AT 800°C - CONSTANT POTENTIAL

Specimen No.	Treatment Time (h)	Atmosphere	Wt. Gain (%)	Structure	Quantovac Reading (a) (mV) C	N
21	0.5	9.1$^{v}/_{o}NH_3/H_2$	0.64	α'	157	143
23	1.0	" " "	0.34	α'	62	206
25	4.5	" " "	0.42	α' + g.b. precipitates	77	147
24	20.75	" " "	0.27		47	152
26	65.5	" " "	0.26		68	152

(a) Actual analysis not quoted because of burn through (see text).

TABLE 29

NITRIDING OF 0.2mm Fe - 0.5^{w}/oC STRIP AT 800^{o}C - CONSTANT POTENTIAL.

Specimen No.	Treatment Time (min)	Atmosphere	Wt. Gain (%)	Structure	Quantovac Readings (a) (m v)	
					C	N
8	5	5.75^{v}/oNH_3/H_2	0.085	$\alpha' + \alpha$	280	149
10	10	" " "	0.26	α'	252	162
9	20	" " "	0.39	α'	223	176
11	40	" " "	0.57	α'	200	174
12	80	" " "	0.81	α' + gb. precipitates	140	191

(a) Actual analysis not quoted because of burn through (see text)

TABLE 30

DECARBURISATION OF 0.75mm Fe-0.5^{W}/oC STRIP AT 780^{oC} IN DRY HYDROGEN.

Specimen No	Treatment Time (h)	Wt. Loss (%)	Ferrite Penetration(μ) Measured	Calculated (a)
57	1	0.050	30	144
59	2	0.102	60	204
58	4	0.212	125	289
60	8	0.292	200	Complete
61	16	0.504	Complete	"

(a) Calculated for a diffusion controlled reaction using

$D_{\alpha}^{C} = 2.3 \times 10^{-6} cm^2/sec$ - Ref 147

$D_{\gamma}^{C} = 2.3 \times 10^{-8} cm^2/sec$ - Ref 136

TABLE 31

NITRIDING OF 0.75mm Fe - 0.5^{w}/oC STRIP IN 5^{v}/oNH_3/H_2 AT VARIOUS TEMPERATURES

Specimen No.	Temperature (°C)	Treatment Time (min)	Weight Change (mg/cm^2)	(%)
99	748	60	+0.593	+0.227
111	"	120	+0.721	+0.289
102	"	240	+0.835	+0.318
113	"	480	+0.798	+0.305
103	"	930	+0.739	+0.287
168	"	1420	+1.147	+0.461
74	780	60	+0.473	+0.181
64	"	120	+0.736	+0.270
77	"	240	+0.761	+0.289
76	"	480	+0.607	+0.228
79	"	980	+0.725	+0.271
119	811	60	+0.517	+0.195
121	"	120	+0.553	+0.213
117	"	245	+0.168	+0.064
129	"	305	+0.658	+0.249
128	"	480	+0.628	+0.240
118	"	960	+0.453	+0.172
171	"	1425	+0.440	+0.174
51	845	60	+0.096	+0.036
48	"	120	+0.114	+0.043
49	"	240	+0.064	+0.023
50	"	480	-0.055	-0.020
143	"	900	+0.008	+0.003

TABLE 32

NITRIDING OF 0.75mm Fe - 0.87^{W}/oC STRIP IN 5^{V}/oNH_3/H_2 AT VARIOUS TEMPERATURES.

Specimen No.	Temperature (°C)	Treatment Time (min)	Weight Change (mg/cm^2)	(%)
101	748	65	+0.405	+0.152
107	"	120	+0.525	+0.193
106	"	240	+0.761	+0.276
112	"	480	+0.833	+0.324
110	"	1005	+0.968	+0.370
170	"	1440	+0.458	+0.165
82	780	60	+0.505	+0.183
84	"	183	+0.614	+0.225
83	"	300	+0.608	+0.234
88	"	540	+0.471	+0.178
85	"	995	+0.460	+0.167
123	811	60	+0.207	+0.078
124	"	120	+0.238	+0.091
125	"	235	+0.016	+0.006
133	"	510	-0.460	-0.173
122	"	960	-0.639	-0.243
148	845	50	-0.077	-0.030
142	"	105	-0.303	-0.112
141	"	150	-0.458	-0.173
139	"	240	-0.635	-0.236
144	"	480	-0.901	-0.332
138	"	970	-1.110	-0.412

TABLE 33

NITRIDING OF 0.75mm Fe - 1,07^{W}/oC STRIP IN 5^{V}/oNH_3/H_2 AT VARIOUS TEMPERATURES.

Specimen No.	Temperature (°C)	Treatment Time (min)	Weight Change (mg/cm^2)	(%)
100	748	60	+0.274	+0.105
105	"	120	+0.406	+0.158
104	"	250	+0.419	+0.161
109	"	480	+0.343	+0.134
108	"	960	-0.071	-0.028
169	"	1440	+0.104	+0.040
95	780	45	+0.224	+0.086
75	"	60	+0.285	+0.114
69	"	120	+0.308	+0.117
73	"	300	+0.089	+0.035
97	"	480	-0.290	-0.113
78	"	960	-0.577	-0.228
127	811	60	+0.090	+0.036
131	"	120	-0.112	-0.043
132	"	135	-0.179	-0.071
130	"	220	-0.142	-0.053
134	"	345	-0.682	-0.257
137	"	480	-0.793	-0.302
126	"	945	-0.651	-0.250
147	845	60	-0.177	-0.069
146	"	120	-0.364	-0.142
149	"	240	-0.926	-0.387
152	"	483	-0.853	-0.339
140	"	960	-1.223	-0.504

TABLE 34

NITRIDING OF 0.76mm Fe-C STRIP AT 845°C WITH A BACKGROUND CARBON POTENTIAL

Specimen No.	Alloy Composition	Treatment Time	Atmosphere	Wt. Gain mg /cm^2	%
160	Fe - 0.5^W/oC	1h - 10 min	10^V/oNH$_3$/1.1^V/o CH$_4$/H$_2$	0.905	0.360
161	" "	4h	" "	1.512	0.595
162	" "	3h. 55min	5 " "	1.205	0.461
163	Fe - 1.07^W/oC	4h	5^V/oNH$_3$/2.3^V/o CH$_4$/H$_2$	1.324	0.494
164	" "	1h 6min	" " "	0.767	0.263
165	Fe - 0.87^W/oC	1h	5^V/oNH$_3$/1.9^V/o CH$_4$/H$_2$	0.690	0.244
166	" "	4h 5min	" " "	0.941	0.346

TABLE 35

D_γ^N AND D_γ^C CALCULATED FROM CONCENTRATION PROFILE CURVES.

Specimen No.	Temperature (°C)	D_γ^N $(cm^2/sec)x10^8$	D_γ^C $(cm^2/sec)x10^8$
99	748	0.554	0.347
102	"	0.699	0.895
103	"	0.494	1.18
74	780	0.745	0.588
76	"	1.14	1.05
79	"	1.03	1.39
119	811	1.38	1.23
117	"	0.820	1.47
118	"	1.50	2.10
49	845	2.37	3.27
48	"	3.37	3.45
50	"	2.06	2.65
101	748	0.600	0.760
106	"	0.616	0.780
110	"	0.735	0.969
82	780	1.21	1.85
83	"	1.11	1.60
85	"	0.990	1.48
123	811	2.16	1.26
125	"	1.69	2.08
148	845	2.37	3.53
141	"	1.92	3.19
144	"	1.58	3.39
100	748	0.637	0.498
104	"	0.850	0.563
108	"	0.701	0.781
75	780	1.25	1.54
73	"	1.36	1.13
78	"	0.720	1.46
127	811	1.71	1.19
130	"	2.13	1.09
147	845	2.66	2.28
149	"	2.08	3.62

Fe - 0.5^W/oC

Fe - 0.87^W/oC

Fe - 1.07^W/oC

TABLE 36

D_{γ}^{N} CALCULATED FROM CONCENTRATION PROFILES OF Fe-C ALLOYS NITRIDED WITH BACKGROUND CARBON POTENTIAL AT 845°C

Specimen No.	Alloy	Atmosphere	D_{γ}^{N} $(cm^2/sec) \times 10^8$
160	Fe - $0.5^{w}/oC$	$10^{v}/oNH_3/1.1^{v}/oCH_4/H_2$	3.27
161	"	" " " " "	3.03
162	"	$5^{v}/o$ " " " "	3.46
164	Fe - $1.07^{w}/oC$	$5^{v}/oNH_3/2.3^{v}/oCH_4/H_2$	4.35
165	Fe - $0.87^{w}/oC$	$5^{v}/oNH_3/1.9^{v}/oCH_4/H_2$	2.50
166	"	" " " " "	2.99

TABLE 37

D_γ^N AND D_γ^C CALCULATED FROM CONCENTRATION PROFILES OF Fe- $0.5^w/o$C SPECIMENS NITRIDED UNDER DIFFERENT POTENTIALS AT 780^oC.

Specimen No.	Atmosphere	Treatment Time. (h)	D_γ^N (cm^2/sec) x10^8	D_γ^C (cm^2/sec) x10^8
62	$20^v/oNH_3/H_2$	2	1.25	1.45
63	$10^v/o$ " "	2	1.11	1.21
65	$2.44^v/o$" "	2	0.661	1.10
89	$10^v/oNH_3/H_2$	8	1.19	1.21
91	$20^v/oNH_3/N_2$	2	1.21	1.02

TABLE 38

NITRIDING OF 0.76mm Fe-0.5$^{W}/_{o}$C STRIP AT 845^{o}C WITH CONSTANT EXCESS CARBON POTENTIAL - VARYING NITROGEN POTENTIAL.

Specimen No.	Treatment Time	Atmosphere	Wt. Gain mg/cm^2	Wt. Gain %
150	19h 40min	5$^{V}/_{o}$NH$_3$/3$^{V}/_{o}$CH$_4$/H$_2$	2.671	1.01
151	19h 45min	10 " " " "	3.755	1.50
153	20h 50min	20 " " " "	3.757	1.44
154	80min	40 " " " "	1.498	0.57
155	19h 30min	" " " " "	2.860	1.14

FIG. 60

KINETIC CURVES FOR IRON-CARBON ALLOYS NITRIDED IN $5^{v}/oNH_3/H_2$ AT 748°C.

FIG. 61

KINETIC CURVES FOR IRON-CARBON ALLOYS NITRIDED IN $5^{v}/oNH_3/H_2$ AT 780°C.

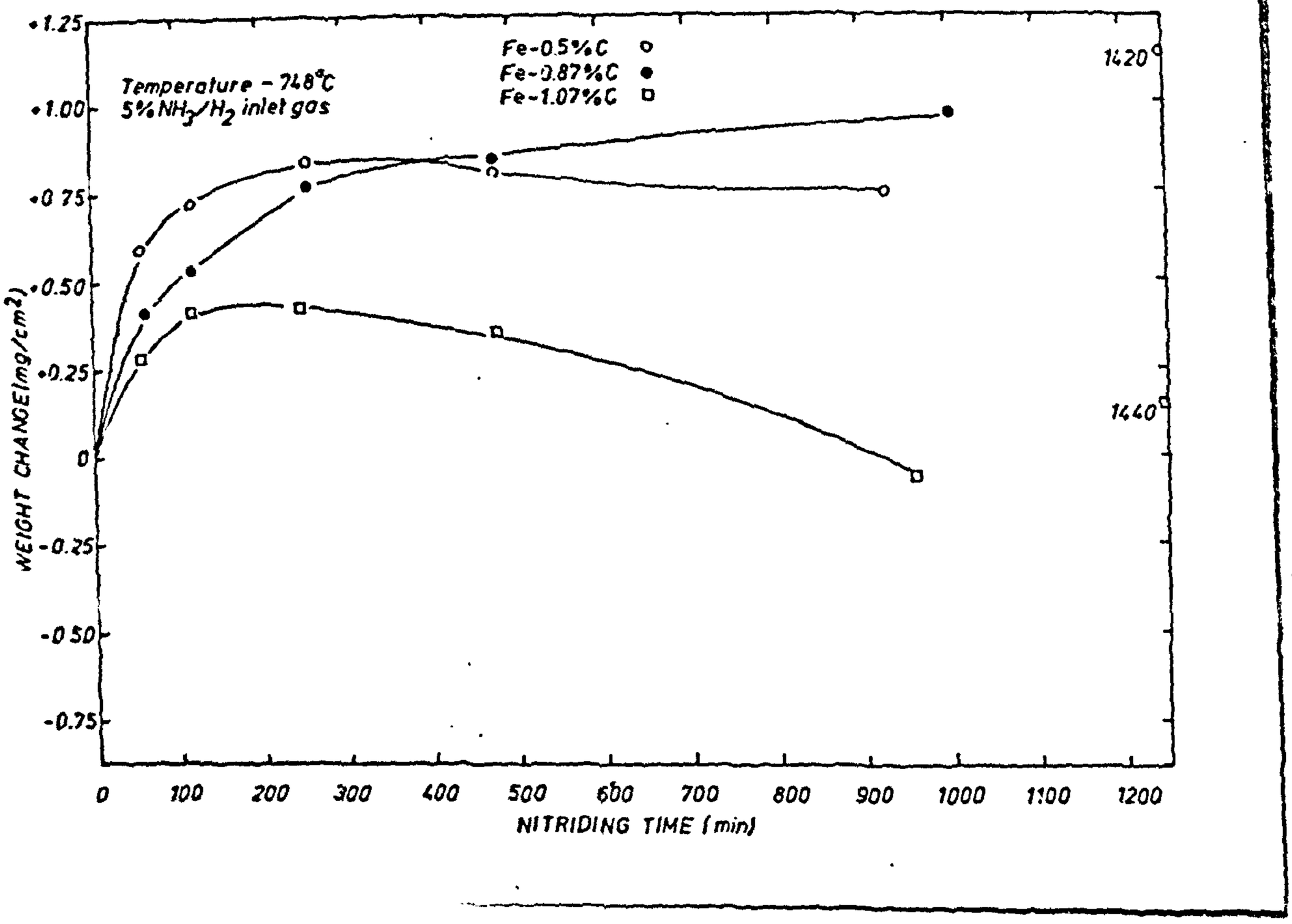
Temperature - 748°C
5% NH3/H2 inlet gas
Fe-0.5%C
Fe-0.87%C
Fe-1.07%C
1.25
1.00
0.75
0.50
0.25
0
-0.25
-0.50
-0.75
1420
1440
0
100
200
300
400
500
600
700
800
900
1000
1100
1200
NITRIDING TIME (min)
WEIGHT CHANGE (mg/cm²)

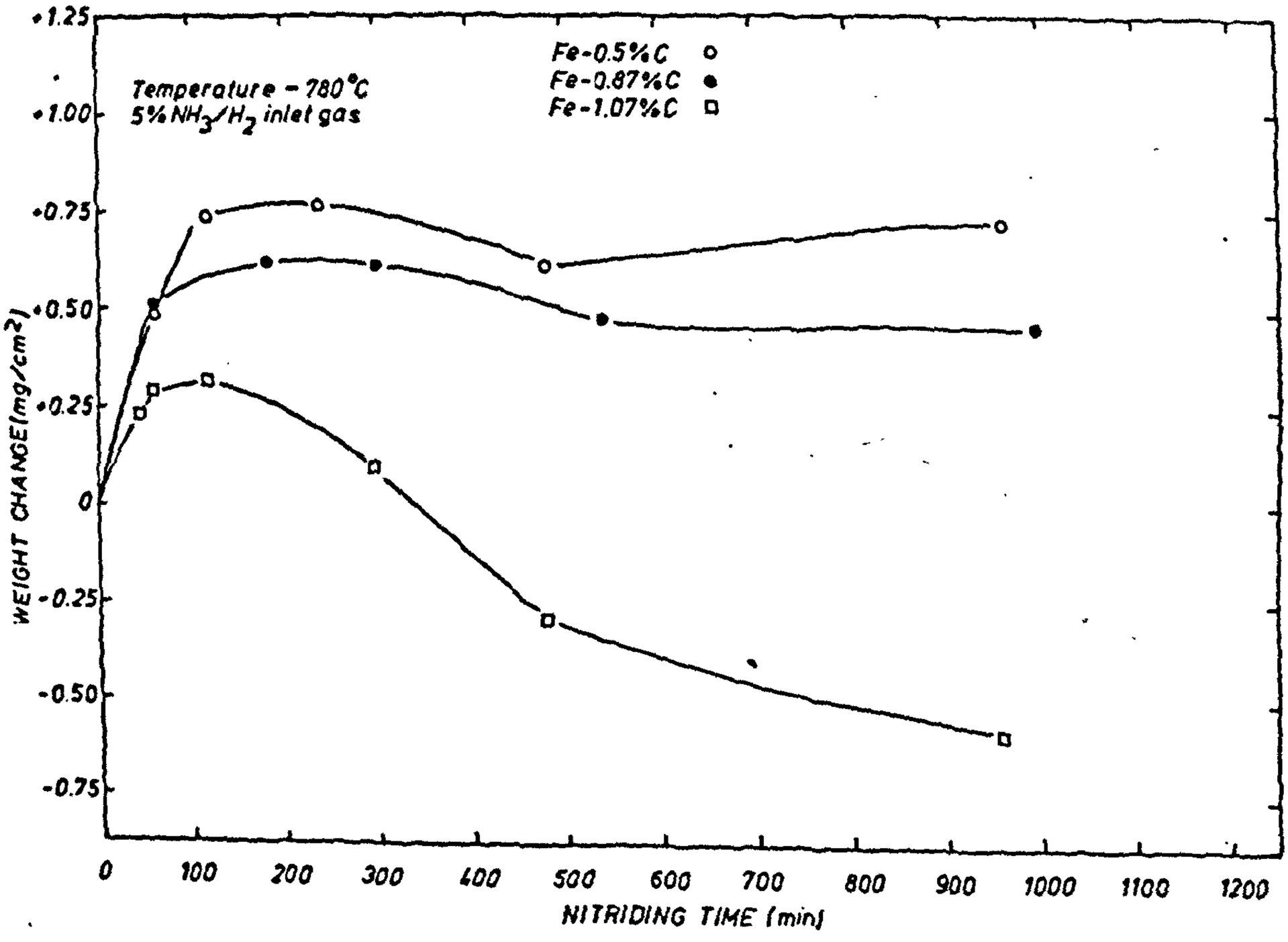
Temperature - 780°C
5% NH3/H2 inlet gas
Fe-0.5%C
Fe-0.87%C
Fe-1.07%C
1.25
1.00
0.75
0.50
0.25
0
-0.25
-0.50
-0.75
0
100
200
300
400
500
600
700
800
900
1000
1100
1200
NITRIDING TIME (min)
WEIGHT CHANGE (mg/cm²)

FIG. 62

KINETIC CURVES FOR IRON-CARBON ALLOYS NITRIDED IN $5^{v}/oNH_3/H_2$ AT 811°C.

FIG. 63

KINETIC CURVES FOR IRON-CARBON ALLOYS NITRIDED IN $5^{v}/oNH_3/H_2$ AT 845°C.

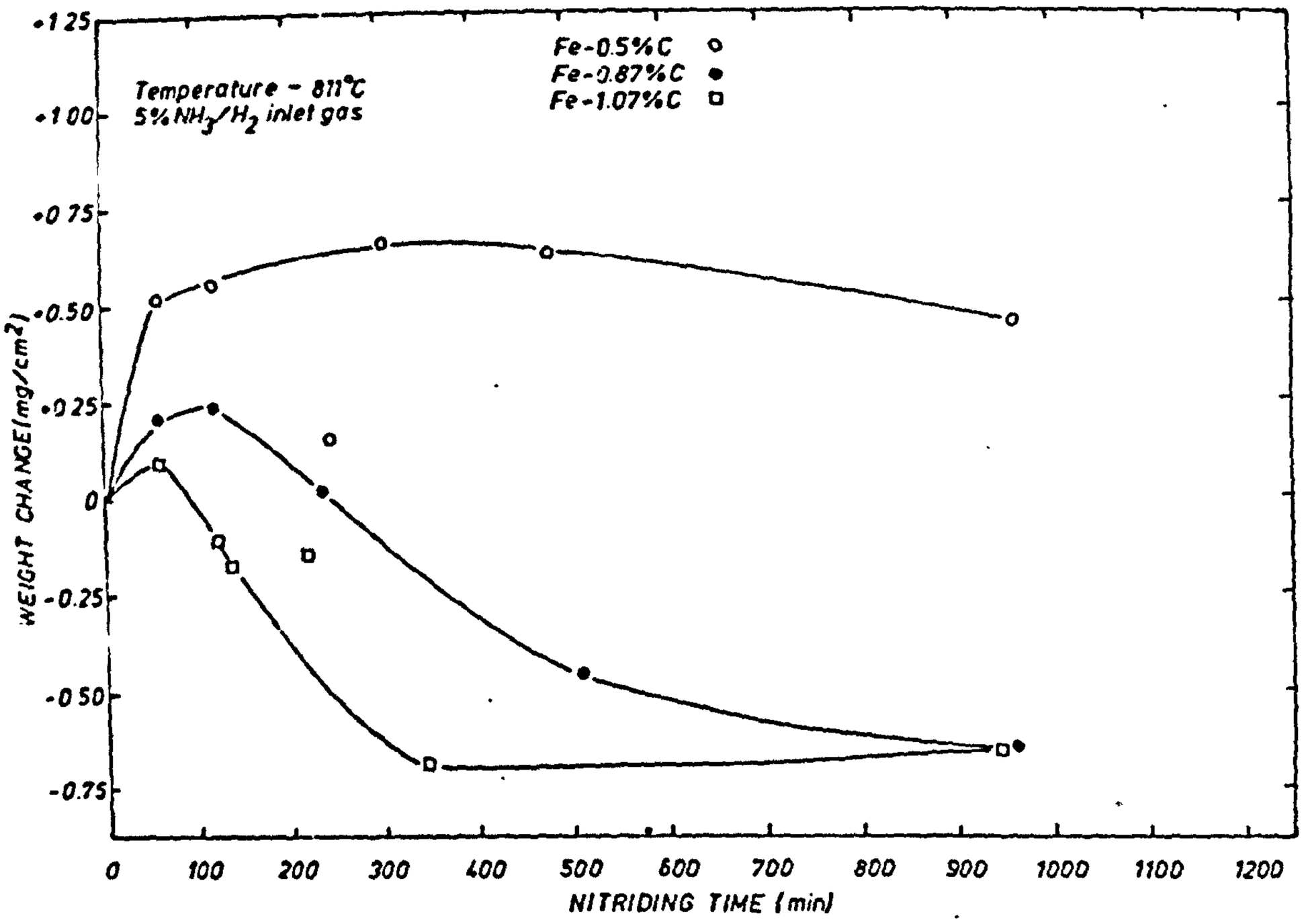
Fe-0.5%C
Fe-0.87%C
Fe-1.07%C
Temperature - 811°C
5% NH3/H2 inlet gas
WEIGHT CHANGE(mg/cm2)
+1.25
+1.00
+0.75
+0.50
+0.25
0
-0.25
-0.50
-0.75
0
100
200
300
400
500
600
700
800
900
1000
1100
1200
NITRIDING TIME (min)

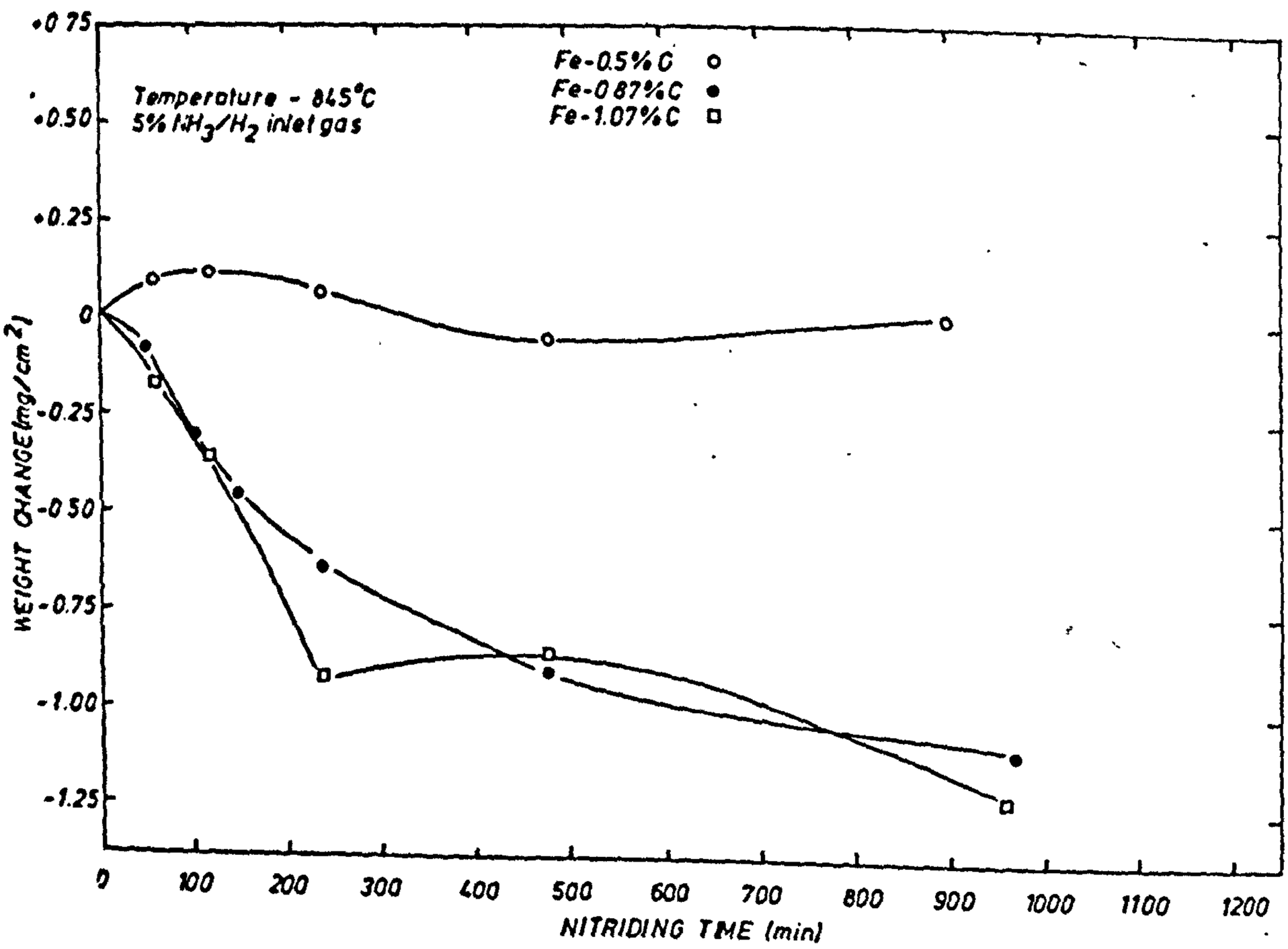
Fe-0.5%C
Fe-0.87%C
Fe-1.07%C
Temperature - 845°C
5% NH3/H2 inlet gas
WEIGHT CHANGE(mg/cm2)
+0.75
+0.50
+0.25
0
-0.25
-0.50
-0.75
-1.00
-1.25
0
100
200
300
400
500
600
700
800
900
1000
1100
1200
NITRIDING TIME (min)

FIG. 64

COMPOSITION PROFILES FOR Fe-0.5^{w}/oC ALLOYS NITRIDED IN 5^{v}/oNH_3/H_2 AT 748°C.

FIG. 65

COMPOSITION PROFILES FOR Fe-0.5^{w}/oC ALLOYS NITRIDED IN 5^{v}/oNH_3/H_2 AT 780°C.

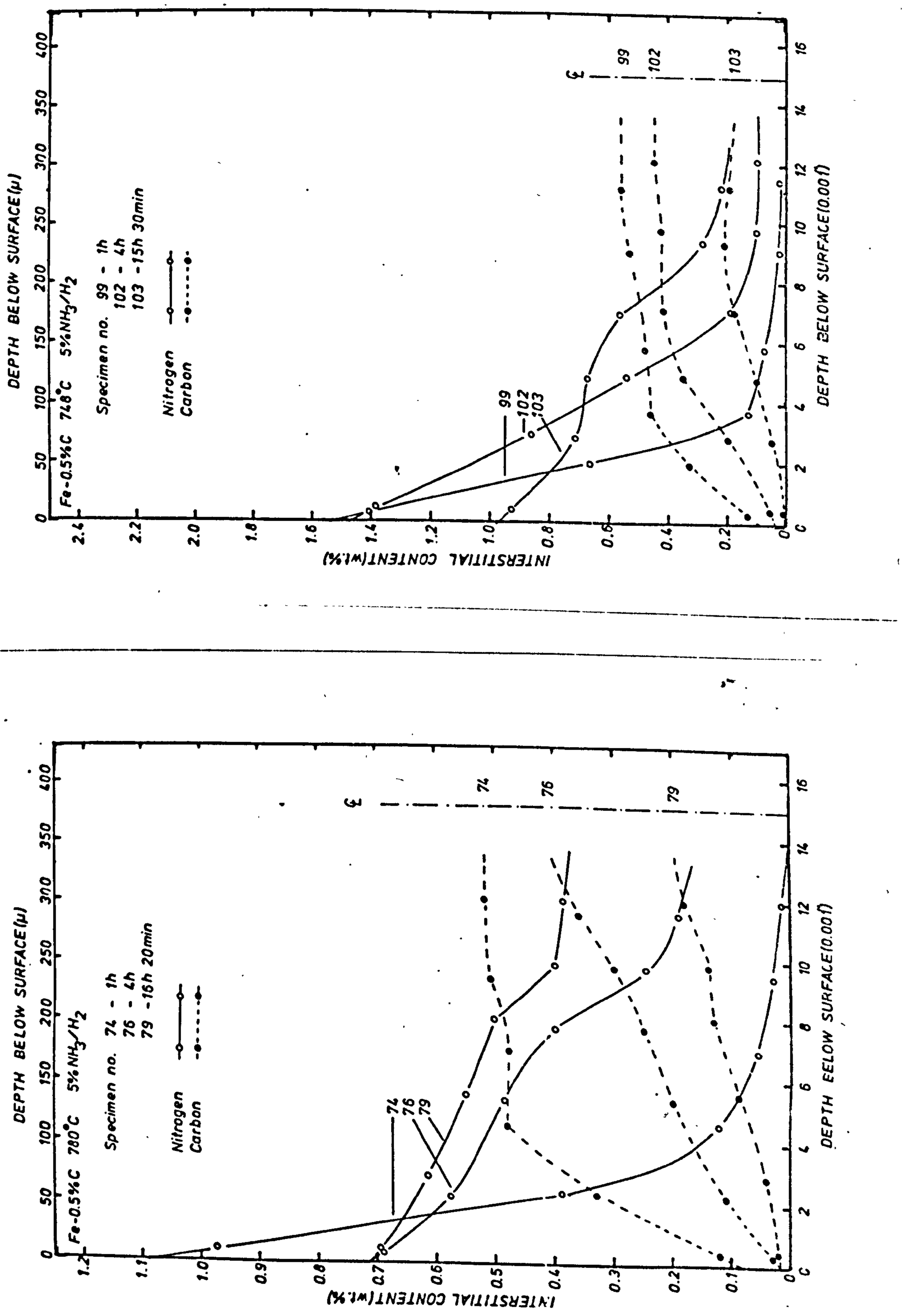
DEPTH BELOW SURFACE(μ)
Fe-0.5%C 748°C 5%NH3/H2
Specimen no. 99 - 1h
102 - 4h
103 -15h 30min
Nitrogen
Carbon
INTERSTITIAL CONTENT(wt.%)
DEPTH BELOW SURFACE(0.001")
Fe-0.5%C 780°C 5%NH3/H2
Specimen no. 74 - 1h
76 - 4h
79 -16h 20min
Nitrogen
Carbon
INTERSTITIAL CONTENT(wt.%)
DEPTH BELOW SURFACE(0.001")

FIG. 66

COMPOSITION PROFILES FOR Fe-0.5^{w}/oC ALLOYS NITRIDED IN 5^{v}/oNH_3/H_2 AT 811^{o}C.

FIG. 67

COMPOSITION PROFILES FOR Fe-0.5^{w}/oC ALLOYS NITRIDED IN 5^{v}/oNH_3/H_2 AT 845^{o}C.

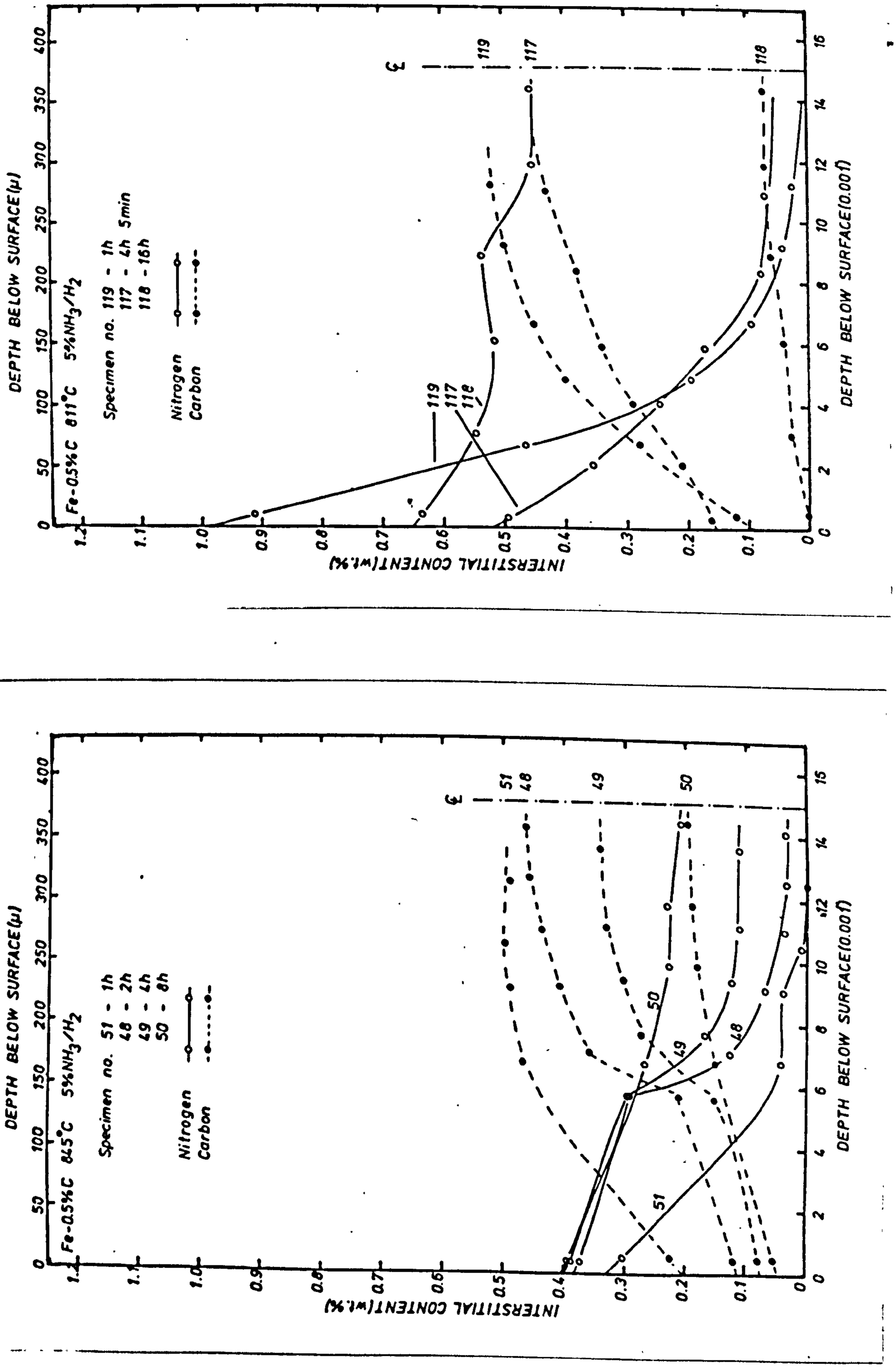
Fe-0.5%C 811°C 5%NH3/H2
Specimen no. 119 - 1h
117 - 4h 5min
118 - 16h
Nitrogen
Carbon
DEPTH BELOW SURFACE(μ)
INTERSTITIAL CONTENT(wt.%)
DEPTH BELOW SURFACE(0.001")
Fe-0.5%C 845°C 5%NH3/H2
Specimen no. 51 - 1h
48 - 2h
49 - 4h
50 - 8h
Nitrogen
Carbon
DEPTH BELOW SURFACE(μ)
INTERSTITIAL CONTENT(wt.%)
DEPTH BELOW SURFACE(0.001")

FIG. 68

COMPOSITION PROFILES FOR Fe-0.87^{w}/oC ALLOYS NITRIDED IN 5^{v}/oNH_3/H_2 AT 748°C.

FIG. 69

COMPOSITION PROFILES FOR Fe-0.87^{w}/oC ALLOYS NITRIDED IN 5^{v}/oNH_3/H_2 AT 780°C.

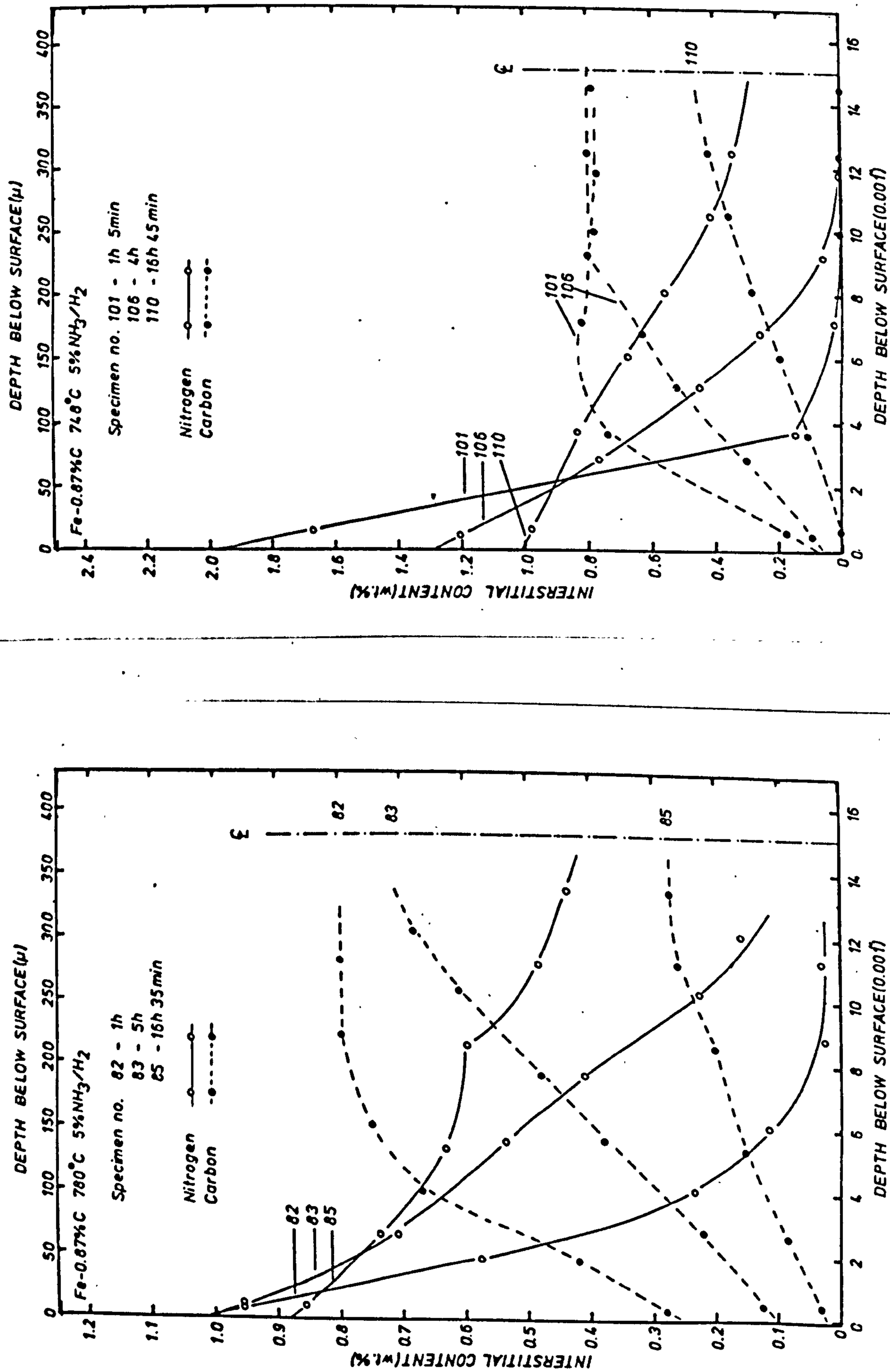
Fe-0.87%C 740°C 5%NH3/H2
Specimen no. 101 - 1h 5min
106 - 4h
110 - 16h 45min
Nitrogen
Carbon
DEPTH BELOW SURFACE(μ)
INTERSTITIAL CONTENT(wt.%)
DEPTH BELOW SURFACE(0.001")
Fe-0.87%C 780°C 5%NH3/H2
Specimen no. 82 - 1h
83 - 5h
85 - 16h 35min
Nitrogen
Carbon
DEPTH BELOW SURFACE(μ)
INTERSTITIAL CONTENT(wt.%)
DEPTH BELOW SURFACE(0.001")

FIG. 70

COMPOSITION PROFILES FOR Fe-0.87^{W}/oC ALLOYS NITRIDED IN 5^{V}/oNH_3/H_2 AT 811°C.

FIG. 71

COMPOSITION PROFILES FOR Fe-0.87^{W}/oC ALLOYS NITRIDED IN 5^{V}/oNH_3/H_2 AT 845°C.

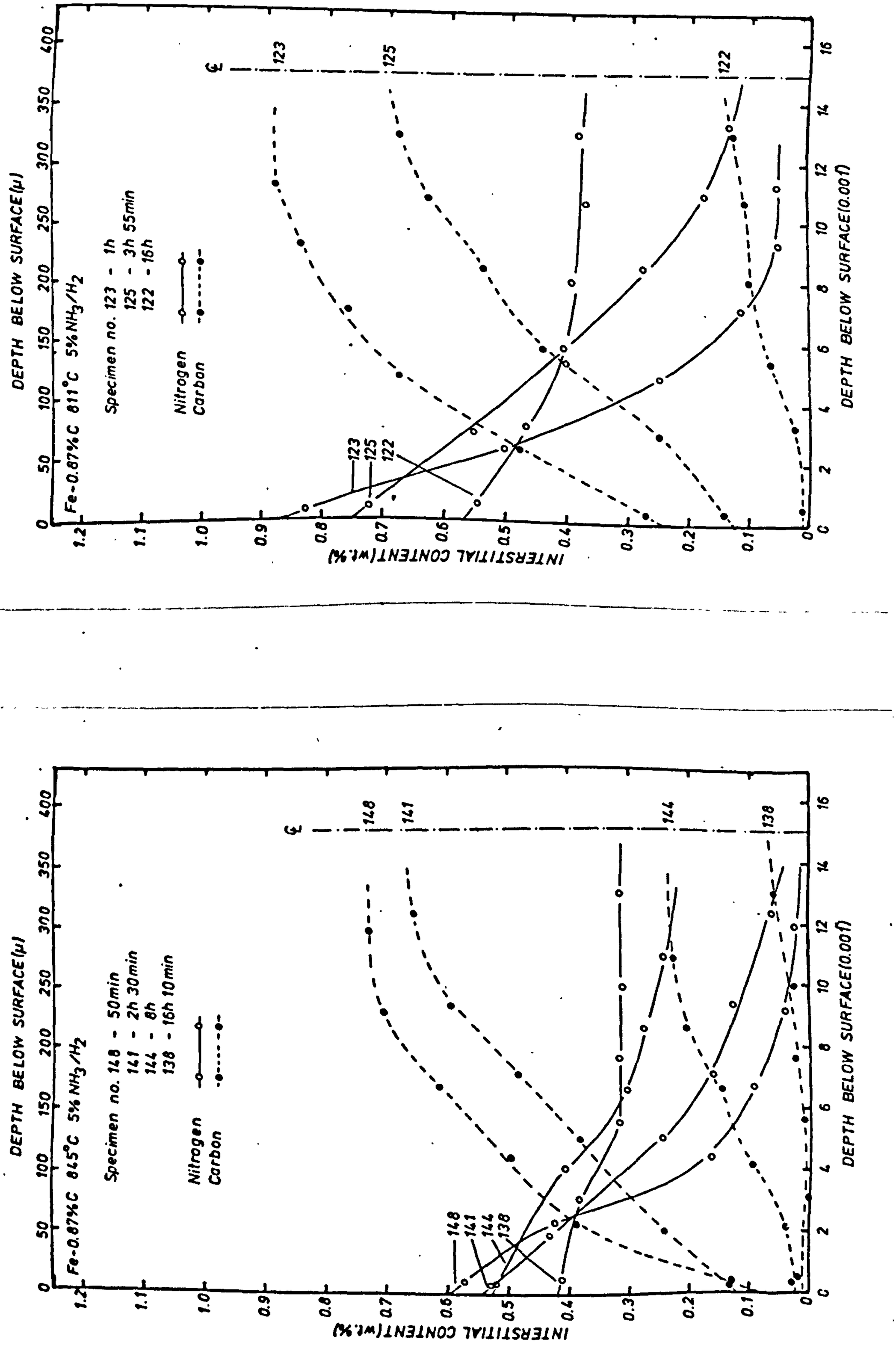
DEPTH BELOW SURFACE (μ)
Fe-0.87%C 811°C 5% NH3/H2
Specimen no. 123 - 1h
125 - 3h 55min
122 - 16h
Nitrogen
Carbon
INTERSTITIAL CONTENT (wt.%)
DEPTH BELOW SURFACE (0.001")
Fe-0.87%C 845°C 5% NH3/H2
Specimen no. 148 - 50min
141 - 2h 30min
144 - 8h
138 - 16h 10min

FIG. 72

COMPOSITION PROFILES FOR Fe-1.07^{W}/$_{o}$C ALLOYS NITRIDED IN $5^{V}/_{o}NH_3/H_2$ AT 748°C.

FIG. 73

COMPOSITION PROFILES FOR Fe-1.07^{W}/$_{o}$C ALLOYS NITRIDED IN $5^{V}/_{o}NH_3/H_2$ AT 780°C.

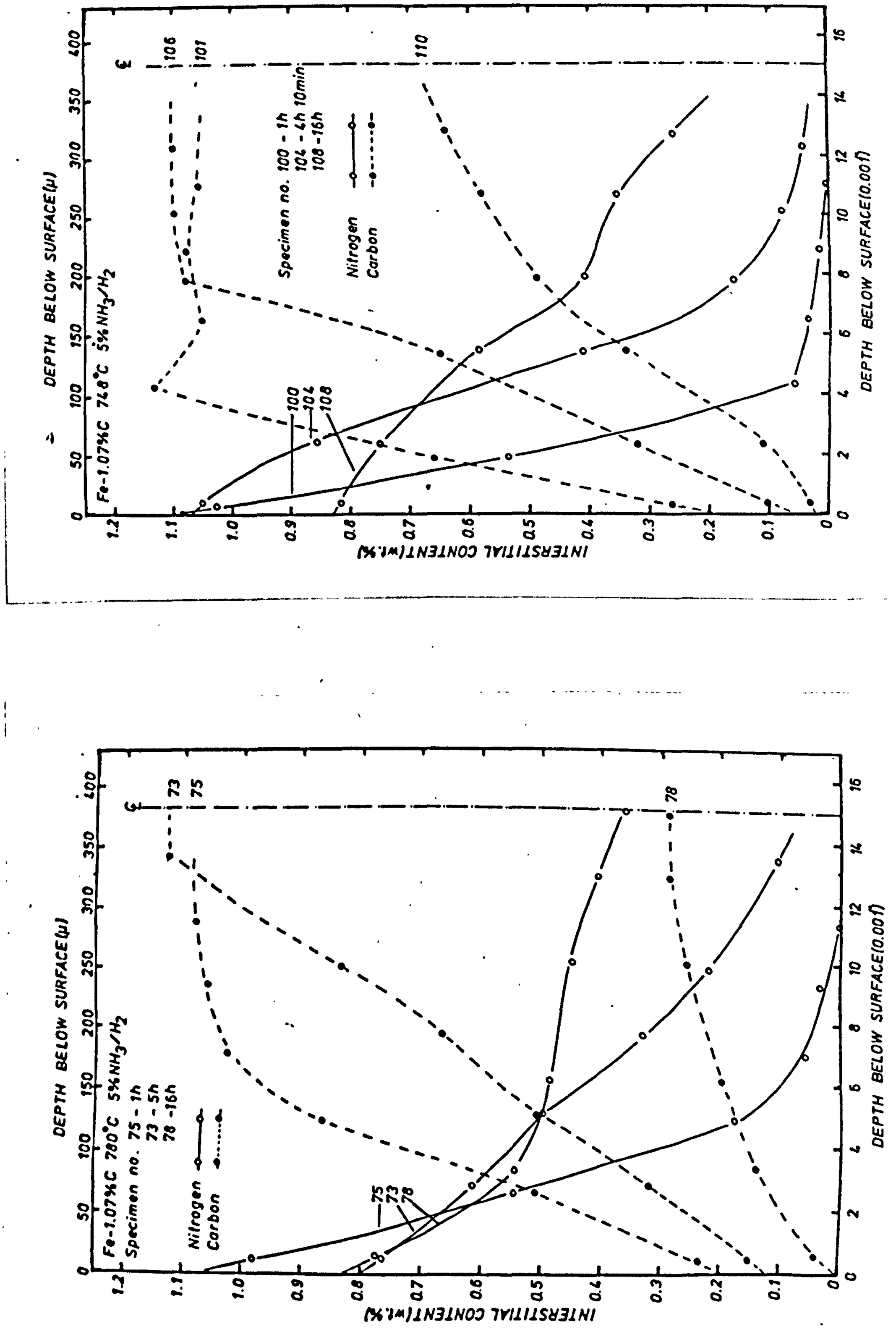
Fe-1.07%C 740°C 5%NH3/H2
Specimen no. 100 - 1h
104 - 4h 10min
108 -16h
Nitrogen
Carbon
100
104
108
110
106
101
DEPTH BELOW SURFACE(μ)
DEPTH BELOW SURFACE(0.001")
INTERSTITIAL CONTENT(wt.%)
Fe-1.07%C 780°C 5%NH3/H2
Specimen no. 75 - 1h
73 - 5h
78 -16h
75
73
78
73
75
78

FIG. 74

COMPOSITION PROFILES FOR Fe-1.07^{w}/oC ALLOYS NITRIDED IN 5^{v}/oNH_3/H_2 AT 811^{o}C.

FIG. 75

COMPOSITION PROFILES FOR Fe-1.07^{w}/oC ALLOYS NITRIDED IN 5^{v}/oNH_3/H_2 AT 845^{o}C.

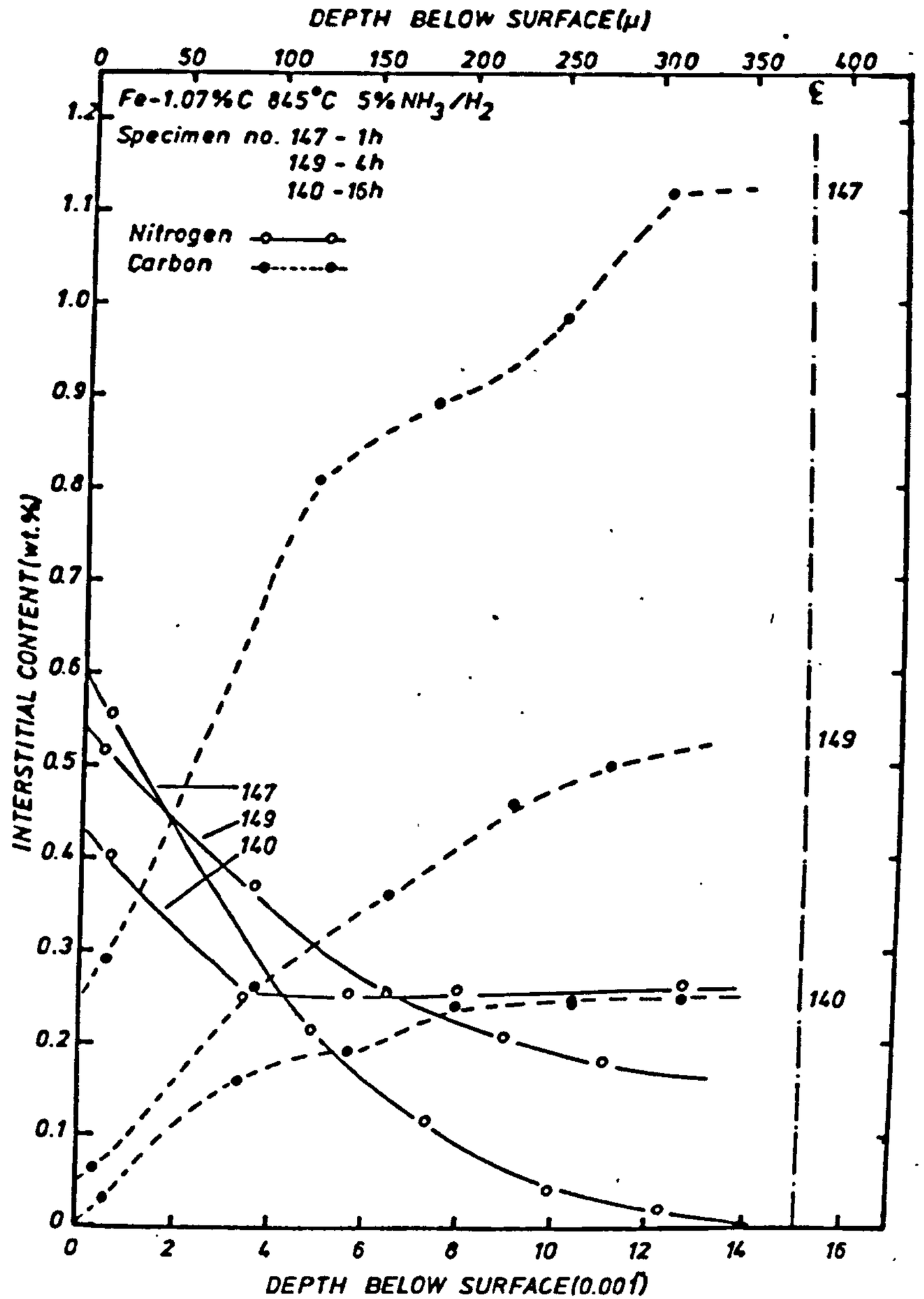
DEPTH BELOW SURFACE(μ)
0 50 100 150 200 250 300 350 400
Fe-1.07%C 845°C 5%NH3/H2
Specimen no. 147 - 1h
149 - 4h
140 - 16h
Nitrogen
Carbon
147
149
140
INTERSTITIAL CONTENT(wt.%)
0 0.1 0.2 0.3 0.4 0.5 0.6 0.7 0.8 0.9 1.0 1.1 1.2
0 2 4 6 8 10 12 14 16
DEPTH BELOW SURFACE(0.001")

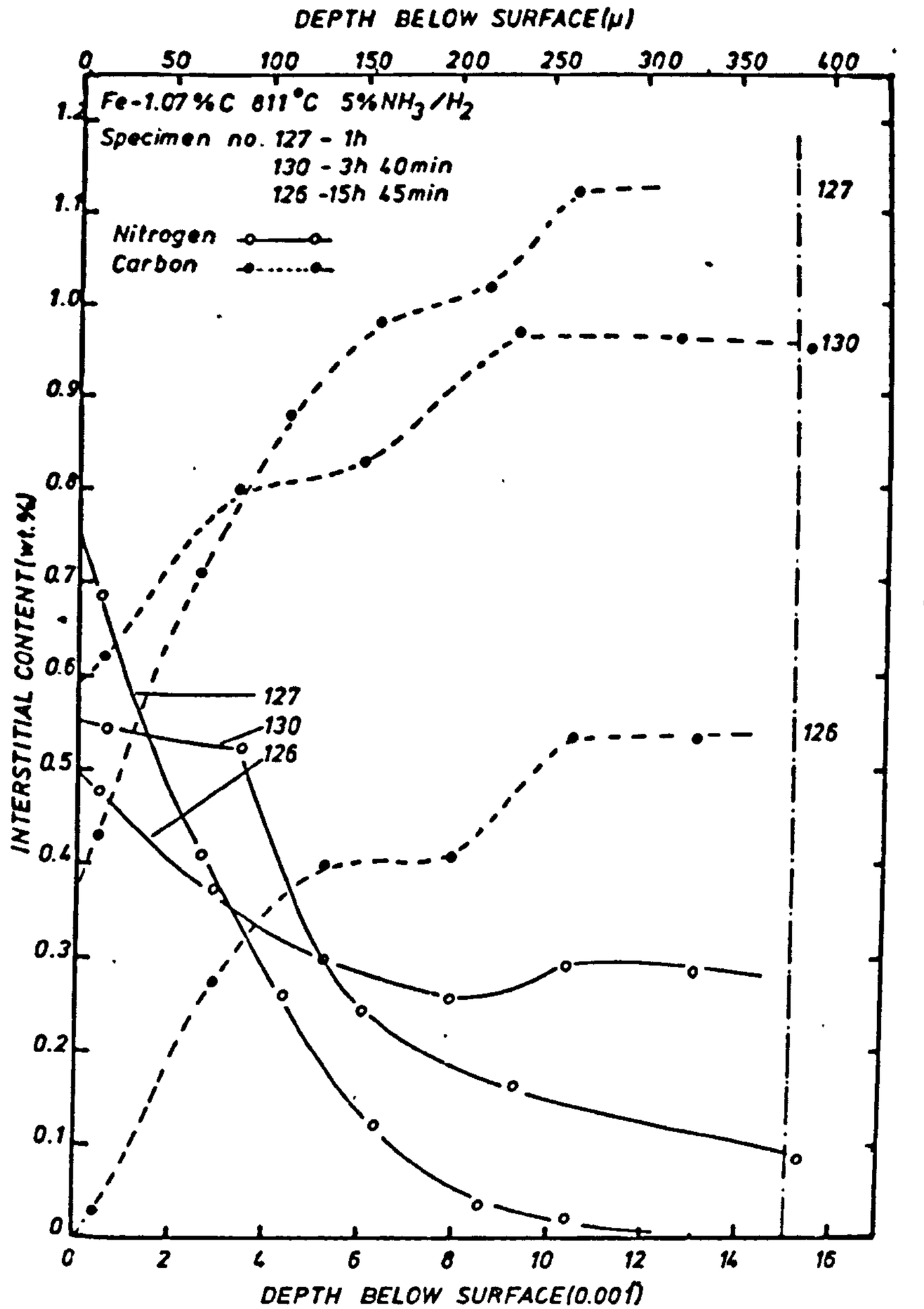
DEPTH BELOW SURFACE(μ)
0 50 100 150 200 250 300 350 400
Fe-1.07%C 811°C 5%NH3/H2
Specimen no. 127 - 1h
130 - 3h 40min
126 - 15h 45min
Nitrogen
Carbon
127
130
126
INTERSTITIAL CONTENT(wt.%)
0 0.1 0.2 0.3 0.4 0.5 0.6 0.7 0.8 0.9 1.0 1.1 1.2
0 2 4 6 8 10 12 14 16
DEPTH BELOW SURFACE(0.001")

127s

FIG. 76

CARBON WEIGHT LOSS FOR Fe-0.5^{w}/oC ALLOYS NITRIDED IN 5^{v}/oNH_3/H_2 FOR TEMPERATURES IN THE RANGE 748°C - 845°C.

FIG. 77

CARBON WEIGHT LOSS FOR Fe-0.87^{w}/oC ALLOYS NITRIDED IN 5^{v}/oNH_3/H_2 FOR TEMPERATURES IN THE RANGE 748°C -845°C.

FIG. 78

CARBON WEIGHT LOSS FOR Fe-1.07^{w}/oC ALLOYS NITRIDED IN 5^{v}/oNH_3/H_2 FOR TEMPERATURES IN THE RANGE 748°C - 845°C.

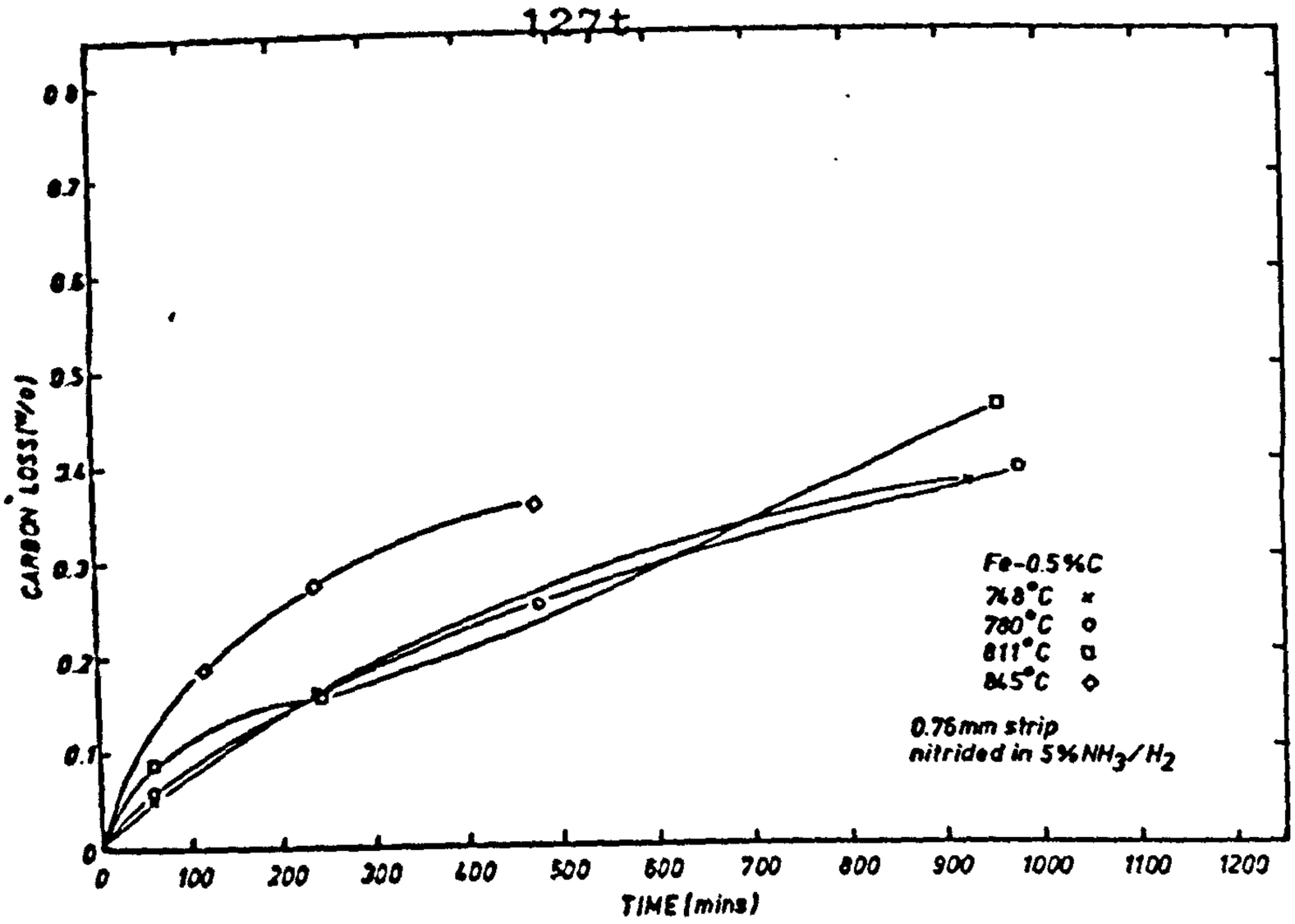
CARBON LOSS(%o)
0.8
0.7
0.6
0.5
0.4
0.3
0.2
0.1
0
0 100 200 300 400 500 600 700 800 900 1000 1100 1200
TIME (mins)
Fe-0.5%C
748°C ×
780°C ○
811°C □
845°C ◇
0.76mm strip
nitrided in 5%NH3/H2

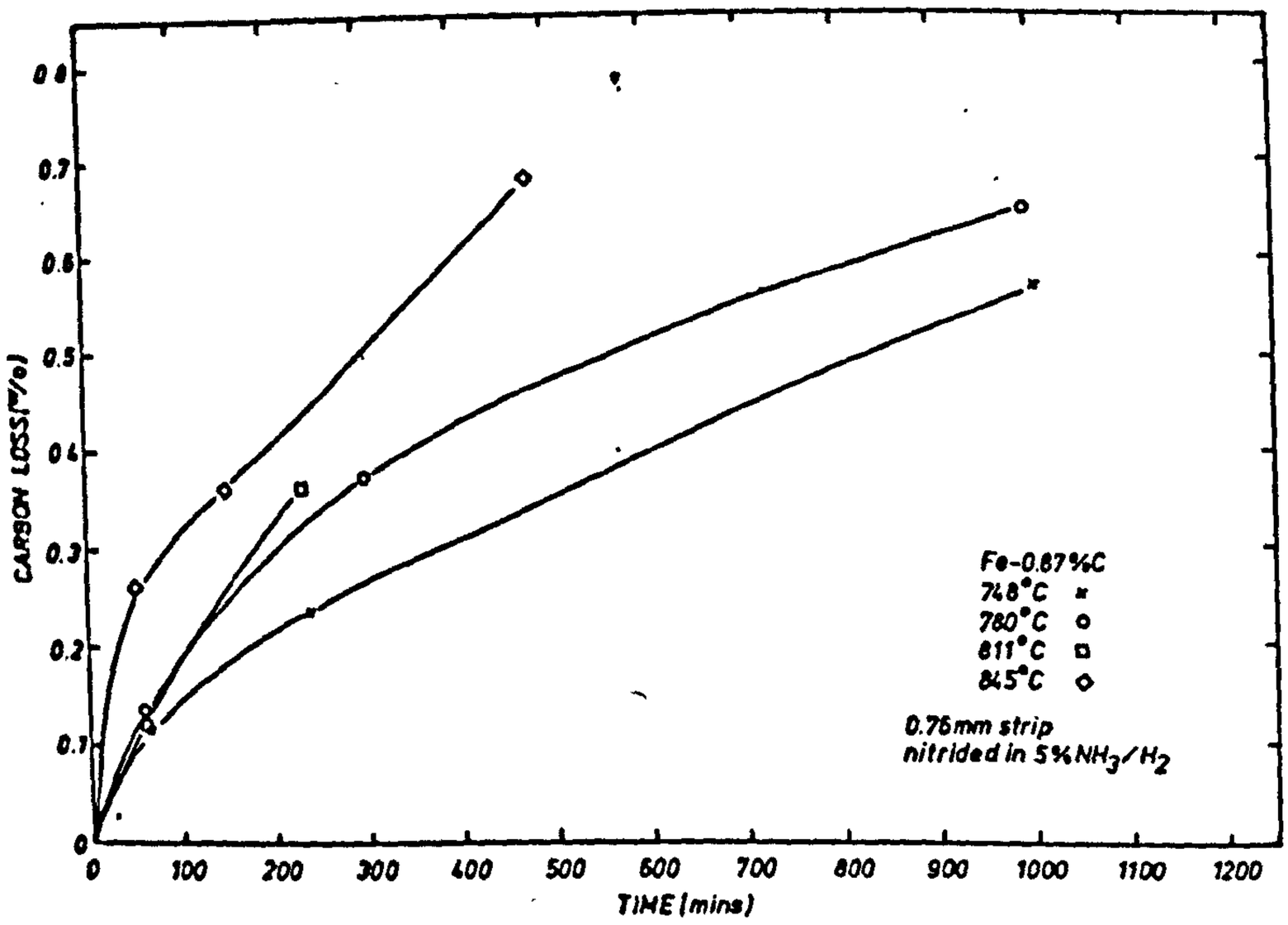
CARBON LOSS(%o)
0.8
0.7
0.6
0.5
0.4
0.3
0.2
0.1
0
0 100 200 300 400 500 600 700 800 900 1000 1100 1200
TIME (mins)
Fe-0.87%C
748°C ×
780°C ○
811°C □
845°C ◇
0.76mm strip
nitrided in 5%NH3/H2

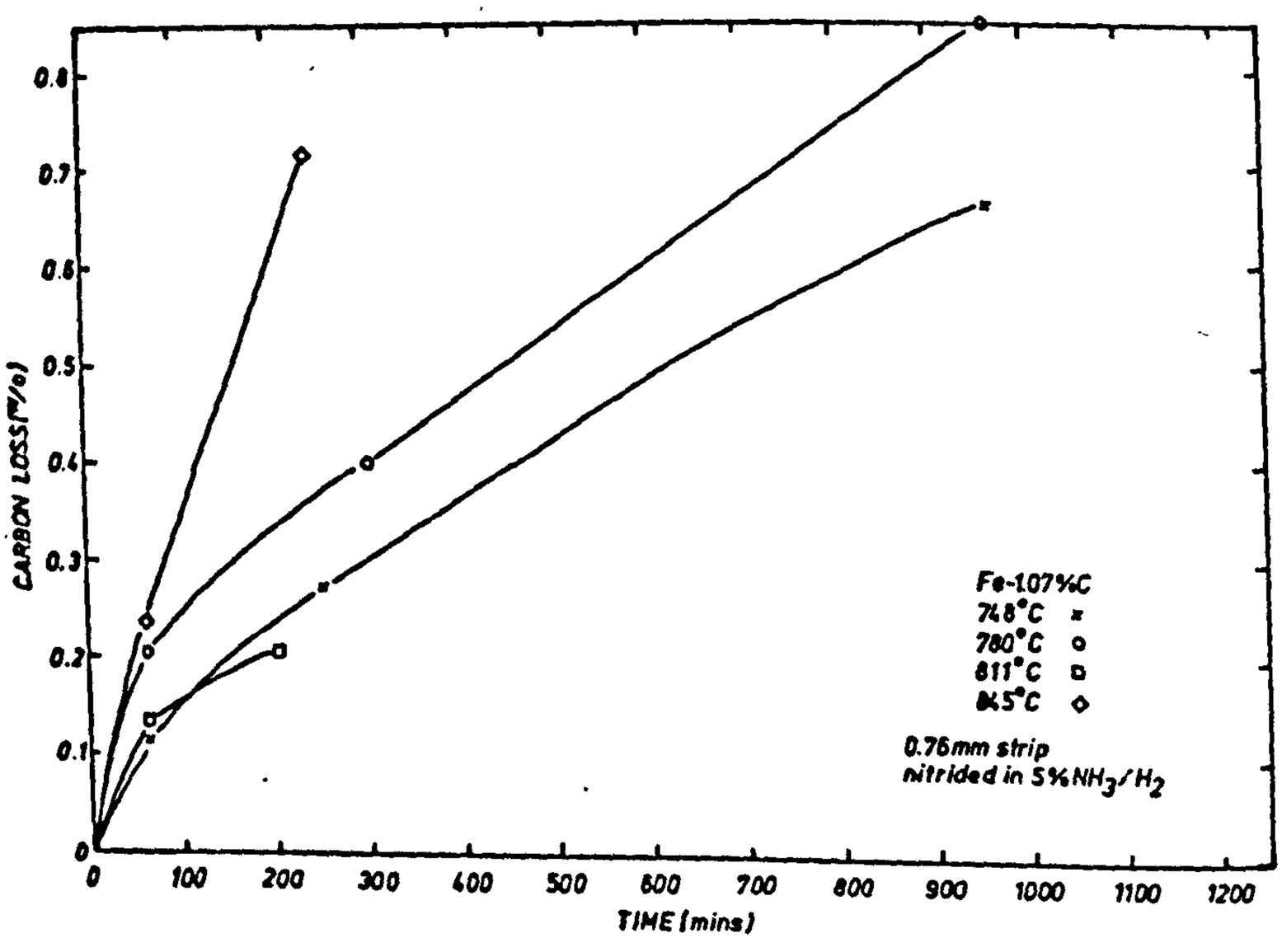
CARBON LOSS(%o)
0.8
0.7
0.6
0.5
0.4
0.3
0.2
0.1
0
0 100 200 300 400 500 600 700 800 900 1000 1100 1200
TIME (mins)
Fe-1.07%C
748°C ×
780°C ○
811°C □
845°C ◇
0.76mm strip
nitrided in 5%NH3/H2

FIG. 79

CONCENTRATION PROFILES FOR Fe-0.5$^{w}/_{o}$C ALLOYS NITRIDED UNDER VARIOUS POTENTIALS AT 780^{o}C.

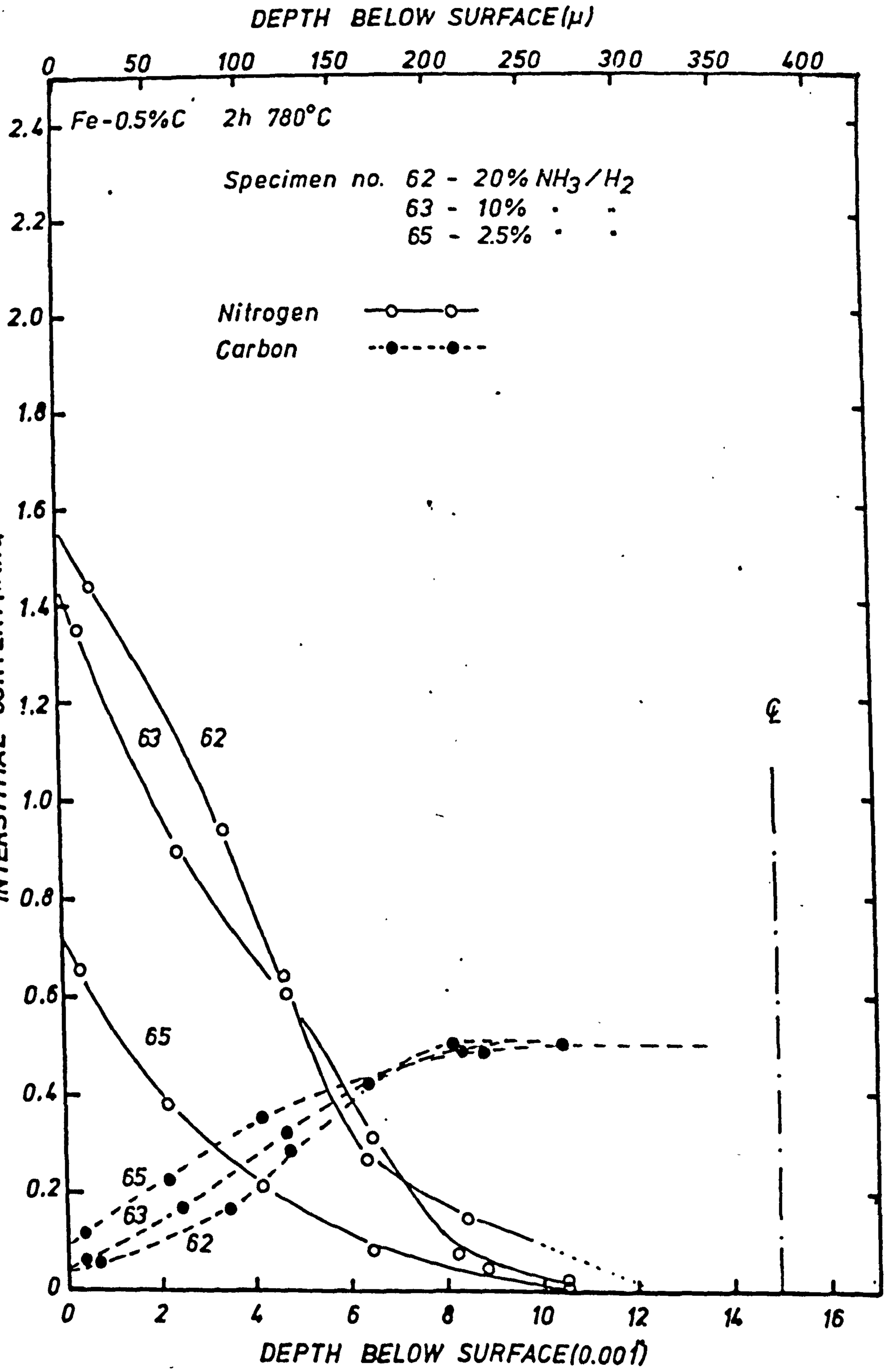
DEPTH BELOW SURFACE(μ)
0
50
100
150
200
250
300
350
400
Fe-0.5%C 2h 780°C
Specimen no. 62 - 20% NH3/H2
63 - 10% " "
65 - 2.5% " "
Nitrogen
Carbon
INTERSTITIAL CONTENT(wt.%)
2.4
2.2
2.0
1.8
1.6
1.4
1.2
1.0
0.8
0.6
0.4
0.2
0
63
62
65
65
63
62
0
2
4
6
8
10
12
14
16
DEPTH BELOW SURFACE(0.001")

FIG. 80

CONCENTRATION PROFILES FOR Fe-0.5$^{W}/_{o}$C ALLOYS NITRIDED IN $10^{V}/_{o}NH_3/1.1^{V}/_{o}CH_4/H_2$ AT 845°C.

FIG. 81

CONCENTRATION PROFILES FOR Fe-0.5$^{W}/_{o}$C ALLOYS NITRIDED IN $5^{V}/_{o}NH_3/1.1^{V}/_{o}CH_4/H_2$ AT 845°C.

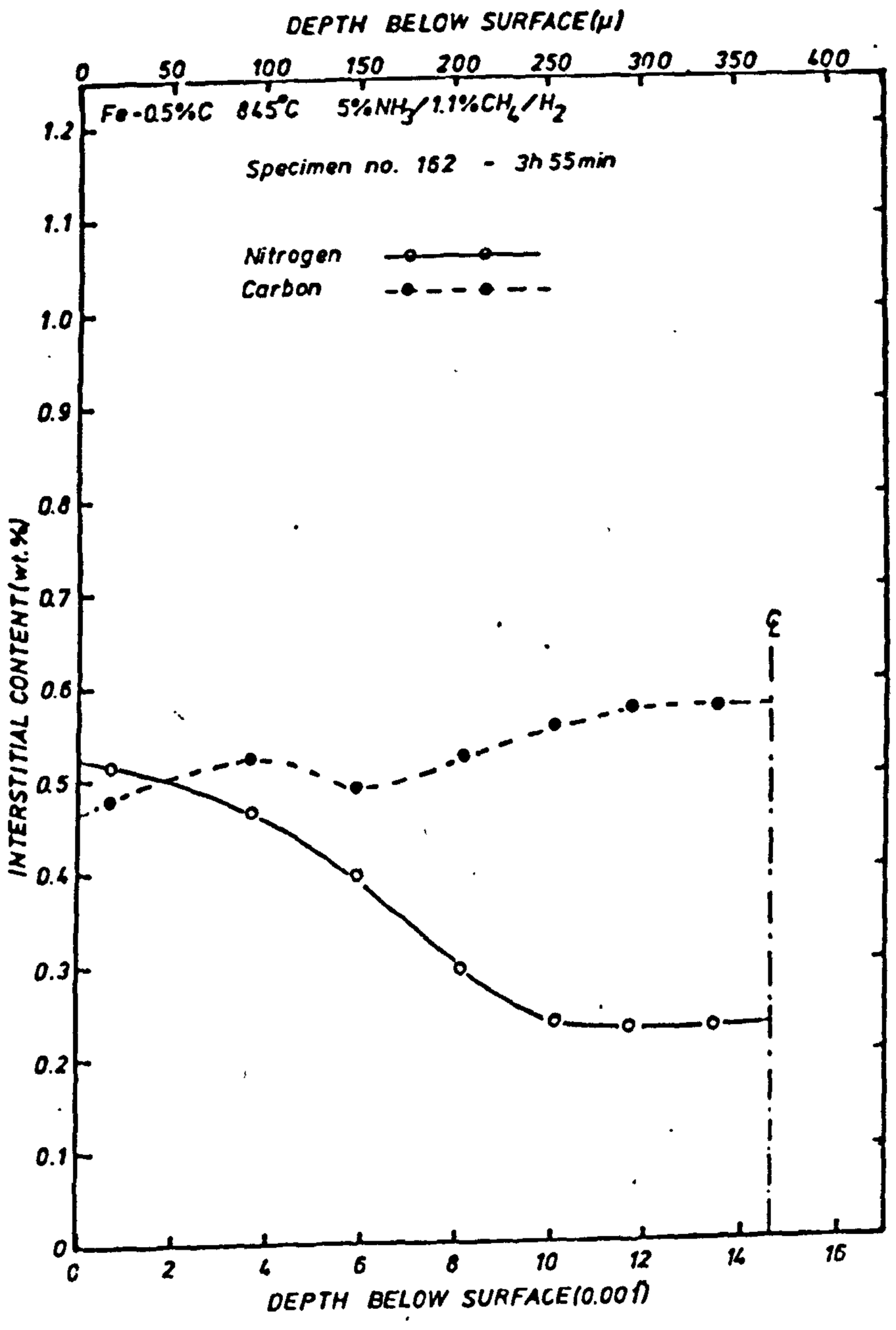
DEPTH BELOW SURFACE(μ)
0 50 100 150 200 250 300 350 400
Fe-0.5%C 845°C 5%NH3/1.1%CH4/H2
Specimen no. 162 - 3h 55min
Nitrogen
Carbon
INTERSTITIAL CONTENT(wt.%)
1.2 1.1 1.0 0.9 0.8 0.7 0.6 0.5 0.4 0.3 0.2 0.1 0
ε
0 2 4 6 8 10 12 14 16
DEPTH BELOW SURFACE(0.001)

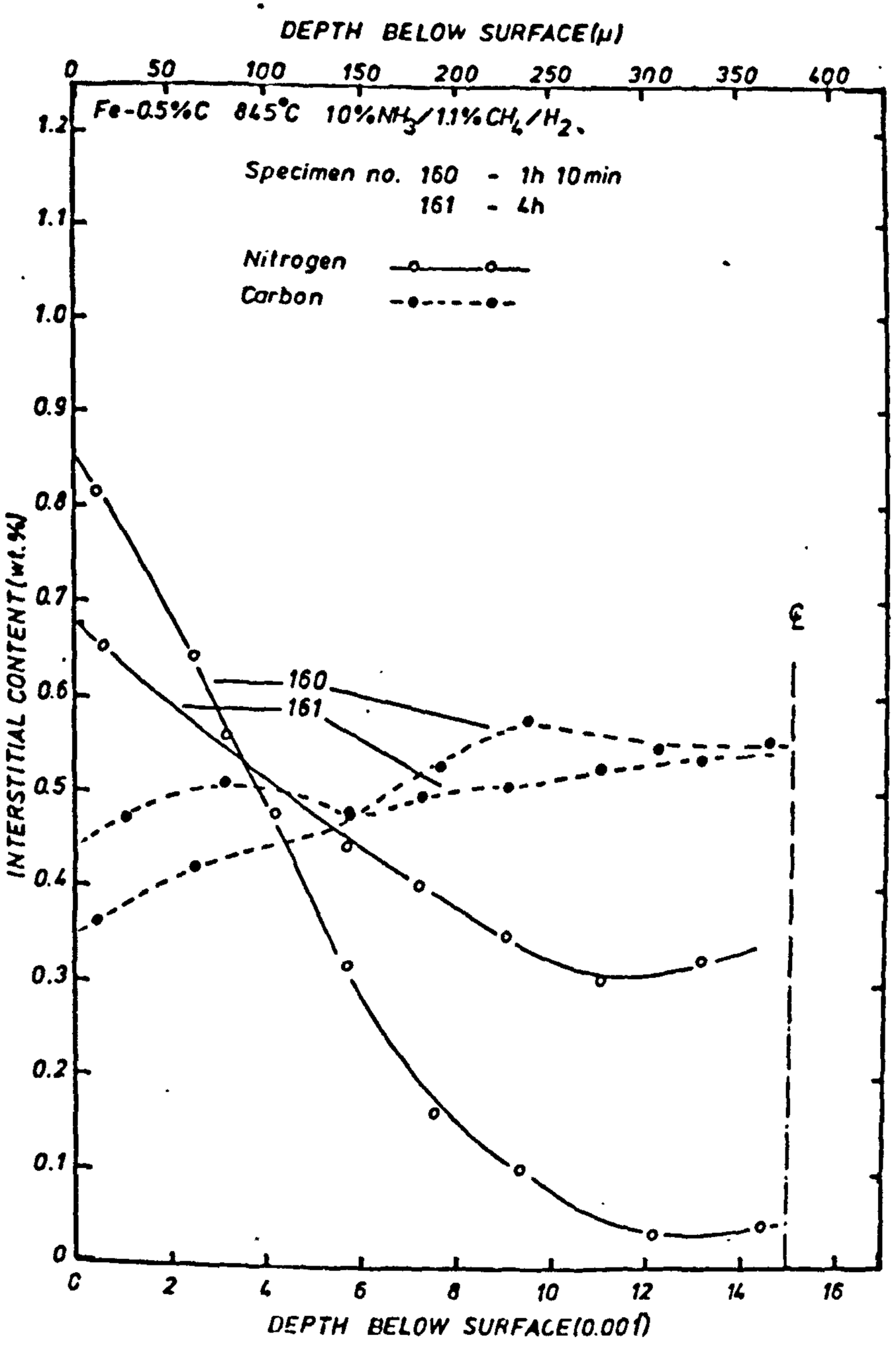
DEPTH BELOW SURFACE(μ)
0 50 100 150 200 250 300 350 400
Fe-0.5%C 845°C 10%NH3/1.1%CH4/H2
Specimen no. 160 - 1h 10min
161 - 4h
Nitrogen
Carbon
INTERSTITIAL CONTENT(wt.%)
1.2 1.1 1.0 0.9 0.8 0.7 0.6 0.5 0.4 0.3 0.2 0.1 0
160
161
ε
0 2 4 6 8 10 12 14 16
DEPTH BELOW SURFACE(0.001)

FIG. 82

CONCENTRATION PROFILES FOR Fe-1.07^{W}/oC ALLOYS NITRIDED IN 5^{V}/oNH_3/2.3^{V}/oCH_4/H_2 AT 845°C.

FIG. 83

CONCENTRATION PROFILES FOR Fe-0.87^{W}/oC ALLOYS NITRIDED IN 5^{V}/oNH_3/1.9^{V}/oCH_4/H_2 AT 845°C.

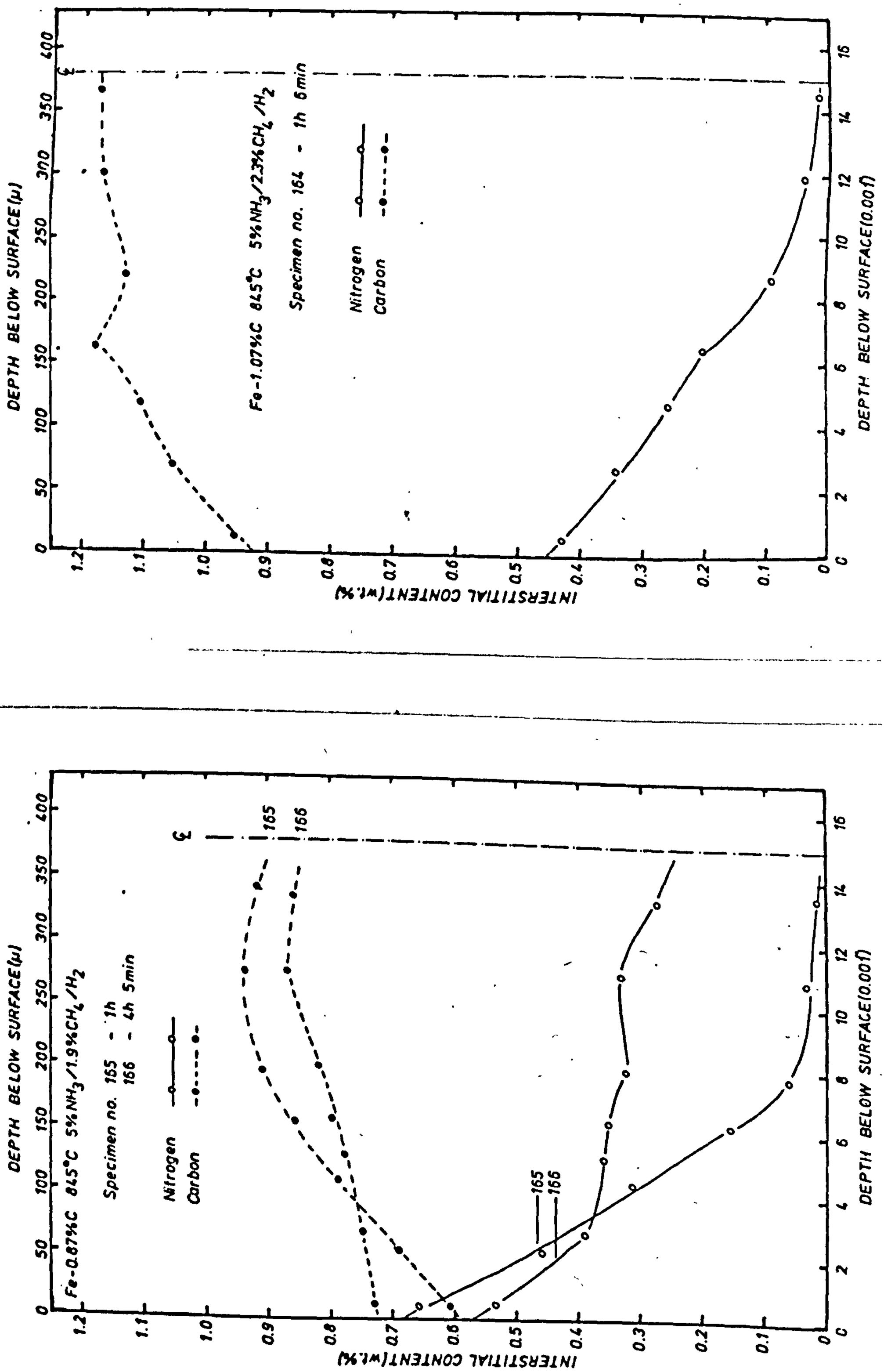
Fe-1.07%C 845°C 5%NH3/2.3%CH4/H2
Specimen no. 164 - 1h 6min
Nitrogen
Carbon
DEPTH BELOW SURFACE(μ)
INTERSTITIAL CONTENT(wt.%)
DEPTH BELOW SURFACE(0.001")
Fe-0.87%C 845°C 5%NH3/1.9%CH4/H2
Specimen no. 165 - 1h
166 - 4h 5min
165
166

FIG. 84

CHANGE IN SURFACE NITROGEN CONTENT WITH TREATMENT TIME FOR Fe-0.5^{w}/oC ALLOYS NITRIDED IN 5^{v}/oNH_3/H_2 AT TEMPERATURES IN THE RANGE 748°C - 845°C.

FIG. 85

CHANGE IN SURFACE NITROGEN CONTENT WITH TREATMENT TIME FOR Fe-0.87^{w}/oC ALLOYS NITRIDED IN 5^{v}/oNH_3/H_2 AT TEMPERATURES IN THE RANGE 748°C - 845°C.

FIG. 86

CHANGE IN SURFACE NITROGEN CONTENT WITH TREATMENT TIME FOR Fe-1.07^{w}/oC ALLOYS NITRIDED IN 5^{v}/oNH_3/H_2 AT TEMPERATURES IN THE RANGE 748°C - 845°C.

127x

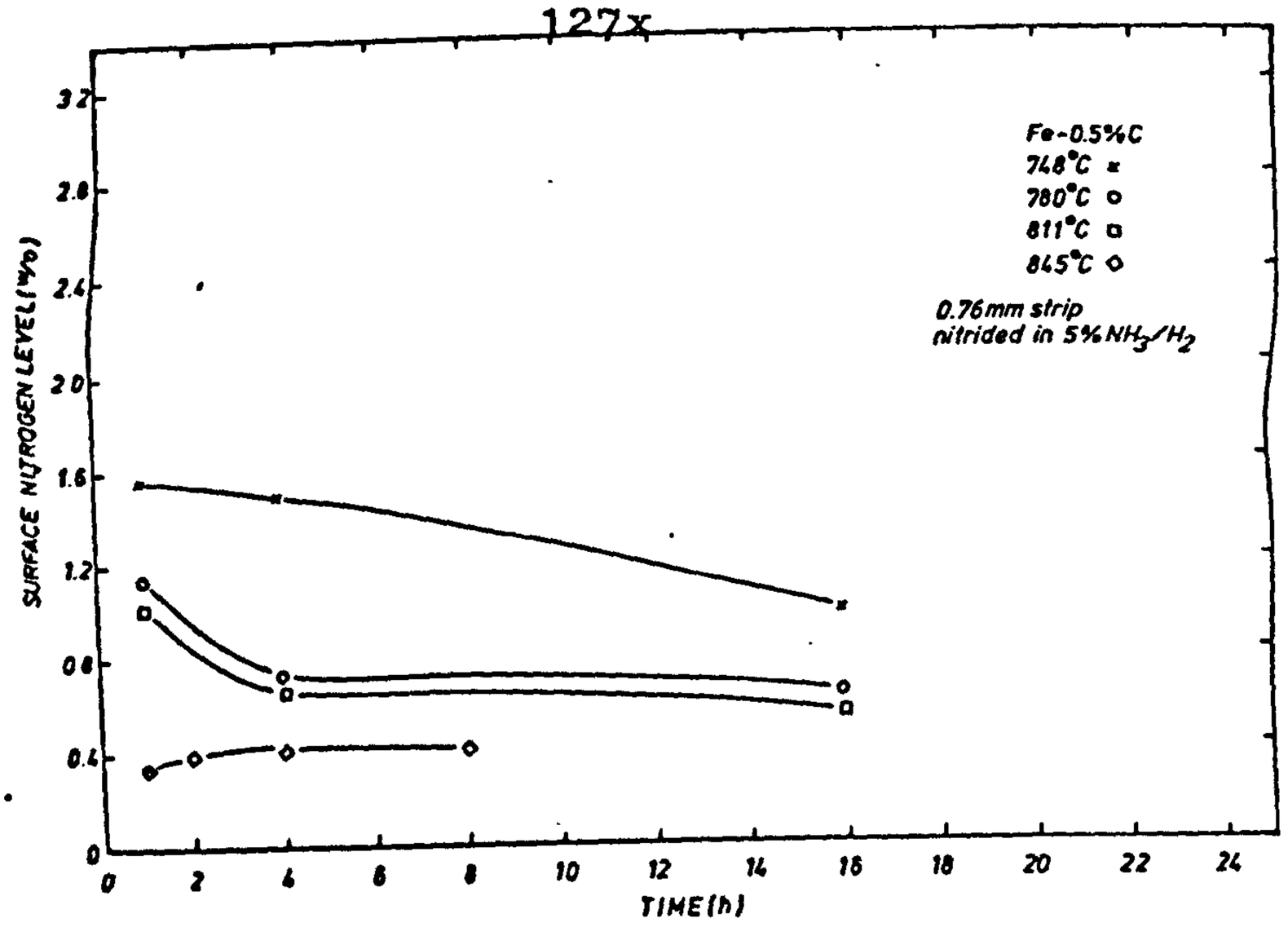
SURFACE NITROGEN LEVEL (wt%)
TIME (h)
Fe-0.5%C
748°C ×
780°C ○
811°C □
845°C ◇
0.76mm strip
nitrided in 5% NH3/H2

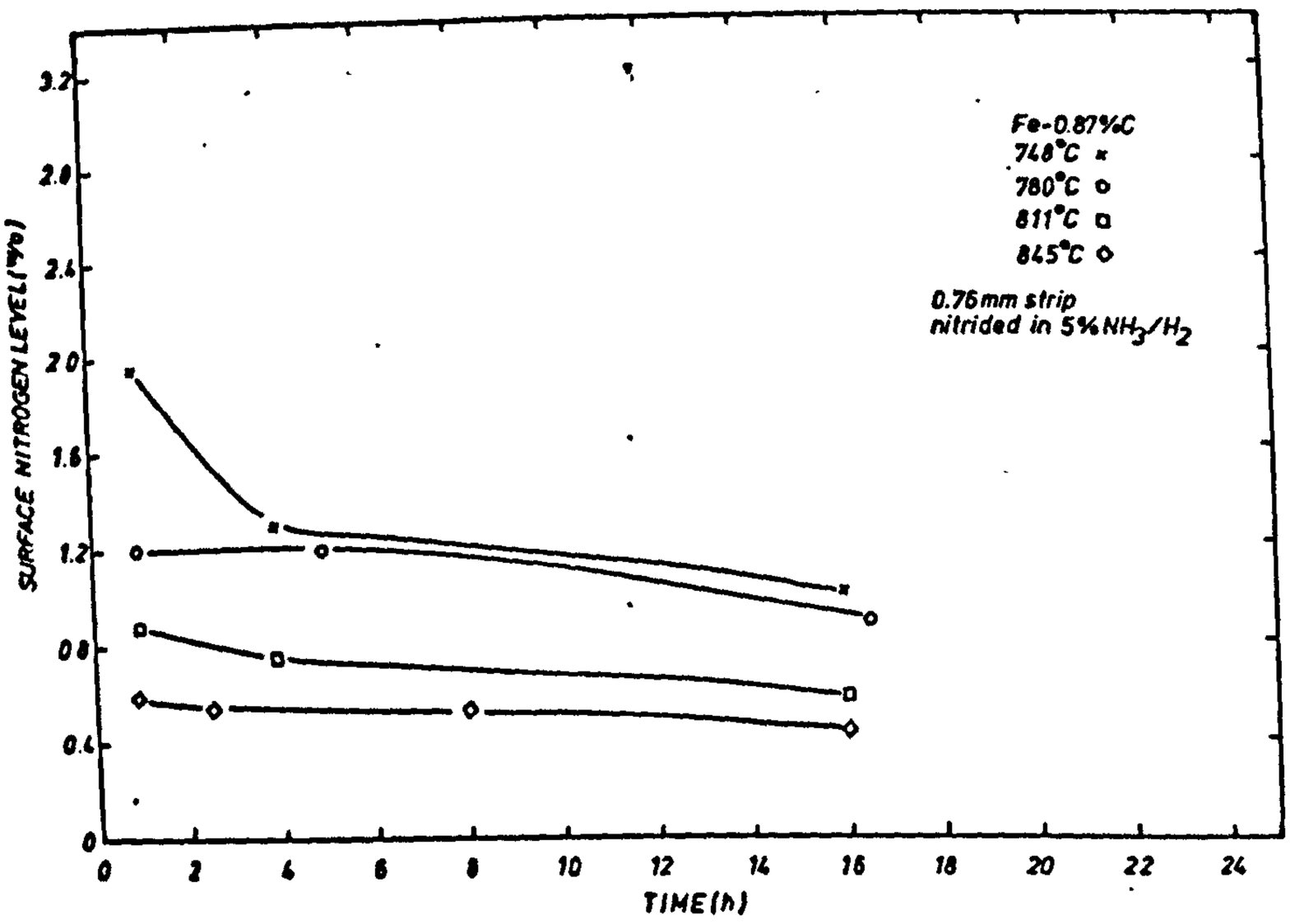
SURFACE NITROGEN LEVEL (wt%)
TIME (h)
Fe-0.87%C
748°C ×
780°C ○
811°C □
845°C ◇
0.76mm strip
nitrided in 5% NH3/H2

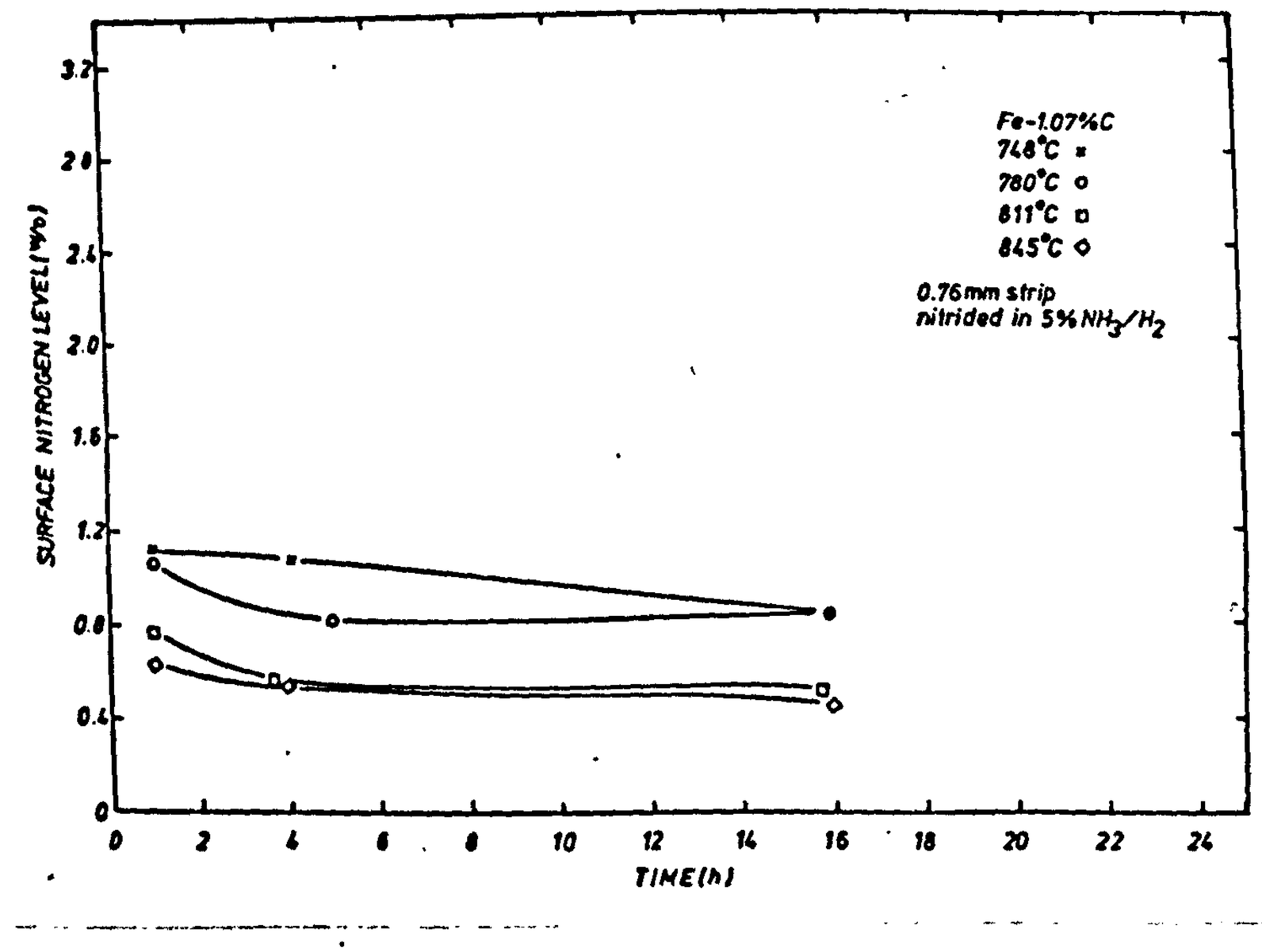
SURFACE NITROGEN LEVEL (wt%)
TIME (h)
Fe-1.07%C
748°C ×
780°C ○
811°C □
845°C ◇
0.76mm strip
nitrided in 5% NH3/H2

FIG. 87

VARIATION OF EXHAUST AMMONIA WITH TREATMENT TIME FOR Fe-C ALLOYS NITRIDED IN NH_3/H_2.

FIG.88

VARIATION OF EXHAUST AMMONIA WITH TREATMENT TIME FOR Fe-C ALLOYS NITRIDED IN $NH_3/CH_4/H_2$.

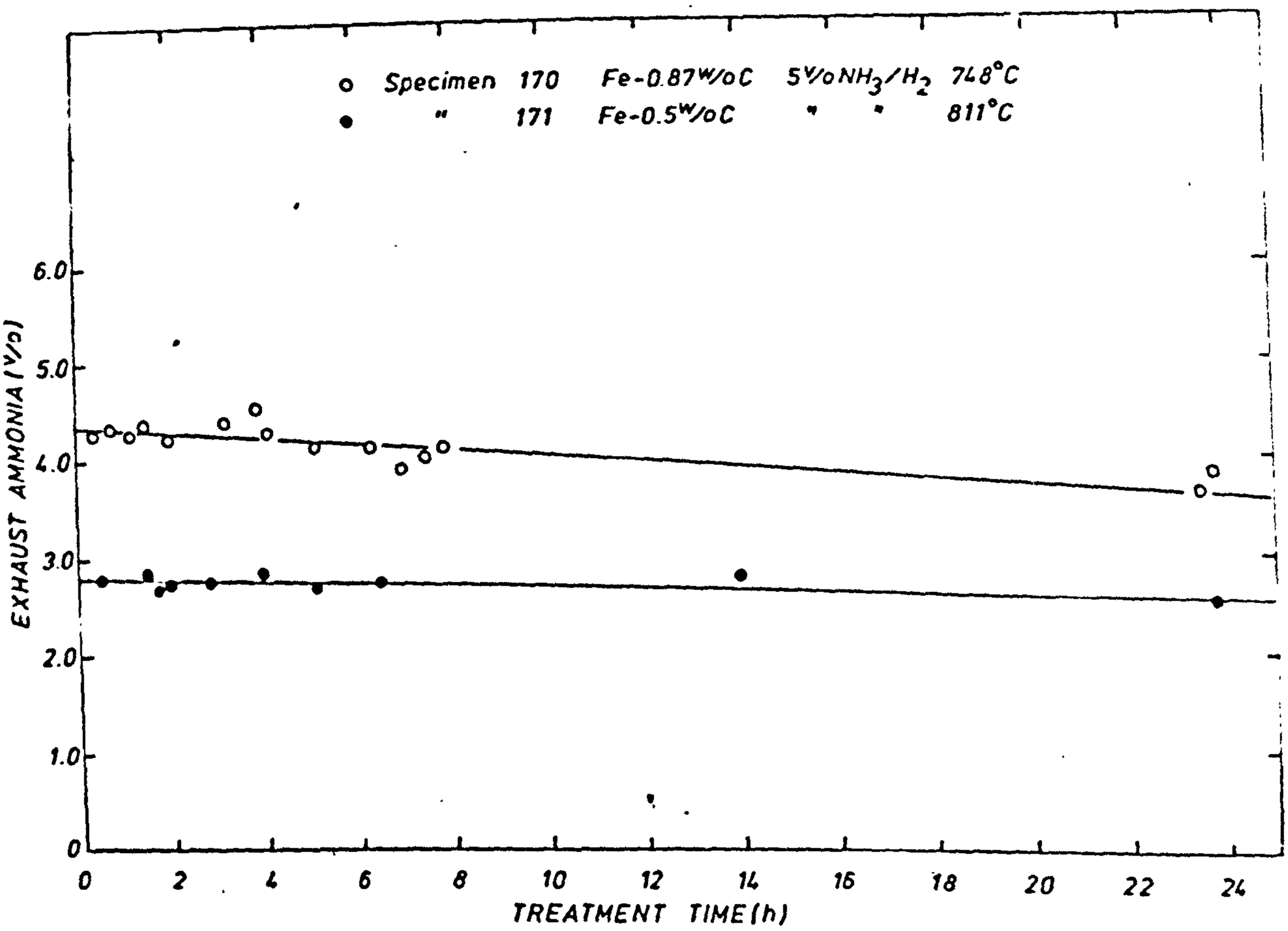
Specimen 170 Fe-0.87W/oC 5V/oNH3/H2 748°C
" 171 Fe-0.5W/oC " " 811°C
EXHAUST AMMONIA (V/o)
6.0
5.0
4.0
3.0
2.0
1.0
0
0 2 4 6 8 10 12 14 16 18 20 22 24
TREATMENT TIME(h)

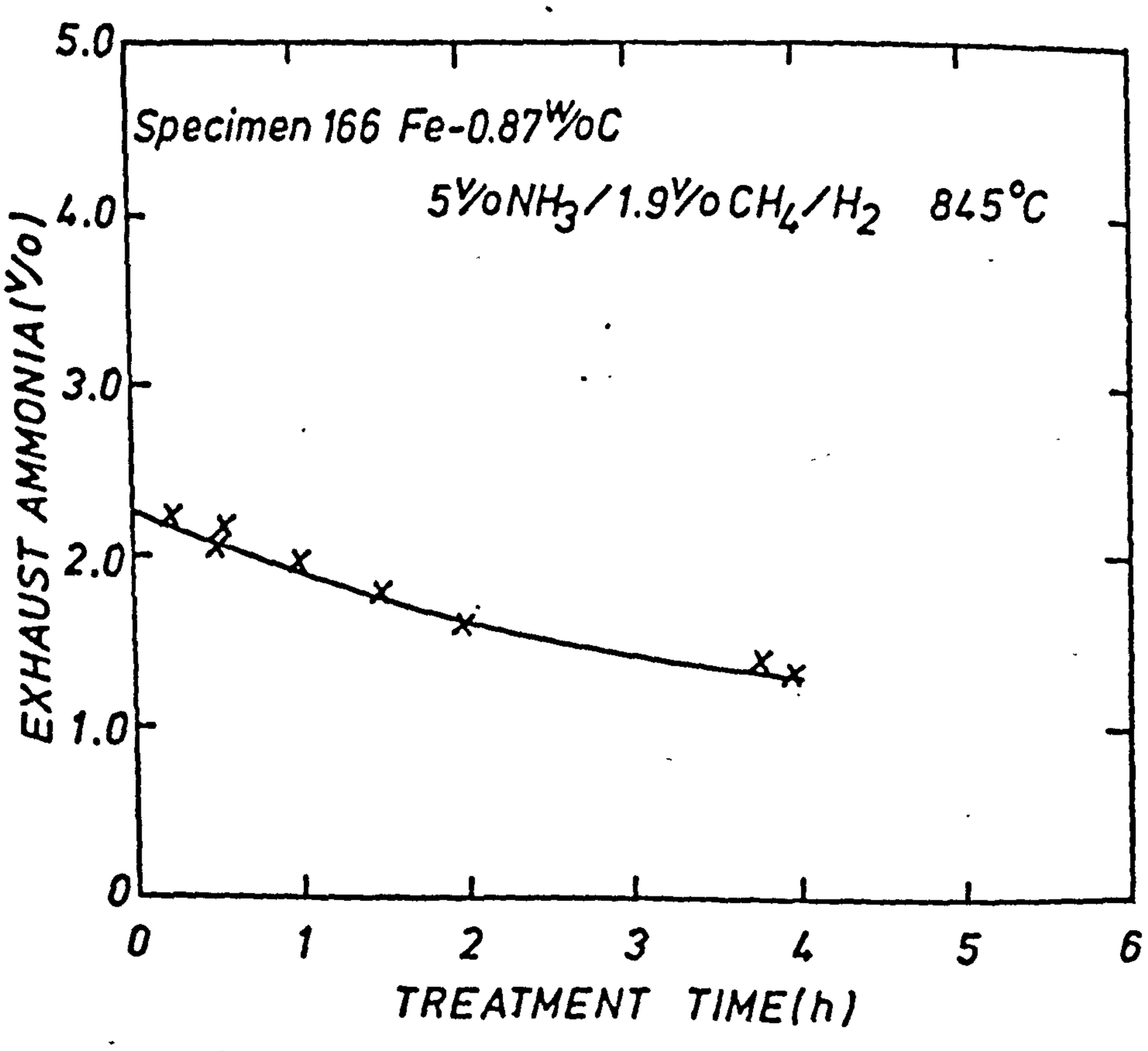
Specimen 166 Fe-0.87W/oC
5V/oNH3/1.9V/oCH4/H2 845°C
EXHAUST AMMONIA (V/o)
5.0
4.0
3.0
2.0
1.0
0
0 1 2 3 4 5 6
TREATMENT TIME(h)

FIG. 89

VARIATION OF D_{γ}^{C} WITH CONCENTRATION.

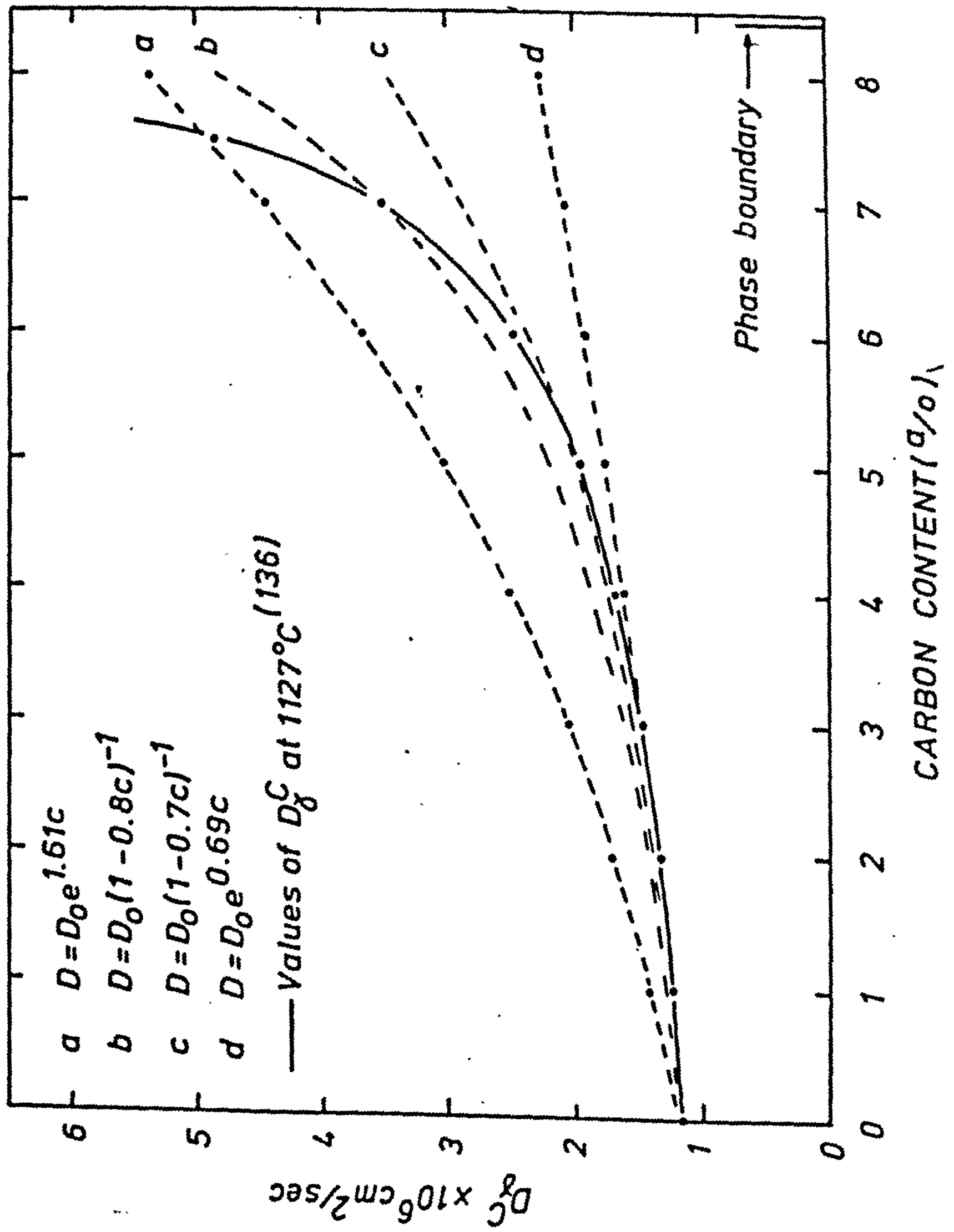
a
b
c
d
Phase boundary
a $D=D_0e^{1.61c}$
b $D=D_0(1-0.8c)^{-1}$
c $D=D_0(1-0.7c)^{-1}$
d $D=D_0e^{0.69c}$
— Values of D_γ^C at 1127°C (1361)
$D_\gamma^C \times 10^6 cm^2/sec$
CARBON CONTENT (% wt)
0
1
2
3
4
5
6
7
8

FIG. 90

CALCULATED AND EXPERIMENTAL CONCENTRATION PROFILES FOR SPECIMEN 62.

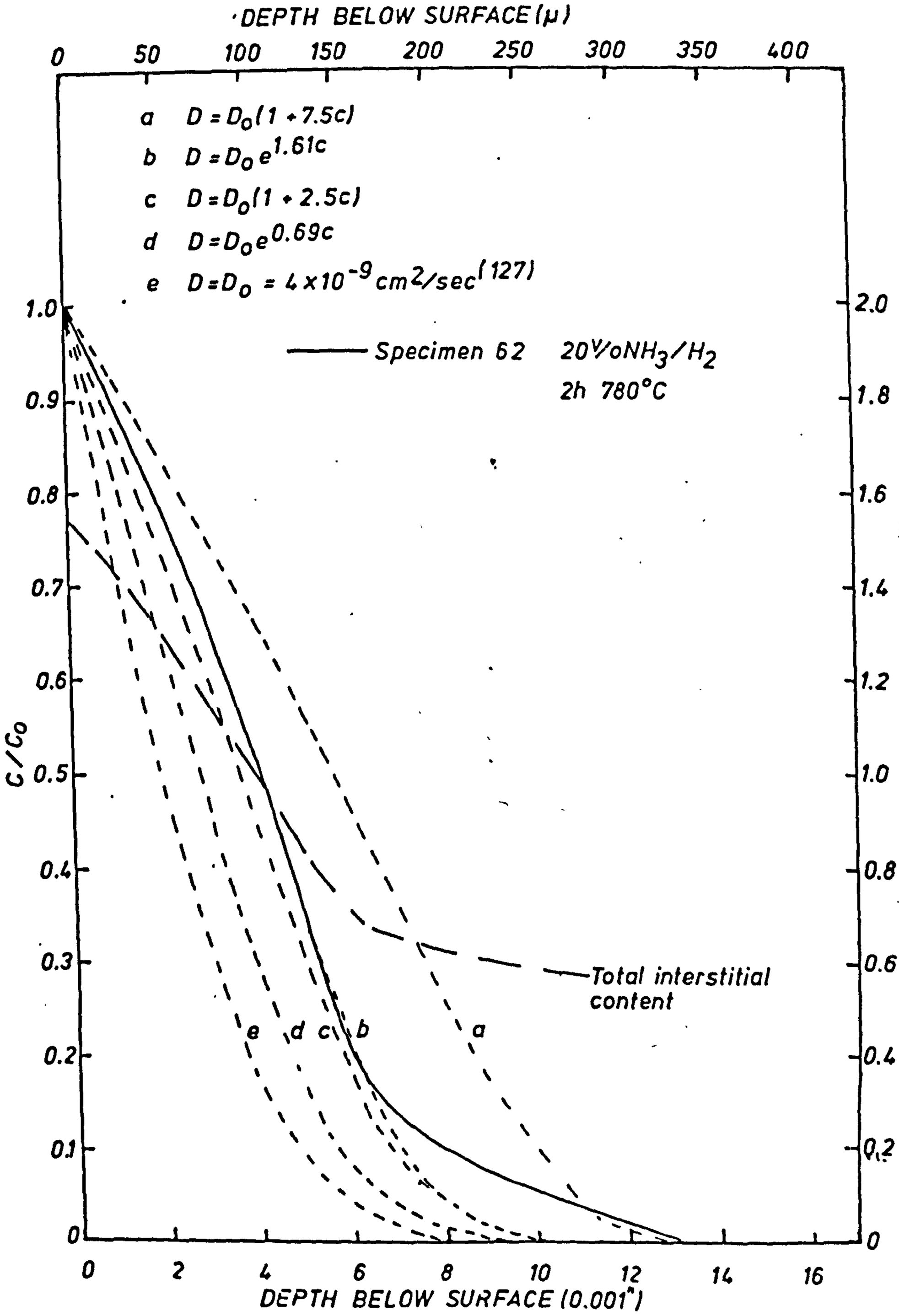
DEPTH BELOW SURFACE (μ)
0
50
100
150
200
250
300
350
400
a $D = D_0(1 + 7.5c)$
b $D = D_0 e^{1.61c}$
c $D = D_0(1 + 2.5c)$
d $D = D_0 e^{0.69c}$
e $D = D_0 = 4 \times 10^{-9} cm^2/sec$ (127)
Specimen 62 20 V/o NH_3/H_2
2h 780°C
C/C0
1.0
0.9
0.8
0.7
0.6
0.5
0.4
0.3
0.2
0.1
0
Total interstitial content
TOTAL INTERSTITIAL CONTENT (W/o)
2.0
1.8
1.6
1.4
1.2
1.0
0.8
0.6
0.4
0.2
0
0
2
4
6
8
10
12
14
16
DEPTH BELOW SURFACE (0.001")

FIG. 91

CALCULATED AND EXPERIMENTAL CONCENTRATION PROFILES FOR SPECIMEN 160.

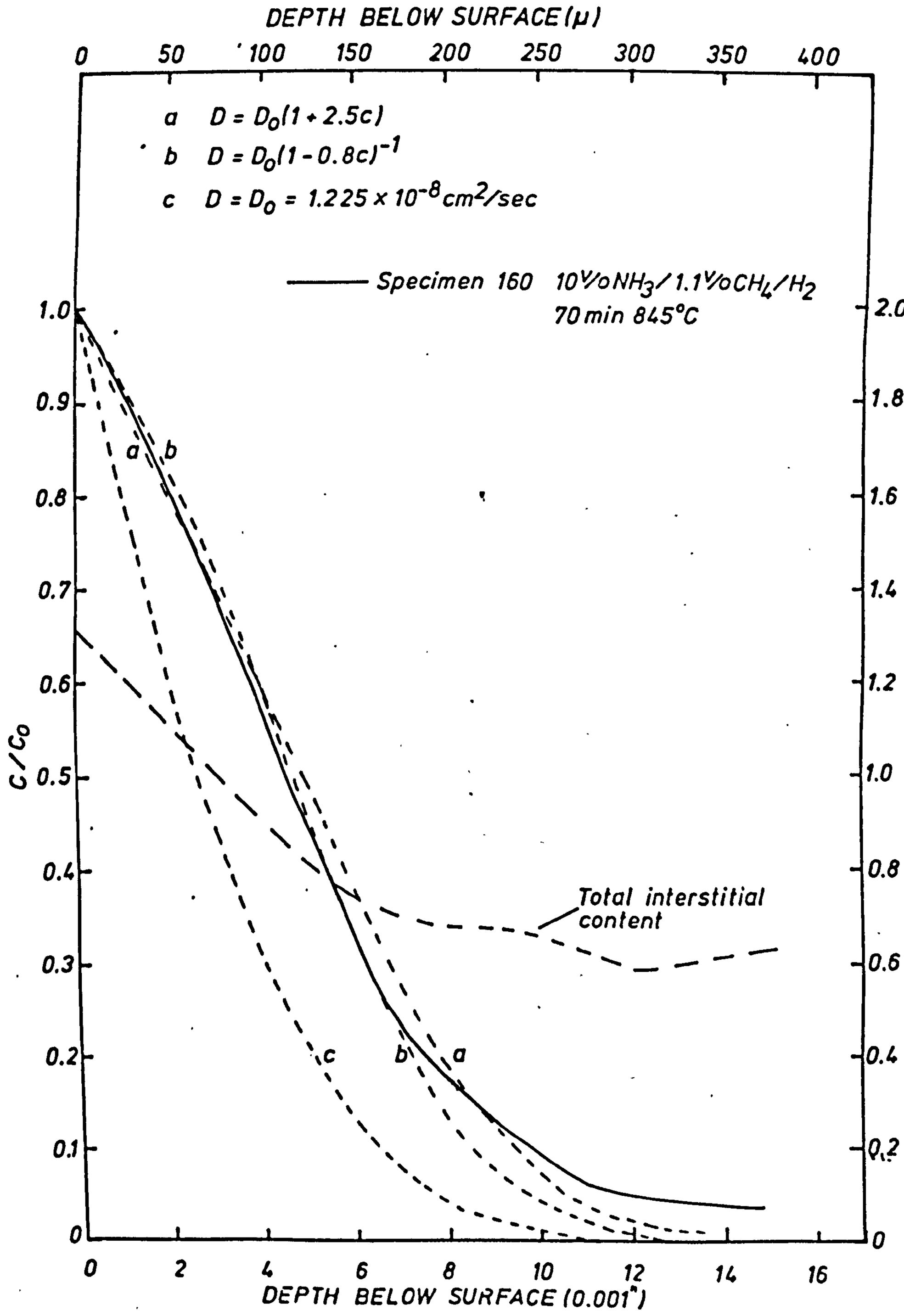
DEPTH BELOW SURFACE (μ)
0
50
100
150
200
250
300
350
400
a D = D0(1 + 2.5c)
b D = D0(1 - 0.8c)^-1
c D = D0 = 1.225 x 10^-8 cm^2/sec
Specimen 160 10 V/o NH3 / 1.1 V/o CH4 / H2
70 min 845°C
C/C0
1.0
0.9
0.8
0.7
0.6
0.5
0.4
0.3
0.2
0.1
0
a
b
c
Total interstitial content
TOTAL INTERSTITIAL CONTENT (W/o)
2.0
1.8
1.6
1.4
1.2
1.0
0.8
0.6
0.4
0.2
0
0
2
4
6
8
10
12
14
16
DEPTH BELOW SURFACE (0.001")

FIG. 92

VARIATION OF D_{γ}^{N} WITH TEMPERATURE.

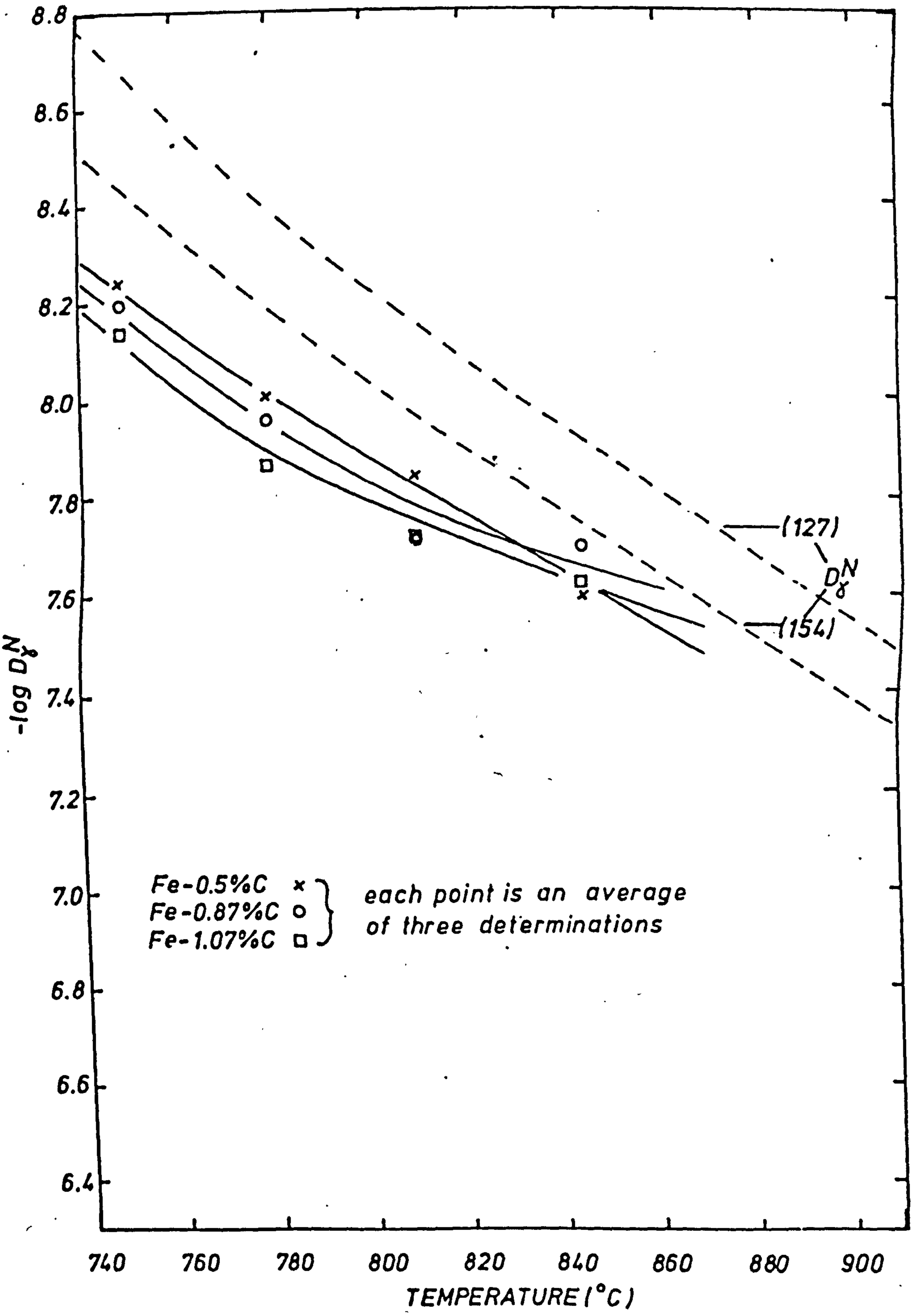
8.8
8.6
8.4
8.2
8.0
7.8
7.6
7.4
7.2
7.0
6.8
6.6
6.4
-log D^N_γ
(127)
D^N_γ
(154)
Fe-0.5%C ×
Fe-0.87%C ○
Fe-1.07%C □
each point is an average of three determinations
740
760
780
800
820
840
860
880
900
TEMPERATURE (°C)

FIG. 93

VARIATION OF D_{γ}^{C} WITH TEMPERATURE.

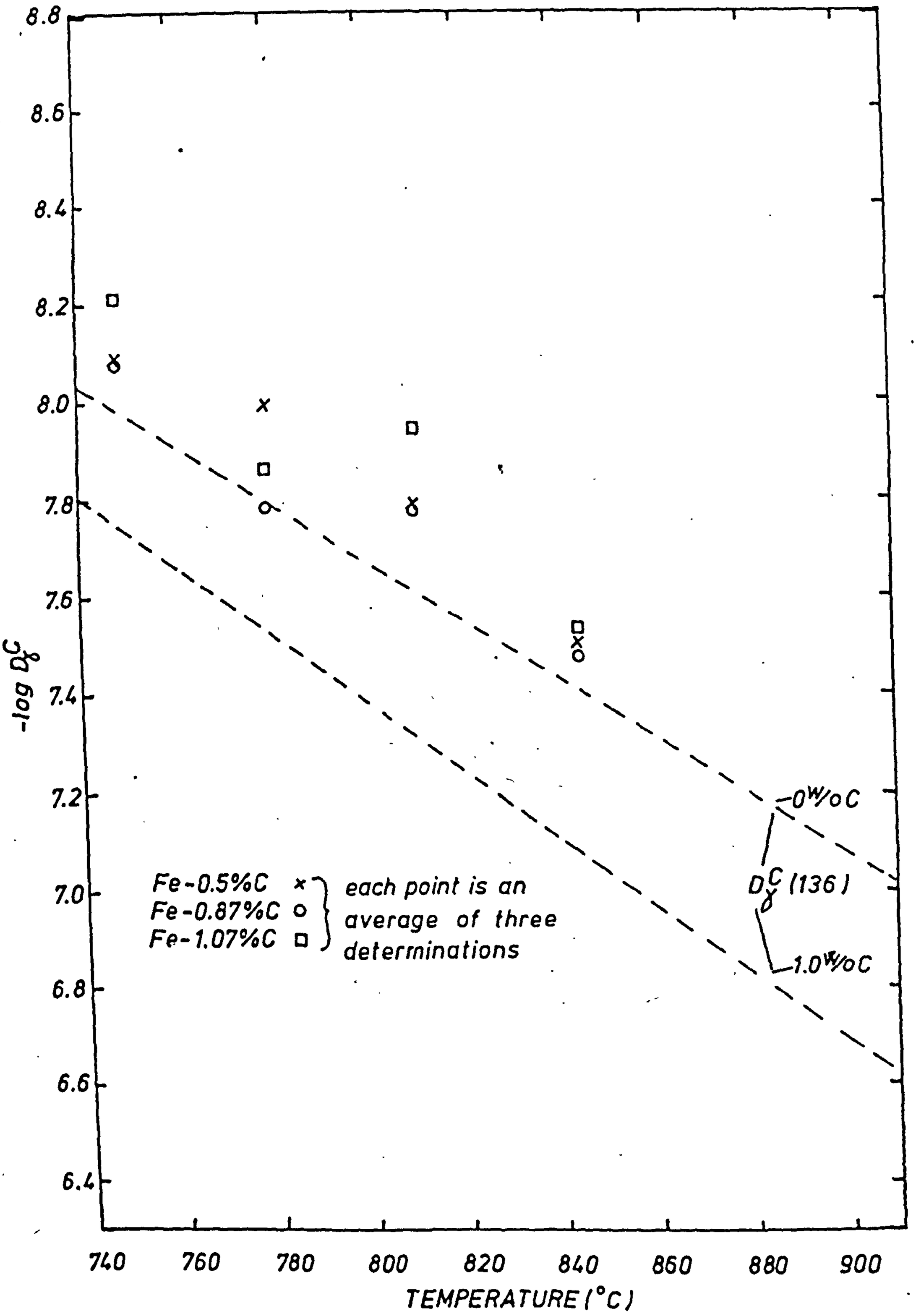
8.8
8.6
8.4
8.2
8.0
7.8
7.6
7.4
7.2
7.0
6.8
6.6
6.4
-log D
740
760
780
800
820
840
860
880
900
TEMPERATURE (°C)
Fe-0.5%C ×
Fe-0.87%C ○
Fe-1.07%C □
each point is an average of three determinations
0 W/o C
D C γ (136)
1.0 W/o C

FIG. 94

CONCENTRATION PROFILES FOR Fe-0.5$^{W}/_{o}$C ALLOY NITRIDED IN $5^{V}/_{o}NH_3/3^{V}/_{o}CH_4/H_2$ AT 845°C.

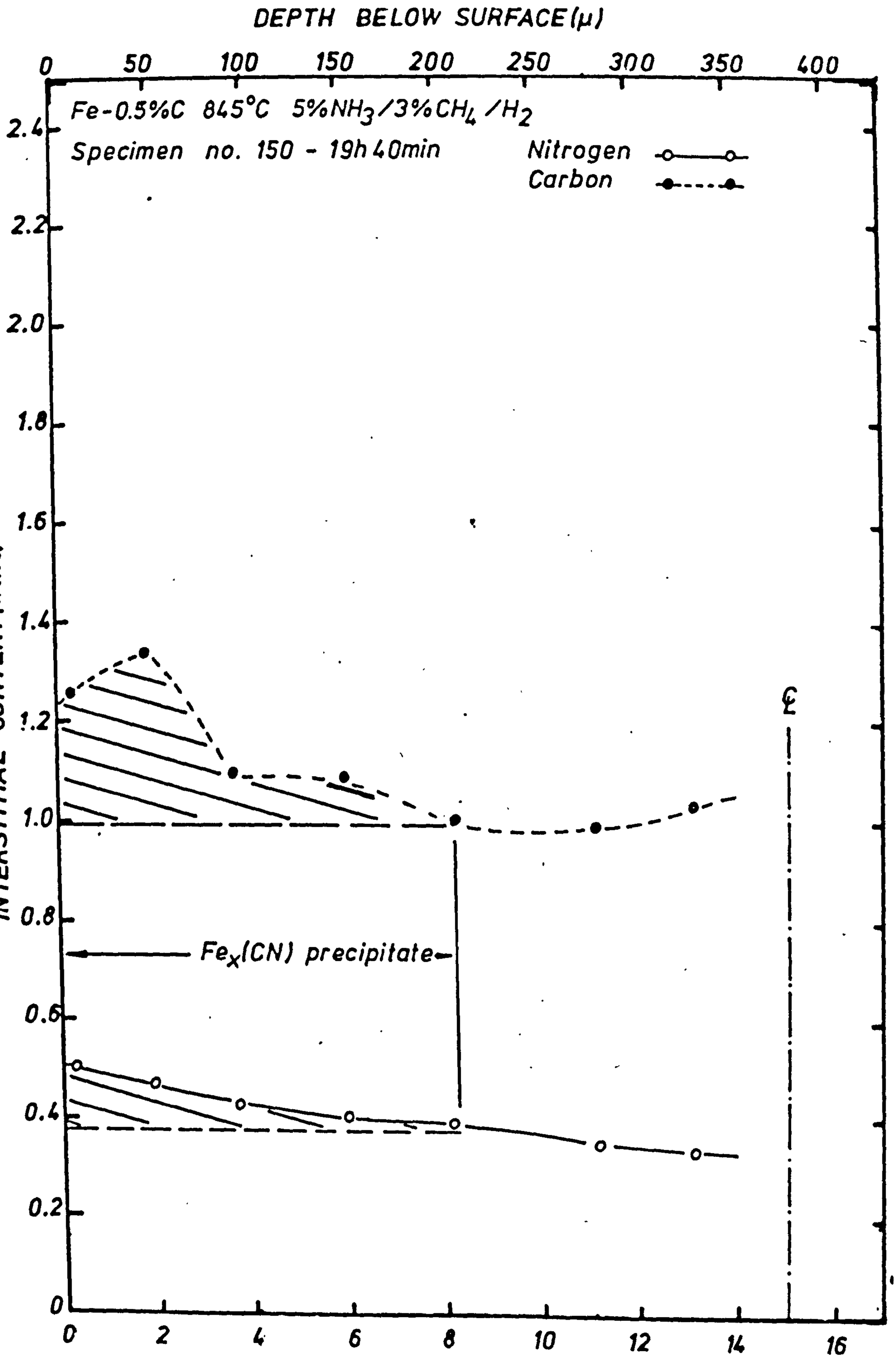
DEPTH BELOW SURFACE(μ)
0
50
100
150
200
250
300
350
400
Fe-0.5%C 845°C 5%NH3/3%CH4/H2
Specimen no. 150 - 19h 40min
Nitrogen
Carbon
INTERSTITIAL CONTENT(wt.%)
2.4
2.2
2.0
1.8
1.6
1.4
1.2
1.0
0.8
0.6
0.4
0.2
0
Fex(CN) precipitate
Fe
0
2
4
6
8
10
12
14
16
DEPTH BELOW SURFACE(0.001)

FIG. 95

CONCENTRATION PROFILES FOR Fe-0.5$^{w}/_{o}$C ALLOY NITRIDED IN $20^{v}/_{o}NH_3/3^{v}/_{o}CH_4/H_2$ AT 845°C.

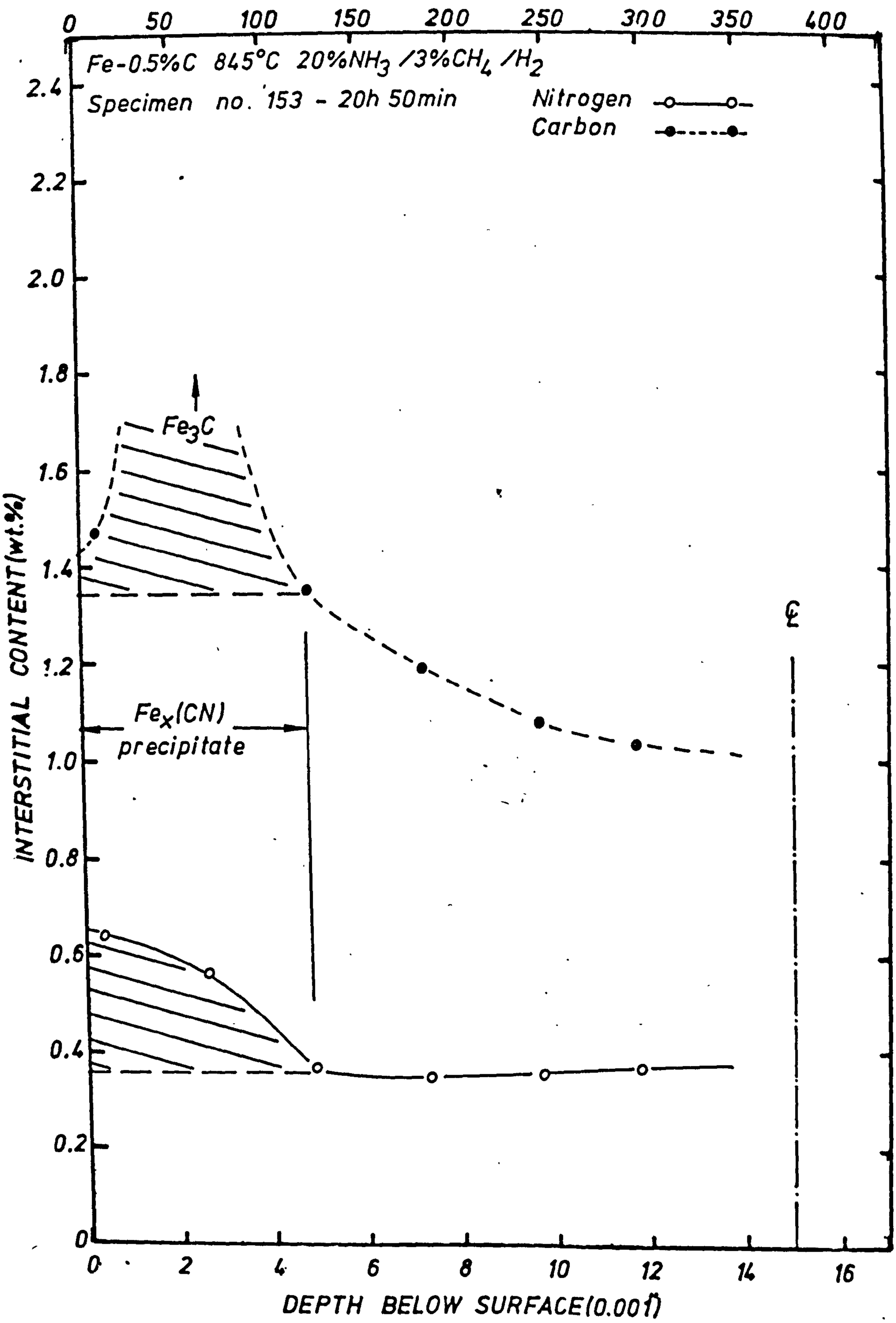
DEPTH BELOW SURFACE(μ)
0
50
100
150
200
250
300
350
400
Fe-0.5%C 845°C 20%NH3 /3%CH4 /H2
Specimen no. 153 - 20h 50min
Nitrogen
Carbon
2.4
2.2
2.0
1.8
1.6
1.4
1.2
1.0
0.8
0.6
0.4
0.2
0
Fe3C
Fex(CN) precipitate
INTERSTITIAL CONTENT(wt.%)
0
2
4
6
8
10
12
14
16
DEPTH BELOW SURFACE(0.001")

FIG. 96

CONCENTRATION PROFILES FOR Fe-0.5$^{w}/_{o}$C ALLOY NITRIDED IN $40^{v}/_{o}NH_3/3^{v}/_{o}CH_4/H_2$ AT 845°C.

127ag

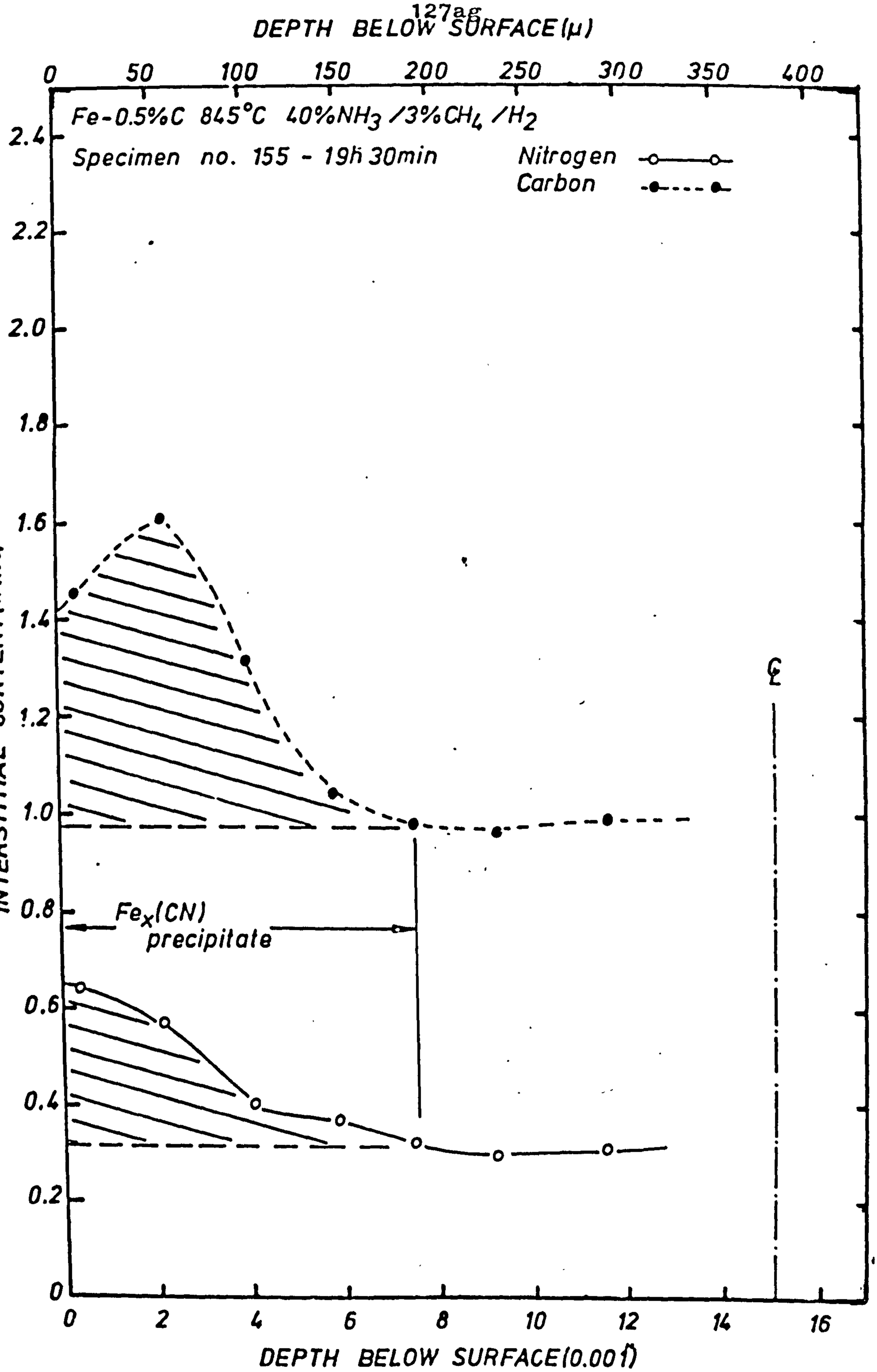
DEPTH BELOW SURFACE (μ)
0
50
100
150
200
250
300
350
400
Fe-0.5%C 845°C 40%NH3 /3%CH4 /H2
Specimen no. 155 - 19h 30min
Nitrogen
Carbon
INTERSTITIAL CONTENT (wt.%)
2.4
2.2
2.0
1.8
1.6
1.4
1.2
1.0
0.8
0.6
0.4
0.2
0
Fex(CN) precipitate
0
2
4
6
8
10
12
14
16
DEPTH BELOW SURFACE (0.001")

FIG. 97

ISOTHERMAL SECTION OF Fe-C-N TERNARY SYSTEM AT 748°C.

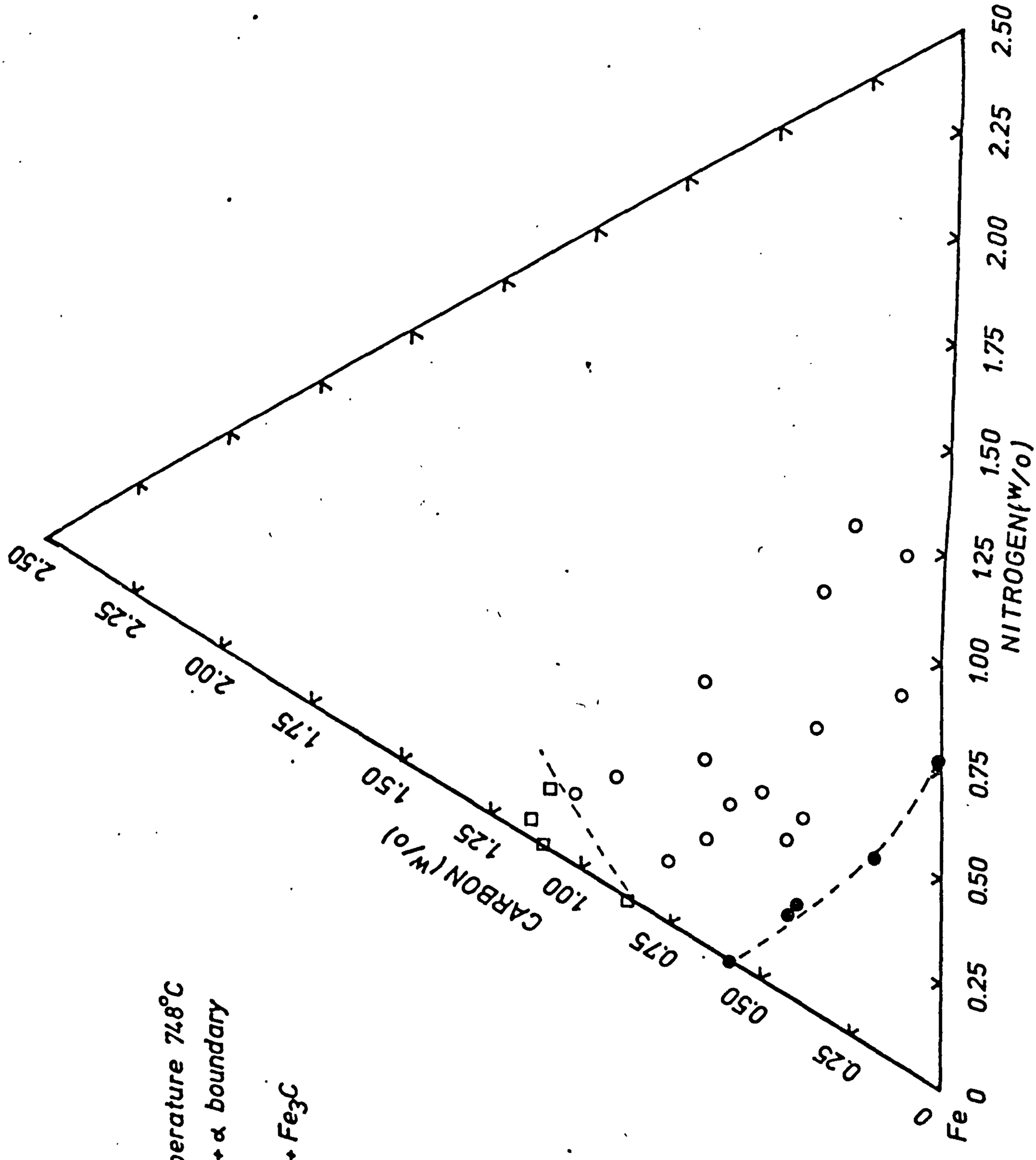
Temperature 748°C
● γ + α boundary
○ γ
□ γ + Fe3C
Fe 0
0.25
0.50
0.75
1.00
1.25
1.50
1.75
2.00
2.25
2.50
CARBON (W/O)
NITROGEN (W/O)

FIG. 98

ISOTHERMAL SECTION OF Fe-C-N TERNARY SYSTEM AT 780°C.

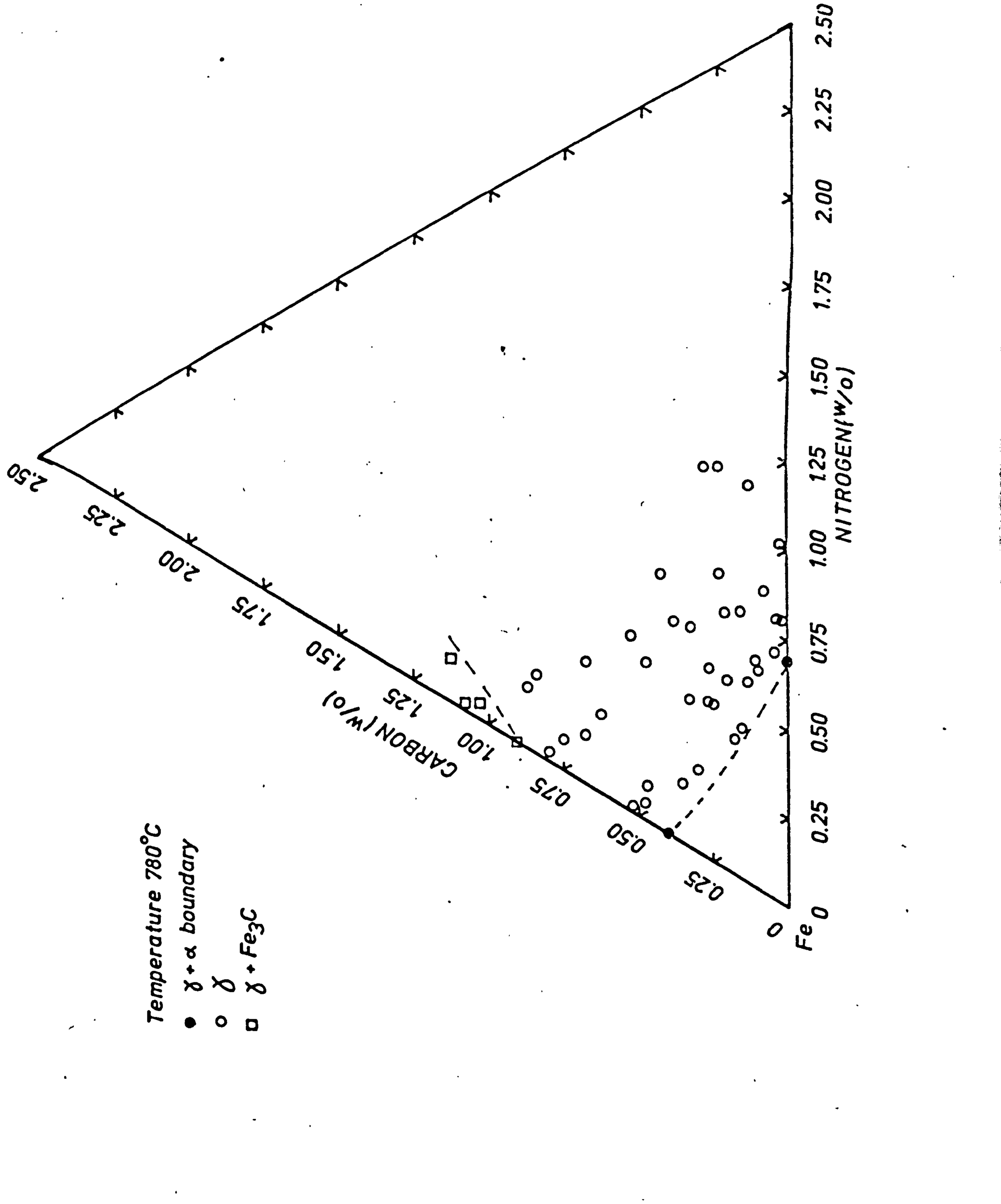
Temperature 780°C
● γ+α boundary
○ γ
□ γ+Fe3C
Fe 0
0.25
0.50
0.75
1.00
1.25
1.50
1.75
2.00
2.25
2.50
NITROGEN (W/O)
0.25
0.50
0.75
1.00
1.25
1.50
1.75
2.00
2.25
2.50
CARBON (W/O)

FIG. 99

ISOTHERMAL SECTION OF Fe-C-N TERNARY SYSTEM AT 811°C.

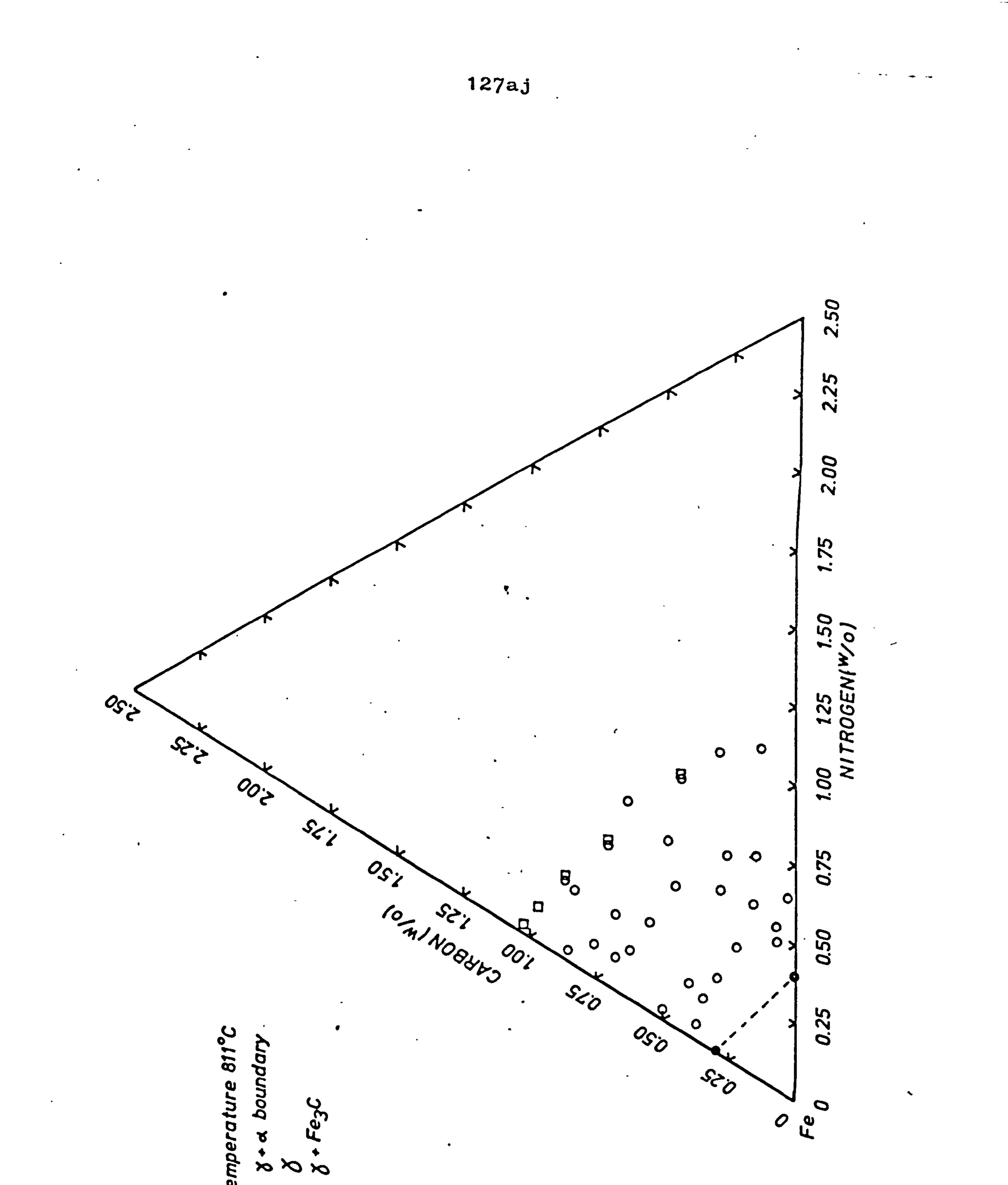
Fe 0
0.25
0.50
0.75
1.00
1.25
1.50
1.75
2.00
2.25
2.50
NITROGEN(W/o)
0.25
0.50
0.75
1.00
1.25
1.50
1.75
2.00
2.25
2.50
CARBON (W/o)
Temperature 811°C
● γ+α boundary
○ γ
□ γ+Fe3C

FIG. 100

ISOTHERMAL SECTION OF Fe-C-N TERNARY SYSTEM AT 845°C.

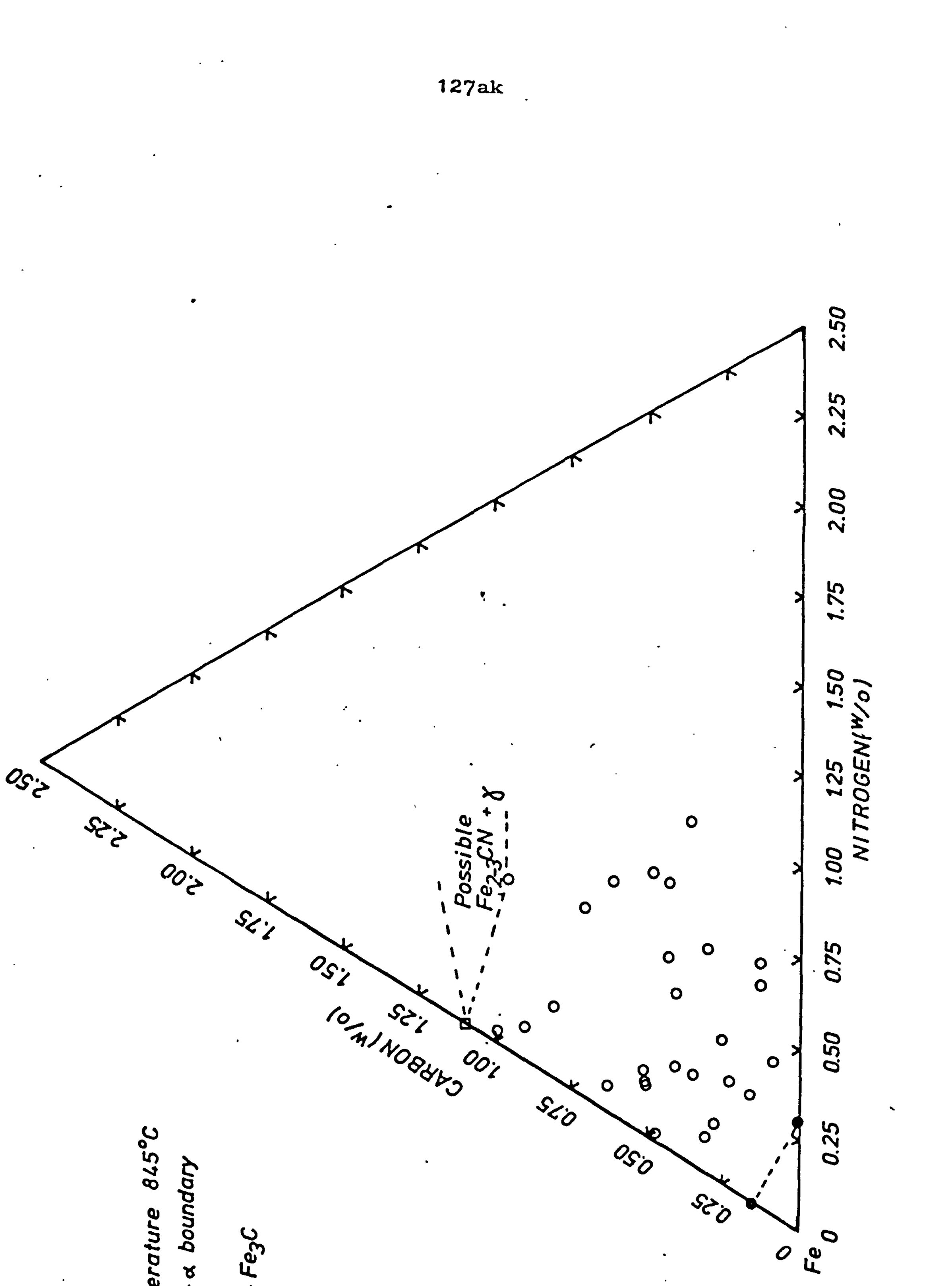
Temperature 845°C
● γ + α boundary
○ γ
□ γ + Fe3C
Possible Fe2-3CN + γ
CARBON (W/O)
NITROGEN (W/O)
Fe
0
0.25
0.50
0.75
1.00
1.25
1.50
1.75
2.00
2.25
2.50
125

CHAPTER 8

SUMMARY, CONCLUSIONS AND FURTHER WORK

(1) It has been shown on a laboratory scale that both infra-red gas analysis and gas chromatography can provide reliable measurement of residual ammonia in heat treatment atmospheres, and hence in turn can determine the nitriding potential of an austenitic nitriding atmosphere. The infra-red system should prove to be the most suitable for any future industrial applications of austenitic nitriding, since it is continuous in operation and more readily adaptable to the full automatic control of heat treatment atmospheres.

(2) During infra-red gas analysis investigations of the austenitic nitriding atmosphere, significant inaccuracies in the measurement of ammonia were detected. It was identified that these inaccuracies were due to overlap of the water vapour and ammonia peaks. This problem was largely eliminated by removing water vapour from the gas stream with a drying agent. As a result, current ammonia infra-red analysers are now designed to avoid this problem.

(3) Ammonia, because of its highly polar nature, has traditionally been a difficult gas to analyse accurately and quickly by gas chromatography. The polar molecule 'sticks' to the column packing material and is not eluted as a sharp peak. This problem has been overcome in the present work by the use of silylation methods combined with high temperature (125°C) column operation.

(4) Instrumentation developments over the past 5 years have allowed light elements such as boron, carbon and nitrogen to be

quantitatively analysed by electronprobe microanalysis techniques. A limitation on the widespread adoption of this technique for the analysis of nitrogen in thermochemically processed specimens has been the lack of suitable standards; the only ones being available were compounds such as boron nitride and silicon nitride. In the present project, two series of standards and calibration curves have been prepared by controlled nitriding techniques (a) 0 - 2.7^{W}/oN for the analysis of nitrogen in austenite (b) 0 - 12^{W}/oN for the analysis of nitrogen in iron-nitride based compounds.

(5) In both the ranges just described, myristate and stoarate analysing crystals can be used to produce nitrogen calibration curves, but the myristate crystal produces considerably less scatter and is preferred for accurate work. Simultaneous determination of carbon and nitrogen can be made using the stoarate and myristate crystals respectively in a microanalyser with two light element spectrometers.

(6) Emission spectrometric techniques for the very accurate, rapid and simultaneous analysis of most elements present in steel have found widespread application over the years as a quality control tool in heat treatment plants. In particular, regular checks of surface carbon contents after carburising and occasional carbon case profiles have proved a valuable means of maintaining heat treatment standards within individual companies. Unfortunately, although many such commercial instruments are capable of detecting nitrogen in steel, there were none available at the start of the present project which could analyse for nitrogen over a substantial range of composition.

Once again this was due to a lack of suitable standards to calibrate the instruments. As part of the present project, a new weight change calibration method for nitrogen was developed, which used iron-carbon alloys nitrided in the austenite phase region. The calibration derived provided an analysis facility over the range 0 - 2.4^{W}/oN to an accuracy of 3% and is now used in the quality control laboratory of Vauxhall Motors, Ellesmere Port.

(7) The diffusion coefficient of nitrogen in austenite at a fixed carbon level has been found to increase with increasing nitrogen concentration; a similar variation to that already known for carbon[136]. The variation can be approximately represented by the expression $D_{\gamma}^{N} = D_{o}e^{1.61c}$; D_{o} is the diffusion coefficient at effectively zero nitrogen content and c is the ratio of the nitrogen concentration at any point along the concentration profile to the surface nitrogen concentration. In these studies, surface nitrogen concentrations of between 1^{W}/o and 2^{W}/o were used. Furthermore, for a fixed base nitrogen level, D_{γ}^{N} increases with increasing carbon content; thus indicating the approximate interchangeability of the two interstitials in their effect on the diffusion coefficient.

(8) The average D_{γ}^{N} value obtained from the nitriding of iron-carbon alloys has a similar temperature dependency to the values obtained by Grieveson and Turkdogan[127] - $D = D_{o}e^{\frac{-40,260}{RT}}$. Whilst Grieveson and Turkdogan obtained a value of 0.91 for D_{o}, values of 2.5 to 3.0 were obtained in this work in Fe-0.5^{W}/oC and Fe-1.07^{W}/oC steels respectively. This data supports the use of Grieveson's data as the base D_{o} value in any equation

for the calculation of concentration gradients based on compositionally dependent diffusion coefficients.

(9) During the nitriding of thin pure iron strip material at temperatures which involve the conversion of ferrite to austenite, severe blistering and void formation has been observed. However, on the basis of the present work it can be concluded that this void formation and associated ferrite reversion only occurs after through nitriding has taken place, but before complete homogeneity can be established. A model for the formation of such voids has been tentatively suggested.

(10) Blistering does not occur, irrespective of section size, during the nitriding of iron-carbon alloys and its absence can be attributed to the diffusion of nitrogen directly into austenite, or at least into a duplex austenite/ferrite matrix.

(11) The austenite phase limits in the ternary iron-carbon-nitrogen system at temperatures above 700°C have in part been delineated. Extensive determination of the system at high temperatures is limited by the rapid thermal decomposition of ammonia at temperatures above 700°C.

(12) During the austenitic nitriding of iron-carbon alloys in ammonia/hydrogen mixtures decarburisation takes place, however under these conditions the decarburisation effect is not diffusion controlled. Furthermore, the assumption often made in decarburisation studies, particularly with single phase systems, namely that the surface carbon content is zero, is not applicable.

(13) Decarburisation can be prevented during austenitic nitriding by providing an appropriate carburising potential with methane during treatment. Under such circumstances, there is a build-up of carbon ahead of the advancing nitrogen interface; a phenomena that has only previously been reported for ferritic nitriding and nitrocarburising treatments.

(14) At a fixed nitriding potential, the surface nitrogen level in nitrided iron-carbon alloys decreases dramatically during the first few hours of treatment. This feature is in fact the reverse of that found during austenitic carburising treatments and can be related to the associated decarburising effects.

FURTHER WORK

The simultaneous investigation into scientific and technological limitations of austenitic nitriding processes has led to the development of several analytical techniques which can form the basis for further development work.

Now that composition profiles can be readily and accurately determined, further work should correlate more accurately the physical and mechanical properties of steels surface hardened with high nitrogen levels.

With the aid of the calibrated microanalyser more detailed study should be made of austenitically nitrided and carbonitrided structures, in order to distinguish some of the structural anomalies which are known to occur.

With the conclusions that gas voids only occur in through nitrided materials, it should now be possible to further investigate the scaling up of the.austenitic nitriding process for industrial applications.

With the aid of the gas analysis methods developed, study should be made of the performance of industrial austenitic thermochemical treatment atmospheres; particular regard should be paid to the attainment of equilibrium between specimens and atmosphere, in view of the known interactions between ammonia gas and other components of the gaseous atmospheres.

REFERENCES

(1) T. Bell, Heat Treatment of Engineering Components
I.S.I. Special report No. 124 P.125

(2) T. Bell, Ph.D. Thesis, University of Liverpool 1965

(3) B.C. Farnell, Ph.D. Thesis, University of Liverpool 1969

(4) J.L. Burns, T.L. Moore & R.S. Archer, Trans ASM 26 1938 P.I.

(5) 'Cassel', Manual of heat treatment and case hardening
7th Edition I.C.I. Ltd., 1964

(6) F.E. Harris, Metals Handbook, American Society of Metals
1948. P.678

(7) Wagman, Kilpatrick, Taylor, Pitzer and Rossini
J. Res. Nat. Bur. Stds. 34 1945 P.143

(8) W.T. Groves, Industrial Heating, June 1949

(9) Leeds and Northrup, Philadelphia USA

(10) R. Littlewood, Steel Times, Sept. 1964. P.423

(11) L.H. Fairbank, Metallurgia 35, May 1969 P.179

(12) R.G.H. Record Metallurgia and Metal Forming 39, Dec.1972
P.413

(13) R.G.H. Record, ibid. 40 Jan.1973 P.19

(14) L.H. Fairbank and L.G.W. Palethorpe, ISI Special Report
No.95 1966 P.57.

(15) K. Nishida and Y. Tanaka Nippon Kinzoju 32(5) 1968 P.435

(16) L.S. Darken and R.W. Gurry Physical Chemistry of Metals
McGraw-Hill New York 1953 Chapt.15.

(17) B.G.F. Roe Unpublished work, International Nickel Ltd.,

(18) L. Salonen and M. Sulonen, Traitment Thermique 73
1973 P.41.

(19) J.M. Bello, F. Medina and B.J. Fernandez, CENIM Meeting
Madrid Sept. 1974

(20) J. Slycke, 16th International Heat Treatment Confernce
Stratford-on-Avon, England May 1976.

(21) V.S. Lomakin, Metallov i term obrab Metallov. 7 1969 P.80

(22) B.J. Fernandez, F. Medina and J.M. Bello, Revista de Met 9 1973(3) P.181.

(23) H.W. Westeren and K. Broadbent, Metals Australia, Feb. 1973 P.3

(24) H.W. Westeren and A. Balaguier. Traitment Thermique 72 1973 P.27

(25) T. Bell, Metals Technology 1, May 1974 P.209

(26) P.C. Jindal, Metal Progress, April 1973, P.78

(27) A. Taylor, M. Eng. Thesis, University of Liverpool 1975

(28) C.K. Jones, S.W. Martin, D.J. Sturges and M. Hudis, Heat Treatment '73, Metals Society London 1976, P.71.

(29) B. Edenhofer, Heat Treatment of Metals 1974 1 No.1 P.23

(30) B. Edenhofer ibid 1974 1, No.2. P.59

(31) J. Sumner, The Engineer 238, 25th April 1974, P.41

(32) B. Edenhofer, Harterei-Tech. Mitt. 28, Sept 1973, P.165

(33) A.U. Seybolt, Trans AIME 245, April 1969 P.769

(34) P. Collignon, G. Hisler, H. Michel and M. Gantois, 16th International Heat Treatment Conference, Stratford-on-Avon, England, May 1976

(35) D. Atkinson, Ph.D. Thesis, University of Liverpool 1966

(36) T. Bell, Survey of the heat treatment of engineering components. The Iron and Steel Instituted, London 1973

(37) J.S. Kirkaldy and G.R. Purdy in Barret and Massalski - Structure of Metals, McGraw-Hill, New York 3rd Edition P.511

(38) B. Prenosil, Harterei-Tech. Mitt 21(3), 1966, P.199

(39) S. Gunnarson, Jernkontorets Annaler 146(5) 1962.

(40) T. Holm, Heat Treatment'73, Metals Society London 1976 P.125

(41) B.G.F. Roe, Unpublished work, International Nickel, Oct'69

(42) C. Razim, Doctoral Thesis, Technische Hochschule Stuttgart '67

(43) C. Razim, Harterei-Tech. Mitt 23 (4), 1968 P.1.

(44) C. Razim, Why Carbon Case Harden. Metal Society Meeting, Coventry, June 1975.

(45) T. Bell and B.C. Farnell, Institute of Metals Monograph, No.33, 1969 P.282.

(46) T. Bell and W.S. Owen Trans AIME 239, 1967 P.164

(47) T. Bell and D. Brough, Metal Science Jnl. 4, 1970 P.17

(48) K.H. Jack, Proc. Roy. Soc. Series A 195, 1948, P.41

(49) F.K. Naumann & G. Langenscheid, Archiv fur Eisenhuttenwes 36 1965, P.677

(50) S.A. Levy, J.F. Libsch and J.D. Wood, Trans AIME 245, April 1969, P.753

(51) J.M. Bello, F. Medina and B.J. Fernandez, Revista de Met 7 1971(2), P.99

(52) R. Chatterjee-Fischer and D. Schaaber, Harterei-Tech Mitt 26 1971, P.108

(53) R. Chatterjee-Fischer and O. Schaaber ibid 24 1969, P.121.

(54) F. Medina, J.M. Bello and B.J. Fernandez Revista de Met 7 1971(5), P.369

(55) K. Ogawa and K. Otomo. The Tokyo Metropolitan Industrial Research Institute 20 1969, P.47

(56) D. Atkinson and C. Bodsworth, JISI 208, 1970, P.587

(57) J. Slycke, Private Communication.

(58) H. Kurabe, Trans I.S.I. Japan 14, 1974, P.404

(59) R. Chatterjee-Fischer and O. Schaaber, Harterei-Tech Mitt 24 1969, P.292.

(60) Z. Kolosvary, V. Sandor and P. Teszler, 14th International Colloquium on Heat Treating, Salzburg 1972, Paper No.14

(61) T. Bell, B. Birch, V. Korotchenko and S.P. Evans, Heat Treatment 73' Metals Society London 1976, P.51

(62) B. Prenosil, Harterei-Tech Mitt 21(1), 1966. P.24

(63) A. Lallemant, Heat Treating, March 1975. P.18

(64) A. Guimier, Spring Heat Treatment Meeting, Sutton Coldfield, June 1974.

(65) B. Prenosil, Harterei-Tech Mitt 19 (1) 1964.

(66) T. Bell, Heat Treatment of Metals 2, 1975 P.39

(67) Alexander Wright & Co. Ltd., Westminster, England.

(68) Glass Precision Engineering Ltd., Hertfordshire, England.

(69) Determination of nitrogen in steel, ISI special report No.62 1962.

(70) The Determination of small amounts of nitrogen in steel. BSC Open Report MG/CC/520/72

(71) Technical data, Ammonia probe Model 8002/2 Electronic Instruments Ltd., Surrey, England.

(72) P.M. Todd, J. Sci. Fd. Agric. 24 1973, P.488

(73) G.K. Buckee, J. Inst. Brew 80 1974, P. 291.

(74) S.P. Evans, Ph.D. Thesis work, University of Liverpool in progress.

(75) B.D. Cullity, Elements of X-Ray Diffraction. Addison - Wesley, 1956. P.485.

(76) K.H. Jack, Proc.Roy.Soc. A208 1951, P.200

(77) Ref. 75 Chapter 11.

(78) R. Coombes Analytical Development Co. Ltd., Hoddesdon, Herts, Private Communication.

(79) R.H. Pierson, A.N. Fletcher and E. St. Clair Gantz Anal Chem. 28 1956 P.1218

(80) D.J. Perkins, Feedback Instruments Ltd., Sussex, Private Communication.

(81) Handbook of Chemistry and Physics, 54th Edition.
CRC Press, Cleveland Ohio, 1973-4

(82) R.M. Bethea and M.C. Meador, J. Chromat Sci. 7 1969, P.655

(83) T.L. Chang, J. Chromatog. 37. 1968 P.14

(84) Waters Associates Inc. Massachusetts. USA.

(85) Johns-Manville Denver Colorado USA.

(86) E.L. Obermiller & G.O. Charlier, J. Gas Chromat. 6, 1968 P.446

(87) R.R. Forsey, J. Gas Chromat. 6 1968, P.555

(88) A. Di. Lorenzo, J. Chromat. Sci. 8, 1970. P224.

(89) D.R. Deans, M.T. Huckle and R.M. Peterson, Chromatographia 4 1971, P.279.

(90) A.G. Kim and L.J. Douglas, J. Chromat. Sci.11 1973, P.615

(91) W.R. Averett, J. Chromat. Sci. 8 1970, P.552

(92) J.E. Lovelock, Anal. Chem. 33 1961 P.162

(93) I.R.M. Wardell and V.E. Coslett, The Electron Microprobe. Proc. Symp. Electrochemical Soc. Washington. P.23

(94) P.S. Ong. ibid P.43

(95) R. Jenkins and J.L. de Vries, Metallurgical Reviews No. 154, 1971, P.125

(96) Applied Research Laboratories, Luton, England.

(97) Japan Electron Optics Laboratory Co. Ltd., Japan

(98) Cambridge Scientific Instruments Ltd., Cambridge, England,

(99) P.M. Martin and D.M. Poole, Metallurgical Reviews No. 150 1971, P.19

(100) V.D. Scott, Advances in analysis of microstructural features by electron beam techniques. Metals Soc. May 1974 P. 141.

(101) G. Love, M.G.C. Cox, and V.D. Scott. J. Phys.D.Appl. Phys.7 1974 P.2143

(102) G. Love, M.G.C. Cox and V.D. Scott. Developments in Electron Microscopy and Analysis EMAG'75. Ed. J.A. Venables Academic Press London 1976. P.145

(103) G. Love, M.G.C. Cox and V.D. Scott, J. Phys.D.Appl.Phys 7 1974, p.2131.

(104) J. Philibert, X-ray Optics and Microanalysis ed. H.H.Pattee, V.E. Coslett and E. Engström. Academic Press, New York 1963, P. 379.

(105) H.E. Bishop, J. Phys. D. Appl. Phys 7, 1974 P.2009

(106) J. Ruste and M. Gantois, J. Phys.D.Appl.Phys. 8 1975,P.872

(107) E. Eichen, J. Tabock and K.R. Kinsman, Metallography 5, 1972, P.151.

(108) J.S. Duerr and R.E. Ogilvie, Anal. Chem. 44. 1972, P.236

(109) J.M. Beswick, Practical Metallography 12, 1975, P.200

(110) E. Kohlhass and E. Scheiding, Archiv. fur Eisenhuttenwes 40 1969, P.47

(111) G.V.T. Ranzetta and V.D. Scott, J.Sci.Instrum. 43 1966 P.816

(112) A.J. Campbell and R. Gibbons. The Electron Microprobe Proc. Symp. Electrochem. Soc. Washington. P.75

(113) Electronprobe Microanalysis Meeting, Hinxton Hall, Saffron Waldon, Oct. 1974.

(114) M.W. Charles, J. Appl. Phys. 42 (9), 1971. P.3329.

(115) D. Atkinson, T. Bell and D. Brough, JISI 203, 1965, P.836

(116) B.G.F. Roe and T. Bell, Developments in Electron Microscopy and Analysis EMAG'75, Ed. J.A. Venables, Academic Press, London 1976, P.149.

(117) K.F.J. Heinrich, Advances in X-Ray Analysis 7 1964 P.325

(118) Telsec Instruments Ltd., Oxford, England.

(119) H.J. Lucas-Tooth and M.S. Banks, 15th International Spectroscopy Colloquium Madrid 1969.

(120) B.J. Price, Metals and Materials 7, 1973, P.140

(121) Telsec Application report No. 72031, Sept. 1972. Telsec Instruments Ltd. Oxford, England.

(122) T. Bell and S.Y. Lee. Heat Treatment'73, Metals Society London 1976, P. 99

(123) K.H. Jack, Acta Cryst. 5 1952, P.404

(124) N. Harris, A. Taylor and J. Stringer, Acta Met 21. 1973, P.1677

(125) C.A. Anderson, The Electron Microprobe. Proc. Symp. Electrochemical Soc. Washington. P.58

(126) J. Crank and M.E. Henry, Trans.Faraday Soc.45 1949, P.1119

(127) P. Grieveson and E.T. Turkdogan, Trans AIME 230 1964, P.407

(128) T. Bell and B.G.F. Roe, previously unpublished work; ref.21 in ref.66.

(129) Balzers High Vacuum Ltd., Berkhampstead, Hertfordshire, Eng.

(130) Shandon Southern Instruments Ltd., Surrey,,England.

(131) Hilger and Watts, - Rank Precision Industries Analytical Division, Margate, England.

(132) V.G. Mossotti, Techniques of Metals Research 3, Chapt.11 - Modern Analytical Techniques for Metals and Alloys. Ed. R.F. Bunshah, Interscience Publishers New York 1970.

(133) J. Gould, Vauxhall Motors, Ellesmere Port, Private Communication.

(134) W. Jost. Diffusion in solids, liquids and gases. Academic Press. Inc. New York 1952, P.69

(135) J. Crank, The Mathematics of Diffusion, Clarendon Press 1964, P.45

(136) C. Wells, W. Batz and R.F. Mehl, Trans AIME 188 1950 P.533

(137) J.D. Grozier, H.W. Paxton and W.W. Mullins, Trans AIME 233 1965, P.130.

(138) A. Silbernagel and R. Sejonoha, Kovove Materialy 6 (4) 1968, P.373.

(139) R.M. Hudson and P.E. Perry Trans AIME 245 1969, P.161.

(140) D. Atkinson and T. Bell Private communication.

(141) R.S. Barnes and R.S Nelson Radiation Effects, Met. Soc. Conf. AIME 37 Ed. W.F. Sheely 1967, P.225.

(142) K.B. Gove and J.A. Charles, Metals Technology 1 (6) 1974, P.279.

(143) E.T. Turkdogan and L.J. Martonik, High Temperature Science 2 1970, P.154.

(144) J.H. Swisher, Trans AIME 242 1968, P.763.

(145) P. Grieveson, Scand. Jnl. of Metallurgy 1 1972, P.231

(146) I. Pyyry and P. Kettunen, ibid 2 1973, P.265.

(147) R.P. Smith, Trans AIME 224 1962, P.105.

(148) Reference 135, Chapter 4.

(149) N. Birks and A. Nicholson, Mathematical Models in Metallurgical Process Development, ISI Publication 123 1970, P.219.

(150) A. Leutgöb and H. Trenkler, Archiv. fur Eisenhuttenwes. 45 (12) 1974, P.871.

(151) A.U. Malik, Ph.D. Thesis University of Liverpool 1975.

(152) Reference 134, P.249.

(153) D.H. Jack , Heat Treatment '73, Metals Society, London 1976, Discussion to Session II, P.178.

(154) J.D. Fast and M.B. Verrijp, JISI 176 1954, P.24.

(155) P. Grieveson and E.T. Turkdogan, Trans AIME 230 1964, P.1604.

(156) F.E. Harris, Metals Technology 14 Tech. Publ. 2216 1947.

(157) C. Wells and R.F. Mehl, ibid 7 Tech. Publ. 1180 1940.

(158) D.P. Whittle and A. Green, Scripta Met. 8 1974, P.883.

(159) G.W. Roper and D.P. Whittle, ibid P.1357.

(160) R.T. DeHoff, K.J. Anusavice and C.C. Wan, Met. Trans. 5 1974, P.1113.

(161) Reference 135, Chapter 12.

LIST OF TABLES

LIST OF FIGURES

QUANTITATIVE ELECTRON PROBE MICROANALYSIS FOR NITROGEN

B.G.F. Roe and T. Bell

Heat Treatment Research Group, Dept. of Metallurgy and Materials Science,
University of Liverpool, Liverpool L69 3BX, England.

Introduction difficulties The lack of accurate data concerning mass absorption coefficients and in the selection of a suitable correction model hinder the application of conventional quantitative microprobe analysis theory to light elements. Progress however is being made along these lines, as evidenced by the recent work of Love et al (1974a, b) and Ruste and Gantois (1975).

An alternative solution is the use of prepared standards of known chemical composition. Such a solution has proved popular for the calibration of microprobes for carbon in iron (Kohlhass and Scheiding 1969, Duerr and Ogilvie 1972, Eichen et al 1972, Beswick 1975), because of the relative ease with which a range of accurate Fe-C standards can be made. In the case of the other light elements such as nitrogen, oxygen and boron, standards are usually limited to specific compounds, such as boron nitride and the oxides of metals. Consequently their range of usefulness in quantitative determinations is limited.

In the field of heat treatment, there is currently considerable interest in thermochemical process developments which involve the diffusional addition of light elements to the surface of ferrous materials. It is therefore essential to be able to determine quantitatively the extent of such additions, in order to correlate process parameters with material properties and structures.

Theory treatment, Our current interest is mainly in the carbonitriding surface hardening where the simultaneous diffusion of carbon and nitrogen into a steel surface takes place. An inherent difficulty in the preparation of iron-nitrogen standards is that the Fe-N system is a metal-gas system which is metastable with respect to pressure. Subjecting iron to nitrogen gas at atmospheric pressure only results in a maximum uptake of $\sim 0.03^{w}/o$ nitrogen at $930^{\circ}C$. To obtain higher nitrogen levels, use is made of the ammonia decomposition reaction (Darken and Gurry 1953),

$$NH_3 \rightleftharpoons N_{(\text{in Fe})} + {}^{3}/_{2}\, H_2$$

which, because of its high chemical potential, provides nitrogen at the specimen surface equivalent to extremely high pressures of nitrogen, and can result in a maximum solution of nitrogen of approximately $12^{w}/o$.

Under static conditions, ammonia thermally decomposes above $600^{\circ}C$, so nitriding above this temperature is normally conducted under dynamic conditions with linear flow rates over the specimen surface of between 0.25 and 1 cm/sec, to provide enough undissociated ammonia at the specimen surface. It has been shown by Atkinson (1966) that the amount of nitrogen taken up by the specimen is proportional to the exhaust ammonia potential when some thermal dissociation occurs, and this has been proposed as a method of controlling the amount of nitrogen in solution for the production of homogeneous Fe-N alloys (Atkinson et al 1965). This method was developed using iron strips less than 0.1 mm thick, and runs into difficulties with problems of gas evolution and severe blistering when greater thicknesses are required. An alternative method has been developed (Roe 1975) whereby Fe-C strip is nitrided at temperatures above the Fe-N or Fe-C eutectoid temperatures to provide homogeneous Fe-C-N alloys. When no background carbon potential is present in the gas atmosphere, decarburisation occurs simultaneously with nitriding and the alloys can be reduced

to homogeneous Fe-N alloys.

Experimental Using a laboratory vertical tube furnace, Fe-C alloys in the form of 25 x 23 x 0.75 mm strip were nitrided in NH_3/H_2 mixtures under the conditions shown in Table 1. The relatively long times are necessary to allow complete diffusion within the sample to occur. The homogeneity of the samples was checked with successive layer analysis by emission spectrometry (Roe 1975), total nitrogen content was also determined by standard Kjeldahl analysis. The specimens were mounted edge-on in Scandiplast resin, carefully polished and finally thoroughly cleaned and degreased with carbon tetrachloride. These standards, unetched, were used for calibration points up to 1.1 w/o nitrogen; for nitrogen contents higher than this the following methods were used.

TABLE 1

DETAILS OF NITRIDING TREATMENTS FOR STANDARDS

NITROGEN (w/o)	ALLOY	TEMPERATURE (°C)	ATMOSPHERE	TIME (h)	THICKNESS (mm)
0	SPEC PURE Fe	——— UNTREATED ———			0.75
0.11	Fe-0.83%C	930	5%NH_3/H_2	8.3	"
0.42	Fe-0.5%C	845	20%NH_3/3%CH_4/H_2 (a)	21	"
0.65	"	811	5%NH_3/H_2	24	"
1.1	SPEC PURE Fe	780	4%NH_3/H_2	4	0.1

(a) Methane used for back-up carbon potential, giving 1% carbon in centre of alloy.

All specimens quenched in brine from treatment temperature.

From the Fe-N phase diagram extended to the high temperature region by Atkinson (1966) Fe-2.47 w/oN is the limit of solubility of nitrogen in austenite in equilibrium with ϵ-nitride at 780°C. By nitriding at a high potential ϵ-nitride forms on the surface with austenite of 2.47 w/oN immediately underneath; suitable conditions are 20%NH_3/H_2 for several hours at 780°C. After quenching, the ϵ-nitride is carefully polished off the surface on a 1μ wheel. The absence of ϵ-nitride and the presence of austenite together with its composition can be checked by x-ray diffraction (Jack 1951, Bell 1965). The flat specimen surface is used for calibration.

Fe-5.9 w/oN This is the composition of the stoichimetric γ' nitride Fe_4N. Suitable conditions for producing this compound on the surface of pure iron strip are 40%NH_3/H_2 at 515°C for 24h. Again the flat surface is used for calibration, without preparation apart from cleaning. The presence of Fe_4N was verified by x-ray diffraction.

Microprobe procedure Specimens were examined in a JEOL JXA 50A instrument fitted with an anticontamination cold finger. An accelerating voltage of 10kV with a specimen current of 0.08μA was used, and pulse height analysis(PHA) was employed in x-ray detection. The two spectrometers were set up for light element detection with myristate and stearate crystals, full details of instrument settings used are given in Table 2. Because of the low countrate associated with light elements, extended count times were necessary, the standard time of 100 seconds being used on all specimens. However this time can be reduced when analysing for high nitrogen contents associated with nitride compounds.

TABLE 2

DETAILS OF JXA-50A MICROANALYSER OPERATING CONDITIONS

Accelerating voltage 10KV

Specimen Current 0.08μA

Pulse Height Analyser (ORTEC)	Myristate	Stearate
GAIN	32 x 4	16 x 4
WINDOW	2.5 VOLTS	2.0 VOLTS
LOWER LEVEL	0.5 VOLTS	0.5 VOLTS
MODE	DIFFERENTIAL	DIFFERENTIAL

Counter. Gas filled proportional 10% CH_4/Argon flowing at 1.4l/h.

Window. Grid supported 2000Å thick polypropylene - 1 mm slit.

Voltage. 1700.

Setting-up is usually performed on the γ' Fe-5.9 w/oN sample. Because of the relatively large currents used, the spot size is also large, approximately 5-8μ as measured on a ZrO_2 standard.

At least 20 separate spot counts have been made on each calibration standard and the mean countrate calculated, normalised to cps/μA. Countrate was shown to be directly proportional to the specimen current, so drift can be easily

compensated. Counting was also monitored from ratemeter traces on a pen recorder and any obvious erroneous results disregarded. The calibration obtained for the two crystals up to the limit of solubility of nitrogen in austenite is shown in Fig. 1. The PHA settings used in this case are those recommended by JEOL, but when the myristate settings are used for both crystals, the calibrations are found to be almost identical. This conclusion can be implied from the work of Charles (1971).

Nitrogen countrate has been found to be unaffected by small increases in contamination, when allowed to build up. Similarly there appears to be no effects of amounts of carbon, up to 1.5^{w}/o dissolved in iron, on the nitrogen countrate.

Applications (a) Nitrogen in austenite: The calibration curve in Fig. 1 covers our current main interest, nitrogen in solid solution in iron. An example of its use is shown in Fig. 2, in the examination of nitrided iron strip. In this situation, analysis was started at least 10μ from the free edge to prevent burning of the mounting compound, and to avoid any problems associated with bevelling of edges during specimen preparation. The nitriding potential used was sufficient to form an austenite phase which penetrates into the ferrite matrix. The shape of the diffusion profile obtained being characteristic of a compositionally dependent diffusion coefficient (Crank and Henry 1949). An average D_N^{γ} value of 1.8×10^{-8} cm^2/sec calculated from this data compares with a value of 5.7×10^{-9} cm^2/sec extrapolated from the data of Grieveson and Turkdogan (1964). Because of the relatively large spot size used, the composition at the actual austenite/ferrite interface is difficult to determine, but values very close to the phase composition limit of 0.46^{w}/oN are obtained.

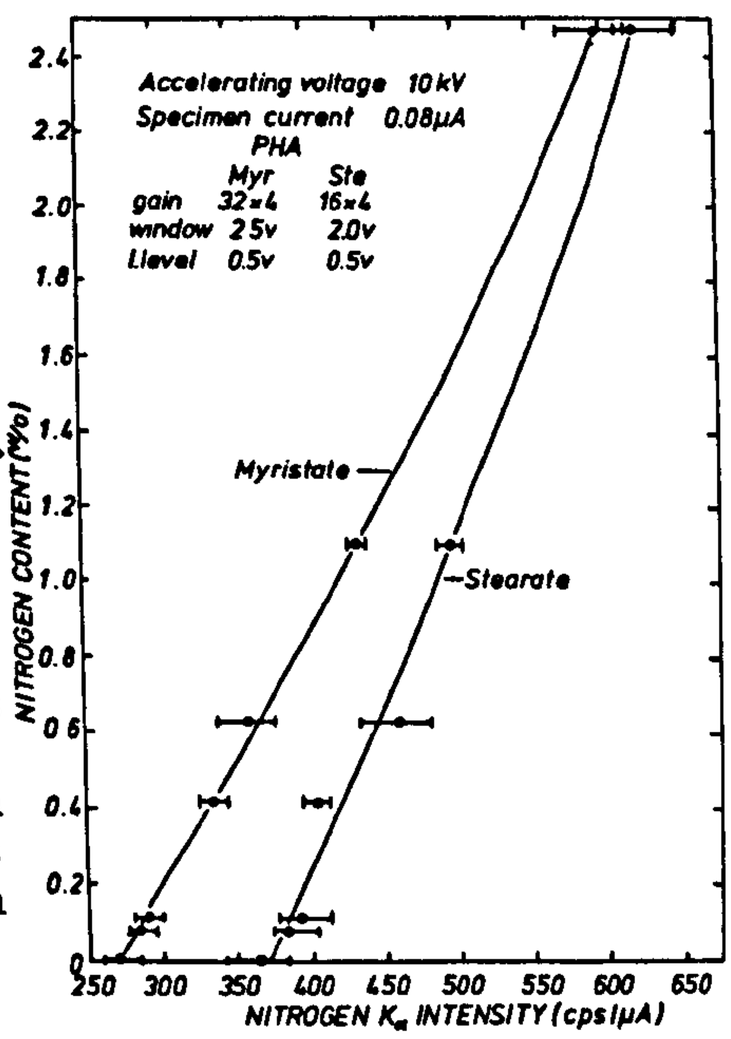

FIG. 1

(b) Iron-Nitrogen compounds: Nitrogen-bearing compounds of iron other than Fe_4N exist, the most common being ϵ-nitride, which is non-stoichimetric and exists over a wide range of composition from 4.5^{w}/o to 11.14^{w}/oN. It is also possible to substitute some nitrogen atoms with carbon to produce structurally similar ϵ-carbonitride (Naumann and Langenscheid 1965). One of each of these compounds have been made and examined by microanalysis.

ϵ-nitride was made by nitriding pure iron strip at 520°C for 48h in 80%NH_3/H_2, conditions which should give ϵ-nitride near to its terminal composition Fe_2N (11^{w}/oN at 520°C)(Jack 1952). The flat surface was used for microanalysis.

ϵ-carbonitride was made by nitrocarburising pure iron strip at 570°C for 3h in a 50%NH_3/50%Endothermic (carburising) atmosphere, a 20μ thick layer of the compound being formed on the surface. The layer has previously been shown by microanalysis traces to be reasonably uniform in nitrogen content across its thickness, and chemically analysed to contain 8.25 $\pm$0.15^{w}/oN (Bell and Lee 1973). The specimen was examined in cross-section, polished but unetched.

Countrates from the two epsilon compounds were obtained using a stearate crystal with the same PHA settings as used for myristate (cf Table 2).

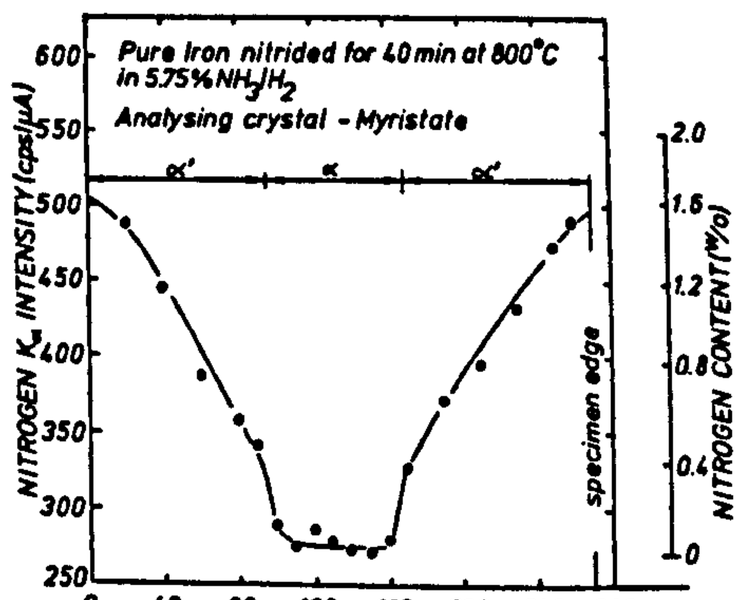

FIG. 2

The γ' nitride Fe_4N was used to extend the calibration curve up to 5.9 w/oN (Fig 3) which within experimental error appears to be a straight line. Some counts approximately 150 cps/μA higher than the indicated mean were obtained, but they were in a minority and outside the normal spread of countrate. It is highly likely that they were due to the presence of a small amount of ε-nitride.

Countrates at spots across the thickness of the epsilon carbonitride layer on the nitrocarburised sample showed only the variation indicated in Fig. 3, for different parts of the layer, and fit a linear extrapolation of the calibration curve (Fig. 3) extremely well, justifying its suggested composition.

The exact composition of the ε-nitride compound is not known, but x-ray diffraction examination using the data of Jack(1952) puts its minimum composition at 9 w/oN, while the maximum possible nitrogen content for ε-nitride at 520°C is 11 w/o from the phase diagram. These values are the compositional limits shown vertically in Fig. 3. If a straight line extrapolation still holds, this would give a nitrogen content at the outermost surface of 10.2 w/o. The countrate obtained on this surface being shown as the horizontal error bar at this point in Fig. 3.

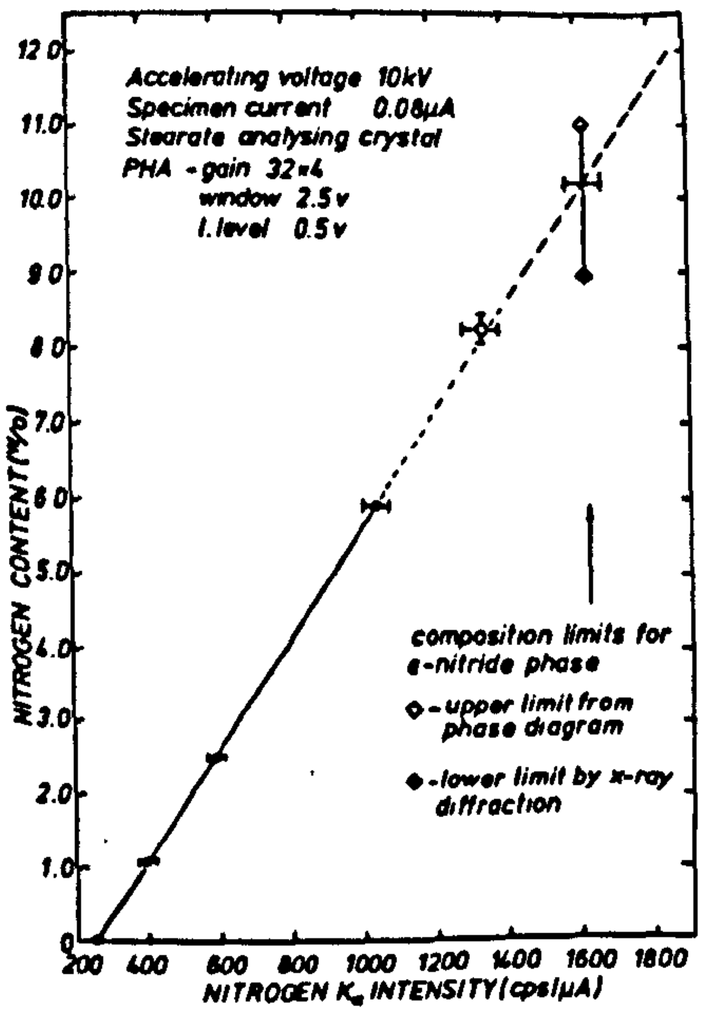

FIG. 3

Acknowledgements The authors gratefully acknowledge SRC for financial support.

References

Atkinson D., Bell T. and Brough D. 1965 JISI 203 p.836
Atkinson D. 1966 Ph.D. Thesis University of Liverpool
Bell T. 1965 Ph.D. Thesis University of Liverpool
Bell T. and Lee S.Y. 1973 Heat Treatment '73 Metals Society conf. proc. (in press)
Beswick J.M. 1975 Practical Metallography 12 p.200
Charles M.W. 1971 J. Appl. Phys. 42 p.3329
Crank J. and Henry M.E. 1949 Trans. Farad. Soc. 45 p.1119
Darken L.S. and Gurry R.W. 1953 Physical Chemistry of Metals McGraw-Hill New York Chapt. 15 p.372
Duerr J.S. and Ogilvie R.E. 1972 Anal. Chem. 44 p.326
Eichen E., Tabock J. and Kinsman K.R. 1972 Metallography 5 p.151
Grieveson P. and Turkdogan E.T. 1964 Trans. AIME 230 p.407
Jack K.H. 1951 Proc. Roy. Soc. Series A 208 p.200
Jack K.H. 1952 Acta Cryst. 5 p.404
Kohlhass E. and Scheiding E. 1969 Archiv. für Eisenhuttenwes 40 p.47
Love G., Cox M.G.C. and Scott V.D. 1974a J. Phys. D Appl.Phys. 7 p.2131
Love G., Cox M.G.C. and Scott V.D. 1974b J. Phys. D Appl.Phys. 7 p.2143
Naumann F.K. and Langenscheid G. 1965 Archiv. für Eisenhuttenwes 36 p.677
Roe B.G.F. 1975 Ph.D. Thesis University of Liverpool
Ruste J. and Gantois M. 1975 J. Phys. D Appl.Phys. 8 p.872